AD-A145 286 HANDBOOK FOR SEA ICE ANALYSIS AND FORECASTING(U) ALASKA 1/4
UNIV FAIRBANKS GEOPHYSICAL INST W J STRINGER ET AL.
JUN 84 NERPF-CR-84-03 N00228-81-C-H553

UNCLASSIFIED F/G 8/12 NL

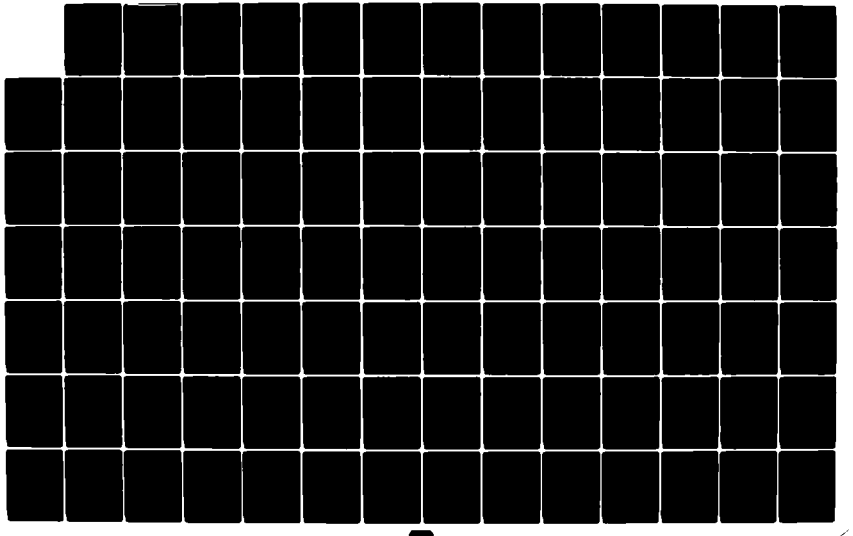

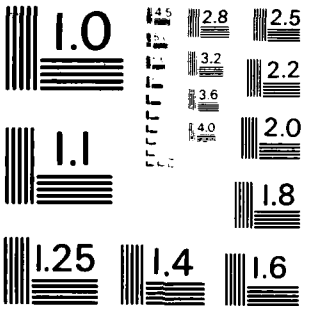

NAVENVPREDRSCHFAC
CONTRACTOR REPORT
CR 84-03

HANDBOOK FOR SEA ICE ANALYSIS AND FORECASTING

Prepared By:

William J. Stringer
Geophysical Institute
University of Alaska at Fairbanks

Don G. Barnett and Raymond H. Godin
Joint Ice Center/Naval Polar Oceanography Center
Suitland, Maryland

Contract No. N00228-81-C-H553

JUNE 1984

Prepared For:
NAVAL ENVIRONMENTAL PREDICTION RESEARCH FACILITY
MONTEREY, CALIFORNIA 93943

UNCLASSIFIED

SECURITY CLASSIFICATION OF THIS PAGE (When Data Entered)

REPORT DOCUMENTATION PAGE		READ INSTRUCTIONS BEFORE COMPLETING FORM
1. REPORT NUMBER NAVENPREDRSCHFAC Contractor Report CR-84-03	2. GOVT ACCESSION NO. AD-A145286	3. RECIPIENT'S CATALOG NUMBER
4. TITLE (and Subtitle) Handbook for Sea Ice Analysis and Forecasting		5. TYPE OF REPORT & PERIOD COVERED Final
		6. PERFORMING ORG. REPORT NUMBER
7. AUTHOR(s) William J. Stringer Don G. Barnett* Raymond H. Godin*		8. CONTRACT OR GRANT NUMBER(s) N00228-81-C-H553
9. PERFORMING ORGANIZATION NAME AND ADDRESS Geophysical Institute University of Alaska Fairbanks, Alaska 99701		10. PROGRAM ELEMENT, PROJECT, TASK AREA & WORK UNIT NUMBERS NEPRF WU OM&N-1
11. CONTROLLING OFFICE NAME AND ADDRESS Naval Air Systems Command Department of the Navy Washington, DC 20361		12. REPORT DATE June 1984
		13. NUMBER OF PAGES 324
14. MONITORING AGENCY NAME & ADDRESS(if different from Controlling Office) Naval Environmental Prediction Research Facility Monterey, CA 93943		15. SECURITY CLASS. (of this report) UNCLASSIFIED
		15a. DECLASSIFICATION/DOWNGRADING SCHEDULE

16. DISTRIBUTION STATEMENT (of this Report)

Approved for public release; distribution unlimited

17. DISTRIBUTION STATEMENT (of the abstract entered in Block 20, if different from Report)

18. SUPPLEMENTARY NOTES

*Authors' affiliation is Joint Ice Center/Naval Polar Oceanography Center, Suitland, Maryland.

19. KEY WORDS (Continue on reverse side if necessary and identify by block number)

Ice
Ice Forecasting
Sea Ice
Polar

20. ABSTRACT (Continue on reverse side if necessary and identify by block number)

Background information and techniques used to analyze and forecast sea ice conditions are presented. Emphasis has been placed on operationally-oriented analysis and forecast rules and aids and the use of climatological charts containing parameters related directly to operational decision-making based on sea ice conditions. Subject material includes sea ice morphology, characteristics and dynamics, global and regional sea ice

DD FORM 1 JAN 73 1473 EDITION OF 1 NOV 65 IS OBSOLETE S/N 0102-014-6601

UNCLASSIFIED

SECURITY CLASSIFICATION OF THIS PAGE (When Data Entered)

Block 20, Abstract, continued.
distribution and benavior, sea ice modeling, remote sensing principles and techniques, remote sensing systems used for sea ice analysis, auxilliary sea ice observations,meteorological and climatological relationships with sea ice, operational sea ice analysis, and sea ice forecasting techniques.

A-1

CONTENTS

FIGURES AND TABLES

FOREWORD

This Handbook for Sea Ice Analysis and Forecasting was developed under the Naval Environmental Prediction Research Facility's continuing effort to improve the quality of naval forecast services in all parts of the world.

A number of excellent publications or articles have been written covering portions of this vital area of interest; the purpose here is to present the most pertinent information available from many sources in a format suitable for use by Fleet forecasters who are unfamiliar with this analysis and forecast problem. Considerable emphasis is placed on operationally-oriented analysis and forecast rules/aids and the use of climatological charts containing parameters related directly to operational decision-making related to sea ice conditions.

It is intended that this document be responsive to current requirements of U.S. Navy operating forces; it has, therefore, been assembled in loose-leaf form. Users are urged to submit to this Command their comments and suggestions regarding contents and changes thereto.

This Handbook for Sea Ice Analysis and Forecasting was prepared by Dr. William J. Stringer of the Geophysical Institute, University of Alaska at Fairbanks, and Mr. Don G. Barnett and Mr. Raymond H. Godin of the Naval Polar Oceanography Center, Suitland, Maryland. This project was funded by the Department of the Navy with additional support from the State of Alaska. Linda Schreurs of the Geophysical Institute, University of Alaska was the project's technical editor. Mr. Samson Brand of the NAVENVPREDRSCHFAC staff served as Project Coordinator.

Kenneth L. Van Sickle
Captain, U.S. Navy
Commanding Officer

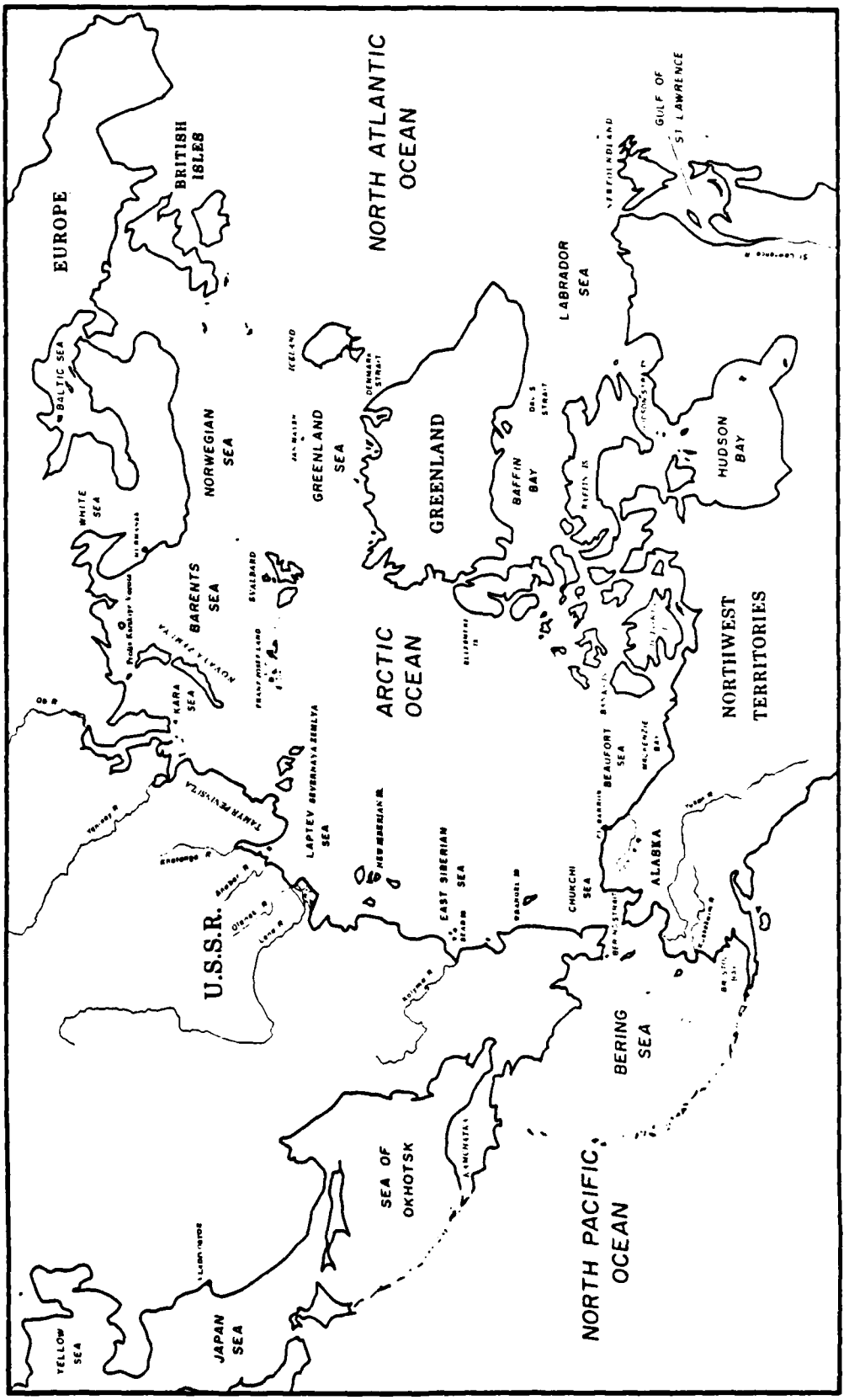

Figure 1. Northern Hemisphere Location Map

Figure 2. Southern Hemisphere Location Map

CHAPTER I. SEA ICE MORPHOLOGY AND CHARACTERISTICS

SECTION 1. FORMATION AND DEVELOPMENT OF SEA ICE

1.1 THE FREEZING PROCESS

1.1.1 Freezing Point of Sea Water. 0° C is defined as the melting point of freshwater ice. Conversely, fresh water can start freezing when it is at 0° C (32° F). Dissolving salts in water lowers its freezing temperature. Sea water contains approximately 35‰ (35 parts per thousand or 3.5 per cent) dissolved salts, most of which is sodium chloride or common table salt. This quantity of salts is sufficient to depress the freezing point of sea water to around -1.9° C (28° F). When applying this concept, it should be remembered that in many nearshore areas, particularly bays and lagoons fed by freshwater streams, the salt concentration in the water is less than 35‰ and its freezing point is correspondingly higher.

1.1.2 Supercooling of Water Before Ice Formation. Water does not actually freeze precisely at its melting point (although the difference can be extremely small). This results from the fact that freezing is a change of phase (as is the transition of water into water vapor). The transition alone requires the withdrawal of 80 calories per gram of water. This is a tremendous amount of energy considering that 1 calorie is defined as the amount of heat required to raise or lower one gram of water by 1° C. Thus, it requires the withdrawal of just as much energy to create one gram of freshwater ice at 0° C as it would to lower the temperature of that gram of water from 80° C (176° F) to 0° C (32° F).

At first, one might think that the only way to satisfy this 80 cal/gm requirement would be to cool the entire quantity of water to be frozen to -80° C before it would suddenly freeze into ice at 0° C. But this is not the case. After the water temperature has been lowered sufficiently below its freezing point (supercooled), small crystals of ice form and the heat of fusion is released into the surrounding water.

As an example, the surface layer of a body of water may be depressed to 0.8° C below its freezing point. This means that each gram of water has had 0.8 calories of heat removed. At 80 calories required to freeze

one gram, the removal of 0.8 calories from each gram of water will freeze .8/80=1/100 or .01 gram. This means that 1% of the surface layer would freeze. No additional heat is transferred into or from the body of water during this process. The energy balance per gram works like this:

1. Before freezing: (supercooled water at -0.8° C)
   1.00 gm water at -0.8° C = 0.8 calories removed from each gram of supercooled sample

2. After freezing: (water and ice mixture at 0° C)
   .01 gm ice at 0° C = 0.8 cal heat of fusion removed from each gram of sample
   \+ .99 gm water at 0°C = 0.0 cal removed from each gram of sample
   = 1.00 gm water & ice = 0.8 cal removed from each gram of sample

Thus, although heat of fusion has been expelled from the water freezing into small ice crystals, it has merely warmed up the surrounding water. No energy need enter or leave during the freezing process.

1.1.3 Frazil Ice Formation. The process of supercooling takes place continuously in freezing water. The small crystals thus formed grow into small disc-shaped platelets of ice with dimensions on the order of 1 or 2 mm in diameter and thickness in the vicinity of 1/10 the diameter. These platelets become the fundamental building blocks of newly forming sea ice. They are nearly pure freshwater ice; the dissolved salts having been excluded during the growth of the crystals into frazil platelets. Clearly, this increases the salt concentration in the remaining water.

1.1.4 Water Density. Here we must introduce the concept of the temperature of maximum density as a function of salinity. First, we will consider the density of fresh water as a function of temperature. Fresh water contracts upon cooling until it reaches 4° C; when cooled further it expands. As a result, when a lake is cooled, the cooled surface water at first sinks towards the bottom because the cool water is heavier than warm water. If water were like most liquids which continue to become heavier with decrease in temperature, a cooled lake would

continue to cool until the whole lake was at its freezing point, then it would begin to freeze. If water in its solid state were heavier than in its liquid state (again like most materials), then newly forming ice would accumulate at the bottom and the lake would freeze from the bottom to the top. Many northern lakes would freeze completely and never thaw except for a surface layer.

Fortunately, as explained above, water is most dense at 4° C and expands when cooled further. Furthermore, ice expands significantly when it freezes (on the order of 10%) so that its solid phase floats. The result of this is that after our hypothetical lake has reached 4° C, water cooled even further - being lighter than the 4° C water - does not sink but remains on the surface. Hence, the bulk of the lake remains at 4° C as ice formation takes place on its surface. After that, additional ice forms on the bottom of the ice surface.

Sea water is a different matter. As salts are added to water, both the temperature of maximum density (starting at 4° C) and the freezing point (starting at 0° C) are depressed. However, the temperature of maximum density decreases faster with salt concentration than does the freezing temperature. These two temperatures coincide at roughly 25‰ salt concentration. Water with greater salt concentration (such as sea water at 35‰) does not reach a maximum density before it freezes. (It does, of course, expand upon freezing.) As a result, the entire sea water column down to some depth requires cooling all the way to the freezing temperature before freezing takes place near the surface. The depth of this cooling depends on several factors including natural layering within the ocean, the surface cooling rate, and wind stress on the water surface. Naturally occurring density layering (as a result of temperature and salinity) tends to limit the depth of mixing. Very low temperatures can cause rapid cooling of the surface layer and its freezing before mixing at depth can occur. Wind stress, on the other hand, tends to increase the mixing depth.

1.1.5 Frazil Ice Depth. Because of the mixing of cooled sea water, it is possible that supercooling and frazil ice formation can take place within a mixed surface layer (at least a meter or two, and perhaps considerably deeper in some situations). Hence, at the very beginning of freezeup of sea water, small frazil discs form as a result

of supercooling within the top layer of the ocean. Frazil ice then becomes the basic building material for the ice forms which follow.

Another way in which the ocean becomes saturated with ice crystals is for snow to fall into an ocean cooled to below 0° C. Since the salt water is cooler than the melting point of the snow crystals, they accumulate as slush which forms a viscous floating mat.

1.2 STAGES OF ICE GROWTH BEYOND FRAZIL AND SLUSH

In this section we will follow sea ice terminology through the nomenclature of terms describing the various stages of growth from frazil crystals to thick first-year ice.

1.2.1 New Ice. This term includes all categories up through a thickness of 10 cm. New ice not only includes frazil and slush ice, but also several other ice types. For the sake of completeness, all ice types in this category will be described here.

1.2.1.1 Frazil Ice. Frazil ice represents the first stage in the freezing process. It consists of fine needles or platelets of ice, suspended in sea water.

1.2.1.2 Slush. Slush consists of snow which has saturated and mixed with the water creating a viscous floating mass of ice crystals within the water. Thus, slush represents an independent process by which ice crystals can be introduced into cold sea water.

1.2.1.3 Grease Ice. This is the next stage in ice formation beyond frazil ice. At this point, the frazil crystals have coagulated to form a soupy layer on the sea surface. Grease ice reflects less light than water and has a dark matte appearance. Grease ice forms regardless of sea state, but tends to increase in thickness with sea agitation.

1.2.1.4 Shuga. With a large degree of wind stress and accompanying wave agitation, grease ice or slush collects into spongy white lumps a few cm in diameter. This ice type is called shuga.

1.2.2 Nilas. As freezing continues, grease ice undergoes a transition to nilas, a thin (up to 10 cm) elastic crust with a matte surface. The only exception to this transition is in cases where the sea state and wind stress are sufficient to cause the formation of shuga (described in 1.2.1.4). When placed under a confining pressure, nilas is easily

thrust into a pattern of interlocking fingers called finger rafting. Nilas is divided into two subcategories:

1.2.2.1 Dark Nilas. Nilas which is under 5 cm in thickness and is very dark in appearance.

1.2.2.2 Light Nilas. Nilas which is between 5 and 10 cm in thickness and is lighter in appearance than dark nilas, but not quite gray.

1.2.3 Ice Rind. This ice develops in areas where water with less salinity than sea water is found. As a result, it forms a brittle, shiny crust either by direct freezing (as on a fresh water pond) or from grease ice. This stage continues for thicknesses up to 5 cm. Because it is brittle, it is easily broken up, usually into rectangular pieces, by wind and gentle waves.

1.2.4 Pancake Ice. (Pancake ice is not truly a thickness category, but it has been included here because it can be a major stage in the development of sea ice.) This ice consists of roughly circular pieces of ice from 30 cm to 3 m in diameter, and up to 10 cm in thickness. The pancakes have a raised rim as a result of their striking up against each other. They develop either on a slight swell from grease ice, shuga or slush or as a result of large swells breaking up previously formed nilas or even thicker forms.

1.2.5 Young Ice. This is ice in the transition stage between nilas and thicker forms. Its thickness ranges between 10 and 30 cm. It is subdivided into gray ice and gray-white ice.

1.2.5.1 Gray Ice. Young ice 10-15 cm thick. It is less flexible than nilas and often breaks under swell (becoming a candidate for pancake ice). It is still sufficiently thin that it will raft under pressure.

1.2.5.2 Gray-White Ice. Young ice 15-30 cm thick. Under pressure, it is more likely to ridge (i.e. break up and form a pile of broken ice) rather than raft.

1.2.6 First-Year Ice. As young ice grows in thickness beyond a thickness of 30 cm, it is call first-year ice. However, this category can be broken down into the following subcategories:

1.2.6.1 Thin First-Year or White Ice. This ice is sufficiently thick to appear white as opposed to the gray appearance of young ice. Its thickness ranges between 30 and 70 cm and is sometimes divided into a first stage (30-50 cm) and second stage (50-70 cm). Although there have been occasional reports of rafting of ice this thick, it usually ridges under pressure.

1.2.6.2 Medium First-Year Ice. This is first-year ice 70-120 cm in thickness.

1.2.6.3 Thick First-Year Ice. This is first-year ice with thickness greater than 120 cm.

1.2.7 Old Ice. This general term is used to describe ice more than one melt season old. Ice which has survived one melt season is called second-year ice, while ice which has survived more than one melt season is called multiyear ice. The reason that a distinction is made for ice surviving a melt season is because of ice strength. When ice forms, the overall salt concentration may be considerably less than sea water (on the order of 6‰) with most of this salt residing as very salty water trapped in the form of brine pockets. The water in these pockets has a very low freezing point due to its high salt content. Because of the pockets, the ice remains considerably weaker than fresh water ice. However, the strength does increase with decreasing temperatures. By 23° F (-5° C), its strength is roughly 75% that of fresh ice.

During the first melt season many of these brine pockets are drained by migration to the underside of the ice or flushed by melt water passing through the ice, leaving the ice considerably less saline. Figure I-1 shows the change of strength of ice with two salt concentrations as a function of temperature. From this figure, it can be seen that as temperatures decrease, old ice will increase in strength earlier than young ice. Furthermore, old ice is stronger than young ice at any given temperature. See section 3.3.1 of this chapter for further discussion.

1.3 ICE THICKNESS GROWTH RATE

Having discussed the range of ice types from frazil to first-year thick, it is worthwhile to consider the rate at which ice grows in thickness. Clearly, for ice to grow on the bottom surface of a floe,

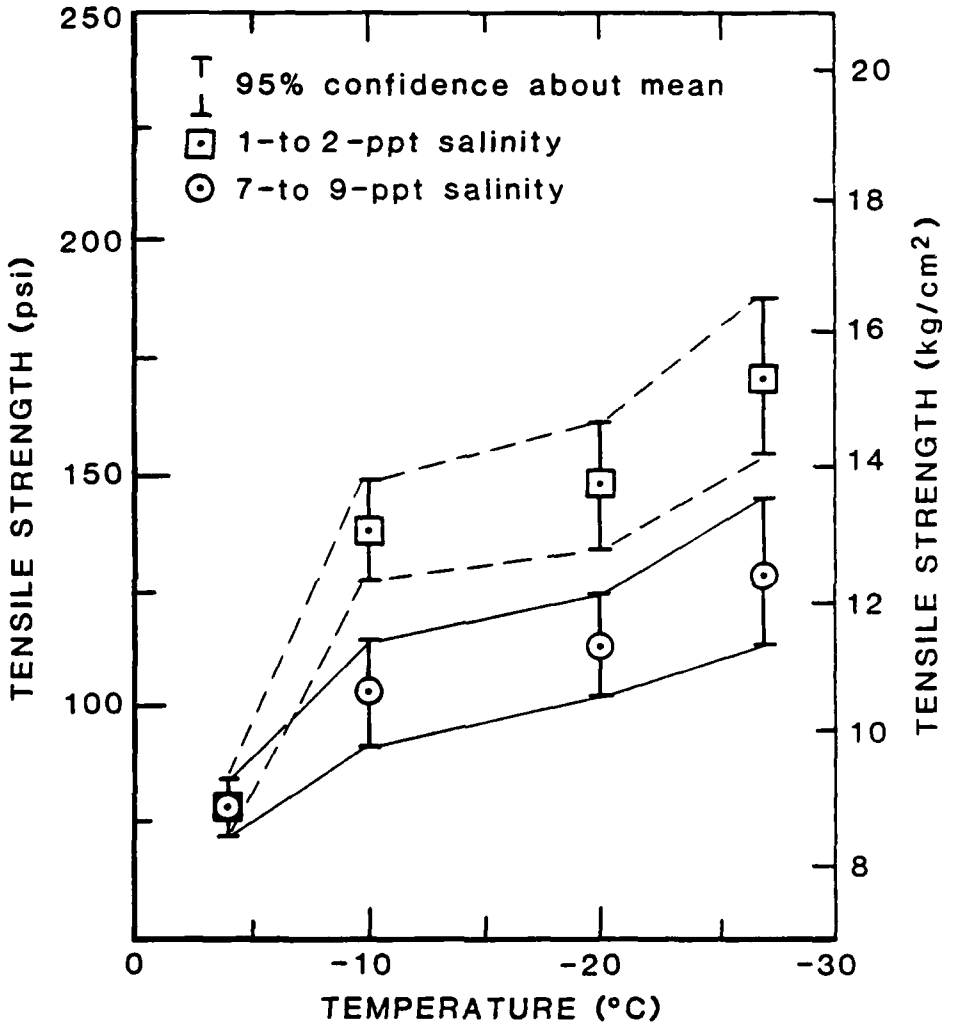

Figure I-1. Shown are results of Dykins (1971) comparing sea ice tensile strength as a function of temperature and salinity. Two salinity ranges were used: 1 to 2 parts per thousand (corresponding to multiyear ice) and 7 to 9 parts per thousand (corresponding to young ice). Envelopes about data points demonstrate data variability.

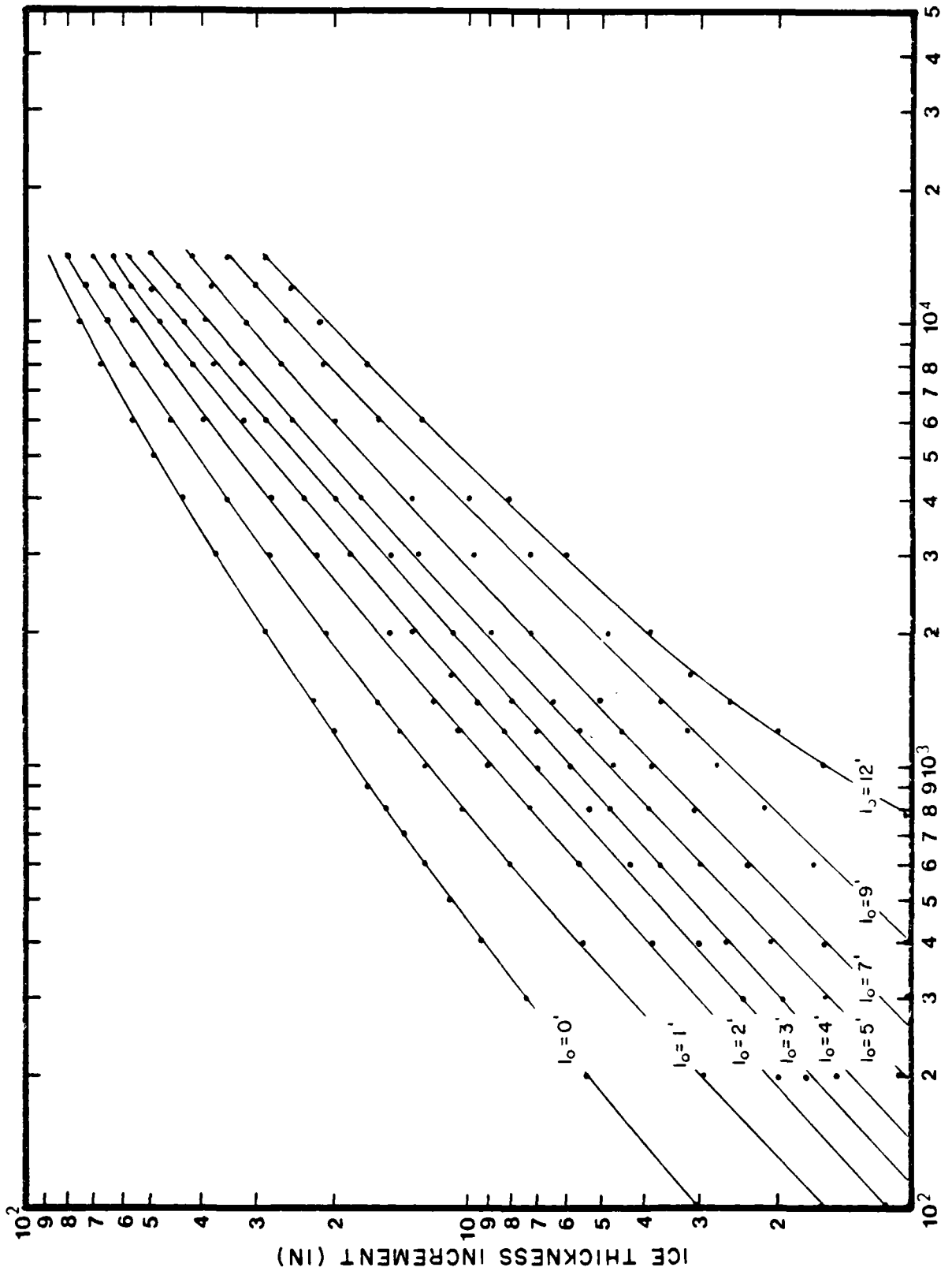

Figure I-2. Relationship between accumulated frost degree days and ice growth increment for various initial ice thicknessess. (From Zubov, 1943).

heat must be removed from its top surface. In general, therefore, the rate of ice growth is proportional to the rate at which heat can be transferred away from the ice and into the atmosphere. Heat transfer is proportional to the temperature difference between the top and bottom surfaces of the ice and the conductivity of the ice, and is inversely proportional to the thickness of the ice.

Thus, we expect ice to grow fastest when the air above it is coldest and when the ice is thin. Everything else being constant, we would expect the growth rate of ice to decrease with increasing ice thickness. In fact, one would expect the growth of ice to cease when equilibrium is reached between the rate at which heat is removed from the top of the ice and the rate at which heat is supplied to the underside of the ice from the water below. Finally, because snow acts as an insulating blanket, snow on the top of the ice limits the heat conduction through the ice and, therefore, its rate of growth and final thickness. The heat conductivity of snow is 1/10 that of ice. Hence, a 10 cm layer of snow on the ice surface would reduce heat transport as much as 1 m of additional ice.

The factors discussed above vary from place to place and with season. However, it is possible to standardize these environmental conditions somewhat by describing the ice growth in terms of accumulation of frost degree days. (The number of degrees below freezing for each day, summed over the number of days under consideration.) On-site measurements of the growth of ice related to frost degree days produced the curves shown in Figure I-2 (Zubov, 1943). Figure I-2 shows the incremental growth in ice thickness in terms of hundreds and thousands of frost degree days for a range of initial ice thicknesses (given in feet). For example, suppose that twenty days ago we had been able to obtain an ice thickness measurement (say 2 feet thick) at a particular location, but had not been able to obtain measurements since. However, we have had continuous temperature measurements and have determined that during the twenty days 900 frost degree days had been accumulated. The growth in ice thickness would be found by first following the curve for I_o = 2' until it intersects a vertical line drawn through the point on the horizontal axis denoting 900 frost degree days. Then, the growth is given by the location on the vertical axis corresponding to this intersection point, or about 8 inches. Hence, the total ice thickness would now be 32 inches.

SECTION 2. FORMS, TYPES, AND CONDITIONS OF ICE

In the previous section we discussed ice terms based largely on age and stage of development. However, there are other terms used to describe sea ice in reference to the size of individual pieces, its mobility, the arrangement of the ice, the nature of openings in the ice (in a macroscopic sense) and other factors.

2.1 ICE TYPES BASED ON MOBILITY CHARACTERISTICS

Regardless of age, oceanic ice can be divided into two broad categories based on its ability to move. These types are fast ice and drift ice.

2.1.1 Fast Ice is defined as sea ice which has formed along or has become attached to the shore, shoals, or to the seaward margins of glaciers. Although the ice is not moving horizontally with respect to shore, it may undergo vertical fluctuations resulting from changes in sea level. Fast ice can form in place or result from the attachment to shore and consolidation of individual floes of any age. It may extend a few meters or several hundred km from shore. Fast ice can be of any age and may be described in age terms (young, first-year, second-year or multiyear). If it has a freeboard greater than two meters, it is called an ice shelf. (Note: A freeboard of two meters implies a total thickness of around 20 meters.) The following terms are used to describe fast ice:

2.1.1.1 Young Coastal Ice. This term is used to depict early stages of fast ice. The ice has usually progressed to the nilas or young ice stage. However, it should be emphasized that ice this thin can easily be detached from shore and later stages of fast ice may not develop from a particular occurrence of young coastal ice.

2.1.1.2 Ice Foot. As fast ice grows in thickness, a narrow fringe of ice along the shore becomes frozen to and even into the bottom. This fringe is called the ice foot. There is usually a series of tidal cracks separating the ice foot from the floating fast ice which rises and falls with sea level changes. This crack region is often referred to as the hinge between the ice foot and the floating fast ice. If the floating fast ice is broken loose and transported away, the ice foot generally remains in place.

2.1.1.3 Grounded Ice. Grounded ice can occur within the floating fast ice or as individual pieces of ice grounded in shoal waters. For instance, grounded ridges and hummocks (see "Sea Ice Structures", 2.5) can occur within the floating fast ice. In such cases, they act to even further stabilize the fast ice. The remnants of hummocks and ridges can remain in nearshore areas well into the melt season. These are sometimes called stamuki. Islands of grounded ice can occur on shoals located beyond the fast ice. Stranded ice consists of ice which had been floating, but has been deposited on land exposed by retreating water.

2.1.1.4 Anchor Ice. Regardless of the nature of its origin, ice which is submerged or attached to the ocean bottom is called anchor ice.

2.1.2 Drift Ice generally replaces the historical term pack ice. It is a very broad category which includes any area of sea ice other than fast ice regardless of its form or arrangement. If freshwater ice is present it is called floating ice. The term pack ice may be used at concentrations of 7/10 and higher. We have already described many terms used to describe the development of drift ice. There are two other series of terms describing drift ice; one series is based on size and appearance of ice pieces and the other is based on percent ice cover.

2.1.2.1 Ice Terms Based on Size and Appearance of Individual Pieces of Drift Ice:

2.1.2.1.1 Pancake Ice. This ice consists of roughly circular pieces of ice from 30 cm to 3 m in diameter, and up to 10 cm in thickness. The pancakes have a raised rim as a result of their striking up against each other. They develop either on a slight swell from grease ice, shuga, or slush or as a result of large swells breaking up previously formed nilas or even thicker forms. Pancake ice is actually a form that new and young ice can assume over a range of thicknesses. On the other hand, it can be such a major stage in the development of ice cover that we have already listed it under development categories (see I-1.2.4). Below, several other forms of oceanic ice are defined which are largely independent of development stage.

2.1.2.1.2 Ice Breccia. This is an ice condition that results from several cycles of ice breaking into pieces and the freezing of the voids created between the pieces. The result is an expanse of ice pieces of different ages (and, therefore, most likely different thicknesses) frozen together.

2.1.2.1.3 Brash Ice. This term is used to describe accumulations of floating ice made up of fragments not more than 2 m (six feet) in largest dimension.

2.1.2.1.4 Ice Cake. This term is used for a piece of relatively flat ice not more than 20 m (60 feet) in its largest dimension. Small Ice Cakes are ice cakes less than 2 m in horizontal extent. Hence, brash ice is composed of small ice cakes.

2.1.2.1.5 Ice Floe. This term describes any piece of ice, regardless of age, more than 20 m in dimension. Floes are subdivided in terms of size:

small floe:	20-100 m
medium floe:	100-500 m
big floe:	500-2,000 m (.5-2 km)
vast floe:	2-10 km
giant floe:	greater than 10 km

2.1.2.2 Drift Ice Terms Based on Percent Cover:

2.1.2.2.1 Ice Cover is the ratio of an area of ice of any concentration to the total area of sea surface within some large geographic region; this may be global, hemispheric, or prescribed by a specific oceanographic entity such as Baffin Bay or the Barents Sea.

2.1.2.2.2 Concentration is the ratio expressed in tenths, describing the mean areal density of ice in a given area.

2.1.2.2.2.1 Compact Pack Ice. Pack ice in which the concentration is 10/10 and no water is visible.

2.1.2.2.2.2 Consolidated Pack Ice. Pack ice in which the concentration is 10/10 and the floes are frozen together.

2.1.2.2.2.3 Very Close Pack Ice. Pack ice in which the concentration is 9/10 to less than 10/10.

2.1.2.2.2.4 Close Pack Ice. Pack ice in which the concentration is 7/10 to 8/10 composed of floes mostly in contact.

2.1.2.2.2.5 Open Drift Ice. Drift ice in which the ice concentration is 4/10 to 6/10 with many leads and polynyas and the floes are generally not in contact with each other.

2.1.2.2.2.6 Very Open Drift Ice. Drift ice in which the concentration is 1/10 to 3/10 and water preponderates over ice.

2.1.2.2.2.7 Open Water. A large area of freely navigable water in which sea ice is present in concentrations less than 1/10 and no ice of land origin is present.

2.1.2.2.2.8 Bergy Water. An area of freely navigable water in which ice of land origin is present. There may be sea ice present but the total concentration shall not exceed 1/10.

2.1.2.2.2.9 Ice Free. No ice present. If ice of any kind is present, this term should not be used.

2.2 ICE TERMS BASED ON BREAKS OR OPENINGS IN THE ICE

Openings or breaks within the ice can be very important from the points of view of transportation or operations upon the ice cover and navigation through the ice. For this reason, a number of terms are used to describe in a specific way openings in terms of width, location, and navigability.

2.2.1 Fracture. This term, rather than lead (defined below) is the basic descriptor of openings or breaks within the ice. A fracture is defined as any break or rupture through fast ice, pack ice with concentration 9/10 or greater, or even a single floe. The length of a fracture can vary from less than one m to many km. In cases where fractures have a finite width, they may contain brash ice and/or be covered with nilas and/or young ice. In general, the two sides of a fracture appear as if they could be rejoined to form a solid sheet of ice. Fracture Zone describes an area with a great number of fractures. Often the fractures in a fracture zone have a regular pattern resulting from stress having been applied somewhat uniformly over a large area. Terms based on width of fracture are as follows:

crack: < 1 m (One specific type, tidal crack, is between the ice foot and the floating fast ice.)
very small fracture: 1-50 m

small fracture: 50-200 m
medium fracture: 200-500 m
large fracture: wider than 500 m

2.2.2 Polynya. A polynya is an irregularly shaped opening enclosed by ice. As opposed to a fracture, the sides of a polynya could not be refitted to form a uniform ice sheet. Polynyas may contain brash ice or uniform ice of markedly thinner ice than the surrounding ice. Terms based on a polynya's location or persistence are as follows:

2.2.2.1 Shore Polynya. A polynya located between drift ice and the coast or between the drift ice and an ice front (ice front defined in 2.6.2.3).

2.2.2.2 Flaw Polynya. A polynya located between drift ice and fast ice.

2.2.2.3 Recurring Polynya. A polynya which occurs at the same location every year.

2.2.3 Lead. A lead is a fracture through sea ice sufficiently wide to permit navigation by surface vessels. As with polynyas, some leads are defined in terms of their location:

2.2.3.1 Shore Lead. A lead located between drift ice and the shore or between drift ice and an ice front.

2.2.3.2 Flaw Lead. A lead located between drift ice and fast ice.

2.2.4 Flaw. Strictly speaking, the flaw is the line of fracture between the fast ice and drift ice when they are in close proximity. A variety of conditions can be found associated with such a flaw. It may consist of a series of polynyas along the fracture separated by linear regions where drift ice has been piled into a shear ridge (see later definition). Such a flaw is generally created when the drift ice is driven along the fast ice edge with a component of compressive force (thus creating a "shear") between the two ice masses. There may be regions of the flaw filled with brash ice and there may be signs of freezing of ice to the new or young stage within the polynyas if the shearing motion responsible for formation of the flaw has ceased.

2.3 TERMS DESCRIBING THE PHYSICAL ARRANGEMENT OF SEA ICE

Sea ice can be found in a variety of arrangements. A series of distinctive terms have been defined to aid the description of sea ice in narrative accounts and messages.

2.3.1 Terms to Describe the Size of an Aglomeration of Floating Ice.

2.3.1.1 Ice Patch. An area of floating ice less than 10 km in horizontal dimension.

2.3.1.2 Ice Field. An area of floating ice with dimensions greater than 10 km. Size distinctions are:

small ice field:	10 to 15 km
medium ice field:	15 to 20 km
large ice field:	greater than 20 km
ice massif:	a large ice field which is found in the same general location every summer.

2.3.2 Terms to Describe the Configuration of a Patch or Field.

2.3.2.1 Strip. A strip is defined as a long, narrow (1 km or less) patch or field of drift ice and often consists of brash ice and sometimes new ice forms. Strips are often generated as smaller ice fragments are detached from the main body of drift ice and run together under the influence of wind, waves, or swell.

2.3.2.2 Belt. A drift ice field which is considerably greater in length than width is called a belt. The width of a belt can vary between 1 and 100 km. Ice of any size or age may be contained.

2.3.3 Terms Used to Define Pronounced Features in the Boundary Between an Ice Field and the Surrounding Water.

2.3.3.1 Tongue. This term is used to describe a projection of an ice field into the adjacent ocean area with a markedly lower ice concentration. Tongues are often caused by winds or currents and are sometimes transformed into a swirl-like structure.

2.3.3.2 Bight. An indentation in an ice edge. As with tongues, their topological opposites, bights are often caused by winds and currents.

2.3.4 Terms Involving the Extent of Ice.

2.3.4.1 Ice Edge. This term is used to denote the boundary between ice of any concentration or type and the open sea. It can be described as compact or diffuse depending on how well defined it appears.

2.3.4.2 Ice Limit. This term is based on a statistical computation of the extreme minimum or extreme maximum location of the ice edge for a given period (for instance, the month of March) over a period of several years. The term "ice limit" is preceeded by either minimum or maximum.

2.3.4.3 Mean Ice Edge. As with ice limit, the mean ice edge is a statistical term. The mean ice edge is simply the average position of the ice edge as measured over some specified period of time.

2.3.4.4 Mean Maximum or Mean Minimum Ice Edge. This term is used to denote the geographical location of the average of the extreme summertime or wintertime locations of the ice edge over a period of years. These two statistical locations are often indicated on atlases.

2.3.5 Terms Describing Boundaries Within The Ice.

2.3.5.1 Fast Ice Boundary. This term is used to denote the boundary at any time between the fast ice and drift ice. (If no drift ice were present, it would be called the fast ice edge.)

2.3.5.2 Concentration Boundary. A line approximating the transition between two regions having different drift ice concentrations.

2.4 TERMS DESCRIBING THE APPEARANCE OF THE ICE SURFACE

2.4.1 Snow-Related Factors.

2.4.1.1 Bare Ice. Ice without snow cover.

2.4.1.2 Snow-Covered Ice. Ice with snow cover. Snow-covered ice is usually more white in appearance than bare ice during winter months, regardless of thickness. As a result, a snow cover on ice makes estimating its thickness very difficult.

2.4.2 Melt Season Factors. As the summer season approaches, the occurrence of water on the ice surface causes a sequence of events resulting in a changing appearance of the ice.

2.4.2.1 Puddled Ice. At the beginning of the summer season melt water from snow and ice accumulates on the ice surface, presenting a pattern of dark patches. Ice at this stage is referred to as puddled ice.

2.4.2.2 Flooded Ice. This term is used to refer to ice that is largely covered with water, either from extensive melt water or river water spread upon the ice.

2.4.2.3 Dried Ice. Eventually the flooded ice drains through cracks and thaw holes developed in the ice. The drained ice whitens considerably. Large portions of floes remain wet and many areas of open water now occur. The white portions of the ice are called dried ice.

2.4.2.4 Rotten Ice. The term rotten ice refers to ice during an advanced stage of melting. Very little ice still maintains sufficient freeboard to appear white. Most of the ice surface is wet and the ice is honeycombed.

2.5 TERMS RELATED TO SEA ICE STRUCTURES

The terms in this category generally derive from compressional forces within sea ice which results in ice raised above the normal ice surface. Although sizes of these features can vary, the presentation here will be generally in order of increasing size.

2.5.1 Standing Floe. A single floe standing vertically or inclined to the ice surface and surrounded by relatively smooth ice.

2.5.2 Rafted Ice. Ice which has been forced to override other ice as a result of compression. Although rafting is most common among thinner forms of ice, there have been reports of rafted ice 2 m thick overlapping by over 100 m in the horizontal.

2.5.3 Hummock. A hillock of broken ice which has been forced upward by pressure.

2.5.4 Hummock Field. A collection of hummocks. A hummock field which has survived one or more melt seasons is called a second-year or multiyear hummock field. Such older hummock fields can form large, thick and relatively strong floes.

2.5.5 Ridge. A line or wall of ice forced up by pressure. A ridge can vary in length from a few hundred meters to over a hundred

kilometers. Many observers make a distinction between a pressure ridge which appears as a relatively short, somewhat irregular pile of ice and a shear ridge which appears as a sinuous mound of piled ice stretching relatively long distances across the ice. Shear ridges are created as a result of differential motion between two regional ice bodies (often the drift ice against fast ice). Very often a shear ridge consists of many parallel bands of piled ice, some with vertical walls 2 to 3 m in height. Pressure ridges are more local in nature and result from purely compressional forces within the ice. Ridges may be divided by age in the following way:

2.5.5.1 New Ridge. The ice blocks are simply piled together. Sharp blocks are piled at roughly a 40° angle of repose.

2.5.5.2 Consolidated Ridge. A ridge which has been exposed to sufficient cooling that its base has frozen together.

2.5.5.3 Aged Ridge (also known as second-year or multiyear ridge). A ridge which undergoes a melt season has brine drained from much of its ice. Furthermore, fresh melt water from the ridge sail (the exposed upper portion) tends to freeze together the ice blocks composing the keel of the ridge. This process continues with each melt season with the result that the ridge becomes stronger, both as a result of the filling of voids and the rejection of salt. During this process the surface appearance of the ridge becomes less angular and more gently-sloped.

2.5.6 Floeberg. This is a massive piece of ice, either a hummock field or a portion of a massive ridge system which has become frozen together. Floebergs with freeboards of 5 m have been observed.

2.6 TERMS RELATED TO GLACIAL ICE STRUCTURES AND FEATURES

2.6.1 Sources:

2.6.1.1 Glaciers are created by the accumulation of snow. There are a number of glacial forms. However, in all cases the accumulated snow is metamorphosed into ice through a process of compression, thawing and refreezing, and water vapor transport. The glacial ice then slowly advances downslope. In the case where a glacier enters the sea, it may be pushed sufficiently seaward that it is afloat.

2.6.1.2 Ice Shelves are defined as a floating ice sheet of considerable thickness with a freeboard greater than 2 m. Ice shelves are distinguished from floating glaciers in that ice shelves are usually of great horizontal extent. An ice shelf can be created as a result of a number of processes or even the combination of several processes including: annual snow accumulation on the ice surface, growth of ice on the undersurface, and the seaward extension of glaciers from the surrounding land. The surface of an ice shelf is usually flat or gently undulating.

2.6.2 Nomenclature of Glaciers and Ice Shelves:

2.6.2.1 Glacier Tongue. This term is used to depict the seaward projection of a glacier. In some cases, portions of glacier tongues can be afloat. In Antarctica, glacier tongues may have dimensions on the order of tens of km in length.

2.6.2.2 Ice Wall. This term depicts the seaward margin of a glacier extending into the sea but which is not afloat. Thus, an ice wall extends to the sea floor.

2.6.2.3 Ice Front. This term depicts the seaward margin of either a floating glacier or an ice shelf.

2.6.3 Nomenclature of Ice Calved from Glaciers and Ice Shelves. The breaking away of a floating ice mass from an ice wall, an ice front, or another floating ice mass is called calving. In the following paragraphs the various designations for calved ice will be defined.

2.6.3.1 Icebergs. A massive piece of ice calved from an ice wall or ice front. Icebergs are usually irregular in shape and may be described as tabular, dome-shaped, sloping, pinnacled or weathered.

2.6.3.2 Tabular Berg and Ice Island. These terms have essentially identical definitions. Their distinction is that of location. Ice islands are found in the arctic ice pack while tabular bergs are found in the ice and open ocean surrounding Antarctica. Both features are flat-topped icebergs and can range in size from a few thousand square meters to over 100 square kilometers. They are usually characterized by a regularly undulating surface which gives them a ribbed appearance when viewed from above. Ice islands are calved from arctic ice shelves, while tabular bergs are usually calved from antarctic ice shelves and

sometimes antarctic glaciers. Ice islands have a maximum freeboard on the order of 3-5 m while tabular icebergs can have significantly greater freeboards.

2.6.3.3 Bergy Bit. This term is used to signify a large piece of calved ice with a freeboard between 1 and 5 m and with an area between 100 and 300 square m.

2.6.3.4 Growler. This term designates a piece of calved ice smaller in size than a bergy bit (less than 1 m freeboard and less than 100 m^2 in extent).

SECTION 3. PHYSICAL CHARACTERISTICS OF SEA ICE

3.1 ALBEDO

One of the most obvious physical characteristics of sea ice is the relative amount of visible light reflected from its surface. As the descriptions of ice types have shown, this factor - known as albedo - is an important quality when determining the early stages of ice growth. Here we will briefly summarize the relationship between albedo and ice thickness.

Albedo	Thickness	Type Designation
very low, ice areas appear dark against water surface	ice crystals contained within the water column up to 5 cm in thickness	New ice forms up to dark nilas stage
low, ice appears dark gray	between 5-10 cm in thickness	light nilas
moderately low, ice appears gray	between 10-15 cm in thickness	gray ice stage of young ice
moderate, ice appears light gray	between 15-30 cm in thickness	gray-white ice stage of young ice
moderately high, ice appears very light gray when compared against snow-covered ice	greater than 30 cm in thickness	first-year ice

To this point we have only dealt with the albedo of ice in the visible spectrum. In later sections, we will deal with the reflectance of ice in terms of other wavelengths.

3.2 SALINITY

The salinity of sea ice is an important characteristic. It plays a large role in determining the strength of ice and to some extent, reflects the age of a particular piece of ice.

Although sea water has a salinity in the vicinity of 35 ‰, ice grown from sea water seldom has a salinity greater than 1/3 or 1/4 this

value. In fact, frazil ice crystals are nearly pure water. However, when a mass of frazil crystals congeal to form nilas, they entrap pockets of sea water between them, some of which may have an elevated salt content caused by the expulsion of salts during the freezing of the frazil crystals. Measurements have shown that the top few centimeters of ice usually contain 8 to 10‰ because of this process. In general, the depth of this layer depends on the thickness of the frazil ice layer at the time of formation of nilas. This, in turn, is usually related to winds and sea state. (The deeper the surface supercooling layer, the more frazil ice formed. The greater the sea agitation, the longer frazil crystals accumulate before congealing.)

After the formation of the first crust of ice on the sea surface, the freezing process changes. In order to grow new ice on the undersurface of the nilas, heat must be conducted through the ice layer to the atmosphere. This will generally be an orderly process and will not result in a soup of frazil crystals in the water below the ice. The growth of crystals becomes much more orderly. The crystals are oriented so that the plates which form extend downward with their flat sides having a strong tendency to arrange themselves in a parallel fashion. The result of this growth pattern is to create the appearance of many vertical columns of ice grown together. This zone is called the columnar region. As a result of this more orderly growth pattern, less dissolved salt is entrapped and an average salinity of around 6‰ results after the crystals have grown in size sufficiently to fill most of the voids.

However, at any given time there will be a layer of incomplete crystal growth at the bottom of a growing ice cover. At its very bottom, this layer has the appearance of an open lattice. Since this lattice forms the skeleton around which ice crystals will grow, it is called the skeletal layer. Because this layer contains pockets of salt water which are not yet excluded, its salinity is somewhat higher (around 10‰) than it will be after it becomes part of the columnar zone. Hence, at any given time, one would expect to find a c-shaped profile of salinity with depth through a growing ice cover, with salinities around 10‰ at the top and bottom of the "c" and salinities around 6‰ in the middle of the "c".

3.2.1 Variations in Salinity. It should be pointed out that the description just presented is quite general in nature. For instance, the salinity in the center of the profile just discussed can easily vary by $\pm 2‰$ as the result of a number of factors, but largely related to the rate of crystal growth at the time of freezing and warming cycles during the winter. Furthermore, measurements have shown that the salinity at a given ice depth can vary by $\pm 0.6‰$ on the average over distances of a meter or two. Finally, not all water which becomes sea ice has a salinity as high as $35‰$, and the ice which is subsequently formed from this water will have a correspondingly lower salinity.

3.2.2 Salinity vs. Age of Ice. It is well known that old ice (i.e. ice older than one melt season) has a greatly reduced salt content compared to first-year ice. The precise process by which this "freshening" of the ice takes place is a matter of current debate and may be actually the result of a number of processes. The end result, however, is a floe with nearly no salinity above sea level and a gradual increase to a salinity of around 3.0 to $3.5‰$ with increasing depth below sea level. The overall average salinity for such a floe has a limiting value somewhere in the vicinity of $2‰$.

3.3 STRENGTH OF SEA ICE

Obviously the strength of sea ice plays a major role with regard to navigation in icy waters. This characteristic is also an important factor to be considered in predicting sea ice behavior. The strength depends a great deal on the particular stress applied. The resistance to compressive stresses (the compressive strength) is much greater than the resistance to tensile stresses (the tensile strength). As a result, for any given thickness the ice is much more easily pulled apart than piled together.

3.3.1 Salinity and Temperature. The strength of sea ice is known to depend on its temperature and salt content. However, the measurement of ice strength is a difficult process, and the exact form of the relationship between ice strength and these factors has not been determined. In general, sea ice is weaker than fresh water ice and its strength increases as the salt content decreases. Furthermore, the strength of sea ice increases as its temperature decreases.

The theoretical concept describing the strength of sea ice is based on the observation that as ice is formed from sea water, the dissolved salts are excluded from the ice crystals during the freezing process. However, some of the salts are trapped in brine pockets (giving first-year ice an overall salt content of around 5‰). Because of the salt content of these brine pockets, their freezing point is lowered and, therefore, they remain unfrozen. These unfrozen pockets yield an ice which is weaker than ice without pockets such as freshwater ice.

Theoretical models of ice strength vs temperature (Assur, 1958) have been based on the physics of processes within the brine pockets as the ice becomes colder. In general, as the brine within the pockets becomes colder, water is frozen out, creating smaller brine pockets and, thereby, increasing the strength of the ice.

In addition, from chemical principles it is known that when temperatures are sufficiently low, the dissolved salts precipitate out in the form of solid hydrates. It has been proposed that these solid hydrates add to the overall strength of the ice.

The first salt hydrate to precipitate should be that of sodium sulfate, $Na_2SO_4 10H_2O$ (the sulfate ion is the second most abundant dissolved salt ion in sea water at a concentration of 2.6‰, compared to a concentration of 19‰ for the chloride ion). Starting at -8.2° C the strength of ice should be increased by the presence of this precipitate. However, it is not clear how rapidly the strength increases.

The next salt hydrate to precipitate should be the hydrate of sodium chloride, $NaCl\ 2H_2O$. Theoretically, the precipitate of this hydrate should increase ice strength rather abruptly starting at -22.9° C.

Because ice strength is difficult to measure, and because of variations from sample to sample, there is a wide variation in measured strengths for each temperature. As a result, the data do not resemble lines, but rather envelopes. From the shape of the envelopes, it can be seen that ice strength increases with colder temperatures, but it is not possible to tell whether the formation of solid precipitates are responsible or whether the increase in strength is a result of the general decrease in the size of the brine pockets.

Figure I-1 shows data relating the tensile strength of ice and temperature for ice of two salinities. The strength can be seen to increase as temperatures are lowered and to increase more rapidly for ice with low salinities. The lower salinity used here (1-2‰) corresponds to multiyear ice while the upper salinity (7-9‰) corresponds to newly formed young ice. First-year ice has a salinity content between these two ranges. The ice samples used in these measurements were taken so that this strength measurement applies to the vertical direction within the ice.

It should be borne in mind that only the top surface of an ice layer will be at air temperature (or even higher if there is a snow cover) and that the temperature will increase down through the ice reaching the temperature of the water underneath (somewhere around -1.9° C) at the bottom surface. Furthermore, since snow has a heat conductivity only 1/10 that of ice, the temperature at the ice surface beneath the snow can be considerably greater than the air temperature, and the entire ice layer will be correspondingly warmer and, therefore, weaker.

3.3.2 Age. Since salinity decreases with age, it is reasonable to anticipate that strength increases with age. Figure I-1 shows that old ice can be between 10 and 40% stronger than first-year ice (depending on temperature and whether one is comparing strengths above or below sea level). However, this comparison is valid only for an ice floe. In the case of a pressure ridge or floeberg the increase of strength with age can be much more pronounced. This results from the filling of voids both above and below sea level with fresh water ice during the melting and refreezing process. By this means, the relatively weak bonding between ice blocks in these features is greatly increased with age.

3.3.3 Loading Rate. Ice is a plastic substance and will deform under stress. As it deforms, the force required to break it becomes greater. If stress is applied slowly, its breaking strength becomes greater and it becomes able to withstand a larger stress before failing than if the stress were applied suddenly.

3.3.4 Strength vs. Size of Sample. The strength of sea ice depends a great deal on the size of the sample being measured (or the scale of the measurement). A great deal of work has been done in laboratories where relatively small samples (on the order of 10-100 cm in dimension)

can be placed under stress in relatively controlled conditions. The failure strength is the pressure (force per unit area) at which the ice sample "fails" and ceases to offer resistance to applied stress. The greatest ice strengths are measured at this laboratory scale. This is largely because the samples tested have the greatest chance of being homogenous with few internal flaws along which failure can take place.

The next sample size is what might be called the field test scale. This size is determined by the amount of stress which can be applied to an ice test sample in the field under conditions which allow accurate measurement of the stress. This sample size varies over the range of 1 to 10 m in dimension. Some control over sample composition and thickness is possible, but other factors such as temperature cannot be controlled. Although such tests are more realistic, it is often difficult to acquire data over the entire range of desired parameters. The measurements of ice strength at field test scale tend to be lower than laboratory scale strength measurements because the samples generally contain more flaws and are less homogenous than laboratory specimens.

A third sample size which produces crude but useful strength values for operational uses is on the order of 100 to 300 m. This sample size category might be called an operational scale. At this scale, floes are instrumented with stress transducers in anticipation of the floe either encountering a natural obstruction or the ramming of the floe by an ice-strengthened ship. These are very realistic measurements when considered full-scale tests (that is, the strength of a floe when encountering a man-made obstruction), but there are many difficulties involved.

The fourth sample size category is what would be called a regional scale. This is the scale generally of most interest to ice analysts. At this scale, the strength of an area of ice with dimensions on the order of 10 to 50 km is important. Typically, a region of ice not only contains floes of various thicknesses, but leads and polynyas. Often large lead systems will be found frozen to stages of thickness less than the first-year category (i.e. less than 30 cm). Obviously, as the ice is compressed, leads and polynyas will be closed rather easily. Following this, thinly frozen leads will be closed with the consequent ridging of the ice in the lead. Next, leads with thicker ice and thin floes will be piled in large ridges or hummock fields. Thus, a compressive force

on the ice will encounter an increasing ice strength as the pack is compressed. This is a rather complicated strength relationship which requires measurements on a regional scale. The stress (force per unit area) on the ice is obtained by measurement of winds on the top surface and oceanic currents beneath. A new quantity, the strength modulus is found by measuring the strain (amount of compaction) from satellite imagery and baseline measurements and dividing the stress by the strain. True failure does not take place. (The entire ice pack does not suddenly shatter and pile up.) Instead, the stress required to produce further compaction increases as the compaction (strain) increases.

Numerically, the relationship can be expressed as follows:

$$\text{stress} = K \cdot \text{strain}$$

K is a property of the ice pack. For purely compressive forces, this equation implies the following relationship: the stress (force per unit area) equals the strength modulus, K, (also in units of force per unit area) times the strain (the compaction expressed as a fraction). Thus, if applying a stress of 1,000 pounds per square inch in an ice pack produces a compaction of 1 km in 100 km, we have:

$$1000 \text{ psi} = K \cdot \frac{1 \text{ km}}{100 \text{ km}} = K \cdot \frac{1}{100}$$

or

$$K = 1000 \text{ psi} \cdot 100 = 100{,}000 \text{ psi}$$

To apply this relationship, we see that for any given strain, a strength is implied. For instance, if the ice pack is compressed 5 km in 100 km, we have a strain of 1/20 and:

$$\begin{aligned}\text{strength (stress within the ice)} &= K \cdot 1/20 \\ &= 100{,}000 \cdot 1/20 \\ &= 5{,}000 \text{ psi}\end{aligned}$$

So that in this example, an ice pack compressed to 19/20 its original dimension has a strength of 5,000 pounds per square inch. A stress greater than this value would be required to produce further compression.

In practice, if one assumes the thickness of the ice pack to be its average thickness, the regional strength it acquires through compression never comes close to the failure strength of a laboratory sample. However, in those areas of the pack where stress is concentrated and ice

is crushed and piled up, the stress applied is clearly greater than the ice failure strength.

3.3.5 Crystal Orientation. Another interesting property of sea ice is the orientation of the individual crystals of ice. As explained earlier, ice crystals form in flat platelets. These platelets result from a preferential growth pattern in the structure of the crystal. In order to provide a coordinate system for reference purposes, the direction perpendicular to the flat sides of the crystal is called the c-axis of the crystal. Thus, we can say that the crystal tends to grow in directions perpendicular to the c-axis.

When frazil crystals collect to form dark nilas, the c-axes are mostly in the horizontal plane (the crystals stand vertically) but they are oriented randomly in that plane (looking down, the platelets have random alignment). However, several observations of the columnar ice forming below the initial layer indicate that often after a transition zone, the c-axes are aligned, meaning that the surfaces of ice crystal platelets are growing parallel to each other. It is generally thought that this results from a preferential growth of ice crystals in the direction of the motion of the water which supplied material for crystal growth. In this way, the c-axis orientation within a floe would become a record of the floe's orientatiton relative to the currents beneath the ice.

CHAPTER II. SEA ICE DYNAMICS

SECTION 1. GEOSTROPHIC WIND FIELDS

This section describes what is meant by the term geostrophic wind, which is the horizontal wind velocity for which the coriolis acceleration exactly balances the horizontal pressure force. This term reflects what is probably the most fundamental concept in meteorology. Although we will not be able to develop our understanding along lines of mathematical physics, we will be able to compile a working knowledge of this term in a way which is useful to the ice observer and short-term forecaster.

1.1 ATMOSPHERIC PRESSURE

The basic tool in determining the distribution of wind velocities over a region of the earth is the barometric pressure chart. This chart is a contour map of atmospheric pressure at some prescribed altitude. The terminology used requires some explanation.

The millibar is the basic unit of atmospheric pressure measurement. By definition, this is 1/1000th of a bar which is the pressure generated by a force of 100,000 newtons acting on an area of one square meter. Long-term measurements have shown that the average sea level atmospheric pressure is 1,013.25 millibars (abbreviated mb). In terms perhaps more familiar, this is 14.7 pounds per square inch. The atmospheric pressure record used most often in sea ice analysis is called the Synoptic Mean Sea Level Pressure Analysis. These charts display contours of atmospheric pressure corrected to mean sea level. Other charts sometimes used give altitude contours for the height of a particular atmospheric pressure above mean sea level (for instance, the 750 mb chart). At 500 mb, half the atmosphere is below and half above the point of observation. This turns out to be a height of around 5 km or 3 miles. Obviously, the atmospheric density does not vary linearly with altitude, as a pressure of 1 mb is not reached until heights on the order of 30 km are attained.

Atmospheric pressure is measured by instruments called barometers. It is quite easy to make very sensitive barometers. An altimeter is little more than a sensitive barometer, which to be accurate, must be

calibrated against the sea level pressure directly beneath its location. In order to measure pressures at various altitudes, balloons are released which climb at a known rate and radio back pressures measured by a "throw-away" barometer.

1.2 MOVEMENT OF AIR RESULTING FROM ATMOSPHERIC PRESSURE SYSTEMS

The variations in atmospheric pressure are complex and arise from a number of factors. The sun is, of course, the primary source of energy to the earth's atmosphere. This energy is absorbed in some places, like oceans, and reflected in other places, such as areas covered with snow and ice or clouds. A great deal of this energy finds its way into the atmosphere, both in the form of direct heating and the added heat of evaporated water. As a result of the complexity of this process, regions of relatively high and relatively low atmospheric pressure are created. Much of what we commonly call "weather" is created as these pressure systems attempt to even out and come to equilibrium. As we shall see, this process would be much simpler if the earth were not turning one revolution per day on its axis. Were the earth not rotating, areas of high and low pressure would come to equilibrium by simply exchanging sufficient air to possess equal pressures. The rate of exchange of air or wind speed would depend on the spatial rate of change of pressure, or pressure gradient. Hence, the greater the pressure change in mb per unit distance, the greater the wind. Furthermore, the wind would be along the direction of greatest change in pressure (i.e. perpendicular to the contours of equal pressure or isobars).

If the earth were not rotating, the acceleration experienced by the air particles would be given by:

$$a_p = -\frac{1}{\rho}\frac{\Delta p}{\Delta x}$$

where: ρ is the atmospheric density

$\Delta p/\Delta x$ is the change in pressure over a given distance divided by that distance (this is the pressure gradient). The negative sign arises because the air is accelerated from high pressure to low pressure, in the opposite direction to the positive pressure gradient.

The formula reflecting the affect of the earth's rotation on wind speed is given in II-1.2.2.

1.2.1 Coriolis Force. When we fire a bullet, we expect that in the absence of winds or other external forces, it will travel in a straight line (although it will change its elevation as it travels along this straight line). But where is this straight line actually drawn? About three centuries ago, Isaac Newton came to the conclusion that in fact the straight line is drawn with respect to the distant stars and not the surface of the earth, which is actually turning on its axis. Sometime later, a man named Coriolis determined the exact value of this small discrepancy.

In order to understand this concept, imagine standing exactly at the north pole on a day in early spring when the sun is just above the horizon (where it will stay all day as the earth rotates). Imagine that you have placed a target 300 m away and just as the sun (a reasonably distant star) passes behind the target, you fire a bullet with a muzzle velocity of 300 m/sec at the target.

In reality, the bullet is traveling toward the sun and the target just happens to be between you and the sun when the bullet was fired. It will be 24 hours until the target is between you and sun again. Meanwhile, the target is moving eastward (counterclockwise) at a rate of 2.2 cm per second. (The target travels 2π x 300 m in 24 hours or 1,884 m. This divided by [24 hours x 60 min/hour x 60 sec/min] or 86,400 equals .022 m/sec or 2.2 cm/sec.) Therefore, to actually hit the center of the target, the bullet should have been aimed 2.2 cm to the east of the target's center when it was fired.

Coriolis realized that most of us here on the earth think of our reference frame as the earth and not the fixed stars. Not being aware of the fixed star reference frame, most of us would fire the bullet straight at the target. We now know that it would land 2.2 cm to the west of the target's center, as if a mysterious force actually acted on the bullet to accelerate it off target. All moving things on the earth's surface are subject to coriolis acceleration. However, usually the deflection is not noticeable.

Coriolis worked out the equation to describe this acceleration in the horizontal plane. It is given by:

$$a_c = + 2w\ v \sin \phi$$

where: w is the rotational velocity of the earth in radians per sec.
v is the velocity of the object
ϕ is the latitude of the object

The reason for the dependence on latitude may be a little puzzling at first, but a little thought will explain why. Consider the above target practice being carried out at the equator instead of the north pole. If the bullet were fired at a target due north or south, it would travel parallel to the earth's axis (which is fixed with respect to the stars) and would not be deflected. Similarly, if the target were due east or west, the bullet would be deflected up or down but not north or south. There would be no deflection in the horizontal plane.

1.2.2 Geostrophic Winds. What really happens to the particles of air in our atmosphere is the result of the interaction of the pressure gradient acceleration and the coriolis acceleration. A complete explanation of how these factors combine is beyond the scope of this handbook. In fact, even an accurate explanation is beyond the scope of many meteorological texts. However, the result is a steady wind along the pressure isobars given by:

$$v_g = \frac{1}{2w \sin \phi} \cdot \frac{1}{\rho} \frac{\Delta p}{\Delta x}$$

Here we recognize the first term as related to the coriolis acceleration and the second as the pressure gradient acceleration.

As a result, instead of atmospheric high and low pressure cells creating winds directly across the isobars, the winds created are along the isobars. The direction along the isobars is easy to understand. Imagine looking down on a high pressure cell in the northern hemisphere. Because of the high pressure, the air wants to expand in all directions. Consider air particles attempting to move southward in terms of the example of the southward-fired bullet. Coriolis acceleration will direct the air to the west. Similarly, air particles attempting to move eastward will be deflected toward the south. The result of this deflection will be a clockwise motion about the center of the high pressure cell. Similarly, coriolis acceleration will produce counterclockwise motion

about a low pressure cell. A little thought will show that these motions are reversed in the southern hemisphere.

The geostophic wind related above describes to a first approximation the motion of air in our atmosphere. However, it does not take into account a number of factors such as the motion of pressure cells and increasing or decreasing pressure. Also, surface effects can completely distort geostrophic winds so that the geostrophic wind concept can only safely be applied to altitudes somewhat higher than the geographic relief in an area.

1.2.3 Modification of Geostrophic Winds by Surface Effects. The winds of most interest to sea ice forecasters are those at the surface of the ice. Hence, the "surface" chart is used. However, at this level, the motion of the air is not purely geostrophic: (1) Even for a smooth surface there will be frictional effects. (2) Mountains and hills can considerably alter surface winds. (3) Cold air generated on large glacial ice masses can create violent local winds. We shall consider these in turn.

Before discussing these modifications to surface winds due to local causes, it is useful to consider the manner in which pressure charts are created. Barometric pressure is only measured at a relatively few locations, particularly in the arctic and antarctic. Yet, detailed pressure charts are drawn based on these data. This is much like constructing a geographic contour map based on a handful of altitude measurements. The result is an overall pattern which is generally correct, but the precise configuration of the isobars cannot be obtained. Therefore, the geostophic winds, which are determined by the density of isobars ($\frac{\Delta p}{\Delta x}$ is simply the number of isobars per unit distance), are also only generally correct. There is simply no way to account for local effects except through observation and experience.

1.2.3.1 Frictional Effects. The standard height for surface wind measurements is 10 m. This is usually sufficiently high to eliminate purely site-specific effects. Yet, even above smooth ice, the winds at 30 m are not geostrophic - that is, along the isobars. In fact, a height of around 500 m is required to reach geostrophic winds. Below that altitude there is sufficient friction to appreciably slow the wind.

This slowing alters the balance between the pressure gradient acceleration which remains largely constant, and the coriolis acceleration. (Remember, coriolis acceleration is directly proportional to v.) As a result, as the surface is approached, the winds are deflected less by coriolis acceleration and have a component along the pressure gradient. The amount of this effect is around 15° over open water and around 20-25° over ice.

1.2.3.2 Mountains and Hills represent barriers to air motion and can alter completely the direction of winds in their vicinity. In some of these locations, the local winds show a strong tendency to be along a particular direction regardless of the geostrophic pattern. Local wind patterns such as these can considerably alter sea ice motion for relatively large distances (20-50 km) from the mountain barriers. These effects are only known through site-specific experience. These alterations are known as orographic effects.

1.2.3.3 Offshore Winds are also caused by katabatic winds. These are winds created in sloping mountain valleys as the air is cooled in the evening and, being heavy, "slides" downslope. This effect can be particularly strong from glaciers and sloping glacial ice fields. Antarctica is particularly well known for katabatic winds. When these winds reach the water, they can move ice floes considerably seaward, creating an appreciable flaw. The effect of katabatic winds is limited to distances less than 40 km from coasts.

SECTION 2. OCEANIC CURRENTS AND TIDES

In addition to winds, the motion of the ocean has a major influence on the motion of ice. There are several sources of oceanic currents causing them to be quite complex at times. The motion of water due to tides can also be complex, particularly in shallow and long embayments. This short section cannot possibly attempt a complete treatment of this subject. However, some topics of interest to the ice analyst can be outlined.

2.1. OCEANIC CURRENT SYSTEMS

Several centuries of observations have yielded considerable knowledge of the major current systems in the earth's oceans. Yet, as late as 1961 a major and important current in the equatorial Pacific Ocean was discovered. Although published charts of oceanic currents appear to imply steady and constant currents, this is not really the case. These charts represent averages and generalizations. The two accompanying charts show the known current systems in the arctic and antarctic. Where data are available, the magnitude of these currents is given in knots as well as the direction of the current (Figures II-1, and II-2).

The magnitudes of oceanic currents are not large compared to wind velocities. Nevertheless, they are much more constant and, therefore, can add a significant component to ice drift, especially over periods of time greater than a day.

In addition to their importance as a means of transporting ice, currents are a major source of energy transport to arctic regions. This energy is supplied in the form of storms generated from the warm currents as well as the transport of warm water. In later sections, the impact of current systems will be discussed in terms of ice behavior in specific regions.

2.2 OCEANIC TIDES

The detailed description of tidal behavior and related causes can easily fill an entire book. All we can hope to do here is present the sea ice analyst with sufficient background to understand tidal phenomena which might have a bearing on sea ice behavior.

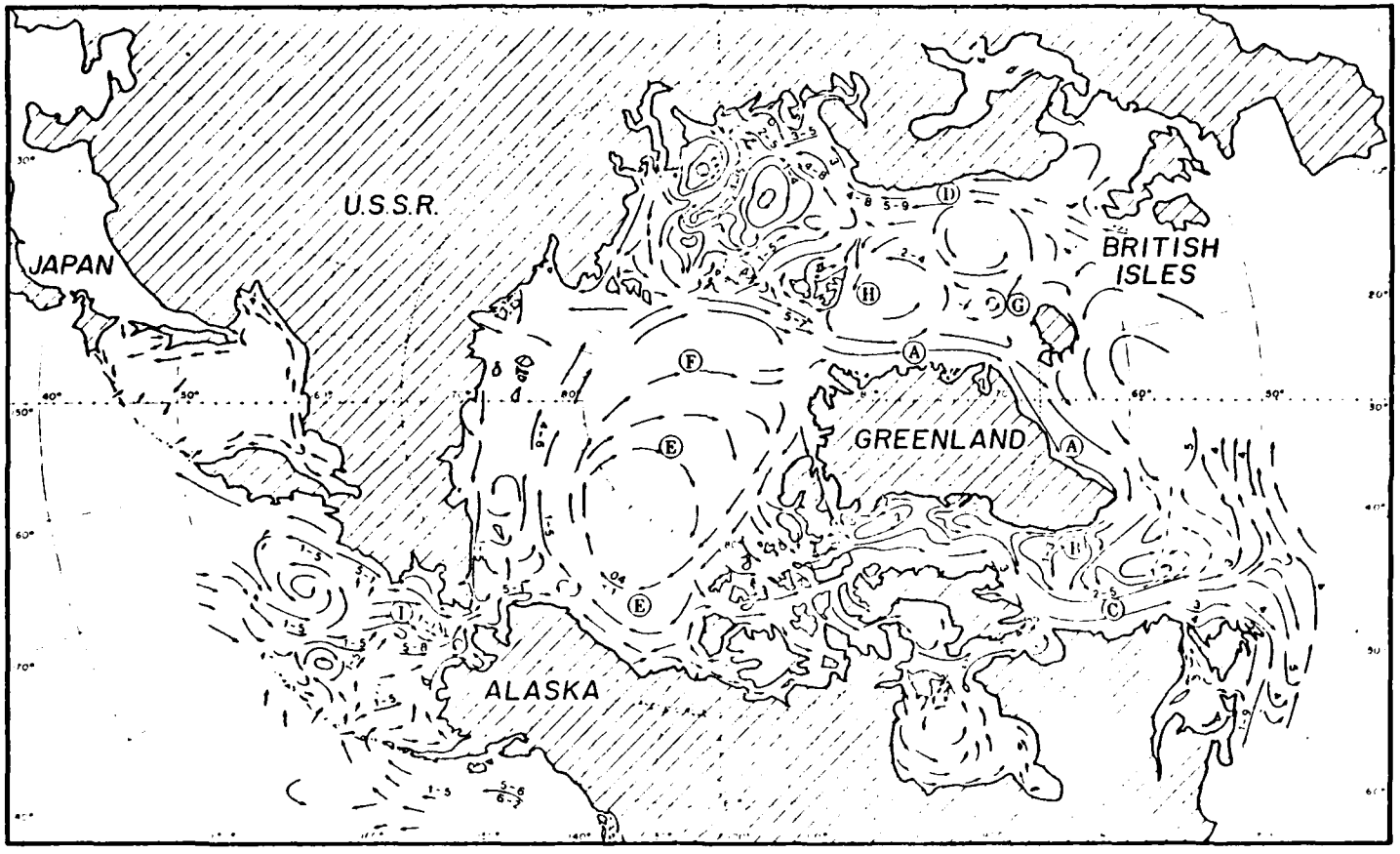

Figure II-1. Arctic Oceanic Currents. Current values shown are in knots. Current names are as follows: (A) East Greenland Current, (B) West Greenland Current, (C) Labrador Current, (D) Norwegian Current, (E) Beaufort Gyre, (F) Trans-polar Drift Stream, (G) Jan Mayen Current, (H) West Spitsbergen Current, (I) Pacific Current.

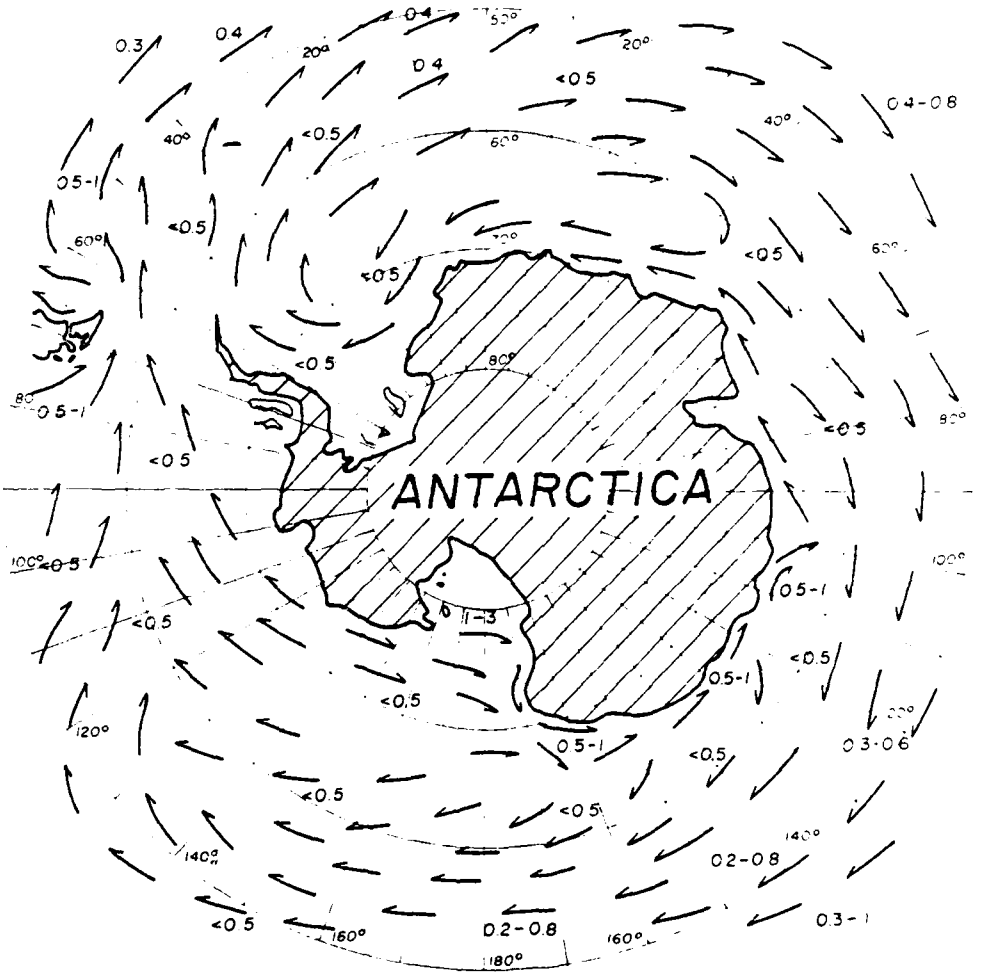

Figure II-2. Antarctic Oceanic Currents.
Current values shown are in knots.

2.2.1 Causes of Tides. Oceanic tides are not only caused by gravitational attraction of the moon and sun for the earth's water but also by the centripetal acceleration of the planet's water surface as both the earth-moon pair and the earth-sun pair revolve around their common center of mass.

The effect of either the sun or moon acting alone would be to cause two high tides and two low tides per day. On a planet covered completely with a deep ocean, the high tides would occur when the celestial body was directly overhead and directly underneath the point of observation. However, the tides caused by the sun and moon add to yield two high tides and two low tides simply as addition of the two separate tidal waves. However, the timing of tides changes during the month because the relative position of the moon and sun changes over that period. Twice a month, when the sun and moon are together and when they are opposite each other, the tidal waves of each combine to cause very high tides (spring tides). Similarly, when the sun and moon are 90° apart (first quarter and third quarter), the tides are their smallest (neap tides).

Even during spring tides, one cannot expect the high tides to occur at noon and midnight. This is because the actual configuration of the ocean and shoreline embayments alters the timing of tides considerably. (Although the relative positions of the tide states will remain in phase.) Because of these site-specific effects, a tide table must be consulted for tide stages at various locations.

2.2.2 Magnitudes. In the open ocean, tidal magnitudes are only a few centimeters. The really noticeable tidal effects are caused by interaction of the tidal bulge with the shore where water can pile up in shallow areas. The coastal tidal range can vary from ten or twenty cm on the shore of the Beaufort Sea to nearly 16 m in the Bay of Fundy, Nova Scotia. Again, tide tables must be consulted to find the tidal range to be expected at various locations.

2.2.3 Geometric Effects. The particular geometry of a sound, inlet, bay or any partially closed body of water will have a great bearing on the tidal range and timing within that feature. In addition, because coriolis acceleration causes a turning motion to the right in the northern hemisphere [and to the left in the southern hemisphere (sh)], tidal waters entering a partially enclosed body will tend to pile on the

right ($left_{sh}$) shore and exiting will tend to accumulate on the left ($right_{sh}$) shore. (Right and left taken in terms of facing the entrance of the water body from the outside.) Furthermore, the tidal range will be much larger on the right ($left_{sh}$) shore.

In some waterways the speed of advance of the incoming tide can be several knots and in extreme cases, a tidal bore or wall of advancing water will be created. Turnagain Arm of Cook Inlet, Alaska can be host to both sea ice and a tidal bore.

2.2.4 Resultant Ocean Particle Movement. Here it is instructive to consider the actual movement of water due to tidal currents. (The motion of ice on a moving body of water will be discussed later.) In a narrow waterway, the tidal currents are greatest when the tide state is changing most rapidly. This occurs roughly halfway between high and low tides. The current which preceeds high tide is called the flood tide current and the current which preceeds low tide is called the ebb tide current. In this case, the path of a particular particle of water is roughly one-dimensional. However, in the case of a larger water body, a particular particle of water tends to undertake an elliptical path as a result of the coriolis acceleration described above. These ellipses tend to be counterclockwise in the northern hemisphere and clockwise in the southern hemisphere (viewed from above the earth). When considering the effect of tides on ocean particle movement, it is important to remember that the tidal ellipse is superimposed on any other current which may be acting in the area. In that case, the particle motion will not necessarily be a closed figure.

2.3 PERTURBATIONS TO OCEANIC FLOW ARISING FROM METEOROLOGICAL CONDITIONS

Meteorological conditions can alter oceanic flow by means of two major mechanisms.

2.3.1 Wind Stress on the water surface obviously creates waves. More importantly for this discussion, it creates a surface current. The precise relationship between wind and the induced currents is not well known. However, there is general agreement that the force on the water surface (the wind stress) is roughly proportional to the wind speed squared. Hence, a 40 knot wind will produce 16 times the water stress

that of a 10 knot wind. Because of coriolis acceleration (described in 1.2.1 of this chapter), the water (and ice moving freely upon it) will actually move to the right ($left_{sh}$) by 20 to 40 degrees. Wind stress can cause a storm surge tide as great or even greater than astronomical tides. In the Beaufort Sea, for instance, the astronomical tide is less than one meter. In that same region storm surges of several meters have deposited ice high above the normal high tide line.

2.3.2 Sea Level Tilt can be created by the piling of water by wind stress. This can become particularly important when a storm surge encounters land and the piled water must flow away according to its slope just as a river runs downhill. Again, coriolis acceleration becomes important to the water moving downslope, tending to turn it to the right in the northern hemisphere.

Sea level tilt can also result from atmospheric pressure variations. This mechanism has been found to be an important factor in creating a southward flow of water (and ice) through the Bering Strait between Alaska and Siberia. Barometric pressure-induced sea level tilt is particularly effective in shallow and constricted waters such as the Bering and Chukchi Seas.

SECTION 3. MOTION OF ICE UNDER THE COMBINED EFFECTS OF WINDS, CURRENTS, AND CORIOLIS ACCELERATION

3.1 HISTORICAL VIEW

In 1893 a Norwegian, Fridtjof Nansen, initiated a transpolar drift across the Arctic Ocean aboard a specially constructed ship, the Fram. Among the many observations made by this expedition was that ice floes on the water surface drifted between 20 and 40 degrees to the right of the surface wind direction. Nansen correctly recognized this as an effect of coriolis acceleration and suggested to a Norwegian physicist, Ekman, that this effect might warrant theoretical investigation. Ekman's subsequent work resulted in the accurate prediction of a large range of oceanic effects related to coriolis acceleration and other phenomena.

The U.S.S.R. has long depended on her northern ports and seaways for transportation of goods within that country and for export/import purposes. Since the late 1920's, the soviets have sent numerous expeditions to the arctic to conduct detailed scientific investigations. By 1943, sufficient information had been obtained that N.N. Zubov could write a massive book of 500 pages (when translated into English) at a time when very little scientific work on arctic ice had been performed in other countries, particularly the United States. Zubov's work touched on almost every imaginable subject related to oceanic ice. Of interest to us here will be his treatment of ice drift as a result of synoptic winds.

Since that time, the soviets have continued their efforts and considerable work has been done by other countries as well. In recent years, the U.S. effort has had two main directions. The first was a large experiment and theoretical program to understand and develop a numerical model to describe drift ice behavior under bounded conditions such as exist in the U.S. portion of the Beaufort Sea. This project was referred to as AIDJEX (Arctic Ice Dynamics Joint Experiment). The second aspect, a major part of which is underway at this writing, is to understand and model the behavior of drift ice in the marginal ice zones (MIZEX). In these regions, ice is growing or melting and usually freely drifting under the direct influences of winds and currents. It is generally presumed that this contrasts with the behavior of drift ice

under the bounded conditions studied under AIDJEX where forces can be transmitted considerable distances (on the order of hundreds of km) within the drift ice. However, the importance of this contribution to the movement of the ice is a matter of debate even today. Fortunately, it does not appear to be of great importance to predicting the location of the drift ice edge.

The movement of sea ice resulting from winds, currents, and coriolis force is a complex subject. A great deal of effort has been made to develop sets of equations which allow ice analysts to make predictions of ice motions based on geostrophic winds (taken from pressure charts) and currents. There are many difficulties. First, there is the question of whether the ice in question is open drift ice, closed pack ice, a few isolated floes, or the drift ice edge. Second, it is often difficult to obtain adequate knowledge of the geostrophic winds in polar regions because of inadequate barometric measurements. Finally, currents are hard to measure and in some areas can change on a relatively short time scale, making the use of standardized current charts questionable.

The problems mentioned above present difficulties not only to the sea ice analyst, but also to the scientists attempting to determine the equations describing ice motion. Despite these problems, some rather consistent equations have been derived.

3.2 OVERVIEW OF THE RELATIONSHIP BETWEEN GEOSTROPHIC WINDS AND ICE MOVEMENT WITHIN THE DRIFT ICE

3.2.1 Geostrophic Winds and Direction of Floe Motion. Although winds at sea level provide the force for moving ice, surface wind values are generally not available to the ice analyst. In order to derive surface wind values, geostrophic wind values must be altered by an appropriate angle to correct for surface friction as described in II-1.2.3.1. This angle is around 25° to the left. However, as described in II-1.2.1, coriolis force alters the direction of moving objects on the earth's surface, turning them to the right (in the northern hemisphere). For sea ice, this angle ranges from 30° to 40° from the surface wind. As a result, sea ice motion is usually between 5° and 15° to the right of the geostrophic wind.

3.2.2 Geostrophic Winds and Ice Velocities. Fluids generally exert square-law forces on objects placed within them. That is:

(1) $F = K V^2$

or the force is equal to the velocity squared times an empirical constant which is related to the viscosity of the fluid and surface friction characteristics of the object. Sea ice has two such forces acting upon it: winds and currents.

Although we do not know the ratio between the geostrophic winds and the surface winds, we can assume it is a constant factor, K_1, so that:

(2) $V_S = K_1 V_G$ where V_S = surface wind speed and V_G = geostrophic wind speed

Using equation (1), the propelling force on an ice floe due to surface winds is:

(3) $F_P = K_2 V_S^2$ where K_2 is a constant combining air viscosity and upper surface friction factors.

Using equation (2), this becomes, in terms of geostrophic winds:

(4) $F_P = K_2 (K_1 V_G)^2$

Again using equation (1), the retarding force on the floe due to water stress is:

(5) $F_R = -K_3 V_F^2$ where V_F is the floe speed in the water and K_3 is related to the water viscosity and lower surface friction characteristics. The negative sign indicates that the water stress retards the floe motion.

When ice is moving at a steady speed, the wind force is balanced by the water stress:

(6) $F_P = -F_R$ or, substituting from (4) and (5):

(7) $K_2(K_1 V_G)^2 = +K_3 V_F^2$

Solving this equation for the floe speed, V_F, we have:

(8) $V_F = \left[K_1\sqrt{\frac{K_2}{K_3}}\right] V_G = C V_G$ since $K_1\sqrt{\frac{K_2}{K_3}}$ is a constant, C.

In other words, the floe speed is related to the geostrophic wind through a simple constant which is likely to be nearly the same for all floes with the same upper and lower surface friction characteristics.

Considerable efforts have been made to determine with greater precision the values of α (the turning angle) and C (the scalar drift coefficient). The results to date support the following values:

$C = .008$ (under constrained drift conditions, winter and spring with small ice velocities)

$C = .01$ (under free drift conditions, summer with higher ice velocities)

$C = .008 \leq C \leq .01$ (intermediate drift conditions)

$\alpha = 30\ e^{-1.7\ V_G}$ (α decreases as the geostrophic wind increases)

where e is the base of the system of the natural logarithms ($\approx$2.71828)

Typical values given by this equation are:

$\alpha = 5°$ (to the right) (for moderate wind speeds $\approx$12 kt)

$\alpha = 18°$ (to the right) (for low wind speeds $\approx$5 kt)

3.2.3 Application of Wind-Drift of Ice Equations. The equations for wind-drift of ice given in the previous section are generally correct for drift ice conditions in areas far [100-150 nautical miles (nm)] from the influence of shore or shorefast ice. If the motion of ice under these conditions is to be forecast, site-specific alterations to these rules may need to be employed. Furthermore, although these relationships are generally correct, they represent data with an uncertainty of around $\pm$ 20%. Therefore, when applying these equations, one should not expect the prediction of any one ice event to be any more accurate than $\pm$ 20%.

3.3 CURRENT-DRIFT OF ICE

Oceanic currents in deep arctic and antarctic waters appear to be relatively constant. This contrasts with shallower areas where meteorologically driven currents are possible. Hence, published current charts can be used in these areas. The currents shown are usually on the order of 1 nm/day. Their directions, as shown, are probably correct to within a few degrees. Studies have shown that the current-driven component of ice drift is most accurate when used to predict drift over

periods of time on the order of a month or more. On shorter time scales, local fluctuations and deviations of currents become significant.

Current-drift of ice appears to be completely free from shoreline interactions at distances greater than 250 nm from shore. Care must be taken when predicting drift ice behavior based on currents and winds at distances closer than this since it is possible that drift rates may be less.

3.3.1 Short-Term Current-Drift of Ice. The short-term component of ice drift can become very important in regions near shore. In these regions the magnitude of currents can be considerably larger than in areas with deep ocean currents because of meteorological forcing and bathymetric configuration. In these cases, coriolis effects may become significant, tending to pile ice against coastlines to the right of a current or creating a polynya to its left. These currents are difficult to predict. Their behavior depends to a large degree on site-specific interactions which, if understood at all, are cataloged for each general area.

3.4 INTERNAL FORCES WITHIN THE DRIFT ICE AND THEIR INFLUENCE ON ICE MOVEMENT AND DEFORMATION.

It has been known for a long time that large forces can develop within drift ice. While the most dramatic demonstration of these forces has been the occasional crushing of ships caught in the ice, the most common indication of large forces within the ice is the occurrence of pressure ridges. Pressure ridges occur when the internal forces within the ice pack exceed the failure strength of the ice. The fact that pressure ridges can be found almost anywhere within the ice demonstrates that such forces are common.

For some time it has been thought that in order to accurately predict drift ice motions, it was necessary to take into account these internal ice forces. This adds a great deal of complication to the forecasting of ice motions since these forces can be transmitted great distances and arise from distant sources. Recently, however, it has been shown that even in close pack conditions, it may not always be necessary to take these forces into account in an explicit way.

Internal forces within the ice are generally even less important when predicting the motion of the drift ice edge than when predicting movements within the ice. As a result of this, ice analysts generally do not take internal forces into account in a rigorous way when predicting pack advances and retreats.

The treatment just given for the motion of ice under the influence of winds and currents is essentially an outline of the basic concepts. In Chapter IV two approaches are described that deal with the problem of predicting sea ice motions.

CHAPTER III. GLOBAL/REGIONAL SEA ICE DISTRIBUTION AND BEHAVIOR

SECTION 1. ICE DISTRIBUTION IN THE NORTHERN HEMISPHERE

The general configuration of the Arctic Ocean in the northern hemisphere is largely that of an ocean bounded by continental land masses. As a result, the variation in ice cover is limited by geography more than thermodynamics. In the polar basin, the variation in ice cover is largely limited to the relatively shallow nearshore areas. The greatest variation in ice cover occurs in the marginal seas: the Chukchi and Bering Seas and Sea of Okhotsk on the Pacific side and the Greenland and Norwegian Seas and Baffin Bay on the Atlantic side.

The arctic ice edge climatology charts were constructed by graphically compositing the maximum and minimum ice edge extremes from eleven years (1972-1982) of Joint Ice Center operational eastern and western arctic ice analyses centered closest to the fifteenth of the month. The medians were constructed by graphically determining the median ice edge from two sets of ice edge summaries consisting of data from 1972 through 1978 and from 1979 through 1982. The medians for the seven and four year data summaries were then combined. The final median line was weighted toward the seven year median in areas where a large difference was observed. In the presentation of ice edge locations, no distinction is made between areas identified as open water or sea ice free. They are both treated as ice free, thus enabling recurring leads and polynyas to be reflected in the climatology.

JANUARY

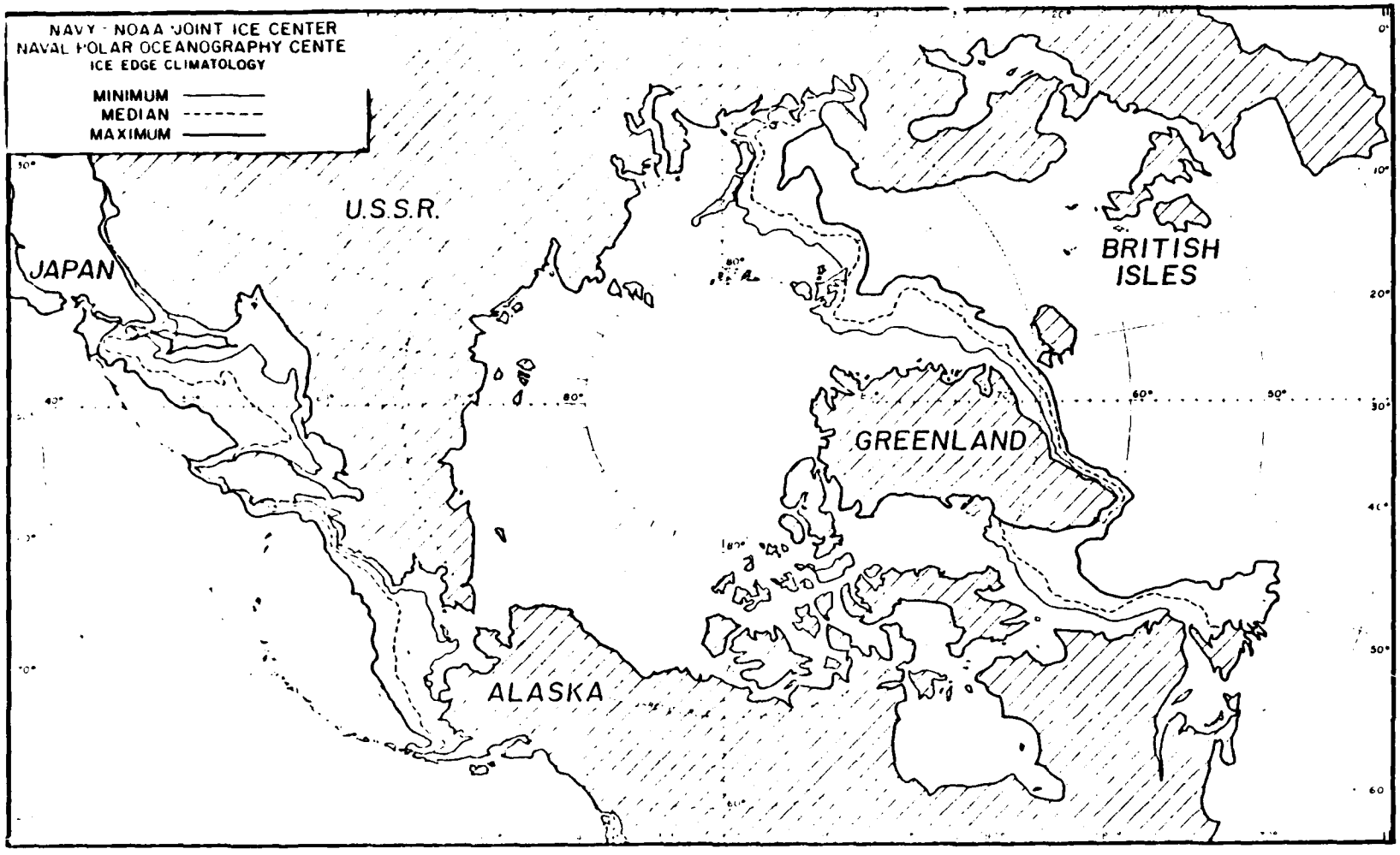

Figure III-1. Statistical Ice Edges In The Northern Hemisphere For January

FEBRUARY

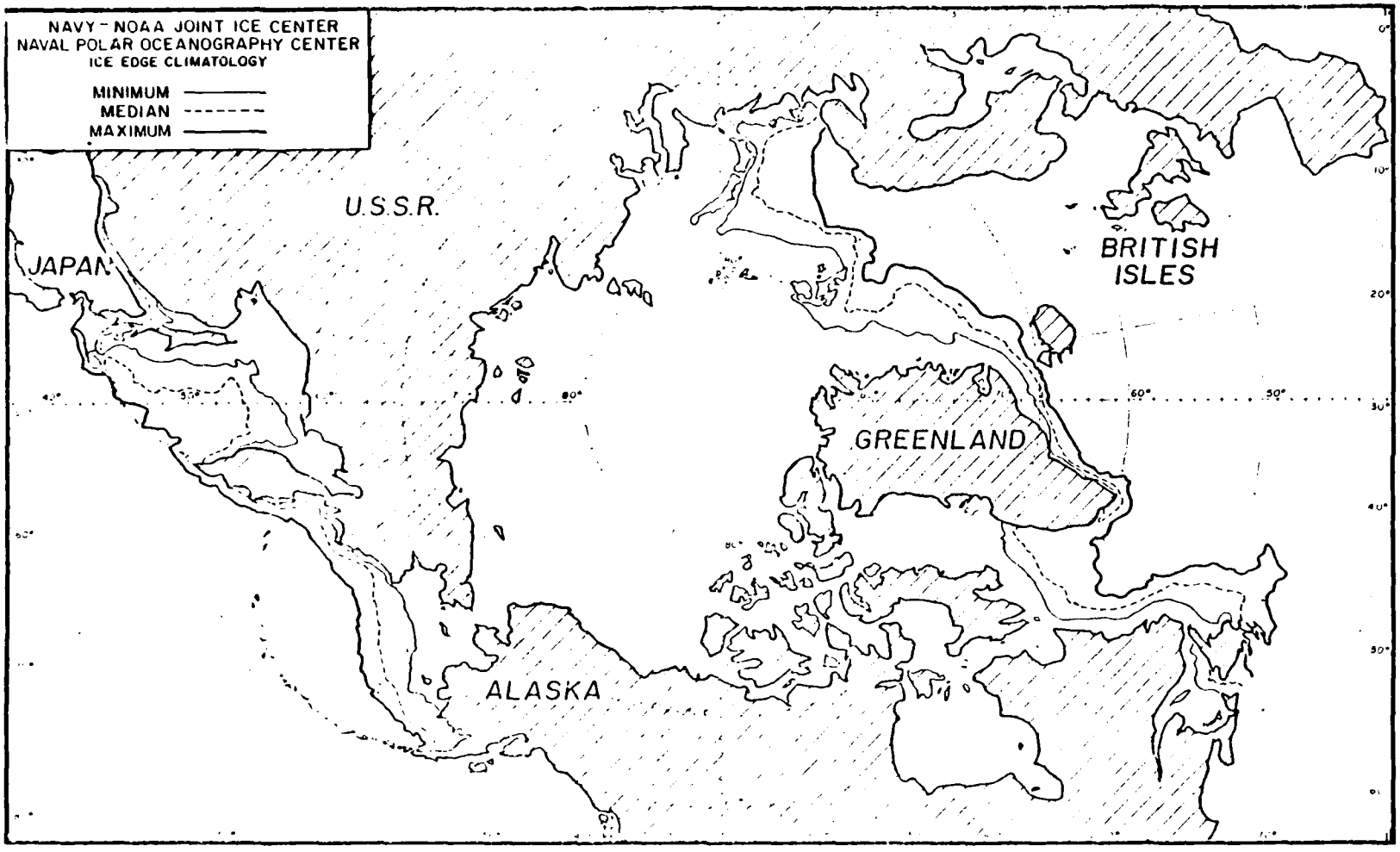

Figure III-2. Statistical Ice Edges In The Northern Hemisphere For February

MARCH

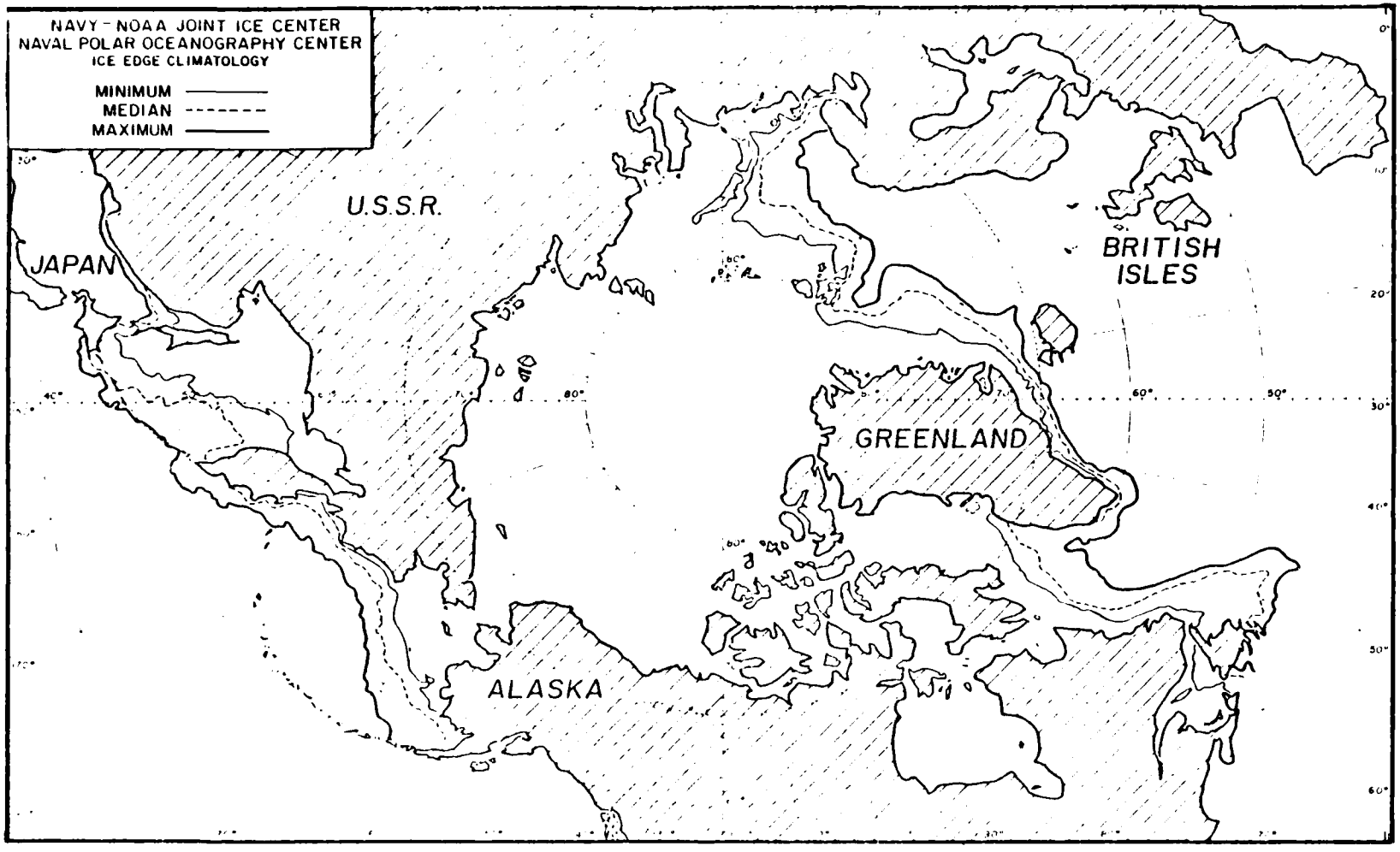

Figure III-3. Statistical Ice Edges In The Northern Hemisphere For March

APRIL

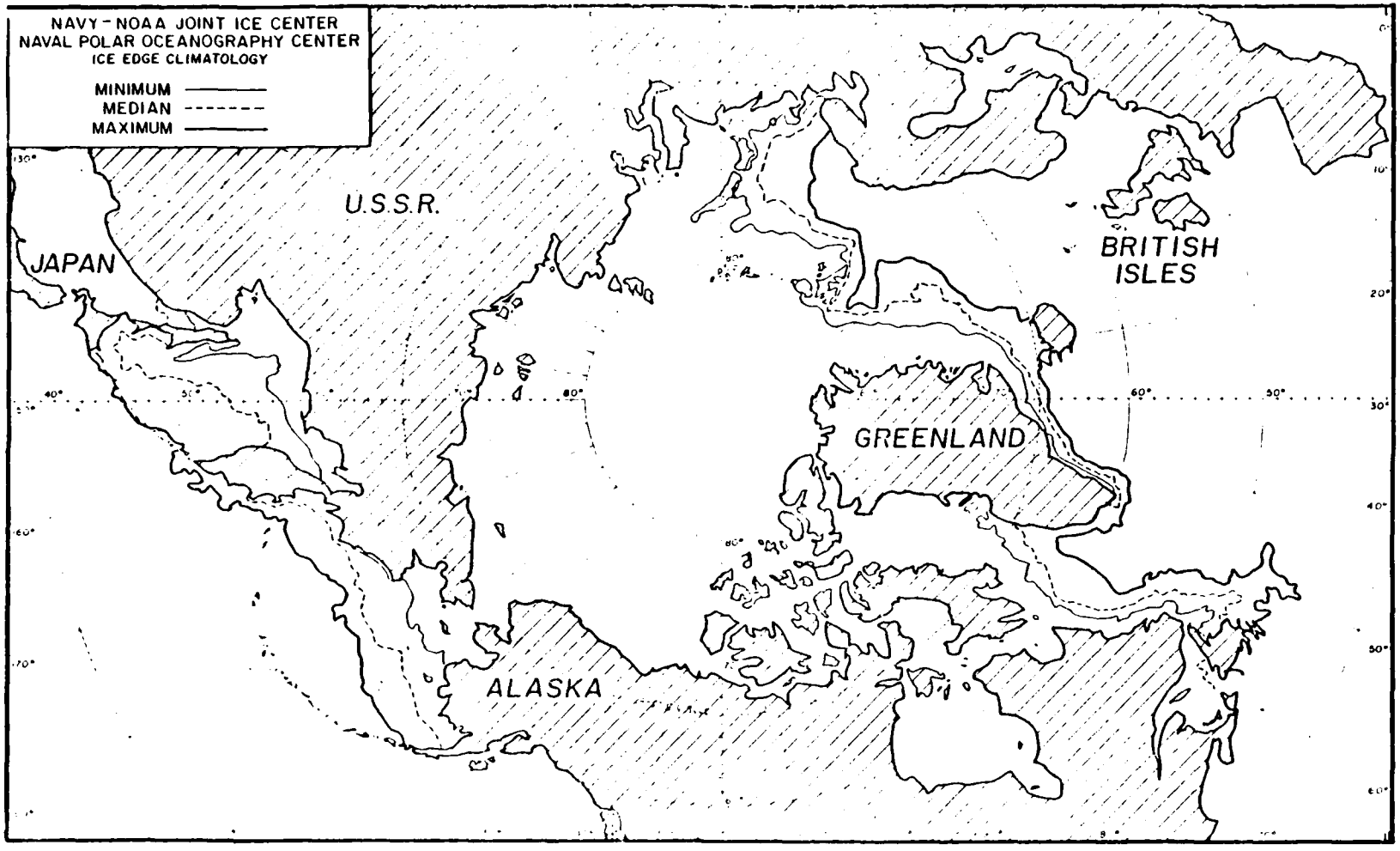

Figure III - 4. Statistical Ice Edges In The Northern Hemisphere For April

MAY

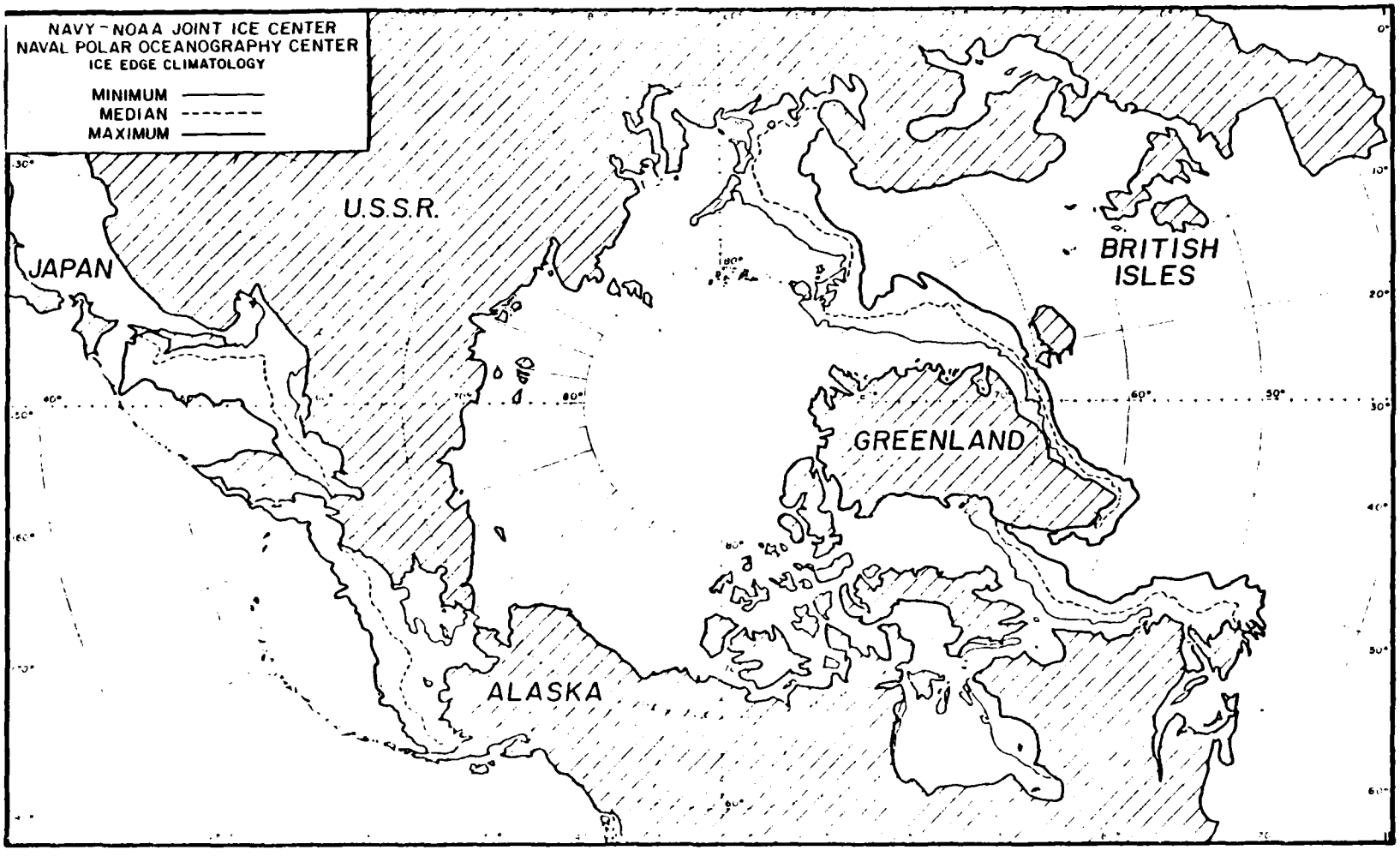

Figure III-5. Statistical Ice Edges In The Northern Hemisphere For May

JUNE

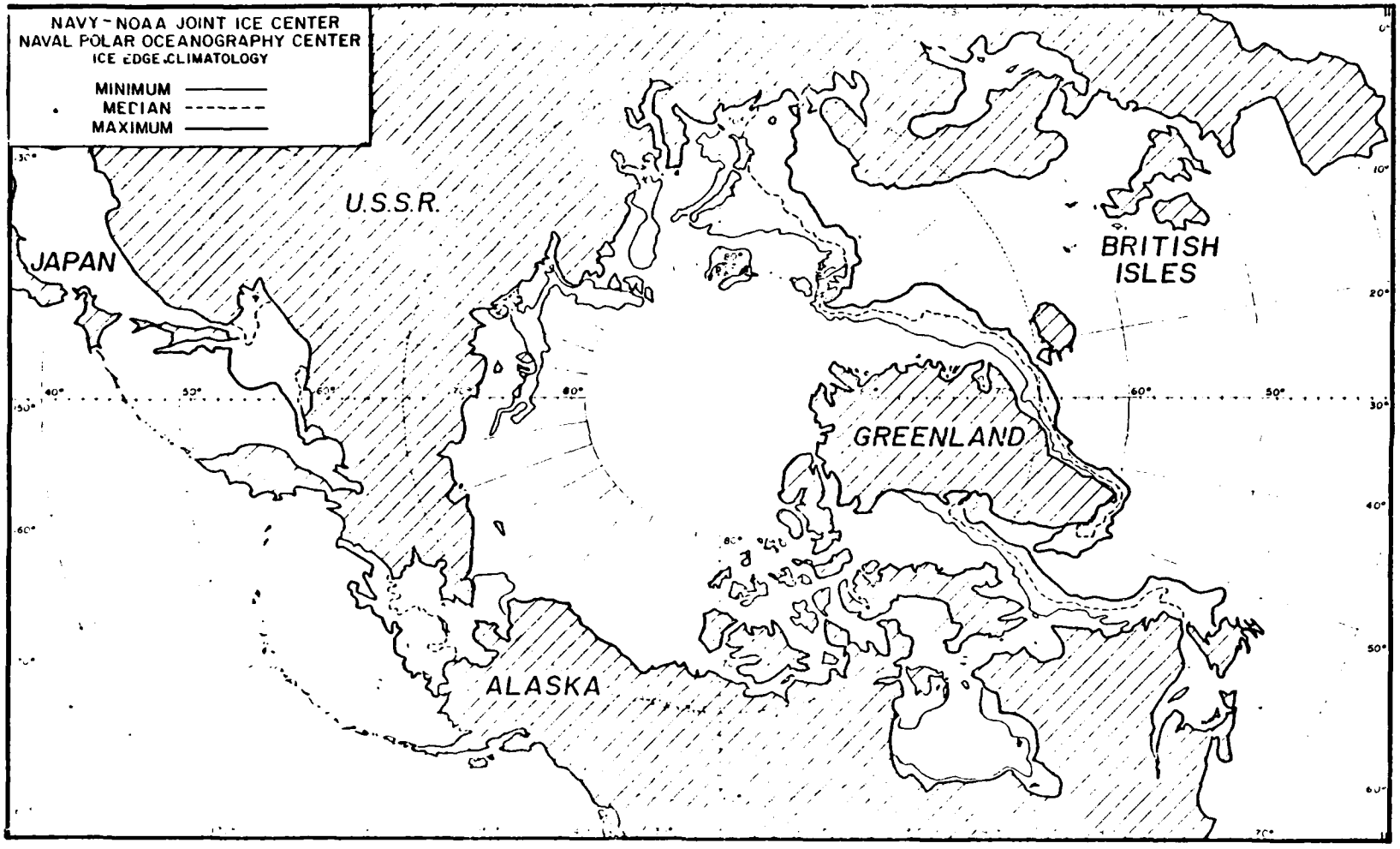

Figure III-6. Statistical Ice Edges In The Northern Hemisphere For June

JULY

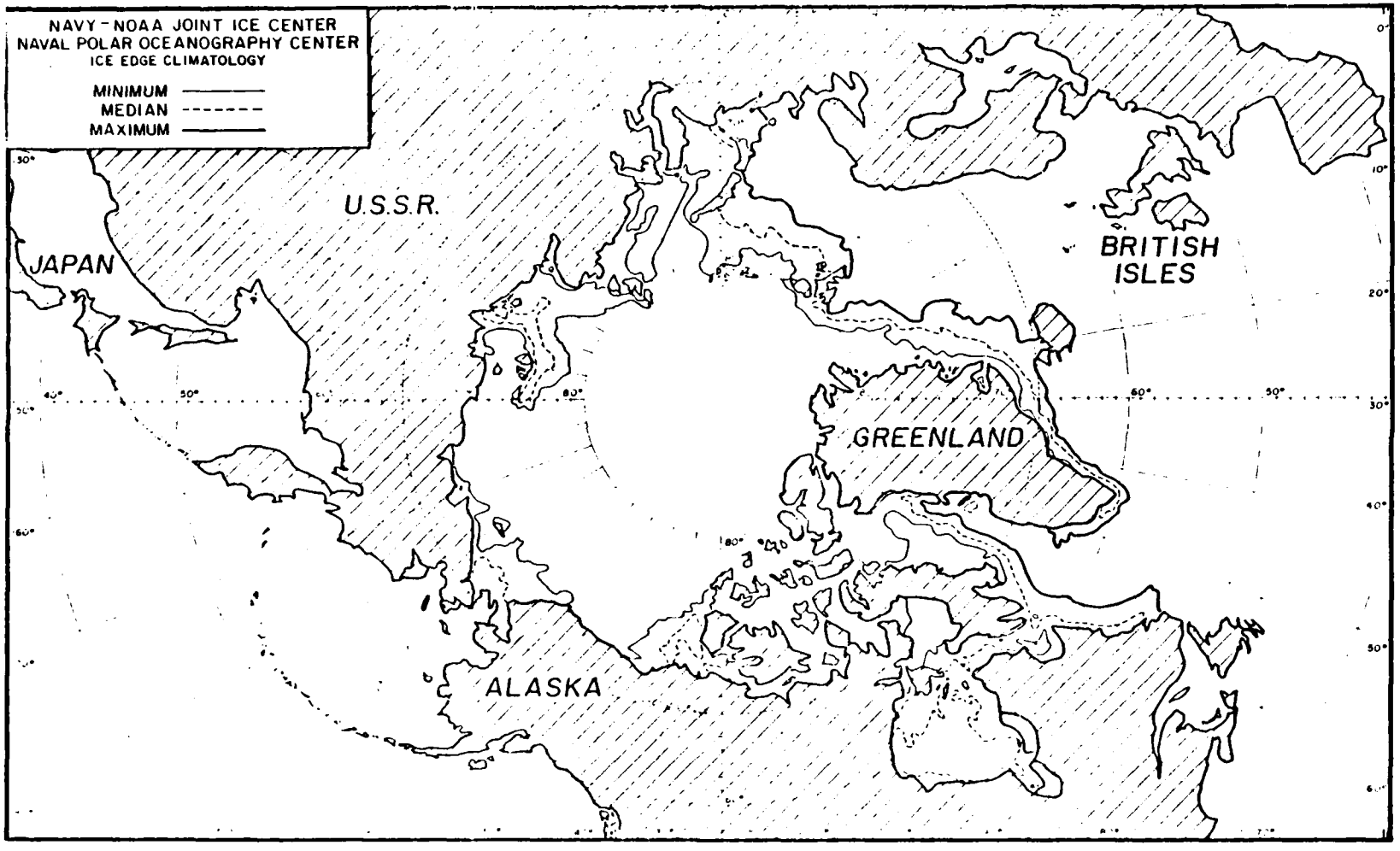

Figure III-7. Statistical Ice Edges In The Northern Hemisphere For July

AUGUST

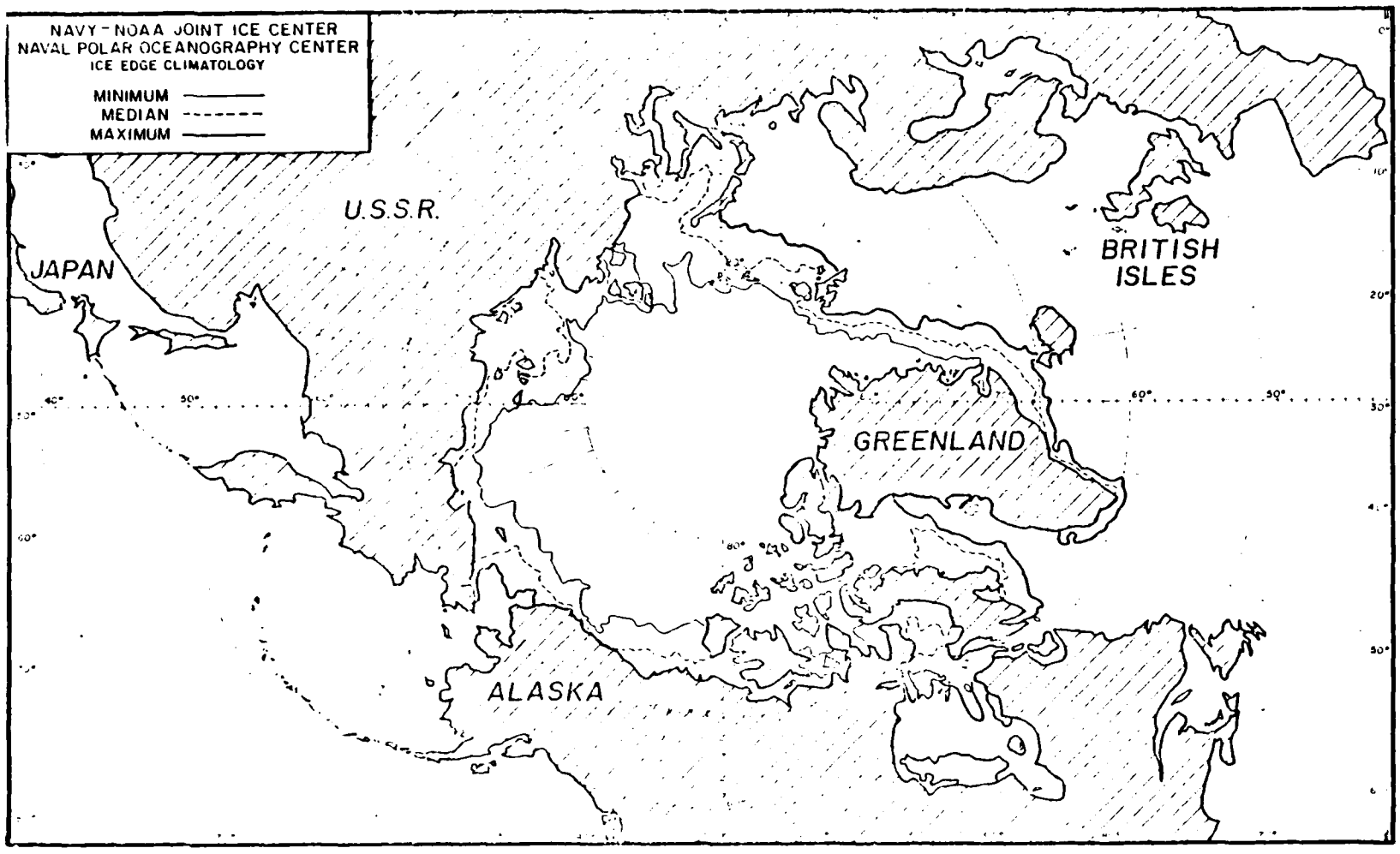

Figure III-8. Statistical Ice Edges In The Northern Hemisphere For August

SEPTEMBER

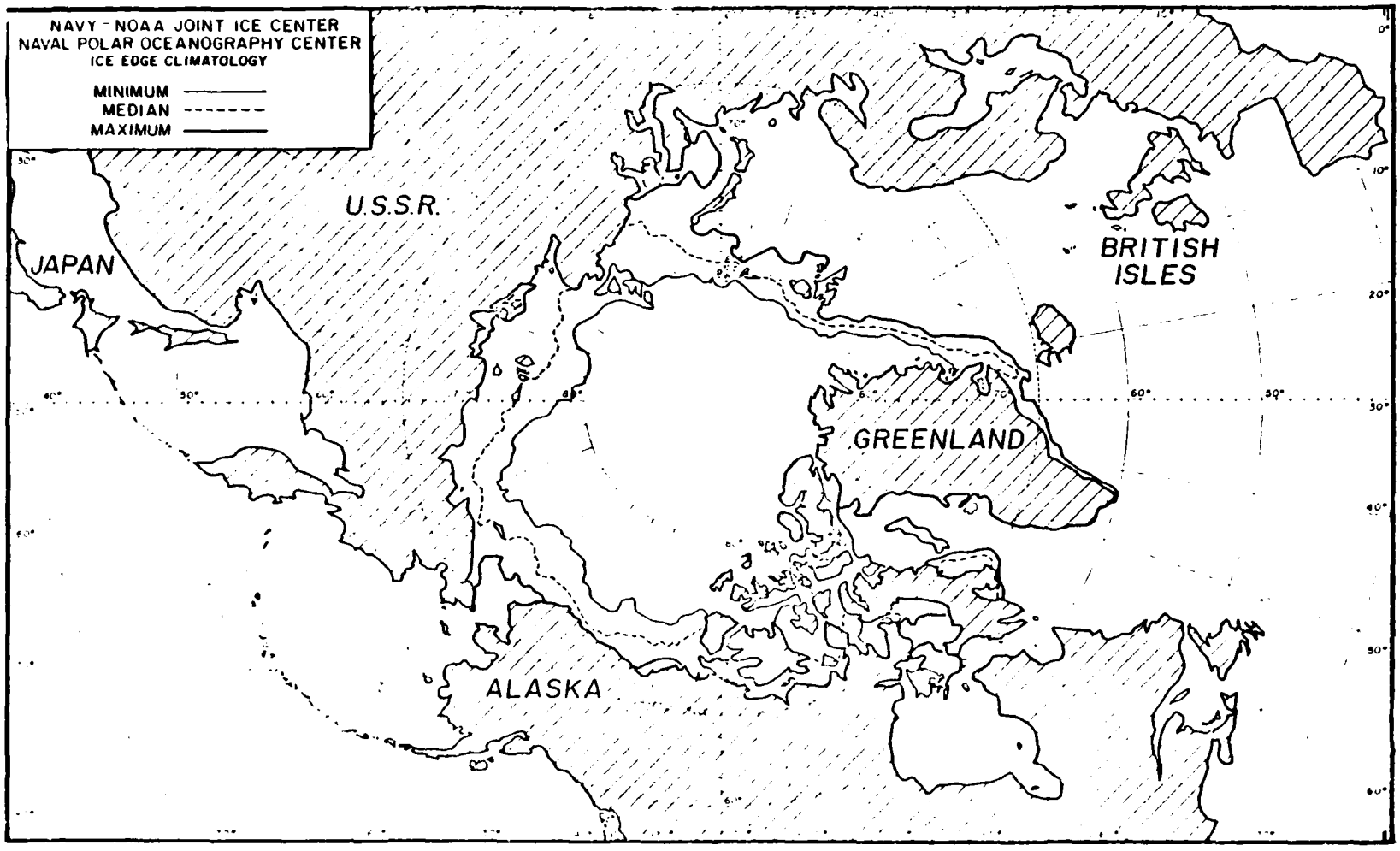

Figure III-9. Statistical Ice Edges In The Northern Hemisphere For September

OCTOBER

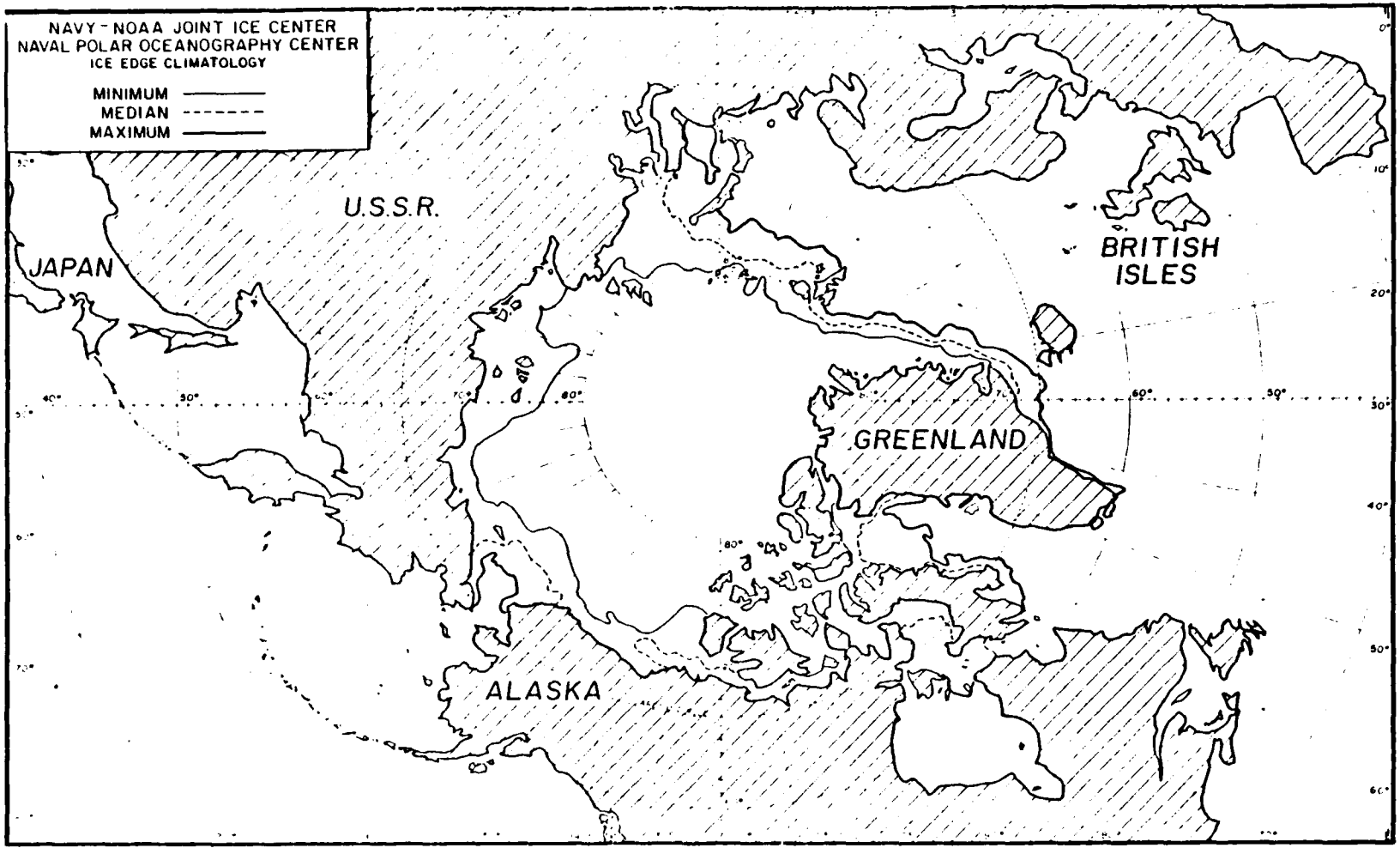

Figure III-10. Statistical Ice Edges In The Northern Hemisphere For October

NOVEMBER

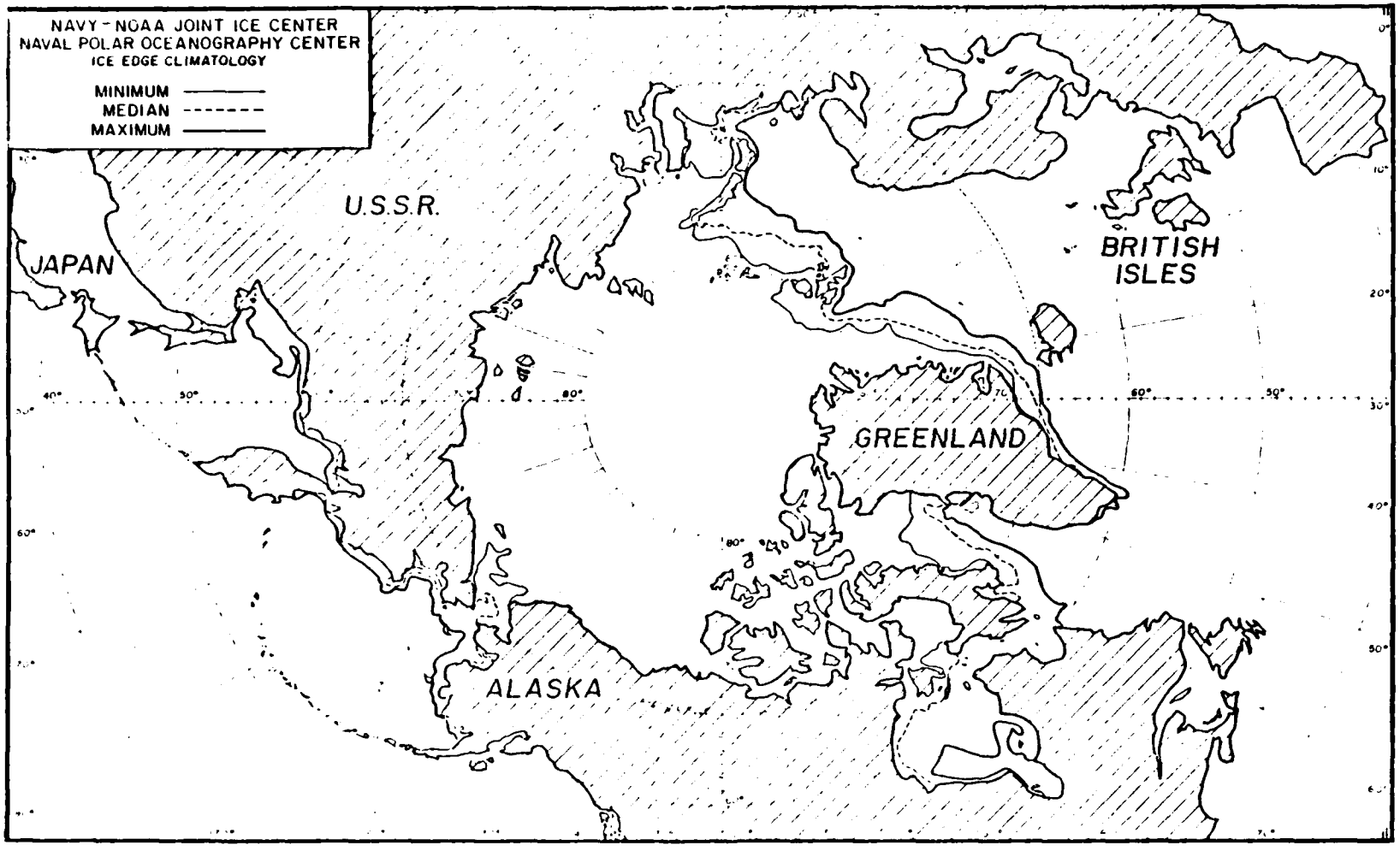

Figure III-11. Statistical Ice Edges In The Northern Hemisphere For November

DECEMBER

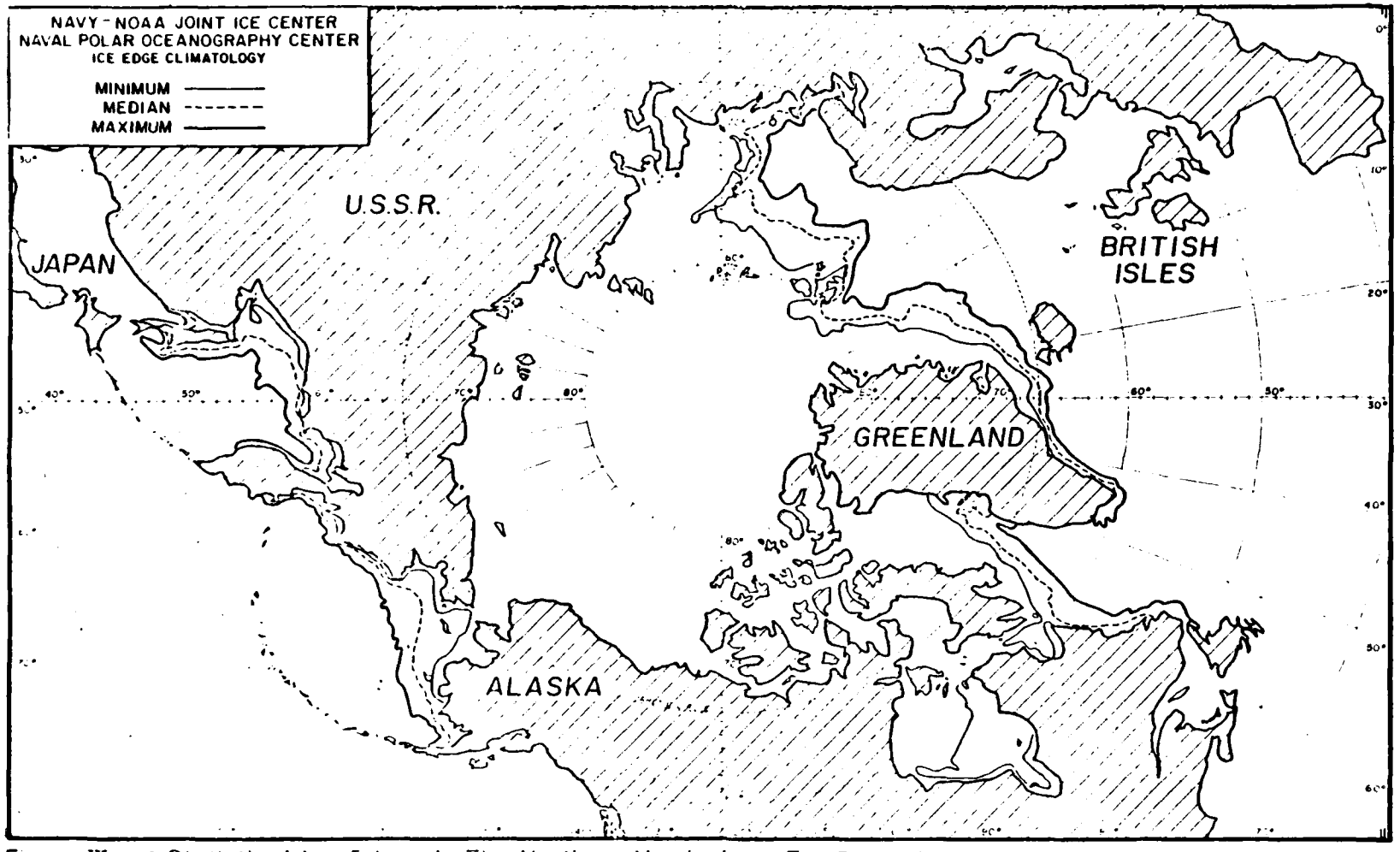

Figure III-12.Statistical Ice Edges In The Northern Hemisphere For December

1.1 DISCUSSION OF VARIATION OF ICE EXTENT IN NORTHERN HEMISPHERE

1.1.1 Atlantic Sector. Sea ice extent is generally greatest in March-April and least in September-October. The actual ice configuration at any time results from a combination of oceanic currents and climatological conditions; the variations that occur continue to reflect these conditions. For instance, the warm Atlantic Current (see Figure II-1) continuously transports heat into the Norwegian Sea. As a result, the ice edge in the eastern Atlantic sector is indented poleward during all seasons. Comparing the April and September maps, we see that the statistical ice edges all remain in the vicinity of Svalbard (Spitsbergen) throughout the year. In the Barents Sea to the east, where the effect of the Atlantic Current dies out, the sea ice extent varies significantly between summer and winter.

On the western side of Svalbard and along the eastern coast of Greenland, the sea ice extent remains nearly constant throughout the year. This is largely due to the southerly Greenland Current which advects ice south throughout the year.

On the western side of Greenland, in the Baffin Bay-Davis Strait region, the Greenland Current swings northward around the southern tip of Greenland before joining the Labrador Current southward along the Newfoundland coast. Note that this current effectively limits maximum ice extent in this region while the minimum ice extent extends as far northward as Ellesmere Island.

1.1.2 Pacific Sector. Here the variation in ice extent occurs in the Chukchi and Bering Seas. In this region, the mean current is northward through Bering Strait. (Although during certain conditions it can reverse for a short time.) This carries warm water into the Arctic Ocean and helps create the minimum ice extent seen there in September.

During winter, a large stable high pressure cell helps to create severe freezing conditions over the Chukchi and Bering Seas and the ice edge moves correspondingly southward, well into the Bering Sea. Here again, however, the effects of warm currents can be seen (see currents on Figure II-1). Because of the Aleutian Archipelago, the Pacific Current enters the western side of the Bering Sea and causes a northerly indention in the statistical ice edges there. On the eastern side, the current effect is lessened and winds advect ice and freezing conditions farther to the south.

Finally, as in the north Atlantic, there is a southerly coastal current along the east-facing coast bounding the sea (in this case, the Asian coast). This current advects ice down the coast of the Kamchatka Peninsula where, in the Sea of Okhotsk, a similar situation occurs as in the Baffin Bay-Davis Strait region. However, removal of ice in the Sea of Okhotsk in summertime is complete.

SECTION 2. ICE DISTRIBUTION IN THE SOUTHERN HEMISPHERE

2.1 INTRODUCTION

The configuration of the polar seas in the southern hemisphere is just opposite that of the northern hemisphere. Whereas in the northern hemisphere the polar ocean is bounded largely by continental land masses, in the southern hemisphere the continental land mass is completely surrounded by an ocean which becomes ice-covered. Because there is no artificial boundary to ice growth in the southern hemisphere, sea ice extent is limited only by climatological and ocean current effects. Consequently, the annual variation in ice cover in the antarctic is several times the annual variation in the arctic ice cover.

The antarctic ice edge climatology charts were constructed using 1973-1982 Joint Ice Center weekly antarctic ice analyses centered closest to the first of the month.

The construction of the maximum, median, and minimum ice edge climatology followed a procedure similar to that used in the construction of the arctic climatology. The medians were constructed through a graphical determination of the ten-year ice edge summary.

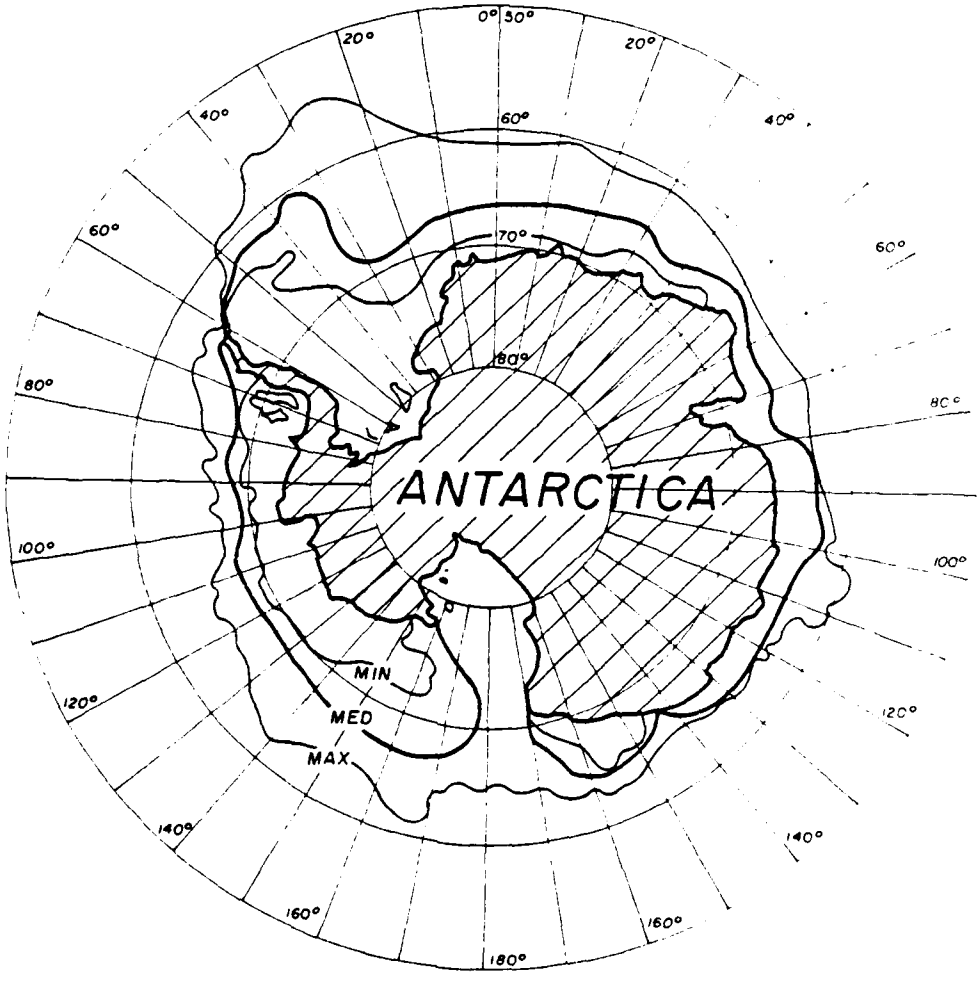

Figure III-13. Statistical Ice Edges in the Southern Hemisphere for January.

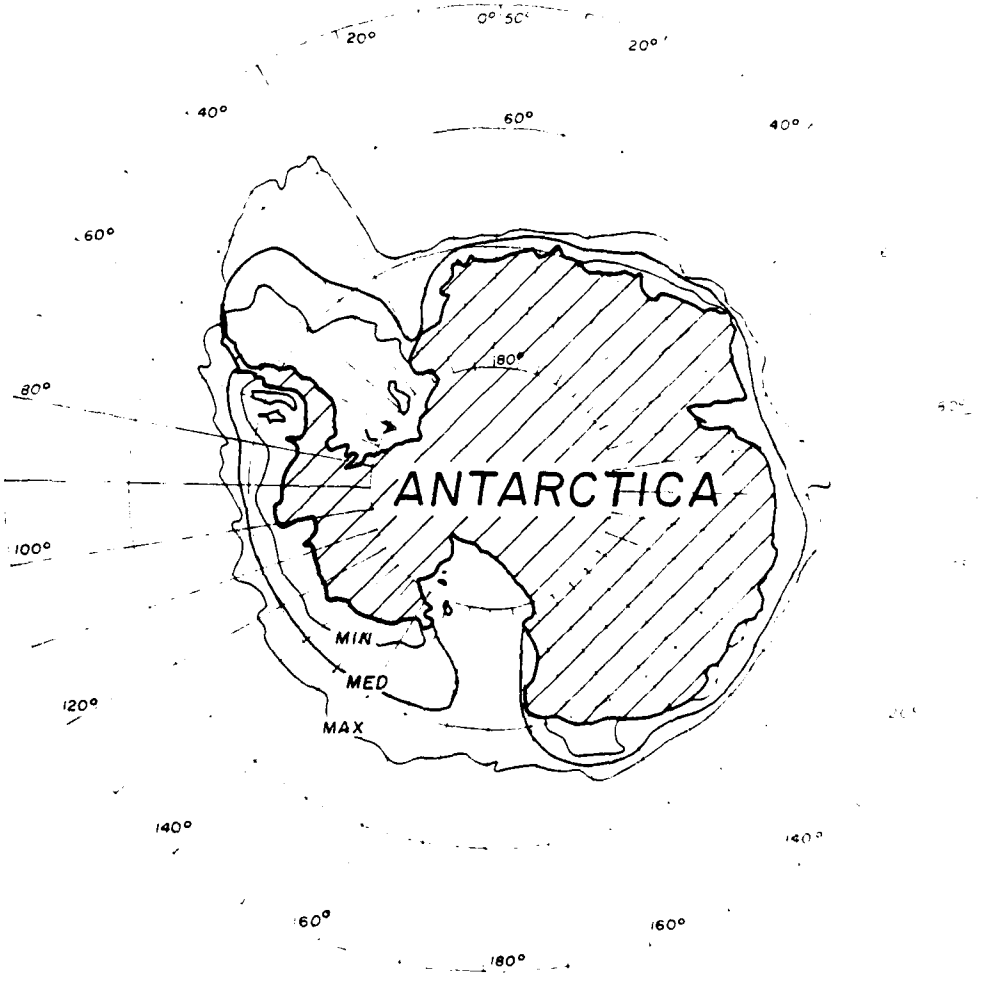

Figure III-14. Statistical Ice Edges in the Southern Hemisphere for February.

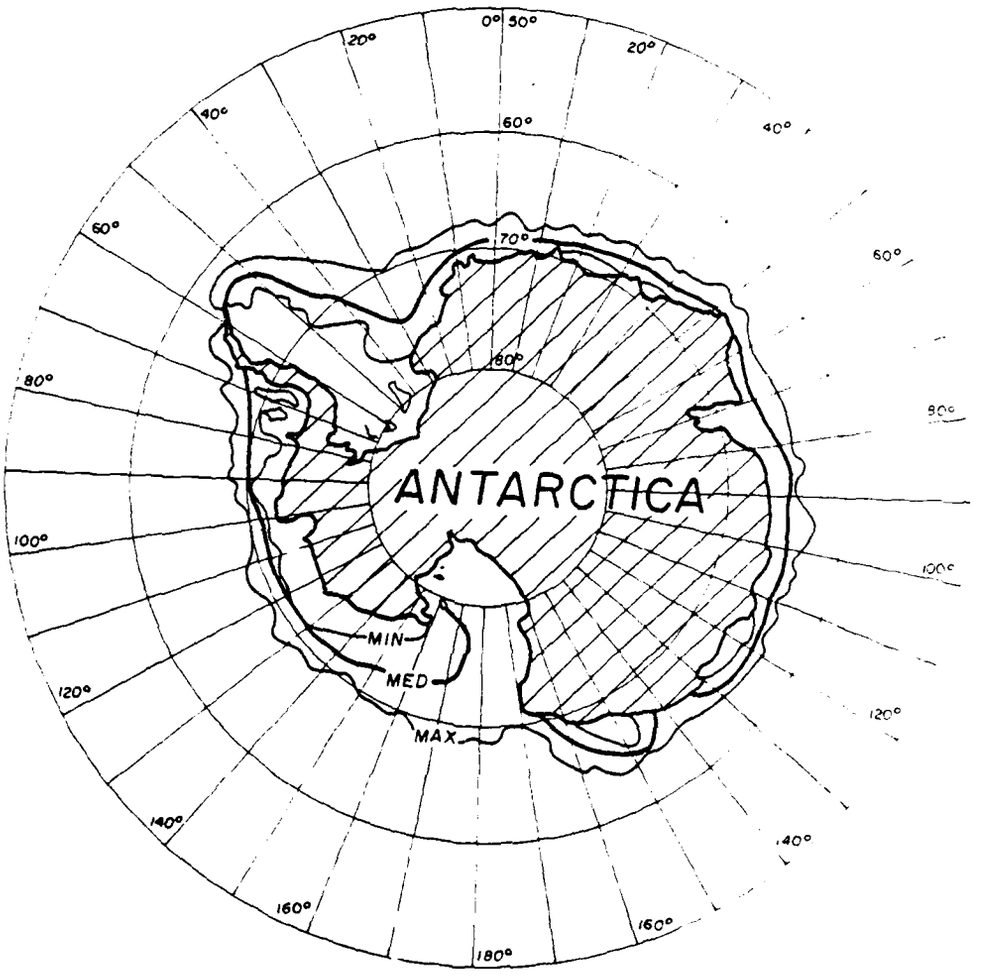

Figure III-15. Statistical Ice Edges in the Southern Hemisphere for March.

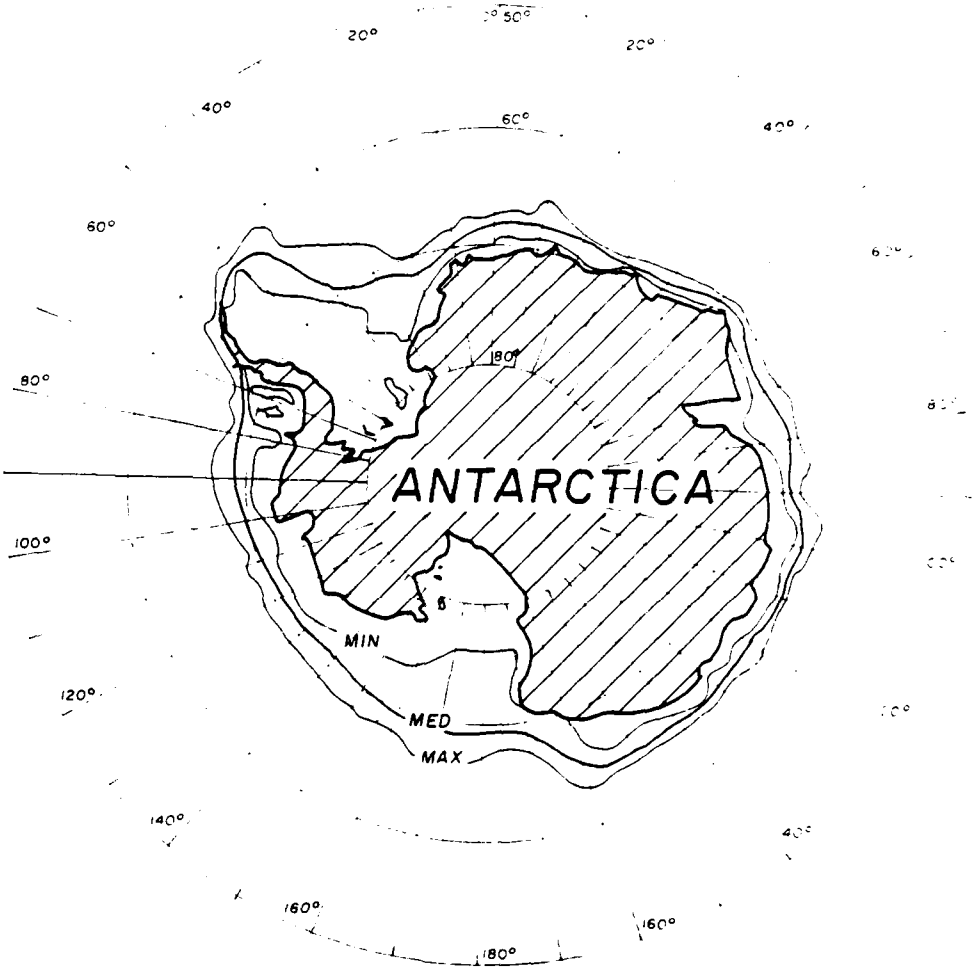

Figure III-16. Statistical Ice Edges in the Southern Hemisphere for April.

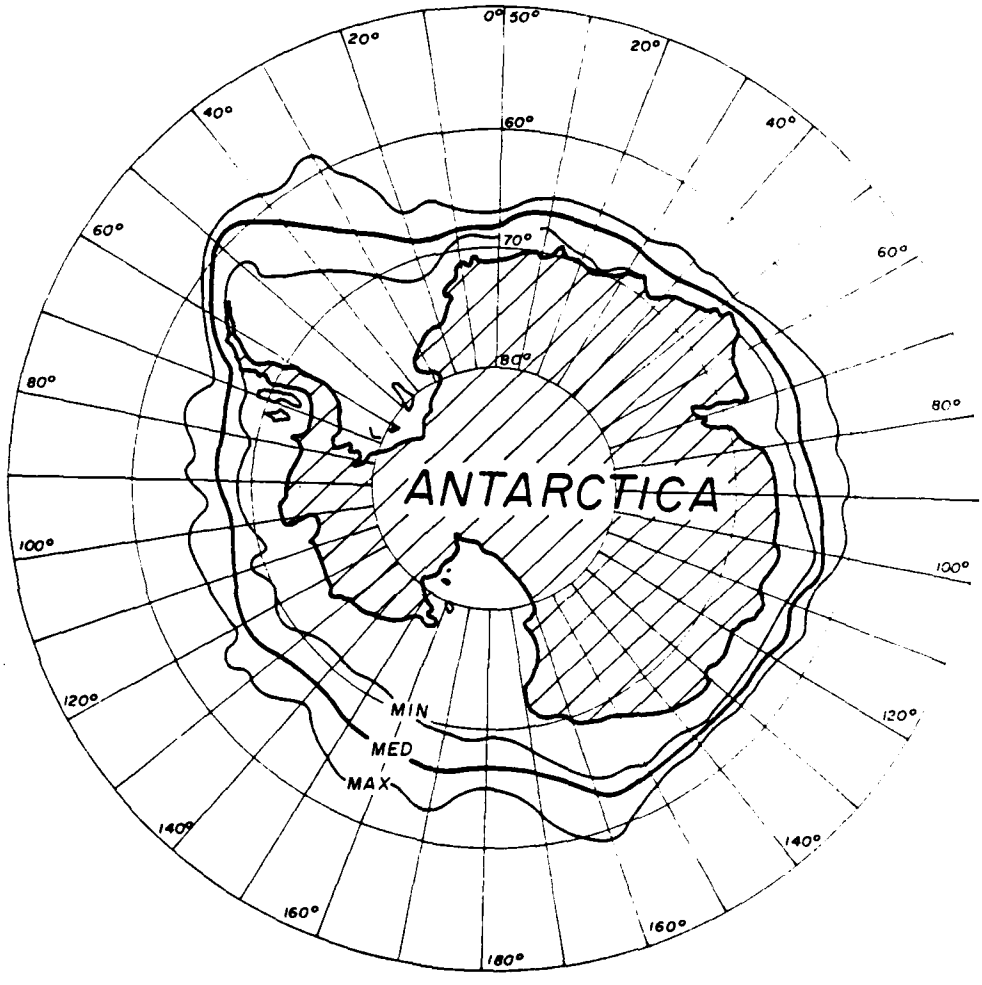

Figure III-17. Statistical Ice Edges in the Southern Hemisphere for May.

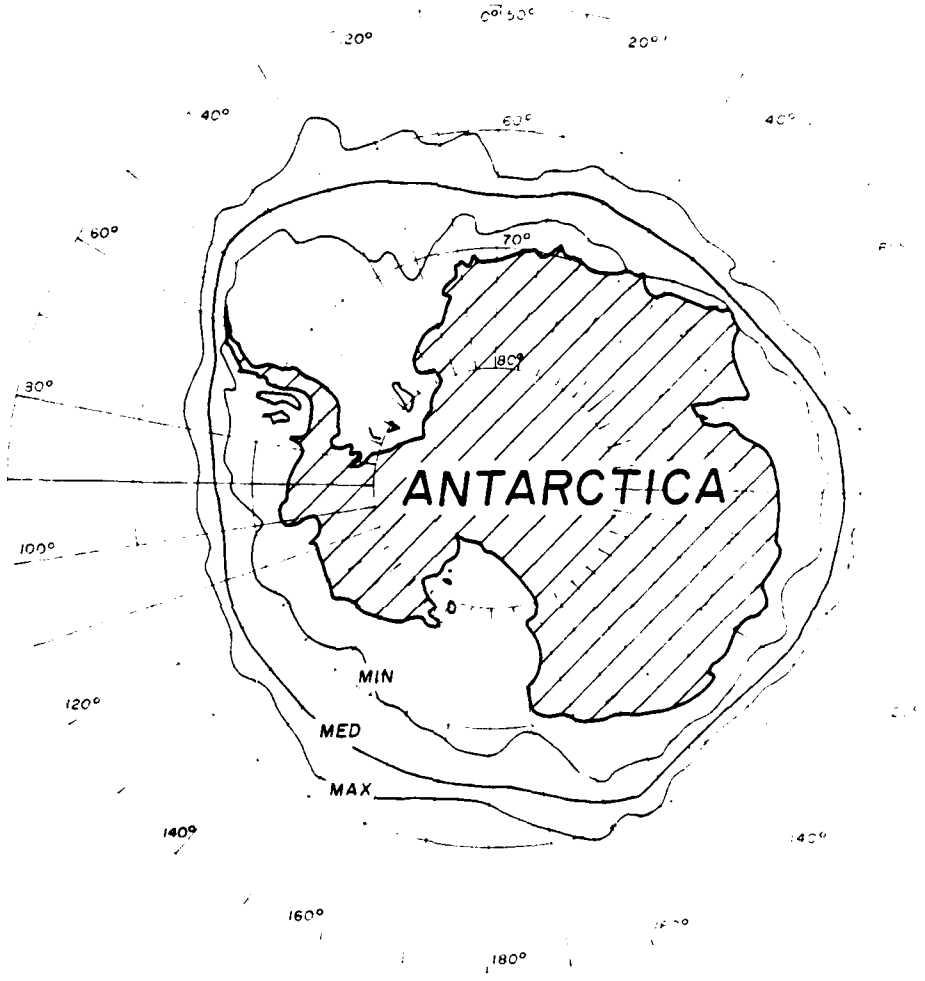

Figure III-18. Statistical Ice Edges in the Southern Hemisphere for June.

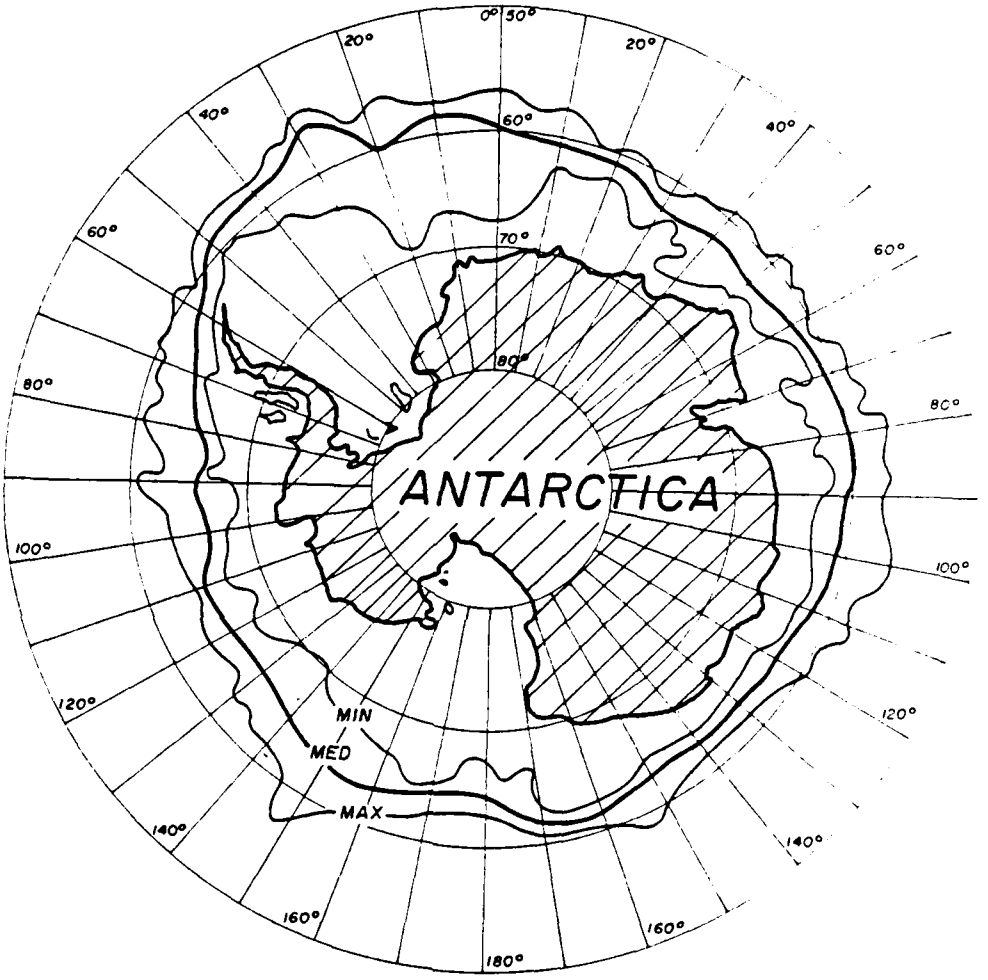

Figure III-19. Statistical Ice Edges in the Southern Hemisphere for July.

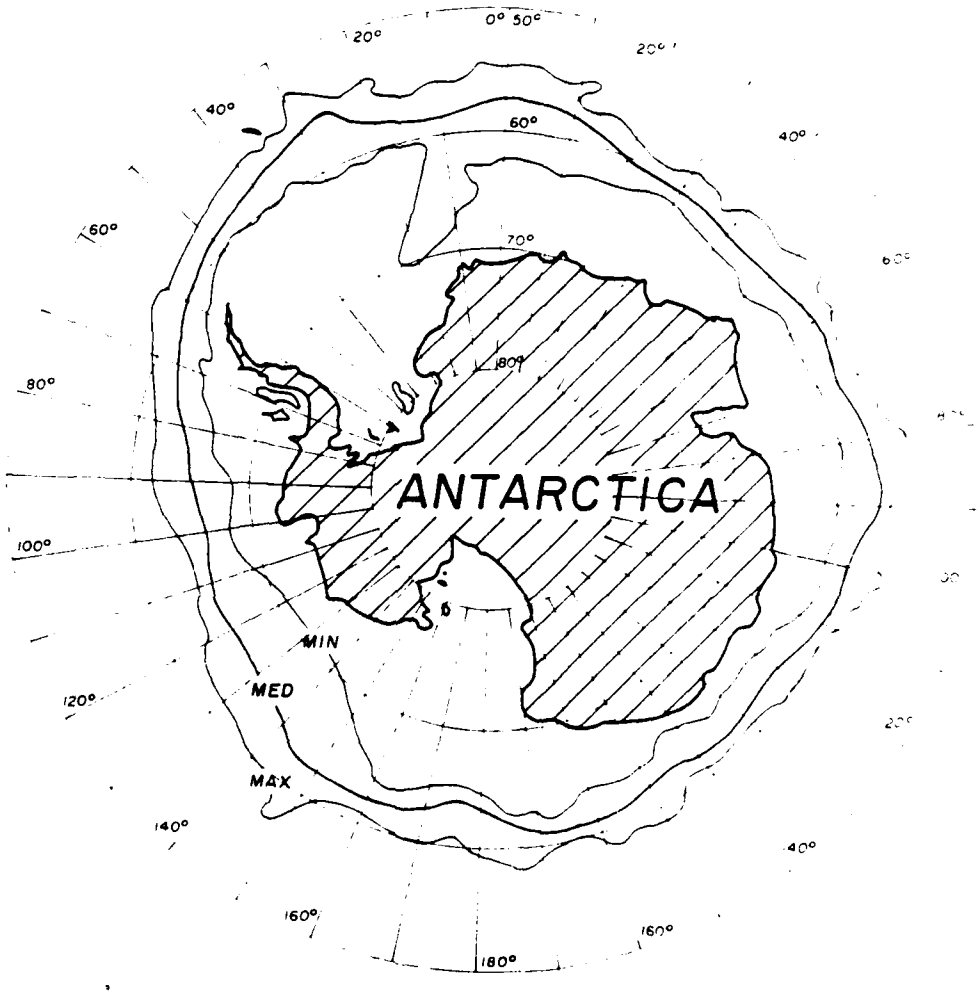

Figure III-20. Statistical Ice Edges in the Southern Hemisphere for August.

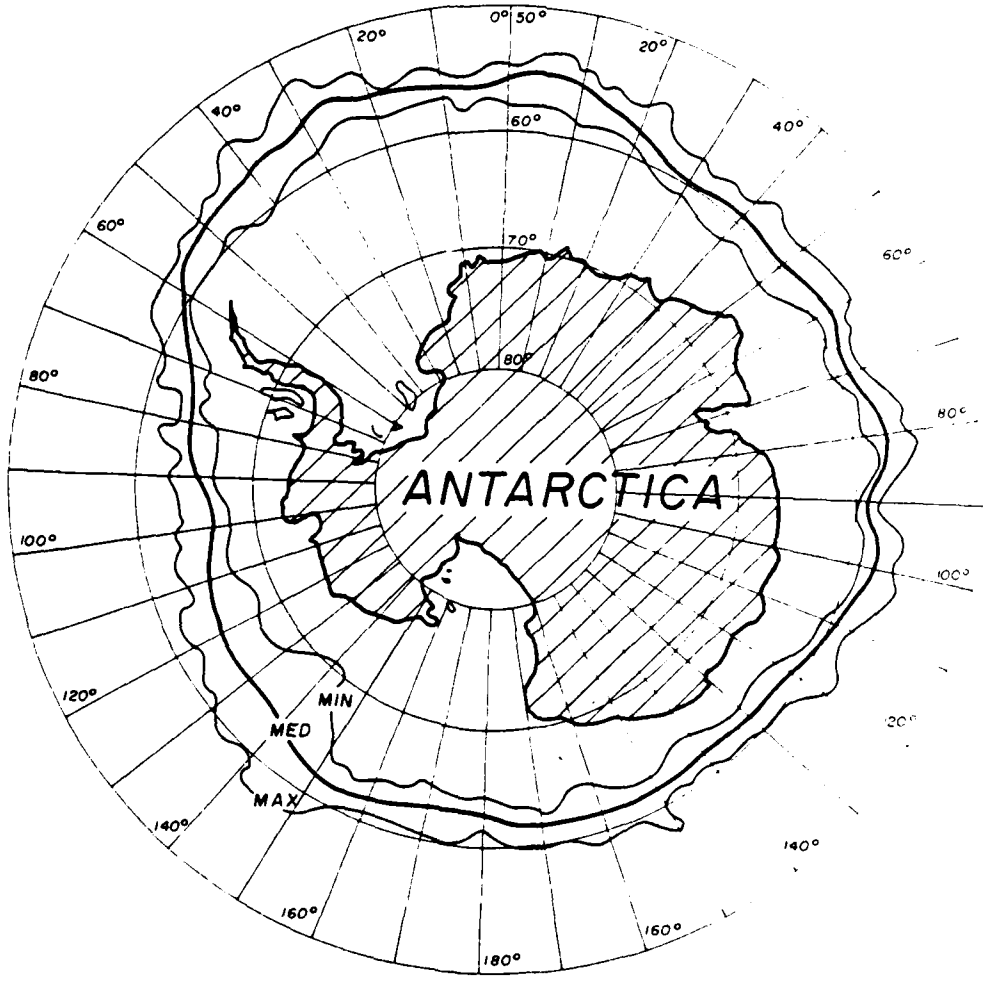

Figure III-21. Statistical Ice Edges in the Southern Hemisphere for September.

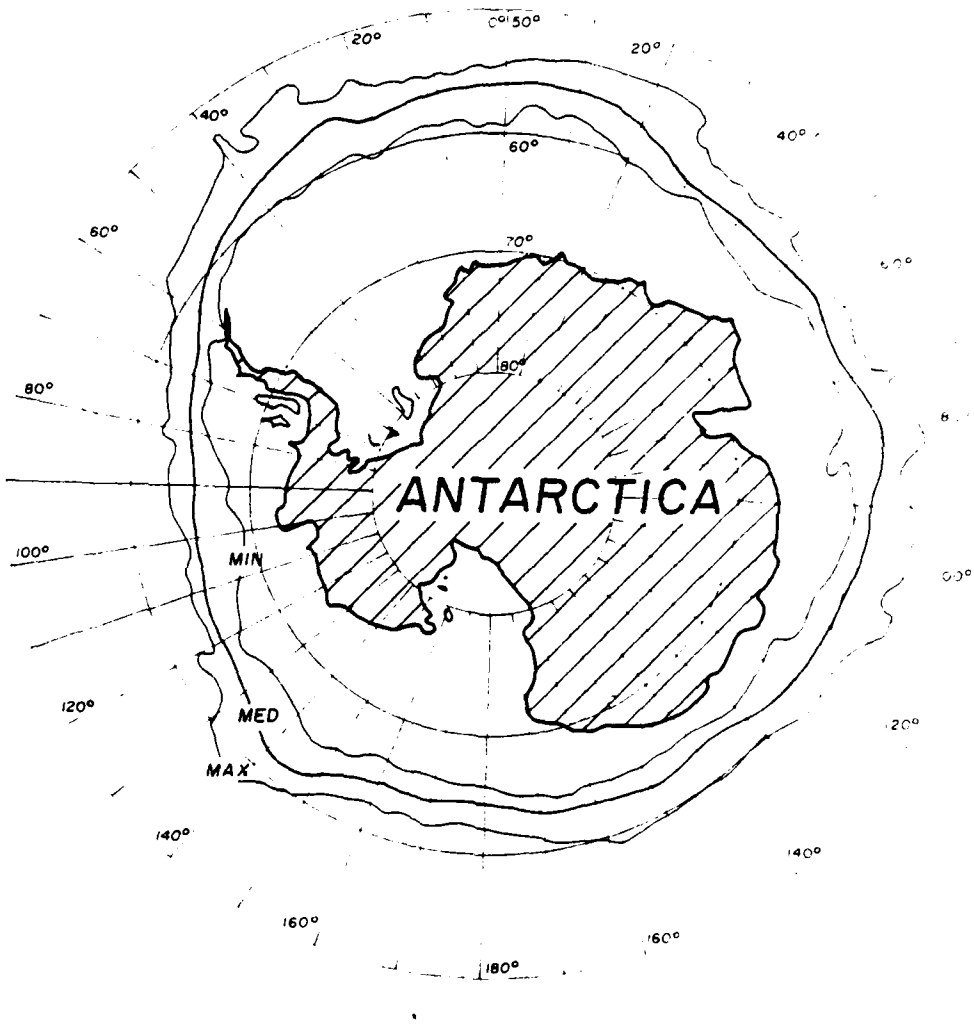

Figure III-22. Statistical Ice Edges in the Southern Hemisphere for October.

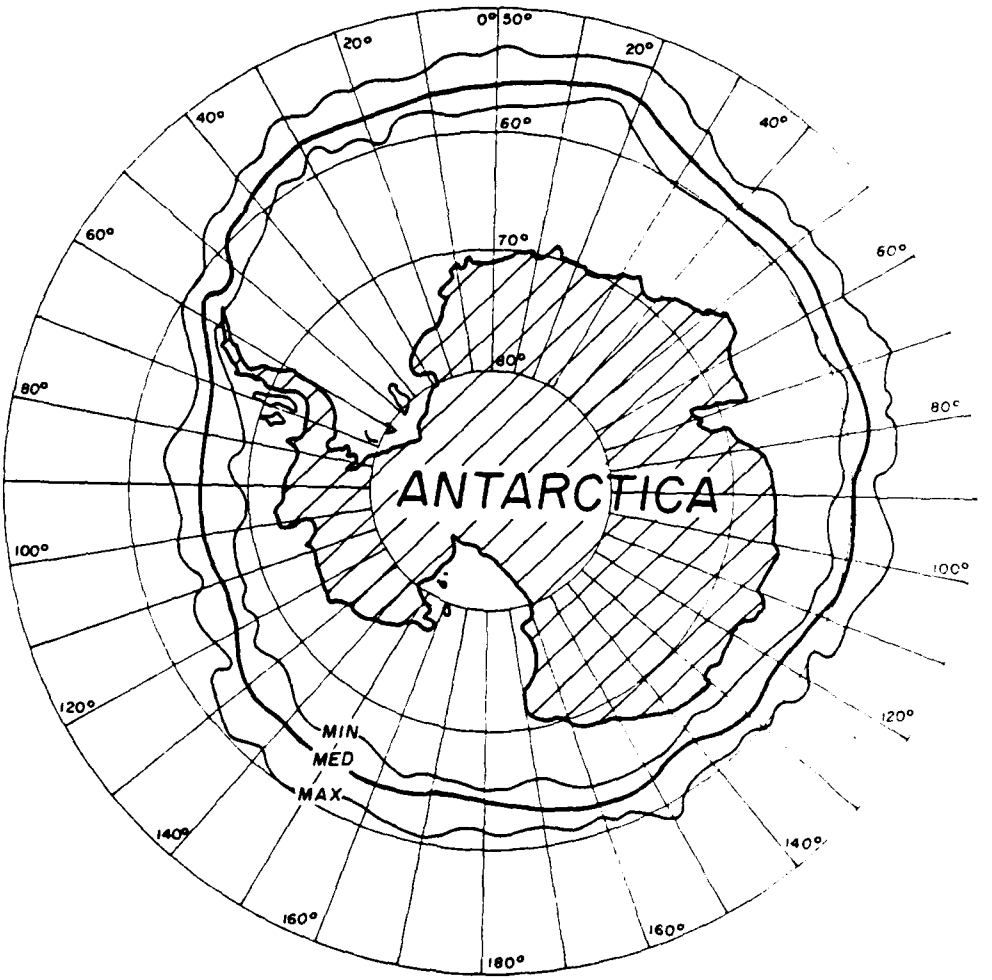

Figure III-23. Statistical Ice Edges in the Southern Hemisphere for November.

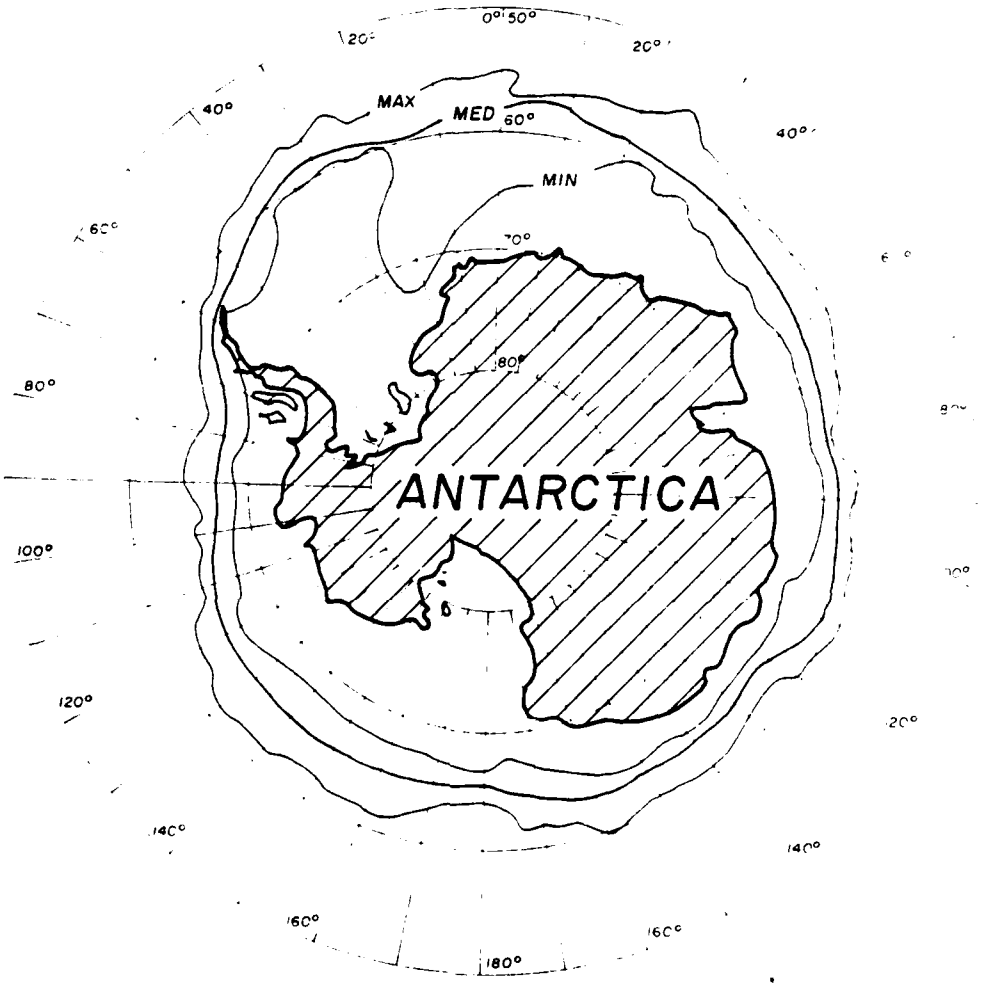

Figure III-24. Statistical Ice Edges in the Southern Hemisphere for December.

2.2 DISCUSSION OF VARIATIONS OF ICE EXTENT IN SOUTHERN HEMISPHERE

Ice extent in the southern hemisphere is at a minimum at the end of the antarctic summer (February-March) and at a maximum at the end of the antarctic winter (October-November). At minimum, the ice extent is close to the coast or ice shelf everywhere except in the Weddell Sea off the Ronne Ice Shelf. While at maximum, the ice has expanded to 60°S latitude in most locations and to 55°S latitude in the Atlantic sector.

Antarctica has two large embayments, the Ross Sea and the Weddell Sea. Both embayments are partially filled with glacial-fed ice sheets: the Ross Ice Shelf and the Ronne Ice Shelf. During summer the ice edge receeds toward these ice shelves, creating the most southerly open water in the Antarctic. When winter arrives, these areas freeze earliest to bring the average ice edge out to an approximate uniform perimeter around the continent. As a result, the absolute amount of ice growth is greatest in these two areas.

As winter advances, the statistical ice extent advances more or less uniformly around the continent except in the regions seaward of the Ross and Weddell Seas. Here the ice advance is statistically greater as the ice covered areas expand under the influence of currents and winds.

This effect is most pronounced in the Weddell Sea area where the ice advances through the South Orkney Islands and into the Scotia Sea. Here the average ice limit becomes greatest, approaching 55 S.

Although its causes are not well understood, a large polynya is often formed in the center of the Weddell Sea. Looking down on a polar projection map, ice development in the Weddell Sea expands in a clockwise fashion as winter advances, very much as would be implied by the currents shown in Figure II-2 showing antarctic oceanic currents. As the ice advances clockwise in the direction shown by the current pattern, a polynya is left in the center of this circular ice advance. This polynya sometimes persists throughout the winter season.

SECTION 3. FACTORS INFLUENCING BEHAVIOR AND EXTENT OF ICE IN SPECIFIC REGIONS

3.1 INTRODUCTION

The following section presents a discussion of ice conditions in several of the major ice affected seas of the world. It is anticipated that other areas will be added as enhancements to this handbook.

The information is intended to begin the education of novice sea ice analysts. Specifically, it is intended to introduce a particular sea of interest and to provide the preparatory knowledge necessary to anticipate the range of ice conditions that occur in the area. An emphasis has also been placed on conditions unique to individual seas and the causal mechanisms involved.

The information presented is almost entirely empirical, based on 17 years of experience with operational weather satellite imagery and 10 years of experience with passive microwave imagery. Minimum and maximum ice limits for the northern and southern hemispheres are shown in section 1 and 2 of this chapter. Sea ice atlases produced by the Naval Polar Oceanography Center (years 1972 to present) will also be useful to the reader. To locate places used in the following discussion, see Figure 1 at the beginning of this publication.

3.2 BARENTS SEA

The Barents Sea is the only soviet arctic sea which is not totally ice covered during the winter. Parameters which play a major role in determining sea ice characteristics and distribution are: (1) the influx of warm Atlantic water (2) the general ocean circulation within the sea (3) predominate southerly air flow (4) the large island groups on the borders (5) bathymetry.

3.2.1 Currents. Even in the most severe winters, the southwest Barents Sea remains ice free. Freezeup is prevented by the relatively warm Atlantic water carried into the sea from the west in an extension of the gulf stream known as the North Cape Current. This current flows eastward in the southern Barents, then divides to send a branch northward along the east coast of Novaya Zemlya. The effect of this branch can be observed frequently during the winter (especially in mild winters) in the form of a northward to northeastward indentation in the ice edge

just west of Novaya Zemlya. There are two other currents which also have a major effect on ice distribution. One current flows southward east of Svalbard and carries old ice in a broad tongue from the Arctic Ocean into the Barents to the vicinity of Bear Island. Another significant current also carries old ice into the sea from the Arctic. This south and westerly setting current enters the Barents just east of Franz Josef Land, then turns westward narrowly along the archipelago. To the west of Franz Josef Land, it turns southwestward as it merges with the south setting current east of Svalbard. Normally, little or no old ice exists in the Barents Sea outside these two current systems. Their influence is quite evident when seasonal melt begins to accelerate in the northern Barents in late June. Because of the greater thickness of the old ice and because of continuous influx of colder arctic water, ice melt in these drift streams lags the melt of adjacent areas. As a result, in average years the Barents becomes ice free south of 80°N latitude between 45° and 55°E by 1 August. However, in adjacent areas to the east and west ice persists southward to 79°N latitude throughout the summer.

3.2.2 Winds. From November through April, the southern Barents Sea is normally under the influence of southwesterly winds as a result of the seasonal deepening of the Icelandic low pressure system. This milder maritime air provides an additional modifying effect which inhibits substantial ice growth in the southern half of the sea. Occasionally, however, southeasterly winds predominate due to an abnormal orientation of the Icelandic low and the Siberian high. If this much colder, continental flow persists during the winter and early spring, ice conditions become abnormally severe (e.g. 1966 and 1976). Nearly 90% of the Barents Sea can become ice covered in these unusual winters compared to about 70% in a normal winter and less than 50% in an unusually mild winter. Because there is a time lag between establishment of these pressure patterns and maximum ice extent, these abnormal ice conditions can usually be anticipated one to two months in advance.

3.2.3 Island Groups. The island groups of Novaya Zemlya, Franz Josef Land, and Svalbard all influence ice conditions in the Barents Sea. Collectively, they provide a buffering effect, limiting interaction

of ice and water masses of the sea with those of bordering ice covered seas. In addition, the location of the Franz Josef Land archipelago affects both wintertime ice distribution and the spring/summer melt pattern within the northern Barents. Throughout the winter a nearly permanent area of weakness exists along the southwest to northwest coasts of the archipelago. Under the influence of normally persistent easterly winds, ice is driven offshore and is rapidly replaced by young and new ice due to refreezing. This polynya frequently extends to more than 100 kilometers offshore from the outer islands. It also has a significant influence on the spring melt. Because the thinner ice within the weakness south of the archipelago melts before the thicker ice to the east and west, and the open water within the lead ceases to refreeze with the warming air temperatures, the entire Barents from the Franz Josef Land to the ice edge becomes ice free by about 1 August.

All of the major island groups of the Barents contain glaciers which calve occasional icebergs. Although it is reported that icebergs have been observed as far south as the mainland coast, they are normally restricted to areas near their source and are quite small and infrequent.

3.2.4 Bathymetry. The Barents Sea has the second greatest average depth of the Eurasian arctic seas. Variations in bathymetry, however, are an important factor in the formation and distribution of sea ice in several areas. There are two areas of particular interest. A group of relatively shallow areas (150 to 200 m) lays between 74° and 76°N and between 35° and 40°E. After about mid-January, an outbreak of colder air from the north can cause new ice formation over these shoals. This formation will many times appear in a circular area isolated from the main pack to the north. With continued cold airflow, the main pack will extend southward to include the ice over the shoal and it will be evident only as a southerly bulge of the ice edge. The southerly extension of the ice edge toward Bear Island is due largely to the southerly setting current east of Svalbard, but here also, bathymetery has a significant effect on ice conditions. Although ice is carried from the Arctic Ocean southward toward Bear Island by this drift current, it is probable that initially most ice in this area is new and young ice. This results from the freezing of relatively cold water which has fully mixed over shoals that are less than 60 m deep in places. It is also probable that these shoals

AD-A145 286 HANDBOOK FOR SEA ICE ANALYSIS AND FORECASTING(U) ALASKA 2/4
UNIV FAIRBANKS GEOPHYSICAL INST W J STRINGER ET AL.
JUN 84 NERPF-CR-84-03 N00228-81-C-H553

UNCLASSIFIED F/G 8/12 NL

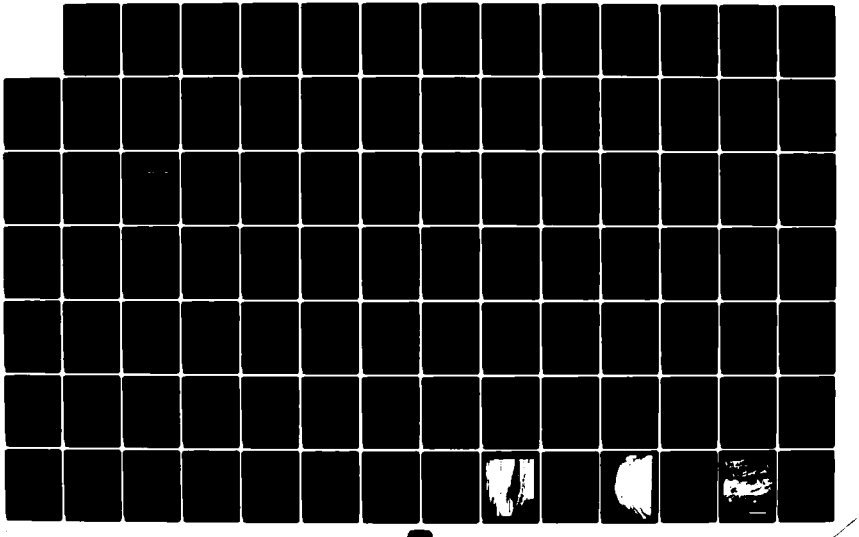

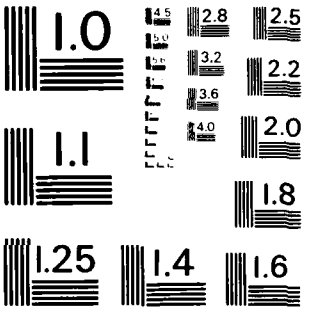

are important in the maintenance of this ice into early summer, while rapid seasonal recession is underway along the remainder of the Barents ice edge.

3.3 KARA SEA

The Kara Sea lays entirely north of the Arctic Circle and is exposed to extremely cold winter temperatures. Beyond this most obvious fact, sea ice characteristics and distribution in the Kara Sea are primarily influenced by four major factors: (1) geography - the Kara's nearly landlocked location (2) southeasterly air flow during the winter (3) river outflow (4) the wide continental shelf in the eastern extremity.

3.3.1 Geography. Warm extensions of the Gulf Stream which influence the Barents Sea are prevented from significantly influencing the Kara Sea by the island of Novaya Zemlya. There is also little interchange between the Kara and Laptev Seas due to the blocking action of the Severnaya Zemlya archipelago. Consequently, with the continent guarding the southern limit of the sea, only the northern opening to the Arctic Ocean allows any significant interaction between the Kara and its neighboring seas.

3.3.2 Winds. From mid-November until late June, little open water exists and even that is transitory. Because of the persistence of southerly winds, ice is constantly removed northward into the Arctic Ocean. Also as a result of this air flow, areas of thin ice are persistently formed to the lee of fast ice boundaries along most of the soviet coasts. Thicker ice is pushed seaward from the fast ice by these winds, and due to refreezing, is rapidly replaced by new ice. This continuous process through the winter results in the thinnest ice normally being found at the fast ice boundary with increasing thickness farther seaward. These areas of new and young ice are prominently visible on satellite imagery (infrared in the dark months and visual in the late winter and spring) and allow the analyst to confidently extract geographic coordinates of the fast ice boundary.

3.3.3 River Outflow. Seasonal breakup begins in late June. Initially the weaknesses adjacent to the fast ice boundary cease to refreeze in the warmer June air and become nearly ice free. These open water areas last only a few weeks, however, because the fast ice then

begins breakup and drifts seaward. The warmer continental waters of the clearing rivers, chiefly the Yenisey and Ob, accelerate melt at first in their estuaries, then in a spreading arc farther seaward. By the ice minimum about 1-15 September, the entire Kara south of 75°N is normally ice free. In extremely mild summers, parts of the sea may become ice free as far north as 80-82°N. An exception to the general south to north ice drift in the Kara is in a southerly setting counter-current along the east coast of Novaya Zemlya. In unusually cool summers, ice continuously fed by this current into the southwest Kara in the vicinity of the north entrance to Proliv Karskiye Vorota fails to totally melt. In those summers ice may be encountered in all but the Yenisey and Ob estuaries and the central portion of the southwest Kara. This uneven and highly variable melt pattern, in combination with increasing cloud cover and a substantial decrease in ice albedo due to surface melt, makes late summer sea ice analysis difficult.

3.3.4 Continental Shelf. As in the Laptev Sea, a wide continental shelf in the eastern Kara provides the mechanics for an extensive area of fast ice. At its maximum in late January until breakup, the fast ice boundary extends up to 100 nautical miles off the mainland and southern Severnaya Zemlya coasts.

3.3.5 Freezeup. Freezeup begins in September with the appearance of new ice in the colder waters of the north Kara. Freezeup in the southern Kara begins in early October where breakup began, in the less saline waters of the estuaries. Rapid freezeup of the remainder of the sea east of 70°E follows. Waters west of 70°E and south of 75°N are more resistant, and in normal years an open water area still exists between Proliv Karskiye Vorota and 100-150 nautical miles northeastward as late as the first several days of November. This open water disappears in late October in severe years, but persists as late as the last half of December in extremely mild years. During the early stages of freezeup, the boundary between the residual first-year ice (which by convention becomes old ice on 1 October) and the new season's growth is relatively easy to judge due to the lesser albedo of the newer ice. As the new ice thickens, however, albedo differences become too small to observe. This fact, combined with the dynamic movement of ice within the sea, renders a confident judgement of the old ice boundary difficult by mid-winter.

3.4 LAPTEV SEA

Sea ice distribution and character within the Laptev Sea are determined by five major factors: (1) an extraordinarily wide continental shelf (2) predominate southerly winter winds (3) the Trans-Polar Drift Stream (4) the Severnaya Zemlya coastal flow (5) the Lena River outflow.

3.4.1 Continental Shelf. From early January until the beginning of breakup in June and July, the Laptev Sea exhibits the widest expanse of fast ice in the world due to its wide continental shelf. Fifty percent of the total area of the Laptev Sea is less than 50 meters deep. South of 76°N, the depth does not exceed 25 meters. Fast ice begins to form in mid-October in the fresh water of the river estuaries and expands to cover most of the continental shelf at its maximum extent up to 155 km from the mainland.

3.4.2 Windflow. This fast ice combines with the normal winter windflow to influence sea ice distribution in the sea still further. Winds persistently push drift ice northward away from the fast ice boundary. Thus, before the moderating temperatures of late May, there is a constant refreezing of newly opened water at the fast ice boundary. This, in turn, is constantly being removed northward. This results in a nearly permanent polynya or area of weakness normally between 10 nm and 60 nm wide at the fast ice boundary. This newer ice is usually removed before reaching more than about 15-30 cm in thickness. Therefore, the polynyas are easily distinguished on imagery. Since they change relatively little in position and appearance during the season, these areas of weakness are not only important sea ice distribution features, but aid in geographic recognition and the gridding of satellite imagery.

3.4.3 Trans-Polar Drift Stream. A third significant factor influencing sea ice distribution in the Laptev is the Trans-Polar Drift Stream which flows from east to west (then turns northwest) across the northern border of the sea. In all but the extreme western Laptev, ice continues its northward drift under southerly winds, becomes entrapped in the Trans-Polar Drift Stream, and is removed from the area. The Laptev Sea is one of the four major Arctic Seas where ice removal is predominate during the winter season. This persistent removal of the thickest ice

and replacement by newer ice quite naturally limits the amount of second and multiyear ice (old ice) found in the Laptev and results in a more extensive summer melt. It is believed that the southern limit of old ice may at times be as far north as 80°N latitude in the central Laptev.

3.4.4 Severnaya Zemlya Coastal Flow. In the western Laptev, along the coasts of Severnaya Zemlya and the Taymyr Penninsula, ice drift is contrary to that elsewhere in the sea. Ice along these coasts is carried southward by the Severnaya Zemlya coastal flow to near the mouth of the Khatanga River. This results in the only significant concentrations of old ice found in the southern Laptev. Since the ice in this coastal band is much thicker, most persists through the summer melt season and would normally present the most serious obstacle to navigation of the southern Laptev during the short summer season.

3.4.5 Rivers. During the months of June to September, a number of siberian rivers discharge fresh, warm water into the southern Laptev, accelerating sea ice melt. The largest of these is the Lena River which accounts for over 70% of the fresh water flowing into the Laptev. In normal years, weakness in the sea ice begins to appear offshore of the Lena delta areas by mid-June. By 1 July a nearly ice free area extends seaward of the delta to about 75°N. Expansion of this ice free area continues until mid-September. At that time most of the sea south of 77°N is ice free except for the areas west of about 117°E where ice usually exists south to 74°40'N in the Severnaya Zemlya coastal flow. Other significant rivers in the area are the Khatanga, Yana, Olenek, and Anabar. Sea surface temperatures may reach 10°C to 14°C at these river mouths. Seasonal freezeup begins in October in the fresher water of these estuaries.

CHAPTER IV. SEA ICE MODELING

One of the principal goals of scientific studies of sea ice is to develop predictive capabilities based on a comprehensive knowledge of sea ice dynamics. Then, given information concerning atmospheric pressure fields, air temperatures, ocean currents and some initial ice conditions, it would be possible to predict future ice growth, movement, and dynamic conditions such as ridge-building events. Such predictions would be based on a model: a set of known relationships among all the relevant physical conditions which, combined with measured environmental parameters, can be used to predict the physical characteristics of the ice cover.

A model need not be so all-encompassing, however. Even a set of curves relating ice thickness to freezing-degree days can be considered a model. More complicated models often require extensive calculations to be performed, and sometimes this is best done on a computer. An example of this is a program used to predict the wind-drift of the ice edge.

A great deal of effort is currently being spent developing models with varying degrees of sophistication to predict ice behavior. The behavior predicted ranges from the value of a simple parameter such as ice thickness to complex matters like the velocity field of the entire ice pack. Because our knowledge of ice and related parameters has increased and because of increased need for accurate sea ice predictions, there is a growing utilization of the more complicated, comprehensive models. The purpose of this chapter is to discuss the general requirements and functions of these comprehensive, computer-driven models so that the ice analyst can develop a background for the application of their results as these models become available.

SECTION 1. MODEL CATEGORIES

As mentioned before, models can range from simple relationships between a single external parameter and a single ice parameter to all-encompassing models relating all external factors with the complete configuration and dynamics of the polar ice pack. In order to discuss models in general, it may be useful to describe the different types of

models in terms of their complexity and capabilities. In this section, we will define such a hierarchy of models.

1.1 FUNDAMENTAL MODEL TYPES

1.1.1 Physical Models. These models use equations based on the laws of physics to predict ice parameters (ice thickness, velocity, etc.) from input environmental parameters (atmospheric temperature, pressure, etc.).

1.1.2 Statistical Models. In these models statistical observations of environmental parameters and ice parameters are used to derive tne equations used in ice forecasting.

1.2 MODEL CATEGORIES BASED ON COMPLEXITY

1.2.1 Single Parameter Models. These are models (either statistical or physical) which relate one environmental parameter with one ice behavior parameter. Many of these models are presented in the form of graphs or simple numerical relationships. Examples of these models include curves such as Figure I-1 which relates tensile ice strength and temperature or Figure I-2 relating freezing degree days and ice thickness.

1.2.2 Multiple Parameter Models. These are models which relate several input parameters with one or more output parameters. These are usually complex models (both physical and statistical) requiring calculations to produce output parameters. The calculations can be relatively simple or computers may be required to produce the desired output.

1.3 MODEL CATEGORIES BASED ON PREDICTED PARAMETERS OR PROCESSES

1.3.1 Ice Drift Models describe the motion of ice under the influence of driving forces (winds, currents, internal ice stresses).

1.3.2 Thermodynamic Models relate ice properties with thermodynamic processes such as rate of ice formation and heat loss by the freezing ocean water.

1.3.3 Ice Strength Models relate external parameters with ice strength. When these models seek to describe ice strength on a regional basis, they take into account the change in strength that results from strain and thermodynamic growth of ice.

1.3.4 Ice Deformation Models describe the deformation of the ice (usually over large areas) as a function of ice strength and stresses placed upon it.

1.4 MODEL CATEGORIES BASED ON SCOPE

1.4.1 Partial Models. It might be argued that all models are partial models. However, this term is generally reserved to describe models which admittedly omit major components which may or may not require addition to accurately describe the particular phenomenon in question. For instance, a partial drift model may describe the wind-drift of ice, but omit long-term oceanic currents. In order to add in this second component of ice drift, an oceanic current model would be required.

1.4.2 Complete Models. These are models which consider all relevant processes and parameters in order to describe oceanic ice within a particular geographic region. (Hence, these are necessarily physical models.) Such models are actually made up of many component models which are made to act together (ice drift, thermodynamic strength, strength vs. strain, ect.). At present there is no operational complete model available for ice prediction.

1.5 ENVIRONMENTAL PARAMETERS

All models require measured values of environmental parameters in order to predict ice conditions. Here we will discuss some of these parameters in terms of how they are obtained and their reliability.

1.5.1 Winds. All ice drift models rely on values for wind speed and direction. Some models require surface winds while others input geostrophic winds directly. Generally, however, surface winds over a large area are derived from the geostrophic winds. Hence, models requiring surface wind input usually require a model for computing surface winds from geostrophic winds.

Geostrophic winds are computed from the atmospheric pressure field which is determined by direct pressure measurements. The accuracy of wind values is, therefore, dependent on the density of pressure measurement

stations. The network of pressure reporting stations has been enhanced in recent years by the presence of drifting buoys placed in the ice pack which report pressure via satellite. When using models dependent on wind fields, it should be borne in mind that considerable error can result in the process of converting atmospheric pressure to winds, particularly in the arctic and antarctic where pressure recording stations are sparse.

1.5.2 Oceanic Currents. Currents play a major role in the movement of ice. In deep water areas, currents are usually not large but can often be the principal factor determining long-term drift. Currents in many deep water areas have been measured over the past hundred years and average values are available from published charts. In shallow areas currents can be sufficiently large to contribute significantly to short-term drifts. These large currents are driven by tides, winds, and the influence of atmospheric pressure patterns. In these cases, the predictions of currents depends on models which themselves can be as complicated as ice drift models. For this reason, most ice drift modeling has been limited to regions not influenced by shallow sea currents.

1.5.3 Surface Air Temperatures. The growth of ice depends largely on surface air and water temperatures. This is not only important in open water conditions where new ice is being formed, but also in floating ice conditions where thickness is increasing and leads are becoming frozen. Extensive surface air temperatures were difficult to obtain in the past, but are now available from satellite imagery (subject to some calibration and atmospheric transmission errors and cloudiness).

1.6 ICE DRIFT MODELS CURRENTLY IN USE AT THE JOINT ICE CENTER

Sections 2 and 3 describe two models which are currently used to predict ice drift. The first was developed by the Pacific Marine Environmental Laboratory, called the PMEL model, for describing ice motions in the Bering Sea. The second model was adapted from work done at the Polar Science Center, Seattle, Washington, and is referred to here as the Fleet Numerical Oceanography Center (FNOC) model.

SECTION 2. PMEL MODEL

2.1 INTRODUCTION

This model predicts ice floe velocities from input surface wind velocities. (Presumably winds are either derived from pressure fields or measured directly.) It is a physical model (containing physical parameters) rather than a statistical model (such as the FNOC model) and was designed for the Bering sea, although it may be applicable elsewhere. A physical model such as this attempts to describe ice motions in terms of actual physical interactions. Notably absent from this model are terms relating internal forces among adjacent ice floes. For this reason, it is termed a free-drift model. Because the Bering Sea opens to the south, is not bounded to the south, and is frequented by winds advecting ice toward the south, it seems reasonable to assume that the ice is often in free-drift. Nevertheless, caution should be exercised when applying this model to nonfree-drift situations such as northerly drifts in compact ice conditions.

2.2 OUTLINE OF METHOD

The method used closely resembles that of Reed and Campbell (1962) which, in turn, was modeled after Shuleikin (1938). The treatment is that of a straightforward problem in physical oceanography. First, it is assumed that the equation of motion is given by the sum of the wind stress, water drag, and coriolis force (all on the ice) set equal to zero. Next, it is assumed the wind stress and water drag are given by quadratic laws: i.e. the wind stress on the ice is proportional (by a constant, C_A) to the wind speed relative to the floe squared, and the water drag on the floe is given by a constant, C_W, times the speed of the water relative to the floe squared. These constants, C_A and C_W, are determined by measurements carried out on ice floes. Wind and water speeds relative to floes in such experiments are usually measured at levels sufficiently distant from the surface that local surface effects are small. These distances are taken here as 10 m and -2 m (below surface) respectively. In this model, it is assumed that the water velocity relative to the earth is generated by the motion of a continuous ice sheet over the ocean surface. Thus, the ice acts as a coupling between the air and

water. Furthermore, it is assumed that this drag-induced current is the only source of ocean movement, although other current components of motion may be added later.

The treatment of the drag-induced current is fairly involved because of the physical oceanographic principles which must be addressed. The ocean is treated as consisting of two layers: a surface turbulent layer moving in the direction of the ice and a deeper layer (called the Ekman layer) whose movement is influenced by coriolis force. The behavior of the surface layer is governed by vertical turbulent mixing (stress constant with depth), and a linearly increasing (with depth) eddy coefficient is assumed. This is a standard treatment for moving fluids near surfaces where turbulent viscosity is responsible for frictional drag. It introduces a constant of proportionality, the Von Karman constant, K, a unitless number which is closely equal to 0.40 for both water and air. The utilization of a linearly increasing eddy coefficient results (through mixing theory) in a logarithmically decreasing velocity profile within the surface layer. The equation relating the surface layer velocity to water stress contains a term involving a roughness parameter, Z_W, which is in turn determined by the water drag coefficient, C_W. Hence, C_W remains the pertinent observational parameter. In addition, another quantity, the friction velocity, determined by the water stress, is identified here. It is assumed that the surface layer extends to a depth, H, which is a constant fraction of the much thicker Ekman layer thickness. This fraction, δ, must be specified when the model is utilized.

In the surface layer the eddy viscosity coefficient was taken to change linearly with depth while the stress was constant with depth. This is a relatively thin layer where vertical turbulance is the prime mechanism for momentum transfer. Now in the much thicker Ekman layer, it is assumed that the mixing length is constant (i.e. the turbulent eddies remain constant in size). Therefore, the eddy viscosity coefficient is constant. However, it is assumed that here the stress does vary with depth. Furthermore, because the mixing length is constant, the Ekman layer can actually be thought of as a series of interacting thin sheets, each obeying the general equations of motion for a fluid subjected to a surface stress. These equations of motion must include a coriolis term.

The effect of this term is that starting just below the surface layer, the top Ekman sheet is driven 45° to the right$_{(n.h.)}$ by the coriolis effect. Through eddy viscosity, this sheet imparts a stress to the sheet beneath it. However, the coriolis effect drives it to the right of this applied stress so that this sheet is driven a little more to the right than the sheet immediately overhead. Thus, each successive sheet within the Ekman layer is driven further to the right than the sheet immediately above, creating a spiral pattern of the velocity vectors. This spiral effect is called the Ekman spiral.

The important contribution to this model from the Ekman layer is the velocity of its top sheet. This velocity is added to the velocity of the surface layer to obtain the water drag velocity on the underside of the ice.

The Ekman layer velocity is derived through solution of a differential equation set up to describe the ocean's motion within the Ekman layer. This velocity is given by a relationship among the water stress, the coriolis factor and a constant of integration, the Ekman depth. This is the depth at which the Ekman spiral velocity reaches a very small fraction of the water velocity at the top of the Ekman layer. The Ekman depth has been found to be proportional to the square root of the water stress by a constant of proportionality known as the Ekman scaling factor (A). This quantity as been the subject of considerable speculation in published literature and remains an important variable in this model. Its value appears to be in the vicinity of .3 or .4.

The relationships described above can be combined into a set of three equations with three unknowns (water stress, the velocity of the ice, and the friction velocity). The equations are nonlinear, but coupled. These equations are actually vector equations and, therefore, consist of real and imaginary parts. The solution is obtained by taking as a first guess the stress applied to the surface layer by the ice as a product of the water density, the air/ice drag coefficient, and the velocity of the air (10 m above the ice). (In other words, it is assumed that the wind stress above the ice is simply transmitted to the water). This value is used to determine a value for the friction velocity which, in turn, is used to determine a value for the floe velocity. This is

then used to produce a new value for the water stress. This new value will very likely be different from the first guess value. The new value is used to determine a second value for the friction velocity and, in turn, floe velocity, and finally a third value for the water stress. This iteration process is continued until successive values for the water stress differ by less than 0.001%. This usually requires five to seven iterations.

2.3 DISCUSSION

This physical model requires a variety of input parameters. Some of these are well known (air, water, and ice densities; coriolis parameter; Von Karman constant). Some are the result of difficult measurements [air/ice drag coefficient (C_A), ice/water drag coefficient (C_W)]. Some are based on reasonable estimates [the ratio of surface layer to boundary layer thickness (δ), the Ekman depth scaling factor (A)], and some are input environmental parameters: the ice thickness, (H_I), and the air velocity at 10 m height, ($\vec{V}_A$).

In principle, such a model has the ability to take into account such variables as ice thickness and upper and lower floe drag characteristics, and even such relatively obscure factors such as variations in δ and A. For this reason a physical model is a useful research tool as well as a forecasting program. However, there can be liabilities as well. The model must be tested over a wide variety of conditions in case some term in the governing equations contributes highly unlikely values under unusual conditions. Also, conditions may be encountered that were not included in the physics represented by the model and the model simply will not be able to take those conditions into account. Therefore, persons using this model to predict ice movement should exercise caution when unusual input values are used. In addition, it should be recalled that the only currents included are those created by the movement of ice above the ocean. Ordinary oceanic currents, tidal currents, and atmospheric pressure-driven currents are not included (but certainly can be added).

Sensitivity tests were performed to determine how various input parameters affected output results. One test, however, showed that the ice drift speeds were quite sensitive to A, the Ekman scaling factor. Increasing the scaling factor increases the Ekman depth and, as might be

expected, this decreases the ice speed. (A deeper Ekman layer means that the wind stress must move more water.) The value assigned to this parameter will be an important feature of this model.

SECTION 3. FNOC "FREE-DRIFT" ICE MODEL

This model is intended as a replacement for the Skiles "free-drift" model. The term "free-drift" needs some discussion here. A true free-drift model is one which models the motion of ice floes with no interactions between floes. If such a model were a physical model (such as the PMEL model), there would simply be no terms in the equations relating to the physics of floe interactions. If the model were statistical (such as this one), the data set would only include situations where the ice floes were not interacting and were clearly in free drift. That is not the case in the FNOC ice model. This model and the Skiles model are based on the assumption that a great number of observed ice motions can be described statistically by only taking the local geostrophic wind into account. This implies that the components of floe motion due to contact forces among floes, wind stress, and water stress are all described to some extent by a single statistical relationship. Furthermore, it is assumed that all these components are directly related to the geostrophic wind. The validity of this assumption is determined by the degree to which the resulting ice drift relationships describe the range of ice motions observed. It is probably more appropriate to refer to this model as a statistical drift model, omitting the word "free".

This model is based on research performed by Thorndike and Colony (1982) on the motions of satellite-tracked position buoys drifting with the arctic ice pack. In addition to providing position information, each buoy contained a barometer, providing needed data to the otherwise sparse network of atmospheric pressure measurements.

In this model, the drift of ice is statistically related to the geostrophic wind. This means the assumption has been made that the atmospheric boundary layer and water drag act in a sufficiently regular way to provide a simple response on the part of the ice to varying geostrophic winds. In fact, the procedure used was to assume that the geostrophic wind only provides a linear modification to the floe velocities:

$$\vec{U} = A\,\vec{G} + \vec{C} + \vec{\varepsilon}$$

where $\vec{U}$ is the vector floe velocity

$\vec{G}$ is the geostrophic wind velocity

$\vec{C}$ is the mean ocean current velocity

$\vec{\varepsilon}$ is the vector residual

A is a complex number, $\mathbf{A} = |A| e^{i\theta}$

It is assumed that **A** is the same for all floes. $|A|$ is the scalar drift coefficient and θ is the vector drift turning angle. This equation was used to describe the motions of a large set of floes for which the individual values of $\vec{U}$ were known from the position buoys and the values of $\vec{G}$ were derived from the atmospheric pressure field. The values of $|A|$, θ, and $\vec{C}$ were determined by least squares fit. In each fitted example a value, $\vec{\varepsilon}$, which was not accounted for by the geostrophic wind or current remained. These values are called residuals.

The method used data from the entire arctic basin for a period of two years. The process assumed that the currents would be constant at each location so that variations from the average ice velocity would be proportional to **A** times the geostrophic wind. Since each calculation would yield a different value of **A**, the average of these values was taken as the derived value of **A** and the variations from this average as $\vec{\varepsilon}$. (Note that each drift measurement would then produce a different value of $\vec{\varepsilon}$.)

Values of **A** were found over the whole arctic basin for the winter-spring, summer and fall season. As might be anticipated, the values varied with season. $|A|$ ranged from 0.0077 for winter and spring to 0.0105 for summer and θ ranged between 5° and 8°. This FNOC model applies the average results: $|A| = 0.008$, $\theta = 8°$ to all cases. It was estimated that using these values would explain 70° of the variance from the mean ice velocity.

This analysis produced one set of average current values for 207 grid points in the arctic basin. It should be pointed out that these values are not actual current measurements, but the steady state component of ice motion remaining after the geostrophic wind-driven component has been subtracted. However, whether these values are actually related to currents or not is irrelevant because this model is purely statistical in nature and these values simply represent a steady state ice drift

which occurs when geostrophic winds are balanced out.

The computations also resulted in values of $\vec{\epsilon}$, the vector residual. This term is a measure of the portion of ice velocities which are not described by the steady drift term or the geostrophic wind term. (This portion was 30%.) Estimates of the sources of error indicated relatively small contributions due to errors of ice velocity and geostrophic wind and a larger contribution due to "neglected physics". This is the portion of motion due to contact forces between floes not contained in the geostrophic wind and current terms.

The scalar value of the residual is ± 4 cm sec^{-1}. This is the size of uncertainty which should be placed on floe speeds derived from this model. Furthermore, it should be emphasized that this error and errors in θ accumlate so that after a few days the total accumulated error can become very large. Thus, this model is only intended for use as a short-term forecasting tool.

SECTION 4. COMPARISON OF FNOC AND PMEL MODELS

These two models are good examples of the differing approaches which can be taken to model ice motion. The FNOC model is based on the statistical relationship between pressure field derived geostrophic winds and ice motion while the PMEL model is based on the physics of ice motion taking into account wind and ocean drag coefficients and a host of related parameters. Ultimately, however, the PMEL model is also driven by winds derived from the barometric pressure field. Both of these approaches have strengths and weaknesses which we will explore in the following paragraphs.

The statistical model (FNOC) used here utilizes only one drag coefficient and turning angle for all cases (although this could be very easily modified). Clearly then, as currently implemented it will not take into account varying ice, oceanographic and meteorological conditions other than geostrophic wind velocity. On the average, the results of short-term predictions will be 70% correct. The user must be careful to recognize situations which may have been rare in the statistical data base used to generate the coefficient and turning angle because there is a good possibility that prediction errors in these cases will be large. For instance, this particular model is based on ice motions measured in the arctic basin at distances far (400 km) from effects of shoreline interaction. Most of the measurements were, therefore, taken at points well within the ice cover. This model should not be expected to predict the motion of the ice edge nearly as well as it predicts ice motions within the ice cover.

The physical model can, in principle, predict ice motions over a wide range of conditions subject to two basic limitations: the physical situation described by the equations of interaction must apply and one must know the values of the various parameters to be used. The ranges of some of these parameters are not particularly well known and, even in cases where there is knowledge about their range, it is not always possible for the ice analyst located far away to know which value applies in a particular situation. In the end, for practical work, average values are used for many of the specified parameters.

There is a major difference between these two specific models which should be borne in mind. The FNOC model is based on arctic basin drift ice statistics, and consequently, the interaction between adjacent floes is implicitly included to the extent possible by the complex linear drift coefficient. The PMEL model was explicitly designed to describe an ice cover in free-drift and was tested against Bering Sea ice motion data (where there is good reason to suspect that free-drift occurs a good deal of the time). It is, therefore, improper to test one model against the other since they actually describe different situations in different regions. We might anticipate, however, that the PMEL model would not work well in the Bering Sea during nonfree-drift situations and that the FNOC model (as implemented) might not work well in truly free-drift situations in the polar pack, for instance near the ice edge during summer.

It should be emphasized that neither model attempts to describe ice movement in the vicinity of shore (not within 400 km in the FNOC model) and that neither takes currents completely into account. The FNOC model explicity uses a long-term average floe motion term and implicity includes floe-motion induced currents in the complex drift coefficient. The PMEL model explicitly includes the floe-motion induced currents, but no others. The excluded short-term arctic basin currents may not be a significant problem for the FNOC model, but the effects of currents in the shallow portions of the Bering Sea region should be added to results of the PMEL model except, perhaps, in the case of extremely high ice velocities.

CHAPTER V. REMOTE SENSING PRINCIPLES AND TECHNIQUES

The purpose of this chapter is to acquaint the reader with the principles and techniques of remote sensing. Sea ice studies and prediction routinely use a wider range of remote sensing techniques than any other environmental surveillance effort. The objective here is to develop a general background so that the reader understands how the various instruments function, and independent judgement is possible. In order to do this, we will examine the general principles of remote sensing: the properties of electromagnetism as it relates to remote sensing and remote sensing systems, the interaction of electromagnetic radiation with the earth's surface - particularly snow, water and ice, and finally, the characteristics and terminology of remote sensing systems. Chapter VI will describe in detail the characteristics of systems used in sea ice analysis.

Section 1. GENERAL PRINCIPLES OF REMOTE SENSING

1.1 USE OF ELECTROMAGNETIC RADIATION FOR REMOTE SENSING

Aerial photography was the earliest form of remote sensing other than the telescope. For a long time, this technique relied on the portion of electromagnetic radiation used by our eyes (the visible spectrum). Early aerial photography was usually obtained on black and white film which responded to light over a broad range of visible light. Later, it was learned that by placing a filter in front of the lens which would pass only a particular color of light, a black and white record could be made of the objects reflecting light in that range. For instance, an aerial photograph of a developed area with a red-passing filter would show bare ground and many man-made surfaces which reflect a significant amount of red light. Hence, this photograph would be useful for identifying man-made features. This technique is used by the Landsat series of satellites today.

Later, as color photography became available, color film was used in aerial photography. Again, filters could be used to enhance particular features.

1.1.1 Near Infrared Aerial Photography. During the second World War there was a need to detect camouflaged objects. Although a great deal of aerial photography was obtained, it was often difficult to detect objects which had been painted green or had been covered with cut tree branches. Some experimental film was developed which responded to to light in the near infrared portion of the spectrum, light just a little more red than the red light detected by the human eye. One of the anticipated uses for this film involved the monitoring of healthy vegetation whose chlorophyll reflects the near infrared extremely well. This film was simply a black and white film with extended sensitivity which would record the near infrared if the visible light was filtered out. Later, a color film was developed which responded to the near infrared as well as visible colors (except blue). This was called color infrared film.

1.1.2 Growth of Remote Sensing. Encouraged by these results, efforts were made to utilize other electromagnetic wavelengths such as heat infrared, microwave, and radar for remote sensing purposes. Here the topic becomes complex because the radiation does not behave exactly as light does and it is not quite as simple to understand as the near infrared.

1.1.3 Imaging Satellite Systems. Another important factor in the development of remote sensing, particularly for ice surveillance, was the development of satellite systems which routinely return images to earth. The first of these systems operated in the visible portion of the spectrum because existing television technology was most easily applied there. Quickly, however, systems were developed to make use of other portions of the electromagnetic spectrum. At this time, satellite remote sensing systems based on radar were being developed.

1.2 ACTIVE VS. PASSIVE SYSTEMS

1.2.1 Source of Electromagnetic Radiation. One of the most important distinctions among remote sensing systems involves the source of the radiation used. The easiest example to use is that of a camera. When a camera is used utilizing sunlight or even ambient light in a room, it is said to be a passive system. On the other hand, when it utilizes flash bulbs, it is an active system. That is, an active system provides

its own radiation. Ordinary radar is an active system, while imaging near infrared systems are passive systems. Passive systems are used when there is sufficient illumination of the object of interest to allow detection. Active systems are used when there is insufficient radiation and it must be provided. A second reason for using passive systems is in situations where the radiation given off is not used for imaging alone, but also quantitatively describes properties of the object. Thermal infrared is an example here. The radiation measured is related to the temperature of the object.

1.2.2 Transmission through the Atmosphere. In all these systems it is necessary for the radiation to pass through the atmosphere (once for passive systems, twice for active systems). Therefore, it is sometimes necessary to keep in mind the interaction between the atmosphere and the radiation. Perhaps the best example of this is the scattering of blue light by the atmosphere. Blue light is actually scattered out of the beam from the sun. It is then scattered toward us from all directions. If blue light were not scattered, the sun would look white instead of red and the sky would be transparent. (We would see stars in the daytime; shadows would be very pronounced.) Ultraviolet light is somewhat "bluer" than blue light and it is scattered even more in the atmosphere than blue light. Furthermore, ultraviolet light will expose photographic film. On a bright day this scattered ultraviolet light will fog a photograph of distant objects. In order to avoid this, we use a filter which passes visible light but not ultraviolet light (called a UV filter). The utilization of almost every remote sensing system used requires some consideration of the transmission and scattering properties of the atmosphere for a particular wavelength. These problems will be discussed where appropriate.

1.2.3 Interaction with the Earth's Surface. A major aspect of interpretation of remotely sensed data is the nature of the interaction of radiation with the earth's surface. Each kind of surface material has its own signature. For instance, a water surface absorbs the near infrared and reflects a fair amount of green light. Snow reflects both. While it is possible for the observer to catalogue these signatures, occasionally he will encounter an object whose signature is puzzling. In those cases it may be necessary to play "detective" and consider the

aspects of the surface which may be producing the signature observed. For instance, the unusual occurrence of a rainstorm upon snow-covered sea ice may create an area with unusual absorption in the near infrared. It is not likely that this signature would be listed in any reference manual.

The nature of the interaction of radiation with the earth's surface can be quite different for active and passive systems. Passive systems depend on illumination from a natural source, usually the sun or radiation emitted from the object. In this case, the angle of illumination is different from the "look" angle. However, usually there is sufficient illumination that there are few total shadows. Actually, we are quite used to this situation since we experience it daily. Most active systems depend on radiation emitted and reflected directly back to the source. This can create effects we do not experience on a daily basis. Consider how things look to you when using a flashlight on a dark night; shadows are troublesome. Yet, this is how the earth looks on airborne imaging radar.

1.3 *LIMITATIONS OF REMOTE SENSING SYSTEMS*

1.3.1 Scale Limitations. There can be a tremendous amount of information available to a remote sensing system. Imaging systems in particular often have more data available than they can collect and transmit back to earth or that can be processed when returned to earth. As a consequence, there are often compromises struck among data resolution, area covered, and frequency of coverage. These compromises can be a cause of some frustration to the image user.

1.3.2 Picture Element Size. There is one feature common to all imaging remote sensing systems which has a direct influence on the analysis of the imagery. This is the size of the picture element, the pixel. Perhaps the best example of pixels comes from photography. Photographic film contains many small silver halide crystals. Exposure to light causes the transparent silver halide crystals to become opaque silver crystals. The objects we see on photographic film are actually composed of many of these silver crystals. These crystals impose the limitation on the size of a clear enlargement which can be made from the

film. The reason that enlargements look "grainy" is that the individual crystals on the original film are becoming separately visible. Obviously, it takes many silver crystals to define an object. For instance, a hundred crystals may be necessary just to make an object identifiable as a human being.

Satellite remote sensing systems divide the earth's surface into an array of rectangular pixels and transmit back to earth a digital signal defining the amount of electromagnetic radiation received at the satellite from that pixel. The size of the pixel on the ground defines the limiting resolution of that particular remote sensing system.

It should be clear that in order to "see" something on an image, its minimum size must be comparable to the size of the pixel. This concept will be discussed in more detail in a subsequent section.

1.3.3 Measurable Levels of Radiation. The interpretation of remotely sensed data is ultimately limited by the amount of radiation received by the recording system. Although some "image enhancement" and even pattern recognition logic can be applied, no magic is possible. This seems like an obvious statement, but very often one finds persons engaged in analysis of remotely sensed data, attempting to identify features or surface cover types when the information needed for their distinction was simply not available to be recorded. Either the reflectance or emission of the object or surface type was not distinctive compared with its surroundings or it was too subtle to be recorded. Occasionally, the analyst must ask himself if there really was a distinctive signal difference available to define the target of interest in the first place. If a negative answer is obtained, a great deal of time may be saved. Later sections will give background material upon which to make such judgements.

1.3.4 Other Limiting Factors. There are many factors which can limit the ability to receive the desired signal even if an adequate signal did originate from the earth's surface. In the case of visual signals, clouds are an obvious example. Clouds can be present over a specific study site a good deal of the time. Figures V-1 and V-2 show the average percent cloud cover over the north polar region during January and July. Examination of the January map shows that the lowest percent cloud cover (35%) is over the central arctic basin. However,

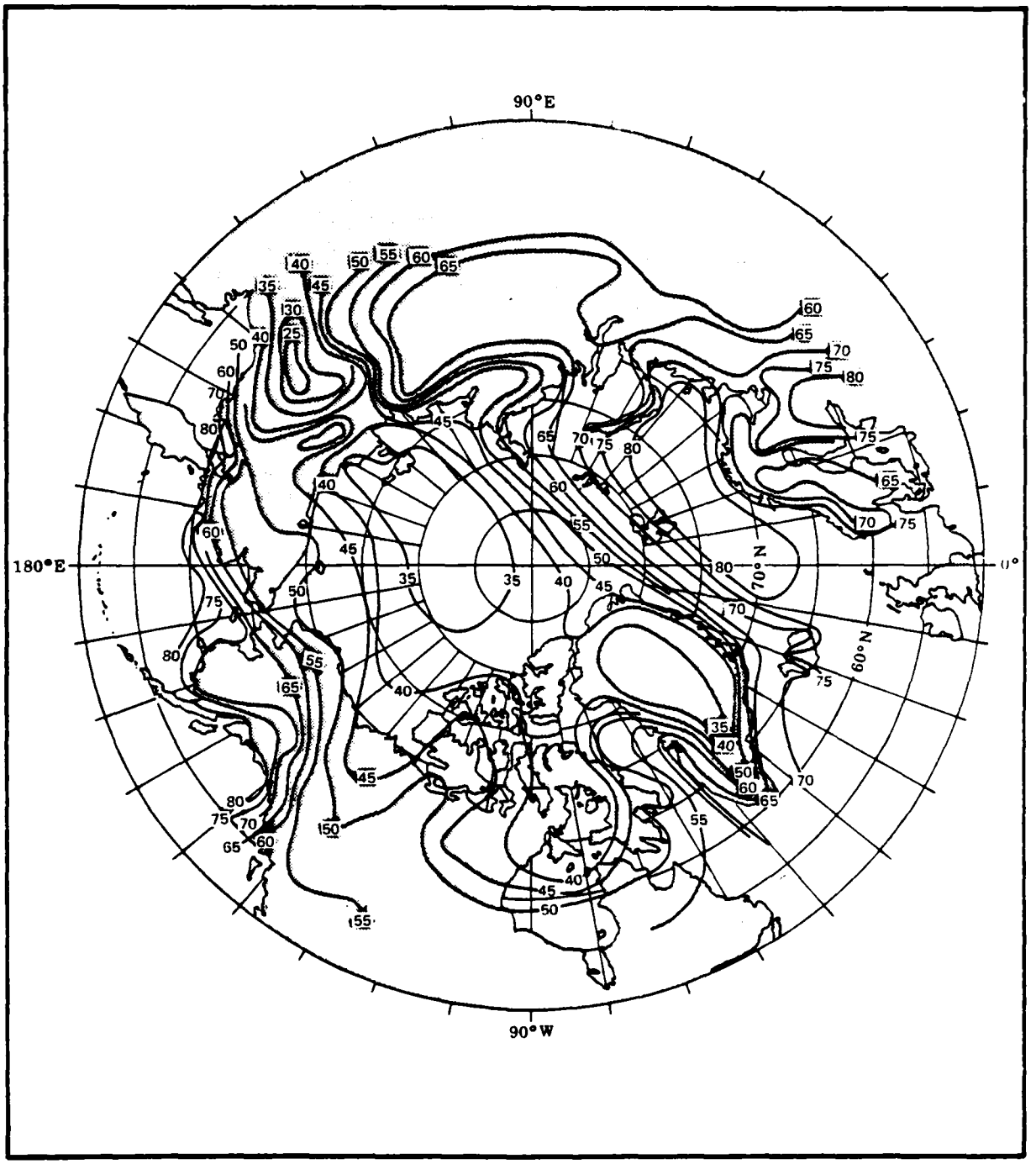

Figure V-1. Arctic Regional Cloud Cover (Percent) for January.

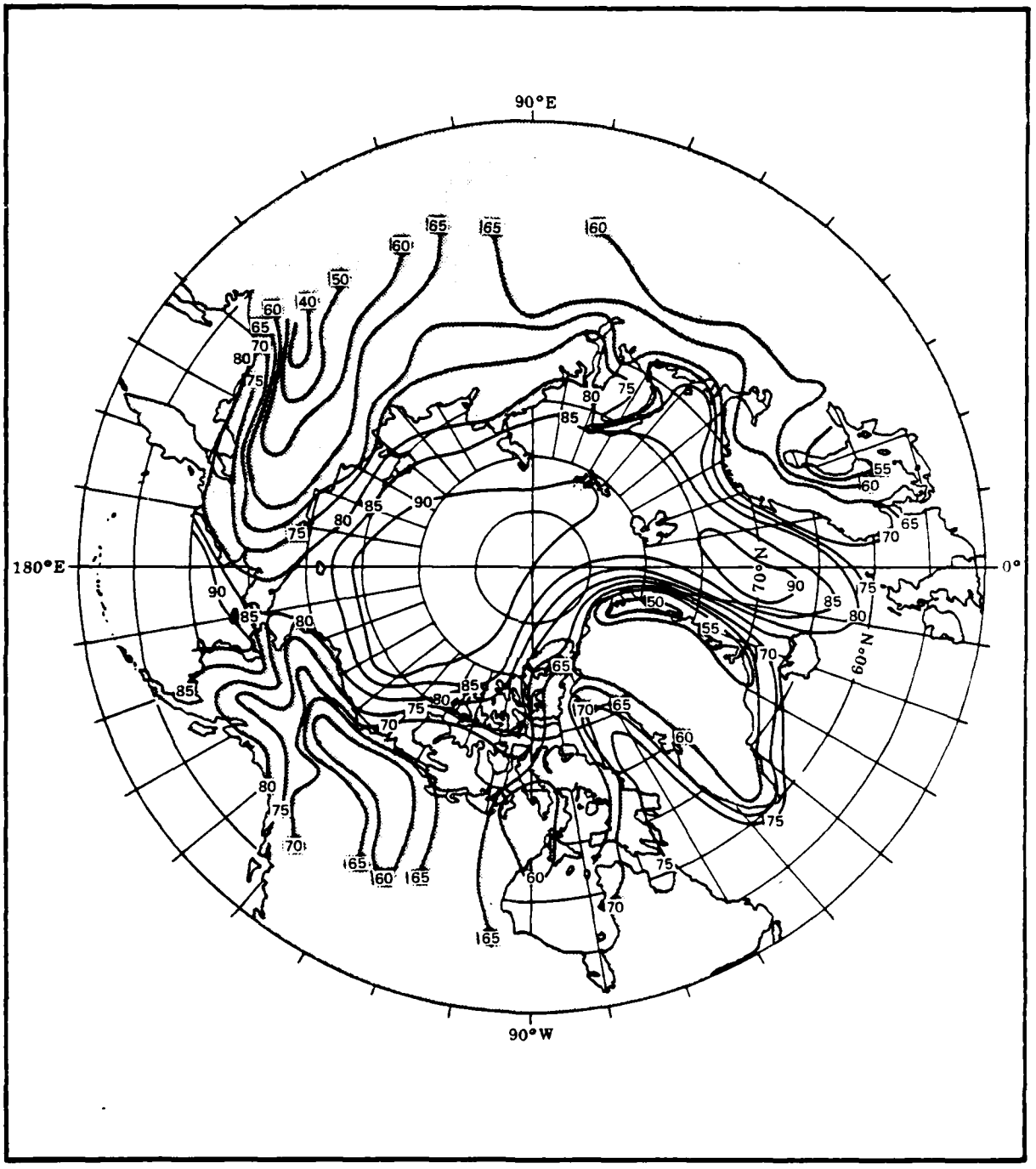

Figure V-2. Arctic Regional Cloud Cover (Percent) for July.

cloud cover over the marginal ice zones where ice edge data is particularly important at this time of year is as high as 80%. Examination of the July map shows a high percentage of cloud cover everywhere. As opposed to the January map, the highest percent cloud cover is now over the central arctic basin (90%). As a result, the cloud cover over the summertime marginal ice zone is also high.

In addition to cloudiness which totally obscures the ice, there are times when thin stratus clouds or surface fog only partly obscures satellite imagery making interpretation of ice features difficult. Many times the presence of these thin cloud forms is not noticeable until imagery is examined in detail. The result, however, is a reduced data content which may not be extremely obvious. Other remote sensing methods also have limitations that are specifically linked to each method. These limitations will be discussed in Chapter VI.

SECTION 2: ELECTROMAGNETIC RADIATION

2.1 BACKGROUND

Experiments with electricity and magnetism in the 1800's developed a body of knowledge which led James Clerk Maxwell to predict in 1886 on purely theoretical grounds that it might be possible for electric and magnetic fields to combine, forming self-sustaining waves which could travel great distances. These waves would have many of the behavior characteristics of waves on water (reflection, refraction, defraction, etc.) and would travel at the speed of light.

These properties gave rise to the possibility that light was an electromagnetic wave, but at that time, there was no proof that electromagnetic waves really existed. In 1888, Heinrich Hertz built an apparatus to send and receive Maxwell's waves. In this case the waves were around 5 meters long. The apparatus worked and, in addition, proved that the waves could be polarized which turns out to be an important property from a remote sensing point of view. After this, it was learned that light, x-rays, infrared, ultraviolet, radio, microwaves, and gamma rays were all electromagnetic waves. The only property dividing them was their wavelength ranges. The names for these divisions arise from the interaction properties each wavelength range exhibits. (For instance, we see light, radio waves are useful for communication, x-rays pass through objects, etc.)

Long before the wave description of light was developed by Maxwell, Sir Isaac Newton had also considered it and discarded the idea. The waves Newton considered were not electromagnetic, but compressional waves in the space-filling ether. Newton's reasoning was sound and based on the fact that the ether waves could not have some of the properties of light which had been observed. (Electromagnetic waves can have these properties.) Instead, he reasoned that light was composed of a vast flow of very tiny particles or corpuscles called photons. He was able to show that the flood of photons could have the known properties of light.

The discovery of electromagnetic waves created the suspicion that the photon concept was incorrect. However, in 1905, Albert Einstein was able to show that no matter how light travels from place to place, it is

emitted and absorbed in small packets of energy (photons again). As a result, electromagnetic waves are dichotomous. They are emitted and absorbed as particles, but travel as waves. Scientific thought concerning this paradox continues to the present. Each representation has been found to have its particular utility.

2.2 CHARACTERISTICS OF THE ELECTROMAGNETIC SPECTRUM

2.2.1 Photon Description. It is useful to think of radiation in terms of photons when considering concepts like detector efficiency, the number of photons required to produce a recognizable signal. Many modern radiation detectors actually count (at ultra high speed) photons as they arrive and send these counts back to earth in digital form. These counts are useful when determining quantities such as signal-to-noise ratios. They are used to answer the question "Is a useful signal even theoretically possible from that object using this system under these circumstances?"

2.2.2 Wavelength/Frequency Relationship. We divide up the electromagnetic spectrum in terms of wavelength, although divisions based on photon energy would be equally valid. Related to wavelength is the concept of wave frequency. These quantities are related by the equation:

$$c = \lambda\nu$$

where c is the speed of light
λ is the wavelength
ν is the wave frequency

Each wavelength has a specific corresponding wave frequency and vice versa. However, because different regions of the spectrum have different applications, some regions are described in terms of wavelengths (light, for instance), while others are described in terms of frequency (radio). The accompanying figure, V-3, shows the portion of the electromagnetic spectrum commonly used for terrestrial remote sensing purposes. Note that the wavelength scale is not linear, but logarithmic. This treatment of the scale is necessary because the wavelengths range over many orders of magnitude. From a remote sensing point of view, it is usually most useful to think of electromagnetic waves in terms of their wavelength rather than their frequency. This is because some

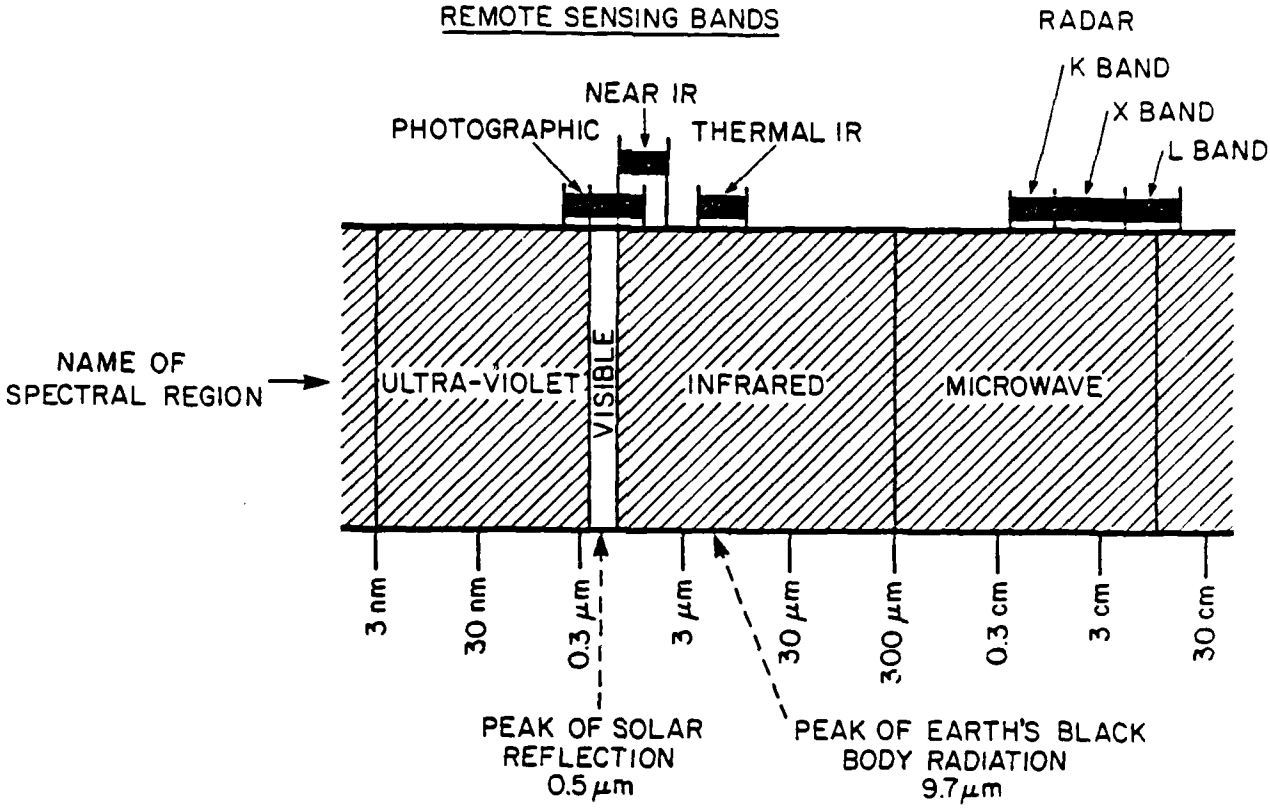

Figure V-3. Nomenclature of Remote Sensing Terms Related to the Electromagnetic Spectrum. Shown here is a map of the portion of the electromagnetic spectrum commonly used for remote sensing of sea ice. The names of the various spectral regions are associated with their wavelength range (bottom scale) while the names and ranges of the various remote sensing regions are indicated at top. Note that the wavelength scale is logarithmic. In addition, the peaks of the solar and the earth's black body spectral radiation curves have been indicated.

judgements concerning the interaction characteristics of radiation can be made in those terms. In general, a wave will interact strongly with objects whose physical dimensions are about one wavelength or larger. The wavelength, then, gives some hint of the sort of response to be anticipated from that spectral region.

2.2.3 Polarization. This is an important concept dealing with electromagnetic radiation. An electromagnetic wave consists of electric and magnetic fields oscillating in the plane perpendicular to the direction the wave is moving. In general, the electric and magnetic fields extend in all directions in this plane (called the wave front). However, it is possible to create waves which have their electric and magnetic fields each confined to a particular direction in the wave front. Such waves are said to be linearly polarized. The polarization is said to be in the direction of the electric field.

Radiation whose electric and magnetic fields extend equally in all directions in the plane of the wave front is said to be circularly polarized. Light emitted by an electric bulb tends to be circularly polarized.

In general, radiation is neither linearly nor circularly polarized, but elliptically polarized, where the strength of the electric field vector varies in an elliptical pattern in the plane of the wave front. The shape of the ellipse is described in terms of magnitude of the electric field strength along the major and minor axes of the ellipse. In nature, these axes are often parallel to the horizontal and the vertical directions. Hence, one speaks of the vertical and horizontal components of an electromagnetic wave. If a wave is circularly polarized, these components are equal. If a wave is linearly polarized in the horizontal direction, then the vertical component is zero. Skylight is elliptically polarized, but the relative magnitudes of the horizontal and vertical components vary in a pattern as one scans around the sun. Circularly polarized light is often changed to elliptical polarization or even linear polarization after being reflected from a surface.

Because electromagnetic radiation has this polarization property, there is actually more information contained in an emitted or reflected signal than just the total signal strength. One can measure the horizontal and vertical components of the electromagnetic signal as if they were two separate sources of information.

2.2.4 Some Characteristics of Various Portions of the Spectrum.

2.2.4.1 Ultraviolet (UV). This wavelength region has not been used to monitor sea ice and it is not likely to be used in the future. Because of the high degree of atmospheric scattering in this wavelength region, there is a tendency for imagery to appear "fuzzy". The radiation source is the sun and the systems used are, therefore, passive.

2.2.4.2 Visible Light. This wavelength region, principally the green and red portion, is used by Landsat and NOAA weather satellites to produce map-like imagery. The green portion is particularly sensitive to ice regardless of whether it is newly formed and thin or old and flooded. This portion of the spectrum is cloud-limited. As with the UV, the radiation source is the sun.

2.2.4.3. Near Infrared. This wavelength region is often detected along with visible light. Landsat and NOAA weather satellites produce images in this wavelength region. The imagery is of great utility to remote sensing of sea ice because it is highly sensitive to water/ice boundaries and water upon ice. It generally presents greater contrast between ice types and ice and water than do the visible wavelengths.

2.2.4.4. Thermal Infrared. This wavelength region is truly representative of heat. However, interpretation of thermal infrared imagery can be somewhat difficult. For many purposes, the best imagery is obtained just before dawn so that solar heating effects are at a minimum. Since the thermal infrared is absorbed by clouds and fog, it is useful to have a visual image as well as a thermal image to help identify them and the areas modified by their influences.

2.2.4.5. Microwave. Data is obtained in this region by both active and passive methods. The earth's surface does emit microwave radiation in very small amounts as a manifestation of its temperature. It is, therefore, necessary to use very sensitive microwave receivers (radiometers) to measure this radiation. This wavelength region is not affected by ordinary cloudiness, but the shorter wavelengths ($\sim$1 cm) can be absorbed by the raindrops in severe storms.

The active systems using this wavelength region come under the heading of radar. Side-scanning radar systems are operated routinely

aboard Canadian ice surveillance aircraft. Imaging radar has also been used experimentally aboard spacecraft and it is likely that data from an operational satellite imaging radar system will be available relatively soon.

The active systems send out and receive back a much stronger signal than the passive microwave systems. Hence, the "background" radiation of the earth does not confuse the signal received.

2.3 SOURCES OF ELECTROMAGNETIC RADIATION

2.3.1 Black Body Radiation. All objects with a temperature above absolute zero emit electromagnetic radiation. The amount of radiation in each wavelength region depends on the temperature of the object in a complicated way but the total radiation is proportional to the object's Kelvin temperature taken to the 4th power (T^4). Hence an object at 373°K (boiling water) emits four times as much radiant energy as water at 273°K (0°C) although its absolute temperature is only 36% greater.

The exact relationship between temperature and radiated energy per wavelength for a perfect radiator is called the black body curve. Figure V-4 shows this relationship for objects at 250°, 275° and 300° K.

2.3.2 The Sun and Earth as Black Body Radiators. The sun's black body curve peaks at a wavelength of 0.5 μm or 0.0005 millimeters, the wavelength of blue-green light. Therefore, the highest radiation level available for remote sensing detectors is at this wavelength. This is also close to the center of the wavelength range of human eyesight. Hence, human eyes are adapted to making the most of the available radiant energy from the sun. However, the sun's black body curve extends from the visible wavelengths to the infrared and even to the microwave region and beyond.

The earth's absolute temperature is around 290°K (17°C). The black body curve for this temperature peaks around 9.7μm. This wavelength is well within the thermal infrared region of the spectrum. However, the earth radiates less energy at all wavelengths than the sun even at this peak for the earth's black body curve. For this reason, daytime thermal infrared measurements can be highly distorted by reflected or back-scattered solar energy.

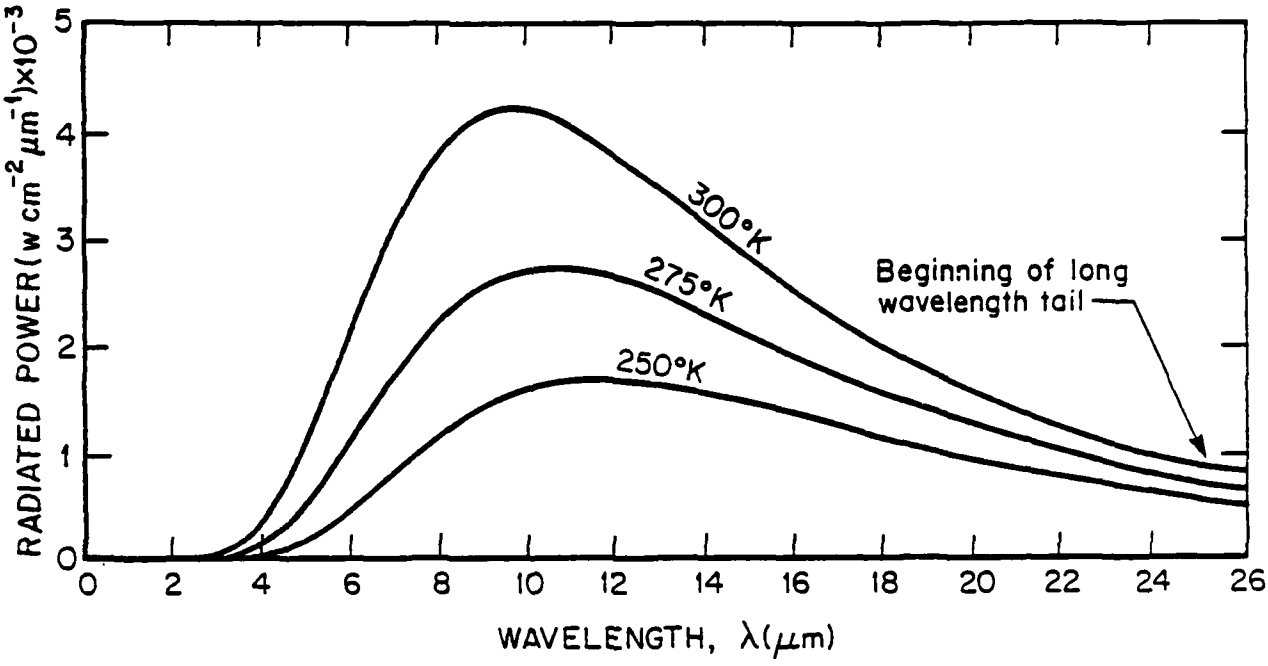

Figure V-4. Black Body Spectral Emission Curves for Temperatures in the Vicinity of the Earth's Average Temperature (290° K). Vertical scale gives radiated power in watts per square centimeter per micrometer of wavelength interval. Horizontal scale gives wavelength in micrometers.

2.3.3 Antennas. Antennas are an optional source of electromagnetic energy. This would be an active rather than passive system. However, antennas are only useful if they can produce more electromagnetic radiation in a selected wavelength band than the earth as a radiator or the earth as a reflector of solar energy. In general, this is difficult to do at visible, near infrared and thermal infrared wavelengths, simply because the earth's radiant power is so strong. (The laser provides a very useful exception to this generalization.) Once the microwave and radar wavelengths are reached, however, it is feasible to generate adequate levels of energy. In order to make the maximum use of the energy available (provided by generators aboard an aircraft or solar panels aboard a spacecraft), the energy is concentrated into a very narrow wavelength range. The narrower the wavelength range for a given amount of power, the "brighter" it will appear. (Remember, in order to be detected it must be reflected from the earth.) There are, however, practical considerations which limit the degree of wavelength concentration possible.

Engineers who build these systems speak of the antenna temperature of their antenna. This "temperature" is how hot a black body (i.e. a perfectly radiating object) would have to be in order to radiate the same energy as the antenna in the same narrow range of wavelengths at which the antenna is radiating. In order to produce radiation brighter than the sun, even in the antennas' narrow wavelength range, antenna temperature must be greater than 6000°K.

2.4 RECEIVING SYSTEMS FOR ELECTROMAGNETIC RADIATION

2.4.1 Cameras. These systems have been in use for about 150 years. The method by which data is recorded has been described in an earlier section. Here we wish to point out some general characteristics of these systems. Film can be made that is sensitive to wavelengths from the ultraviolet to the near infrared. Cameras are relatively simple data recording systems. They have several drawbacks, however: (1) The film must be developed by a chemical process before it can be viewed (2) The data cannot easily be transmitted from place to place (3) It is difficult to accurately compare the quantity of reflected light registered at the center of the image to the quantity of light registered at the film's edges.

2.4.2 Image Orthocon or Vidicon (T.V.) Cameras. These systems electronically register images. Their wavelength range largely coincides with the range of ordinary cameras. Like film cameras, the entire scene is recorded in a very brief interval. But, unlike ordinary cameras, the data can be recorded, transmitted and displayed electronically, providing a real-time capability if necessary. There are some drawbacks concerning the precision of the recorded data. These systems are in use aboard some satellites, but their use is declining.

2.4.3 Line Scanners. These systems operate over the wavelength range of cameras and orthocon and vidicon systems, and also into the thermal infrared. The method of operation is basically that of a telescope which scans the earth's surface from side to side along a path provided by an aircraft or satellite. A device sensitive to the wavelength to be monitored is placed at the focal point of the telescope. As the telescope travels from side to side, it records the amount of radiation received along a narrow line. This record is "chopped" electronically into small bits called pixels. (This term was described previously in 1.3.2 of this chapter.) An image is a mosaic of these pixels. Line scanner images have all the advantages of image orthocon or vidicon images with the added quality of precise measurement of the electromagnetic signal strength.

2.4.4 Antennas. Antennas are used in both active and passive remote sensing systems in the microwave range, and in active radar systems using wavelengths somewhat longer than the microwave range. Generally, active systems use the same antenna to receive and send the signal. Passive microwave antennas must be much more sensitive than their active system counterparts because the earth's microwave signal is much weaker than that produced by an active system. Very often these antennas are called radiometers. These systems produce an image by building up a mosaic of pixels that are similar to those produced by a line scanner. However, the scanning is performed electronically rather than by mechanical pointing.

SECTION 3. INTERACTION OF ELECTROMAGNETIC RADIATION WITH THE EARTH'S SURFACE: PARTICULARLY ICE AND SNOW

3.1 DEFINITION OF TERMS

3.1.1 Reflection. True reflection occurs when radiation which has been incident on a surface at some angle, θ, leaves the surface at that same angle as measured from a normal to the surface.

3.1.2 Scattering occurs when light which has been incident on a surface (or within a volume such as a cloud) leaves at a wide range of angles. Very often the intensity of the scattered radiation varies with scattering angle. In some cases, such as volume scattering within our atmosphere, some wavelengths are scattered more than others. Some wavelengths will be scattered from a surface that will reflect other wavelengths. The general rule is that if the surface roughness elements are long compared to the radiation's wavelength, the radiation will be reflected; if the roughness elements are short compared to the wavelength, it will be scattered.

For instance, a side-scanning radar image of a typical ice scene will show smooth ice as almost black since nearly all the incident radiation is reflected away at the ice surface. There is often a tendency to interpret this as open water. On the other hand, even a small ridge will produce a bright return signal because the incident radiation is scattered in all directions by the many small surfaces of the ice composing the ridge.

3.1.3 Absorption. Except for unusual cases, some of an incident electromagnetic signal is absorbed by the material of the surface it strikes or the medium it passes through. In the case of both active and passive systems, absorption of the electromagnetic signal by the atmosphere plays a major role in determining which wavelengths are used. Water vapor in the atmosphere absorbs many of the microwave wavelengths leaving a few "windows" through which we can transmit and receive this information.

Water strongly absorbs radiation in the near infrared portion of the spectrum used by Landsat band 7 images and NOAA series spacecraft (near IR band images). This absorption is so strong that wet snow and ice can be interpreted as water unless data from other wavelengths are available. Microwave radiation is also strongly absorbed by a thin film of water.

3.2 EMISSION OF ELECTROMAGNETIC RADIATION BY THE EARTH'S SURFACE

3.2.1 *Emissivity*. We have already discussed the "black body" curve relating wavelength and intensity of radiation at each wavelength. The total energy radiated by a perfect radiator is:

$$I_P = \sigma T^4$$

where I_P = the total radiation emitted by a perfect radiator

σ = an empirical constant determined by experiment (known as sigma)

T^4 = absolute or Kelvin temp. raised to the 4th power.

Very few objects are perfect radiators (i.e. black bodies) but their total radiated energy can be related to a black body by a simple constant, ε, called the emissivity.

$$I_R = \varepsilon I_P$$

where I_R = is the actual radiated energy

ε = a constant between 1 and 0 (1 being the emissivity of a perfect radiator)

3.2.2 Brightness Temperature. In terms of total radiated energy it is possible to define an effective temperature, T_B, as the temperature required of a (perfect) black body to radiate as much energy as the nonperfect radiator at temperature T. (Clearly, T_B will be less than T.)

To do this, we relate the energy radiated, I_R, to its effective temperature, T_B, as if the radiating source were a perfect black body:

$$I_R = \sigma T_B^4$$

However, we must understand that T_B is not the source's true temperature, T, but merely its effective temperature.

From above, we have the relationship between I_R and T:

$$I_R = \varepsilon I_P$$

but $I_P = \sigma T^4$ so $I_R = \varepsilon(\sigma T^4)$

and since $I_R = \sigma T_B^4$

we have $I_R = \sigma T_B^4 = \varepsilon(\sigma T^4)$ and $T_B^4 = \varepsilon T^4$

or $T_B = \varepsilon^{\frac{1}{4}} T$

We now have the relationship between an object's true temperature, T, and its effective temperature, T_B. The constant of proportionality is the object's emissivity taken to the 1/4th power.

3.2.3 An Example: Thermal Infrared Temperature Measurement. As an example, if we were to find the effective temperature of a surface with ε = .5 at an actual temperature of 270°K, we would have:

$$T_B = (0.5)^{\frac{1}{4}} \times 270° = 0.84 \times 270° = 227°$$

Thermal infrared scanners are calibrated to give true temperatures of perfect radiators. Thus, if a thermal scanner were aimed at the surface in the example above, it would yield a temperature of 227° although the temperature of the surface was actually 270°. The only way we can get the true temperature of the surface would be by knowing its emissivity and by rewriting the above second equation to yield T:

$$T = \frac{T_B}{\varepsilon^{\frac{1}{4}}} \quad \text{or} \quad \frac{227°}{0.84} = 270°$$

In other words, thermal IR temperatures are obtained by dividing the temperature recorded by the instrument (i.e. the effective temperature) by the emissivity taken to the 1/4th power.

One may wonder why the effective temperature of a material with an emissivity of 0.5 is only 43° cooler than its actual temperature. The reason is that the emissivity relates total energy radiated, but this quantity is proportional to the 4th power of the temperature. Thus, the equivalent of a large change in emissivity can be accomplished by a small change in effective temperature.

So far we have considered the total energy radiated by an emitting body. However, this does not necessarily relate directly to temperature

measurement. The measurement of temperature is one of the most difficult measurements to perform accurately, particularly by remote sensing methods. A great number of methods are used, each with its own characteristic problems, attributes, and particular range of applicability. Here we are only concerned with the measurement of the temperatures of water, ice, and snow over a temperature range from a few degrees above 270°K to about 250°K. There are two principal wavelength regions used: the thermal infrared and the microwave. Because these two methods are essentially quite different, they will be discussed separately.

3.2.4 Thermal Infrared. The methods for sea ice analysis used in this wavelength region measure true temperature to differentiate between ice and water. The instruments used are not much different from those of a line scanner measuring visible light. The thermal scanner accepts a broad range of wavelengths covering the main portion of the black body curve for radiators whose temperatures are in the vicinity of 270° K. The amount of energy in this portion of the black body curve contains most of the total energy radiated and, is, therefore, proportional to T_B^4.

Thus, as discussed previously, small changes of temperature are easily detected because they cause large changes in the energy radiated. Furthermore, the emissivities of water and ice are almost equal (at ε = 0.96), eliminating ambiguities arising from differing emissivities. For example, the 5% temperature change from water at 273°K to ice at 260°K will cause a measured energy change of 21%.

In addition, small changes in emissivity are unimportant since the T^4 influence on energy radiated is much greater. This is convenient because snow has a somewhat lower emissivity (around 0.95). Thus, snow upon the ice surface will lower the energy radiated by only 1% and, therefore, not result in an incredibly low temperature measurement.

The relative independence of water, snow, and ice temperature measurement from the value of emissivity is considered to be an attribute allowing unambiguous differentiation between ice and water. However, it can also be a liability when the ice and water are both close to the freezing point, for then they radiate very nearly the same energy and it is difficult to distinguish between them (see Figure IX-12).

3.2.5 Microwave. As mentioned previously, the methods used in the microwave wavelength region are essentially radio techniques, while thermal IR techniques are basically optical in nature. Besides this difference, there are two fundamental differences between the detection of ice types by these two methods: the relative emissivities are very important in this wavelength region and the energy radiated is directly proportional to the temperature. This sounds like a contradiction compared to the thermal infrared where radiated power is proportional to T^4, but the explanation is reasonably simple. The microwave radiation measured is far into the long-wavelength tail of the black body curve (See Figure V-4). In this wavelength region the energy radiated is approximated by the Raleigh-Jeans equation where it is equal to the emissivity times the first power of the temperature, or simply εT. Hence, in the microwave region it is correct to relate actual temperature (T), brightness temperature (T_B), and emissivity, ε, in the following way:

$$T_B = \varepsilon T$$

However, several factors must be kept in mind. First, although we are detecting water and ice at temperatures around 273°, we are measuring the energy radiated at wavelengths far from the peak of radiated energy. And, although at the peak energy portion of the radiated energy curve the energy radiated is nearly proportional to T^4, at the long-wavelength tail of the curve it is more nearly proportional to T. (Overall, the total energy radiated is precisely proportional to T^4.)

Secondly, ε is wavelength dependent. Here again, because most of the radiated power is concentrated near the peak of the radiant energy curve, ε near these wavelengths becomes the overall emissivity for thermal IR measurement and ε values for long wavelengths where little energy is radiated, can be ignored. However, the emissivities of long wavelengths cannot be ignored when measurements are actually made in this wavelength region. In the 1.5 cm microwave region, water has an emissivity around 0.50 while first-year ice has an emissivity around 0.92. Furthermore, multiyear ice has an emissivity of 0.84 yielding the possibility of making a distinction between these ice types. Finally, snow is essentially transparent at this wavelength which is extremely useful for ice surveys.

3.2.6 Identification of Ice Types on Microwave Imagery. In this wavelength region, both temperature and emissivity are important. Suppose in the 1.5 cm region we have an image containing water at 273° and first-year ice at 250°, the effective temperature of each will be:

$$T_{B\ water} = 0.5 \times 273° = 136° K$$

$$T_{B\ ice} = 0.92 \times 250° = 230° K$$

Because of its much greater emissivity, the ice actually emits more energy than the water, although it is colder.

Thus, in a region where there is only water and first-year ice (for instance, many areas around Antarctica), the ratio of water and ice is roughly the fractional position of the temperature measured between 136° K and 230° K, or:

$$R = \frac{T_B - 136°}{230° - 136°}$$

where T_B is the measured effective temperature.

If $T_B = 136°$, R = 0 (no ice).

If $T_B = 230°$, R = 1 (all ice).

However, the real world is not quite so simple. First, in regions where there is only first-year ice, surface conditions such as wetness can drastically alter the measured effective temperature of the ice, reducing the concentration of ice given by the above ratio. Second, in regions where there is multiyear ice, the ratio can also be lowered in areas with lower emissivity.

The second problem can be eliminated by adding a second microwave channel operating at a different wavelength. The emissivities of first and multiyear ice and water are strongly wavelength dependent. By monitoring emitted radiation on a second channel, entirely new data can be obtained. This data and that obtained on the first microwave channel can be combined in a pair of simultaneous equations to yield the true ice concentration. (Assuming the first problem, wetness, does not exist.)

Wetness can, in principle, be accounted for by adding either a third microwave channel or true surface temperatures as obtained from thermal infrared sensors.

Clearly, the ice analyst cannot solve simultaneous equations on a pixel by pixel basis. This is the sort of problem best performed by a computer. The precise formula the computer uses in making these calculations is called an algorithm. Usually the formulation of the algorithm used to treat ice data is not available to the ice analyst. For instance, the Nimbus Scanning Multichannel Microwave Radiometer (SMMR) data is treated by a computer at the Fleet Numerical Oceanography Center in California and transmitted to the ice analyst. It is important for the ice analyst to know that the SMMR data is being treated by a computer using a man-made algorithm which is not infallible.

3.3 SPECIFIC CHARACTERISTICS OF THE INTERACTION OF ELECTROMAGNETIC RADIATION WITH SNOW, ICE, AND WATER

This section catalogs the interaction of electromagnetic radiation with materials of interest to the sea ice analyst. The order of presentation starts with visible wavelengths and progresses through longer wavelengths.

3.3.1 Visible Light Wavelengths:

3.3.1.1 Green Light (Landsat band 4 and AVHRR visible band).

Snow: High albedo. Light scatters well in all directions regardless of wetness of snow.

Water: Low albedo in deep, clear water. Albedo increases with decreasing water depth from around 10 meters. Suspended sediment greatly increases albedo.

Ice: High albedo relative to red and near IR wavelengths for all ice thicknesses, but varies from low for light nilas to high for first-year gray-white. Highly responsive to thin ice forms. Tends not to differentiate among thicker forms.

3.3.1.2 Red Light (Landsat band 5 and AVHRR visible band).

Snow: High albedo. Light scatters well in all directions. Wet conditions decrease albedo somewhat.

Water: Low albedo in relatively deep and clear water. (Not influenced quite as much as green light by shallow depth or suspended sediment.)

Ice: Albedo varies from low for gray ice to high for thin, first-year (lower than green light). Moderately responsive to

thin ice forms. Thickness differentiation continues to thin first-year stages. Will not repond to thinnest ice forms.

3.3.2 Near IR Wavelengths (Landsat bands 6, 7 and AVHRR near IR).

Snow: High albedo. With dry snow, light is scattered well in all directions. Wet snow conditions drastically reduce albedo.

Water: Low albedo. Not further influenced by water depth over 30 cm. Only responds to very high sediment loads.

Ice: Albedo ranges from low for gray ice to high for first-year ice.

3.3.3 Thermal IR (AVHRR thermal band). Snow, ice, and water all have nearly the same emissivity (ε = .95). Ice and water surfaces are identified in terms of their actual temperature.

3.3.4 Microwave Emissivities of Water, First-Year and Multiyear Ice. In general the emissivity, ε, of various materials is not constant but varies with the frequency of the emitted radiation. Furthermore, the emissivity is different for the two polarization components of radiation, and these emissivities both change with viewing angle. Figure V-5 shows the variation of emissivity with microwave frequency for calm sea water, first-year ice and multiyear ice for both horizontal and vertical polarization components at a 50° nadir viewing angle. (Note: the SMMR microwave radiometers obtain data at this viewing angle.)

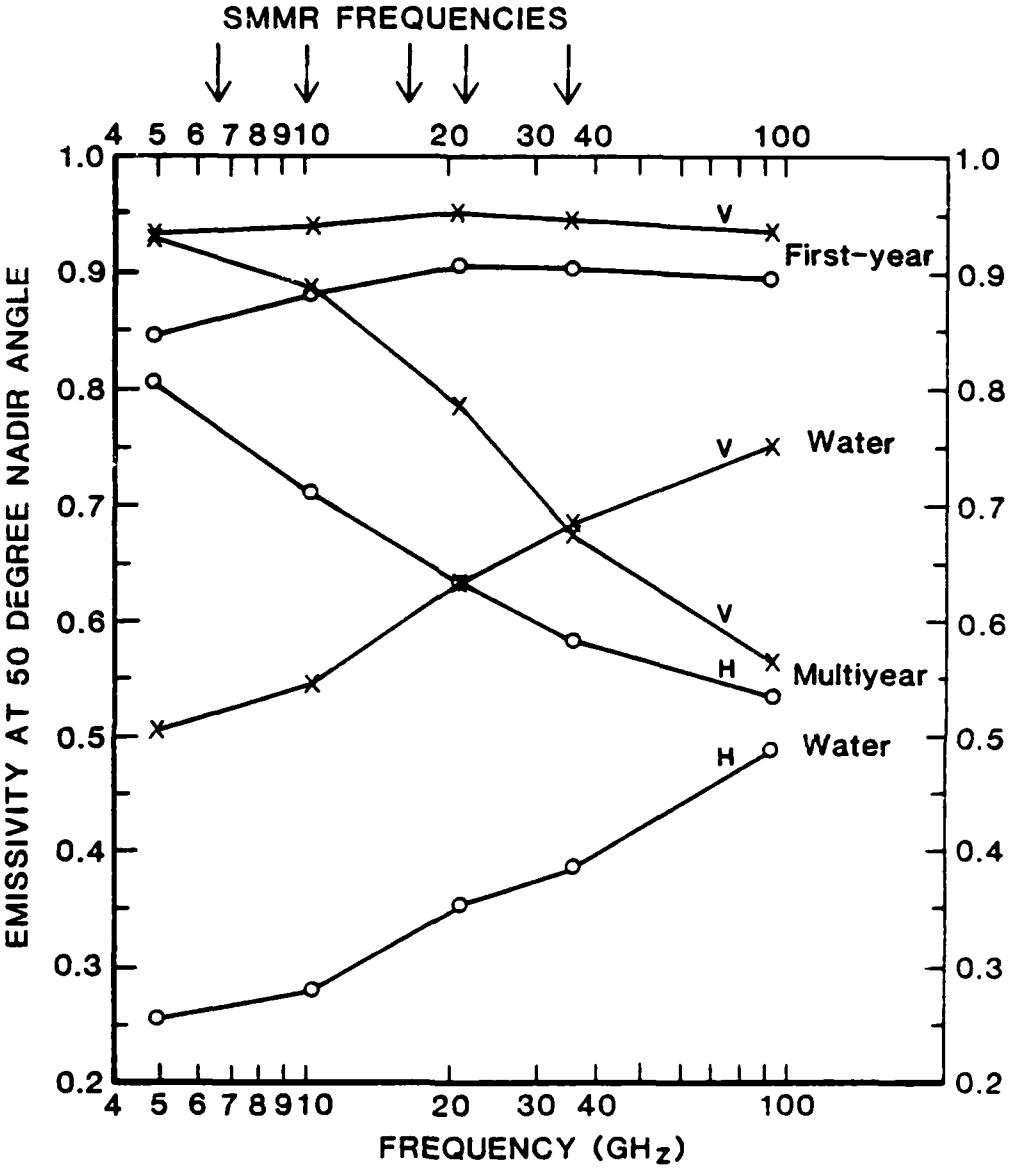

Figure V-5. Variation of microwave emissivities of calm sea water, first-year ice, and multiyear ice. Frequency for horizontal and vertical polarizations at constant 50° viewing angle (as measured from nadir). The five frequencies of the Scanning Multichannel Microwave Radiometer (see Chapter VI, Section 4) are indicated at the top. (Svendsen, el. al., 1983).

SECTION 4. CHARACTERISTICS AND TERMINOLOGY OF REMOTE SENSING SYSTEMS

This section discusses various characteristics of remote sensing systems in general and introduces the terminology used to describe those characteristics.

4.1 DATA ACQUISITION AND GENERATION OF DATA PRODUCTS

We are now ready to discuss in more detail some aspects of data acquisition and the generation of data products which have a bearing on data interpretation.

4.1.1 Orbital Characteristics. There are two basic satellite orbit types used to monitor large portions of the earth's surface. These are the geostationary orbit and the polar orbit. We will discuss the simpler of the two first.

4.1.1.1 Geostationary Orbit. In order for a satellite to attain a desired orbit, it must move at a specific speed. For satellites just above the earth's atmosphere (around 500 mi) this speed is about 17,000 mph. At this speed a satellite orbits the earth in about one and a half hours. As higher orbits are attained (and the satellite is further removed from the earth's gravitational field), the speed required is reduced. At a distance of approximately 23,500 mi, the speed required is 6,150 mph. At this rate the satellite circumnavigates the planet in 24 hours. If the satellite is directly above the equator and traveling in the same direction as the earth is turning (i.e. eastward), it will remain above a particular point on the equator. This is called a geostationary orbit because, with respect to the earth, the satellite is stationary.

A remote sensing system placed aboard a geostationary satellite has the ability to continuously monitor a particular location on the earth's surface, or a whole hemisphere. The GOES (Geostationary Operational Environmental Satellite) is a well known operational geostationary satellite. Images from this satellite are obtained every thirty minutes to give weather forecasters a hemisphere-wide view of changes in cloud patterns.

Unfortunately, the ice-covered regions of the world cannot be seen very well on this imagery because they are viewed at an oblique angle. Its greatest value to the ice analyst comes from the ability to detect ice in the Great Lakes.

4.1.1.2 Polar Orbit. Most of the satellites currently in orbit are in polar orbits. Most of these satellites are at altitudes between 500 mi and 1000 mi and, as described above, require approximately one and a half hours to complete an orbit. However, a wide variety of additional orbital characteristics can be chosen to further define the motion of a satellite. For instance, the locations of successive orbits as projected on the earth's surface can be a very important factor. This characteristic can be adjusted to yield a wide variety of satellite coverage frequencies and repeat patterns. However, some desired factors are obtained at the expense of others, principally the maximum latitude of the satellite's orbit as projected on the earth. Landsat, for instance, does not cover farther north than 80°N, but its frequency of coverage has many characteristics which are desirable to the users of its data.

A point to remember here is that very few polar orbits actually cross the poles.

4.1.2 Picture Element. Most satellite remote sensing systems in current use utilize radio transmission to transmit image information back to earth. The image to be transmitted is divided into small rectangular cells called picture elements (pixels). On the earth, the image is reconstituted by reassembling these pixels into the same array in which they were recorded.

4.1.3 Gray Level. The information recorded for each pixel represents the amount of radiation measured from that area on the earth's surface. In other words, the radiation is averaged over the pixel. When the pixels are reassembled to form the image for viewing, each pixel is given a uniform level of gray or gray level representing the amount of radiation which has been measured from that corresponding area. This process limits the amount of information on a satellite image. If such an image is sufficiently enlarged, the earth's surface appears to be nothing more than an array of rectangles with varying levels of gray.

Gray level can also be used when referring to an object on a satellite image. (First-year ice has a higher gray level than open water on a near IR positive image.) However, the gray levels as seen on an image can be manipulated and care must often be taken to understand what has been done in this regard in order to accurately interpret an image.

4.1.4 Gray Scale. The image interpreter must be aware that the gray levels of pixels as displayed on an image may have been purposely rearranged in some systematic manner from those recorded in order to enhance interpretation. The guide to understanding the system of gray levels as assigned is to examine the image's gray scale. The gray scale of a satellite image is the relationship between the radiation measured at the satellite and the corresponding gray level assigned to pixels. Very often the gray scale appears as a bar broken into bands, each with a particular shade of gray. Corresponding notations describe the relationship between these bands and the radiation level they represent. For instance, the gray scale can be reversed, making white things black and vice versa. (This is called a negative image.) Or certain gray levels can be assigned a new gray level not assigned to any other feature. (For example, thermal IR images are often given gray scales which make ocean temperatures around freezing either very black or white so that the region where freezing is taking place can be identified easily and quickly.)

4.2 FACTORS RELATED TO DATA INTERPRETATION

This section discusses basic satellite parameters which have a significant bearing on satellite image interpretation. These factors are present to one degree or another in all satellite remote sensing systems.

4.2.1 Detectability, Resolution, and Discrimination. These three factors are often mistakenly lumped together under the term resolution. However, each has its own specific definition and use.

4.2.1.1 Resolution. This term has a strict meaning referring to the ability to identify separate objects. When a system is referred to as having a resolution of x meters, it means that the objects must have a physical separation of at least that distance to be identified as separate objects. On satellite images this distance is obviously related

to the pixel size as represented on the earth (pixel footprint). For instance, the pixels representing two bright objects must have one darker pixel between them in order for the viewer to suspect that two separate objects are being represented. For this reason, the pixel footprint size is generally referred to as a particular detector's resolution. As a practical example, the footprint of AVHRR visual channel is approximately 1.1 km. In general, two objects must be separated by that much distance to be distinguishable.

4.2.1.2 Detectability. In some respects this is a more useful, yet complicated term. Even though a single object might be smaller than the pixel footprint or resolution, it may be detected. For instance consider a single narrow lead 1/4 the width of a pixel running across a satellite image. Although the lead is smaller than a pixel, there is sufficient contrast between the black water and the white ice in those pixels containing the lead that they will appear darker than the pixels representing the surrounding ice. Thus, the lead will be detected. Yet, since its size is less than the resolution, it is not be possible to determine whether it is a narrow open lead or a wider lead frozen to some intermediate stage between the water and surrounding ice. In general, highly contrasted objects may be detected when they are smaller than the resolution distance.

4.2.1.3 Discrimination. This term refers to the ability to determine in terms of grey level whether two classes of objects are present (for instance, gray and gray-white ice). Ultimately, discrimination depends on the distinction possible between the gray levels as recorded by the satellite and presented on the image. It may be that there is not sufficient data recorded for two ice types to be represented by two different gray levels. Or the individual steps on the gray scale used to produce a particular image were too close (in terms of shades of gray) for such a distinction to be made. Finally, the physical arrangement of the two ice types (relatively small intermixed floes for instance) may make such a distinction impossible.

4.2.2 Signal Averaging Over Pixels. This subject has been mentioned in the previous discussion in terms of detection of objects smaller than the remote sensing system's resolution. In that case, signal-averaging over pixels allowed the detection of a lead too small to be resolved.

However, this detection was obtained at the expense of an ambiguity concerning the thickness of ice in the lead. This relatively common ambiguity can become a serious problem if the area contained by a pixel contains several ice types or ice with a range of surface conditions. Such averaging presents problems on microwave and thermal IR imagery at the ice/water boundary. The microwave case can become particularly troublesome because the pixel footprint size is very large and often contains many ice conditions. A resulting inaccurate analysis can involve errors whose size ranges over tens of miles. Improved data analysis techniques involving several wavelengths will help to reduce these errors.

4.2.3 Registration of Satellite Data to Maps. The construction of a useful product from remotely sensed data generally depends on the fitting of the data to maps of the earth's surface. This creates problems arising from several factors:

4.2.3.1 Problems Arising from Geometry. It is difficult for remote sensing systems to take into account the viewing angle between the satellite and various points on the earth's curved surface. In general, this problem increases with the field of view of the particular imaging system because more curvature must be taken into account. A computer program may be utilized to perform this function, but it should be kept in mind by the image analyst that this transformation is not always particularly accurate and errors can result.

4.2.3.2 Problems Arising from Pixel Array Warping. Once pixel data are received on earth, the satellite image is compiled using a fixed rectangular grid of pixel locations. This method assumes that the pixel information (i.e. radiation intensity level) was recorded on a corresponding grid aboard the satellite. This requires that the satellite does not roll or pitch while the pixels are being measured and that the measuring system (often a mechanical device) operates very smoothly. This is not completely possible. As a result, data is occasionally assigned to a image pixel that was recorded from the area on the earth assigned to a neighboring pixel. This effect causes a general warping of an image involving distances of up to a few pixels. Accurate correction procedures involve precise knowledge of exactly where a few particular

pixels should appear and a subsequent computer-driven unwarping of the data. This is a complex process and is not done on a routine basis. In practice, the effect is most important near land or shoals. In these cases the imagery is manually registered to these points of interest, leaving increasing errors with distance from shore.

4.2.3.3 Registration to a Particular Map Projection. It is impossible to completely and accurately represent the earth's curved surface on a flat sheet of paper. A large variety of techniques are used to project points on the earth's surface to produce a flat map, each with its own particular utility (preserving angles, preserving uniform distances, etc.). Remotely sensed data is obtained in its own particular projection, depending on the mechanics of how that particular system works. In many cases, the imagery is provided to the ice analyst in that same projection unless it has been transformed by a computer into some other map projection. If accurate mapping is desired, the projections of the data provided and the map to be produced must be taken into account.

4.3 INTERPRETATION AMBIGUITIES

The analysis of remotely sensed sea ice imagery requires constant vigilance to avoid errors arising from ambiguities in interpretation. These ambiguities develop because it is impossible for the remote sensing system to gather complete information concerning the ice. The following sections list some of the more common problems of this type.

4.3.1 Pixel Averaging Ambiguities. These interpretive problems arise because the gray level assigned to each pixel represents an average of the light measured from that pixel's representative portion of the earth's surface. Thus, for example, a pixel containing a thin lead between two floes will appear darker than surrounding pixels representing only floe surfaces. However, this pixel could have just as well contained a wider lead that had frozen over but was still not as white as the surrounding floes. Unless other data is available, such as a second data channel operating at another wavelength, this lack of precision regarding the lead simply remains.

4.3.2 Unanticipated Surface Conditions. Most remote sensing signatures are based on an assumption that some anticipated surface

conditions exist. However, this may not be the case. For instance, on visual wavelength imagery, a recent snow would make many thin ice categories appear identical to thick first-year and multiyear ice. Similarly, a wet surface can make ice appear as ocean on some passive microwave imagery. Such wetness could result from sea state as well as melting.

4.3.3 Incorrect Assumptions Regarding Anticipated Response. Each remote sensing system is based on the physics of a particular portion of the electromagnetic spectrum. However, it is possible for the ice analyst to begin to think in terms of a system responding to particular surface features consistently and anticipate that the same surface feature will always yield the same response. Thus, while thermal imagery actually records the temperature of the earth's surface as modified by its emissivity, there may be a tendency to think that it records the presence or absence of ice. However, when ice is melting, its temperature is very close to that of the surrounding water and it can be invisible on thermal imagery.

CHAPTER VI. CHARACTERISTICS OF REMOTE SENSING SYSTEMS USED FOR SEA ICE ANALYSIS

This chapter lists the remote sensing systems currently in use for sea ice analysis and prediction and gives their characteristics in terms of the nomenclature outlined in Chapter V.

SECTION 1. AVHRR (ADVANCED VERY HIGH RESOLUTION RADIOMETER)

1.1 VEHICLE: TIROS-N SERIES SATELLITES (NOAA)

1.2 NATURE OF SYSTEM

1.2.1 Sensor Description: five channel passive multiband radiometer

1.2.2 Satellite Orbital Characteristics:

orbit: nearly polar, sun synchronous
period: 102 minutes
altitude: 830 km
declination: 8.7 degrees

1.2.3 Coverage. Obtains useful coverage of entire earth each day. However, the highest satellite subpoint is at 81°. As a result, the poles are only seen at image borders. Imagery is wide-angle with great amount of overlap. Images are obtained on both northbound and southbound passes.

1.2.4 Pixel Footprint (Nominal Spatial Resolution). 1.1 km (0.6 nm) at the satellite subpoint, the point on earth directly beneath the satellite. Because this is a wide-angle system, the pixel footprint varies considerably from the satellite subpoint to the edge of the area scanned.

1.2.5 Sensor Characteristics:

Channel	Passband Range	Principal Utility
1	0.55 - 0.90 μm	daytime ice and cloud mapping
2	0.73 - 1.10 μm	daytime ice and water mapping
3	3.55 - 3.93 μm	sea surface temperatures nighttime ice mapping nighttime cloud mapping
4	10.5 - 11.5 μm	sea surface temperatures nighttime ice mapping day/night cloud mapping
5	11.5 - 12.5 μm	sea surface temperatures

Note: Sensor passbands listed here may vary somewhat from satellite to satellite.

1.3 DATA FORMAT

1.3.1 Standard Data Product: 9"x9" black & white facsimile image

1.3.2 Scale: 1:7,000,000 (1" = 110 mi) at satellite subpoint. Note: The normal image format is not rectified with the result that the scale varies from the satellite subpoint to the edge of the image.

1.3.3 Pixel Size: ~0.005 in

1.3.4 Ancillary Information on Data Product:

tracking station providing data
date and time of data acquisition
orbit number since launch
radiometer channel
satellite heading (azimuth)

1.3.5 Global Area Coverage (GAC). This is a secondary data product providing daily visual band coverage of the entire earth at 4 km resolution. This product is provided with coordinate grid, national boundaries and ice/water boundaries. The scale is approximately 1:20,000,000.

1.4 DATA CHARACTERISTICS

1.4.1 General Description. This system (and DMSP, which is s[illegible]r) provides the highest resolution sea ice imagery used for routine analysis. In practice, only band 1 (visual wavelengths) and band 4 (thermal IR) are used for ice analysis. Occasionally, bands 2 and 3 are used.

1.4.2 Conditions Which Can Be Discriminated:

band 1: water/ice boundary
fast ice
leads over 1 km wide
ice concentration
ice types from light nilas to thin first-year

band 2: ice/water boundary (ignores very thin ice forms)
fast ice
leads over 1 km wide
ice concentration
ice types from young to thin first-year

bands 3,4: water/ice boundary
leads over 1 km wide
ice concentration
fast ice
ice types from light nilas to thin first-year

1.4.3 Limitations. Bands 1 and 2 depend on available light. Bands 3 and 4 do not yield results when the ice temperature is near that of the surrounding water. All bands are cloud-limited. Band 2 does not respond to thin ice or ice which is flooded with melt ponds.

1.4.4 Ambiguities. On bands 1 and 2 snow cover can make thinner ice forms appear as older and thicker forms. Band 2 can portray wet ice as open water. Bands 3 and 4 respond to the temperature of objects and, therefore, will not distinguish ice when its temperature is near that of the surrounding water.

SECTION 2. DMSP (DEFENSE METEOROLOGICAL SATELLITE PROGRAM SENSOR SYSTEM)

2.1 VEHICLE: DMSP SATELLITE

2.2 NATURE OF SYSTEM

2.2.1 Sensor Description: two channel multiband radiometer

2.2.2 Satellite Orbital Characteristics:

orbit: nearly polar, sun synchronous
period: 102 minutes
altitude: 830 km
declination: 8.7 degrees

2.2.3 Coverage. Obtains useful coverage of entire earth between 81.3°N and 81.3°S each day. Imagery is wide-angle with great amount of overlap. Images are obtained on northbound and southbound passes.

2.2.4 Pixel Footprint (Nominal Spatial Resolution): 3.7 km (low resolution mode), 0.6 km (high resolution mode)

2.2.5 Sensor Characteristics:

Channel	Passband Range	Principal Utility
1	0.4 - 1.1 μm	daytime water/ice boundaries
2	8.0 -13.0 μm	day/night sea surface temperatures

2.2.6 Resolution. Thermal Fine (TF) resolution data are collected continuously day and night by the infrared detector; Light Fine (LF) resolution data are collected continuously during daytime only by the silicon diode detector. Fine resolution data have a nominal linear resolution of 0.3 nm (0.4 km). Because of the quantity of data collected, it is not possible to store or transmit all of the fine resolution information. Therefore, smoothing (as described below) or selective collection is required. Storage capacity and transmission constraints limit the quantity of fine resolution data which can be provided in the Stored Data Fine (SDF) mode to a total of 40 minutes of LF or TF data per 10 minute Command Readout Station (CRS) readout.

Data smoothing permits global coverage in both Thermal Smoothed (TS) and Light Smoothed (LS) data to be stored on the primary tape

recorders in the Stored Data Smoothed (SDS) mode. This smoothing is accomplished by analog averaging of the fine resolution input from five resolution cells which are contiguous in the across-track direction, then digitally averaging five such 1x5 cell samples in the along-track direction. A nominal linear resolution of 1.5 nm (2.1 km) results. 400 minutes of LS and TS data may be transmitted during a single 10 minute CRS readout.

In addition, a photomultiplier tube allows collection of Light Smoothed (LS) data under quarter-moon or brighter nighttime conditions at 1.5 nm (2.1 km) nominal linear resolution.

A combination of either fine resolution data and the complementary smoother resolution data (i.e., "LF and TS" or "TF and LS") can be provided directly to remote sites in the Real Time Data (RTD) mode. In this mode, only the analog, across-track smoothing is provided before transmission. Along-track smoothing is done by the ground processing equipment.

2.3 DATA FORMAT

2.3.1 Standard Data Product: 14"x22" black & white transparency

2.3.2 Scale: 1:7,000,000 (1" = 110 mi) normal scale (data combined to yield resolution of 5 km)
1:3,500,000 (1" = 55 mi) 2X mode
1:1,750,000 (1" = 27.5 mi) 4X mode

2.3.3 Pixel Size On Data Product:

	Low Resolution	High Resolution
Normal	.01 in	.002 in
2X	.02 in	.004 in
4X	.04 in	.008 in

2.3.4 Ancillary Information. Transparency has attached label listing site of receiver, vehicle providing data, time, satellite track, band, gray scale spread, enchancement, temperature threshhold (if applicable) and scale.

2.4 DATA CHARACTERISTICS

2.4.1 General Description. Although DMSP sensors have a higher resolution than current AVHRR sensors, DMSP data as provided has a somewhat poorer resolution than AVHRR. The reason for this is that data transmission requirements preclude the transmission of large quantities of high resolution imagery (see section 2.2.6) and the pixel-averaged DMSP imagery normally provided has larger pixels than AVHRR imagery.

2.4.2 Conditions Which Can Be Discriminated:

band 1: water/ice boundary
fast ice
leads over 1 km wide
ice concentration
ice types between light nilas and thin first-year

band 2: water/ice boundary
leads over 1 km wide
ice concentration
fast ice
ice types between light nilas and thin first-year

2.4.3 Limitations. Band 1 depends on available light; band 2 does not yield results when the ice temperature is near that of the surrounding water. Both bands are cloud-limited.

2.4.4 Ambiguities. Snow cover can make ice appear as older and thicker. Thin-ice forms may appear as thicker ice with lower concentration.

Section 3. ESMR (ELECTRONICALLY SCANNING MICROWAVE RADIOMETER)

3.1 VEHICLE: NIMBUS SERIES SATELLITES

Note: ESMR was operational between January 1973 and November 1982. It is listed here because ESMR imagery is used as an example of imaging microwave radiometry.

3.2 NATURE OF THE SYSTEM

3.2.1 Sensor Description: single channel microwave radiometer

3.2.2 Satellite Orbital Characteristics:

orbit: nearly polar, sun synchronous
period: 102 minutes
altitude: 830 km
declination: 8.7 degrees

3.2.3 Coverage. Obtains useful coverage of entire earth several times each day. Imagery is wide-angle with very large overlap. Images are obtained on both northbound and southbound passes.

3.2.4 Pixel Footprint (Nominal Spatial Resolution). Varies from 25 km (15 nm) square at satellite subpoint to 160x45 km rectangle at right and left ends of scanner sweep.

3.2.5 Sensor Characteristics:

	Passband Range	Principal Utility
Nimbus V	1.55 cm	day/night ice/water boundary

3.3 DATA FORMAT

3.3.1 Standard Data Product: 35 mm black & white strip transparency.

3.3.2 Scale: varies across film, 1:20,000,000 at satellite subpoint.

3.3.3 Ancillary Information On Data Product. Full scale dot matrix map of geographic coordinates corresponding to area imaged on 35 mm ESMR film.

3.4 DATA CHARCTERISTICS

This system provides reliable, low resolution wide-angle imagery which is used for routine sea ice analysis. Because most weather conditions do not limit observations, ESMR imagery can be used to identify and map

sea ice when higher resolution imagery is not available. However, detailed mapping is not possible because of the combination of the low resolution and wide-angle effects.

3.4.1 Conditions Which Can Be Discriminated:

water/ice boundary

land/water boundary

ice concentration

3.4.2 Limitations. Coarse-grained resolution, poor mapping registration.

3.4.3 Ambiguities. May respond to thin or wet ice as ocean rather than ice.

SECTION 4. SMMR (SCANNING MULTICHANNEL MICROWAVE RADIOMETER)

4.1 VEHICLE: NIMBUS SERIES SATELLITES

4.2 NATURE OF SYSTEM

4.2.1 Sensor Description: 10 channel microwave radiometer.

4.2.2 Satellite Orbital Characteristics:

orbit: nearly polar, sun synchronous

period: 102 minutes

altitude: 830 km

declination: 8.7 degrees

4.2.3 Coverage. Obtains useful coverage of the entire earth in three day's time.

4.2.4 Pixel Footprint (Nominal Spatial Resolution): Depends on channel. See 4.2.5.

4.2.5 Sensor Characteristics. (Note: each channel listed below has vertical and horizontal polarizations, making a total of 10 channels.)

Channel	Passband	Resolution	Principal Utility
1	4.5 cm	150 km	good delineation of ice edge
2	2.8 cm	100 km	good delineation of ice edge
3	1.7 cm	60 km	best delineation of ice edge
4	1.4 cm	60 km	detects atmospheric water vapor
5	0.81 cm	30 km	sensitive to wet ice

4.3 DATA FORMAT

Raw Data: magnetic tape

Analyzed Data: polar projection, color annotated maps generated by computer. (Additional details in next section.)

4.4 ANCILLARY INFORMATION ON DATA PRODUCT

(There are several SMMR data products. This discussion deals with sea ice data products only.) There are separate displays for sea ice concentration and multiyear ice fraction of sea ice. On each of these maps a 32-step color scale is related to values of these parameters.

Additional ancillary information includes the frequency at which a particular map type is produced, the spatial resolution of the parameter portrayed, the orbits from which data is missing, and the dates of coverage.

4.5 DATA CHARACTERISTICS

This sensor system is designed to yield several data products related to water on the earth's surface. The products of interest to sea ice analysts are: (1) sea ice concentration and wind speed over open water (2) thin first-year ice fraction and multiyear ice fraction of sea ice. The effective resolution of these products is around 60 km.

4.5.1 Conditions Which Can Be Discriminated:

ice/water boundary
first-year ice types
large areas of multiyear ice
concentration of ice

4.5.2 Limitations. Coarse-grained resolution, 3-day repeat period for data update. Operationally, data has been found to be displaced by as much as three pixels.

4.5.3 Ambiguities. Wet ice conditions can cause errors in ice edge location, ice concentration, and extent of thin first-year ice. Pixels containing coastlines can show erroneous values because of contribution to signal from land portion of the pixel. Therefore, caution should be used when basing analysis on data from such pixels.

SECTION 5. MSS (MULTI-SPECTRAL SCANNER)

5.1 VEHICLE: LANDSAT (1 THROUGH 4)

5.2 NATURE OF SYSTEM

5.2.1 Sensor Description: 4 channel passive optical scanner.

5.2.2 Satellite Orbital Characteristics:

orbit: nearly polar, sun synchronous
period: 100 minutes
altitude: 930 km
declination: 8-9 degrees

5.2.3 Coverage. Obtains complete coverage of earth's surface in 16-18 day's time, depending on satellite.

5.2.4 Pixel Footprint (Nominal Spatial Resolution): 80 m

5.2.5 Sensor Characteristics:

Channel	Passband Range	Principal Utility
* 4	0.5 - 0.6 μm	detects all ice
5	0.6 - 0.7 μm	detects most ice
6	0.7 - 0.8 μm	detects dry, thick ice
7	0.8 - 1.1 μm	detects dry, thick ice

* Note: Band designations 1-3 are assigned to another Landsat system not customarily used for ice analysis.

5.3 DATA FORMAT

Products:

70 mm, 10" black & white transparencies
10", 20", and 40" black & white prints
10", 20", and 40" color composite prints
10" color composite transparencies

Scales:

70 mm products: 1:3,500,000
10" products: 1:1,000,000
20" products: 1:500,000
40" products: 1:250,000

5.4 ANCILLARY INFORMATION

Each Landsat standard data product displays geographic coordinates around the perimeter of the image. Other information displayed includes: a gray scale, coordinates of the center of the image and the satellite subpoint, the Landsat band displayed, the vehicle producing the image (Landsat 1, 2, 3, etc.), the orbit number, the date, solar elevation and the azimuth.

5.5 DATA CHARACTERISTICS

Landsat imagery has the highest resolution of all satellite imagery produced routinely. Because of the relatively long time required for complete coverage of the area of interest (about two weeks), the cloud cover limitation, and the relatively small geographical area contained on each image, it is not used for routine sea ice analysis on a global scale. However, it is used for sea ice monitoring in the Canadian arctic via a special Canadian ground station. It is also used for specialized sea ice monitoring in the vicinity of Alaska by private industry.

5.5.1 Conditions Which Can Be Discriminated:

ice/water, ice/land, water/land boundaries
thin ice vs. thicker ice
ice concentration
fast ice
large ice ridges

5.5.2 Limitations: Cloud cover, relatively small area of coverage each day.

5.5.3 Ambiguities. It is difficult, if not impossible to discriminate between first-year and old ice. Although thinner ice types can be differentiated in general, snow cover can eliminate the ability to distinguish among ice types in terms of albedo. The exception to this is very thin ice types that are depressed below sea level by the weight of snow and flooded.

SECTION 6. DUAL MODE RADAR ALTIMETER

6.1 VEHICLE: GEOS-3 (GEODYNAMICS EXPERIMENTAL OCEAN SATELLITE)

6.2 NATURE OF SYSTEM

6.2.1 Sensor Description: Active radar altimeter and surface roughness monitor.

6.2.2 Satellite Orbital Characteristics:

orbit: circular, excentric equatorial
period: 102 minutes
altitude: 843 km
declination: 25 degrees

6.2.3 Coverage. Obtains data in narrow strips directly beneath satellite between 65°N and 65°S. Density of strips is a minimum at the equator and a maximum at 65°N and 65°S. The satellite will perform 28 crossings of each latitude per day. (At 60° latitude, this equals one crossing every 500 miles).

6.2.4 Pixel Footprint (Nominal Spatial Resolution). Here this term refers to position resolution along track. Operationally, this distance resolution appears to be 10 km.

6.2.5 Sensor Characteristics:

Channel: 1 Wavelength: 2.15 μm

Mode	Radar Pulse Width	Range Precision With 1 Sec. Averaging
global	200 nsec	60 cm (rms)
intensive	12.5 nsec	20 cm (rms)

6.3 DATA FORMAT

For sea ice analysis purposes, the data format is a computer printout listing a computed ice index in terms of latitude and longitude.

6.4 ANCILLARY INFORMATION

Time to the nearest alternate second, date, orbit and several technical parameters not defined in this discussion. In addition, a surface wind file in m/s is available based on wave height analysis.

6.5 DATA CHARACTERISTICS

The utility of this data to sea ice analysis is that of providing an accurate location of the ice edge regardless of weather or ice surface wetness.

6.5.1 Conditions Which Can Be Discriminated:

sea/ice boundaries

6.5.2 Limitations. Data may not be acquired exactly where needed. Data is not acquired above 65° latitude on present system.

6.5.3 Ambiguities. None observed except positional accuracy inherent from the 10 km operational resolution.

SECTION 7. GOES RADIOMETER

7.1 VEHICLE: GOES (Geostationary Operational Environmental Satellite)

7.2 NATURE OF SYSTEM

7.2.1 Sensor Description: 3 channel radiometer

7.2.2 Satellite Orbital Characteristics:

orbit: geostationary, equatorial. One satellite at 75°W and a second at 135°W

altitude: 35,800 km

7.2.3 Coverage. Each satellite generates an image of the earth every half hour in each of three spectral bands. The satellite subpoint is either 0°N, 135°W or 0°N, 75°W depending on the satellite, with the earth appearing as a disc centering on that point. Consequently the image scale varies radially from that point. Image compression also takes place with radial distance with the result that at a distance of 60° longitude or latitude from the satellite subpoint, little useful data can be obtained.

7.2.4 Pixel Footprint (Nominal Spatial Resolution) varies with angular distance from equatorial satellite subpoint.

Sensor	0° Earth Coordinates	40° Earth Coordinates	60° Earth Coordinates
visible	0.7 km	1 km	2.1 km
infrared	7 km	10 km	21 km
water vapor	7 km	10 km	21 km

7.2.5 Sensor Characteristics:

Sensor	Passband	Principal Utility
visible	0.55 - 0.75 μm	cloud cover mapping
infrared	10.5 - 12.5 μm	cloud top altitude day/night cloud mapping
water vapor	6.7 (peak) μm	monitoring upper level flow

7.3 DATA FORMAT

This data product is generally transmitted by radio or landline facsimile and displayed as hardcopy (film positive transparency or paper

positive). At many locations video recorders are used to permit several hours of images to be viewed sequentially, giving the weather analyst a comprehensive view of the flow of air masses.

7.4 DATA CHARACTERISTICS

7.4.1 General Description. This system was designed to provide nearly hemispheric monitoring of air mass movement. Occasionally sea ice can be seen at the northern or southern extremes of the image. However, this data product is not a primary source of sea ice data.

7.4.2 Conditions Which Can Be Discriminated:

band 1: cloud patterns, occasionally ice/water boundaries
band 2: cloud temperatures, nighttime cloud patterns
band 3: water content of air masses

7.4.3 Limitations. This system has a relatively low spatial resolution which becomes even poorer at high latitudes. While it is useful for monitoring air motion to or from polar regions, it does not monitor air mass motions within the polar regions very well.

CHAPTER VII. AUXILIARY SEA ICE OBSERVATIONS

1.1 VALUE OF AUXILIARY OBSERVATIONS

Although in recent years remotely sensed data has come to play a major role in sea ice analysis, it is not yet possible to compile a complete and accurate picture of sea ice conditions from this data source alone. Auxiliary sea ice observations play a major role in confirming remotely sensed ice information or providing important corrections to the overall picture of ice conditions.

The most important auxiliary sea ice observation is the location of the ice edge. Its value reflects both the importance of the ice edge location in general and the difficulty of accurately locating the ice edge with remotely sensed data. It is also useful to provide a description of the ice edge in terms of indications of freezing or thawing, wind-driven advance or retreat, and compactness or diffuseness.

Other important auxiliary information includes the location of the icebergs, floebergs, ice islands, old ice, ridging and hummocking. These ice features are poorly monitored by remote sensing techniques but are very important aspects of the ice cover.

Another valuable aspect of sea ice that can be reported from all locations within the ice edge is ice concentration. Because of ambiguities that often arise between concentration and albedo, particularly on data with low spatial resolution, information confirming or correcting ice concentration is always valuable to sea ice analysts.

1.2 TIMELINESS AND LOCATION OF AUXILIARY OBSERVATIONS

Although auxiliary observations are an important aspect of ice analysis, their usefulness depends greatly on two features: they must be timely and they must contain accurate location information. Timeliness is particularly important in areas where conditions may change quickly. For instance, it does the ice analyst little good to learn that the ice edge was advancing at 3 kt four days ago. Accurate location information is particularly important when reporting the ice edge because, as has been described earlier, the remotely sensed imagery often does not accurately locate the ice edge. This makes auxiliary observations very useful.

1.3 SOURCES OF AUXILIARY OBSERVATIONS

1.3.1 Shore Station Ice Reports. Obviously, shore station reports are highly local in nature. Unless the observer has access to enhanced elevations, only ice conditions within a short distance from shore can be reported. However limited the extent of these observations, the ice analyst can at least be certain of their location which, under some circumstances, can be of great value. The ice analyst must keep in mind that a shore station observer may be unaware of leads and other features just a few km away from his station. In order to make some judgement about a shore observer's report, it would be useful for the analyst to have some idea of the distance at which ice conditions can be seen from each station. Shore station reports from the following countries are currently utilized:

Source of Data	Area Covered
Argentina	Antarctica
Denmark	Baltic
Denmark	Greenland
Fed. Rep. Germany	Baltic
Finland	Baltic
German Dem. Rep.	Baltic
Norway	Baltic
Norway	Northern Islands
Poland	Baltic
Sweden	Baltic
U.S.S.R.	Baltic
United Kingdom	Antarctica
United States	Antarctica
United States	Alaska

1.3.2 Ship Ice Reports. Ice reports from ships can have great value to the ice analyst since the shipboard proximity to the ice and the motions of the ship allows the ice observer to make an accurate estimate of ice form and thickness and a reasonably accurate estimate of ice concentration. Recent improvements in navigational systems have greatly improved the locational accuracy of ship ice reports so that it should be possible to make precise comparisons with satellite-derived

data. Because of the value of ship ice reports, a special computer program at Fleet Numerical Oceanography Center scans for ice data among the weather reports gathered by the International Ship Weather Reporting System. These ice reports are then transmitted to ice analysts at the Joint Ice Center at Suitland, Maryland.

1.3.2.1 Arctic Ice Ship Reports are obtained from the following sources: U.S. Coast Guard ice breakers, Military Sealift Command vessels, NOAA research ships, merchant and fishing vessels.

1.3.2.2 Antarctic Ice Ship Reports are obtained from the following sources: U.S. Coast Guard ice breakers, Military Sealift Command vessels, research vessels (foreign and U.S.), merchant and fishing vessels.

1.3.3 Aircraft Observations. Aircraft reports have great value to the ice analyst because of the observer's ability to provide ice reports from a large area and, in some cases, from locations specifically requested by the ice analyst. However, it is not always possible for the aircraft ice observer to make as detailed observations as the ship observer. It is possible that errors regarding freezing conditions and other aspects of the ice might be made. As with ship reports, the value of aircraft reports depends a great deal on the ability of the aircraft's navigational system to provide accurate locations for the ice observations.

1.3.3.1 Arctic Aircraft Ice Observations are available from the following sources:

(1) U.S. Navy dedicated sea ice reconnaissance flights. The following observation techniques are available: visual, radar, radiometer (sea surface radiation thermometer) and laser profilometer.

(2) U.S. Navy ice observer flights of opportunity. Observation techniques available are visual and radar.

(3) U.S. Coast Guard International Ice Patrol (visual and radar observations).

(4) Private industry (primarily Alaska sector)(visual observations).

(5) U.S. Navy Patrol aircraft (radar observations).

(6) Canadian Ice Center Patrol aircraft (observations by side-looking airborne radar and visual observation).

(7) Denmark Ice Patrol aircraft (visual and radar observations).

(8) Norwegian Patrol aircraft (visual and radar observations).

(9) Japanese Patrol aircraft (visual and radar observations).

1.3.3.2 Antarctic Aircraft Ice Observations are available from the following sources:

(1) U.S. Navy dedicated ice reconnaissance flights (visual and radar observations).

(2) U.S. Navy ice observer flights of opportunity (visual and radar observations).

(3) U.S. Coast Guard flights (visual observations).

(4) United Kingdom (visual observations).

CHAPTER VIII. METEOROLOGICAL AND CLIMATOLOGICAL RELATIONSHIPS WITH SEA ICE

INTRODUCTION

Since it is clear that the formation and removal of sea ice from the ocean surface are related to meteorological conditions, it would seem logical that the variability of ice conditions would reflect meteorological variability. From this point of view, observed variabilities in ice conditions should be explainable in terms of meteorological events.

However, determining the nature of the relationship between sea ice and meteorology is not simple. One of the biggest problems is a meaningful characterization of the ice. For instance, the terms "late" or "early" are fairly descriptive, but "light" and "heavy" are also terms which have been used to describe ice conditions. Does "heavy" mean thick ice or merely compacted ice? Because of ambiguity in the terms used historically, it has not been easy to relate recorded meteorological data with ice conditions. In recent years studies relating ice and meteorology have defined quantitative measures (or indices) of ice behavior so that numerical ranking of ice conditions can be performed. This technique has considerably improved studies relating ice and meteorological conditions.

SECTION 1. CASE STUDIES OF RELATIONSHIPS BETWEEN ICE CONDITIONS AND METEOROLOGY

1.1 BARENTS SEA

As was described in Chapter III, Section 3, the area of the Barents Sea covered by ice in the winter and early spring can vary between 50% to 90%. This variation results from the configuration of atmospheric pressure patterns which produce either southeasterly or southwesterly flow into the region. Southwesterly winds result in the introduction of air warmed by the north Atlantic Ocean. Southeasterly flow during the winter results in the introduction of air cooled over the snow covered Asian continent. At times, the atmospheric pressure patterns responsible for these flow patterns can remain stationary for periods of up to two

months. Stability of one pattern or the other for a period of this length results in variations in ice extent.

1.2 BEAUFORT SEA

For many years ice conditions in the summertime have been described as heavy or light depending on the ability of ships to navigate around Point Barrow to or from the Chukchi Sea. An analysis was performed to determine whether any systematic relationship could be found between heavy and light ice years and climatic parameters. It was found that during heavy ice years, persistent atmospheric patterns resulting in onshore winds are responsible for holding the floating ice into shore. Melting is minimized because the winds off the ice are generally cooler than offshore winds. Any voids in the pack which do occur are filled due to onshore pressure within the ice pack. Pressure pattern configurations responsible for the onshore flow patterns can persist for periods of two to three months so that once heavy ice conditions are initiated, they can persist for the remainder of what would normally be the ice free season (Rogers, 1978).

1.3 BERING SEA

It has long been recognized that the ice extent in the Bering Sea varies in extent from year to year. Years when the ice was extensive were referred to as heavy ice years and those when the ice extent was limited were termed light ice years. Analysis of storm tracks in the Bering Sea has shown that there are two principal tracks of storms in the area: one parallel to the Aleutian Island chain, and one curving northward into the Bering Sea. Furthermore, light ice years are characterized by many storms penetrating the Bering Sea region, particularly along its western sector. Heavy ice years are characterized by fewer storms entering the region and by a tendency for low pressure centers to be quasi-stationary over the western Gulf of Alaska and southeastern Bering Sea. It has been suggested that ice advance in the Bering Sea is associated with cold continental, northeasterly winds when the arctic high pressure dominates the northern Bering Sea and eastern Siberia, and that storms penetrating the region interrupt these northeasterly winds. Not only can this stop ice advance in the region, but it can also cause its retreat (Pease and Salo, 1981).

1.4 DAVIS STRAIT - LABRADOR SEA

Studies based on a ten-year record of ice in this region identified patterns of "early" and "late" ice advance and retreat. Early ice advance is associated with a high frequency of cold, northerly and westerly air flow which not only forms new ice, but also advects second and multiyear ice into the area. A late ice advance appears to result from an increased frequency of airflow from the east, bringing above average temperatures and resulting in late ice formation.

Ice retreat was found to be related to a general synoptic meteorological feature: the 700 mb trough over the eastern Canadian Arctic. The trough is normally displaced eastward in June, July, and August. Early ice retreats were associated with a relatively small ($\sim 4°$) latitude displacement and late ice retreats were found to be associated with larger ($\sim 8°$) displacements. The small, easterly trough displacements result in strong east-west pressure gradients yielding strong winds and the advection of warm southerly air. The larger trough displacements yield weaker pressure gradients and a reduced frequency of southerly winds (Crane, 1978).

1.5 STUDIES OF COHERENCY OF ICE CONDITIONS

The results of the regional studies suggest that light and heavy or early and late ice years are often the manifestation of shifting climatological patterns. The question naturally arises: Do ice conditions within the entire northern or southern hemisphere become severe or mild at the same time or do severe conditions in one region coincide with mild conditions in another area?

1.5.1 Arctic Example. This is a difficult problem to answer precisely, but there is evidence to support both possibilities. First, there is evidence that the energy stored in arctic ice can vary by ± 20 from the mean value in any given year. Second, studies have shown that during winters when temperatures in Greenland are above normal, temperatures can be below normal in northern Europe. This means that Davis Strait (near Greenland) can have heavy ice conditions at the same time that the Baltic Sea in northern Europe has lighter than usual ice conditions (Allison, 1982).

1.5.2 Antarctic Example. Because of the limiting influence of the arctic continental land masses, it is difficult to assess the influence of regional temperature changes on ice extent. However, the circumstances are reversed in the antarctic where the land mass is surrounded by unobstructed ice. A study using satellite imagery to measure mean air temperatures and ice extent found that a 1° C increase in annual mean temperature corresponds to a shrinkage of the antarctic ice extent by 2.5° of latitude (Ackley, 1979).

1.5.3 Hemispheric Coherency vs. Compensating Variations. The example given for the arctic in 1.5.1 suggests that overall climatic conditions may be stable within a hemisphere, but compensating regional variations take place. In other words, when ice conditions are more severe in one area, they tend to be less severe in other areas, leaving the total ice extent and/or temperatures within average levels. The areas experiencing these compensating conditions can change randomly within the hemisphere. The second example suggests that the entire arctic or antarctic ice extent might vary on a hemisphere-wide basis. Other detailed studies show that both occur. However, the compensating regional variations tend to be stronger than the overall hemispheric variations. The regional variations in ice extent are associated with shifting of average atmospheric pressure patterns while the hemispheric variations are related to changes in net transport of energy into high latitudes.

SECTION 2. VARIATIONS IN ICE EXTENT OVER PERIODS RANGING FROM YEARS TO CENTURIES

2.1 INTRODUCTION

In the previous section we have seen that annual variations in ice extent can occur on a regional or hemispheric basis. The next question that naturally arises concerns interannual variations and their relationship to world climatic changes. In this section we will briefly review variations of this type. Our best long-term records of ice conditions relate to localities, often because important activities such as shipping were mentioned in official records or journals. Some of these records extend back over one thousand years. Records of a more regional nature generally extend no further back than a century and include ship logs and some of the earliest professional government-sponsored observations. Ice records of a hemispheric nature only really began with the introduction of imaging satellites in the late 1960's.

2.2 SHORT-TERM LOCAL ICE VARIATIONS

2.2.1 Barrow, Alaska. A numerical index was applied to summertime ice conditions in the vicinity of Barrow, Alaska based on U.S. Navy ice reconnaissance flight data from 1953 and later data derived from imaging satellites. The index showed that each year divisible by five (1955, 1960, etc.) was a severe ice year. (Indeed 1955 and 1975 were the two most severe years of that period of record, causing great problems for sea-lift operations to stations along Alaska's north slope.) Although attempts were made, no cause for the five-year periodicity was found (no other known climate-related pattern coincides with this apparent cycle). The utility of this cycle as an inclusion in other long-range forecasting methods for the Alaska Beaufort Sea is uncertain. However, considering the relatively short period of observation, any consideration of the cycle should be tempered with caution (Barnett, 1976, 1980).

2.2.2 Greenland Sea. Reasonably reliable records of sea ice occurrence in the Greenland Sea have been maintained since the turn of the century. These records have been analyzed for local trends in ice

cover and it has been found that since 1900 there has been a slight, but persistent trend toward lighter ice conditions - meaning, in this case, less extensive ice cover. However, it should be emphasized that the year-to-year variations can be greater than the total long-term trend from 1900 to the present (Skov, 1970).

2.3 SHORT-TERM HEMISPHERIC VARIATIONS

As has been pointed out previously, the antarctic is a much better location than the arctic for measurement of change in ice cover because of the absence of land masses to limit ice growth. Furthermore, the annual sea ice extent in the antarctic varies by a factor of approximately 2 from summer to winter. Therefore, one might expect the antarctic to be more sensitive to climatic change than the arctic.

Studies based on satellite imagery and other careful measurements from 1966 to 1982 failed to yield a significant long-term trend, but the results did hint at a 10-year cycle of variation. The temporal span of the data sample is much too short to give that suspicion any real validity. The studies have shown that the year-to-year fluctuations in ice extent can be very large and that ice extent variations in a particular sector of the antarctic can be counter to the overall trend (Zwally, et. al., 1983).

2.4 LONG-TERM TRENDS

As discussed earlier, we have no reliable hemispheric long-term data. However, there are records from the north Atlantic sector and from the largely land-locked Baltic Sea. It should be emphasized that these records were not ice observations per se but rather records which made reference to ice conditions in a secondary way. These records usually dealt with navigation problems, and were much more likely to mention severe ice conditions than open water. In general, it can be said that the detail and frequency of reports decreases with time and it is most likely that only the most severe ice events are recorded for times over a few centuries ago.

2.4.1 Ice in the Vicinity of Greenland. Around 800 A.D. the Norse settled in Iceland and around 1,000 A.D. in Greenland. Icelandic trade records indicate that the Greenland colony flourished for over 400 years.

There is evidence that a general cooling of the northern hemisphere took place between 1350 and 1850. Data include crop records in northern Europe and tree ring data from North America. About the start of this period, the Norse in Iceland lost contact with the Greenland colony. The principal reason appears to be that ice conditions prevented trade and communication. Excavation of graves has shown that the last burials occurred around 1450. There is no indication of the colony's existence after that data.

2.5 VERY LONG-TERM TRENDS

The extent of sea ice over a very long term (thousands to hundreds of thousands of years) has been measured by an indirect but apparently reliable method involving plant and animal remains in ocean-bottom sediments. The results echo and elaborate upon what we have known about the earth's climate based on evidence of glacier advances and recessions. At the present time the ice cover on the ocean appears to have the least extent it has had in the last 125,000 years. As little as 12,000 years ago, sea ice extent was at a maximum, perhaps extending as far south as 45° N latitude in the north Atlantic during winters. The records indicate that sea ice extent can change rather quickly (by several degrees of latitude in periods on the order of a century) (Kellogg, 1973).

Although the present extent of sea ice is at a long-term minimum, the past variations in ice extent are so irregular that it is impossible to make any short-term predictions based on past variations in ice extent.

SECTION 3. CLIMATOLOGICAL FACTORS INFLUENCING THE EXTENT OF SEA ICE AND THEIR ROLE IN FUTURE ICE EXTENT

It is well established that the world climate has changed considerably over the past 200,000 years, undergoing significant cold and warm spells during that time. Furthermore, there is evidence that sea ice extent has also varied considerably during that time. At present, there are no firm conclusions about what might be the major factors causing these changes in climate and whether any future variations can be predicted on the basis of these factors. Here we list some of these factors and discuss some aspects of their significance.

3.1 ASTRONOMICAL FACTORS

3.1.1 Long-Term Variations In Solar Energy. Very little is known about the relative stability of the thermonuclear processes in the sun. However, the sun is a type of star which appears to be quite stable. Calculations have been performed which indicate that because of its size, changes in the energy generated from the central core of the sun should not be expected to vary by more than 1% in 10 years. Because of our lack of knowledge concerning solar variability, it is usually assumed to be constant.

3.1.2 Short-Term Variations In Solar Energy. Sunspot activity on the sun goes through an eleven-year cycle. Although sunspots appear to be purely surface phenomena, they appear to change the total energy output of the sun by a few percent over the solar cycle. (Solar output has been extremely difficult to measure at the earth's surface.) Attempts have been made to correlate sunspot activity with climatic changes through a number of indicators, the most promising of which is tree rings. The results have not been very successful. Any effect of sunspot activity on solar heating and ice extent on the earth's surface is probably very small.

3.1.3 Earth's Orbit. The earth's orbit around the sun is not circular, but elliptical with the result that at present solar heating is a few percent greater on January 1 than on July 1. The earth's orbit precesses with a period of 25,800 years. As a result, in 12,900 years the northern hemisphere could expect slightly colder winters and warmer summers than at present. It has been argued that this variation is

sufficient to "trigger" other more significant influences on world climate and in ice extent (Malankovitch, 1930).

3.1.4 Atmospheric Dust. Dust suspended in the high atmophere (30 thousand feet or more) reflects sunlight before it has a chance to heat the earth's surface. Small meteors burned in the entry process are a steady source of dust. Some volcanoes also add to atmospheric dust. The famous Krakatoa eruption of 1883 produced sufficient dust that the color of sunrise and sunset were altered for several months. It has been argued that this eruption altered the world climate to some extent at that time. If this suggestion is correct, volcanic activity might play an important role in short-term variations in climate and overall ice extent.

3.2 OCEANOGRAPHIC VARIATIONS

The world's oceans contain a great deal of heat and apparently act as a gigantic thermodynamic flywheel storing heat from the sun and releasing heat into the atmosphere. Oceanic currents transport a great amount of energy from equatorial latitudes toward polar latitudes and have a significant direct moderating effect on ice extent. In addition, atmospheric storms generated from these currents carry equatorial energies even further into the arctic, having further influences on ice formation, extent, and removal. Oceanic currents undergo significant variations with resulting influences on heat transport by the atmosphere. Perhaps the most pronounced of these variations is the el niño, where equatorial currents off South America in the Pacific Ocean change, causing world-wide alterations in storm tracks, energy transport, and very likely sea ice extent.

3.3 REGIONAL CLIMATIC VARIATION

Perhaps if more were known about the influence of oceanic variations on the atmosphere, this topic would be placed under that heading. For the present, however, we must be content with the observation that in the arctic and antarctic variations in semistatic atmospheric pressure patterns occur which have significant influences on regional climate and ice extent. These pressure pattern changes are becoming more predictable as time goes on, increasing the possibility of making accurate seasonal ice forecasts.

3.4 ATMOSPHERIC PROCESSES

3.4.1 CO_2: The Greenhouse Effect. There is some evidence that CO_2 created by burning of fossil fuels is changing the properties of the earth's atmosphere in a way that traps more solar energy and, thus, heats the earth. This is called the "greenhouse effect". One consequence of this effect would be a decreasing of worldwide ice extent.

3.4.2 Arctic Haze. In the early 1950's, observers on arctic weather reconnaissance flights reported seeing layers of haze at altitudes of only a few thousand feet in the skys above the north polar region. This phenomenon has been termed arctic haze. Subsequent studies have shown that arctic haze is very likely man-made and probably arises from industrial activity in the central U.S.S.R. If this is true, arctic haze is a relatively recent atmospheric feature and any effects resulting from it might be noticeable in recent records. It has been estimated that the most pronounced effect is likely to arise from atmospheric heating by carbon particles associated with the haze and enhanced melting of sea ice because of the decreased albedo from deposition of carbon on the ice. Estimates indicate that a 30 km poleward retreat of the average ice edge would result from this effect. If this is true, then this retreat probably took place between 1935 and 1950. No statistcal ice edge studies have been performed to determine whether such a retreat has taken place. Furthermore, other factors discussed in this section would have to be taken into account in such a study. It would probably be difficult to ascribe a measured average ice edge retreat to arctic haze alone (Shaw and Stamnes, 1980).

3.5 SUMMARY

Although world-wide trends in sea ice extent may be taking place as a result of changes in incident solar energy, these changes are probably very small and are not noticed over periods of several years. More significant long-term changes in world-wide ice extent are very likely caused by increased atmospheric CO_2 if the effect is as pronounced as calculations suggest. Arctic haze may have caused a slight poleward retreat of arctic ice in the past few decades, but this effect would be difficult to measure. On a year-to-year basis, worldwide variations in ice extent are more likely caused by changes in oceanic current patterns

and atmospheric dust. Finally, on a regional scale, the largest year-to-year variations in ice extent are likely to be caused by shifts in atmospheric circulation patterns.

CHAPTER IX. OPERATIONAL SEA ICE ANALYSIS

SECTION 1. PROCEDURES AND CONCEPTS UTILIZED FOR SEA ICE ANALYSIS

Sea ice analysis is the process through which a contemporary picture of sea ice is developed. This picture includes the location of the ice edge, the configuration of ice of various types within the ice edge, ice movement, ice formation, and ice removal. The performance of this task on a worldwide basis is a formidable undertaking. The arctic regions are quite large and ice conditions can change quickly. Consequently, data must be acquired over large regions on a daily basis and analyzed as quickly as possible. Furthermore, no single data source supplies all the required information. Consequently, a scheme of collecting information from several sources must be utilized.

1.1 STRATIFIED SAMPLING IN SEA ICE ANALYSIS

This is the name given to the technique of using many data sets to yield desired information concerning a geographically related phenomena such as sea ice. The technique varies, but in general the practice is to use the most reliable information first and to proceed toward the less reliable to fill remainirg data gaps. This, in most cases, means proceeding from best resolution to the worst resolution data.

Prior to beginning a sea ice analysis, the analyst should be thoroughly familiar with environmental conditions that have occurred in the geographic area of interest since the previous analysis. Familiarity with the ice climatology and the mechanisms which affect ice distribution of the area is also a necessary part of the preparation. This preparatory knowledge should help prevent violation of continuity (see IX-1.2) in an analysis series, aid in detection and elimination of erroneous data, and resolve conflicts in data sources.

The first mechanical step in sea ice analysis is to plot all ground truth data from ship, shore, and aerial observations. Next, data from all available visible and infrared satellite imagery is plotted (both 1 km and 4 km resolution). Due to clouds, darkness, and non-availability of finer resolution data, voids in the analysis will normally still exist. These voids are then filled with passive microwave data (currently SMMR).

The above procedure represents an ideal situation but the preferred order of use should not be equated to the relative importance of the data. Each type of data carries its own unique characteristic, and each varies in importance with the season, the current meteorological conditions, and the nature of the mission being supported. For example, the analysis of SMMR data of 60 km resolution is easily subject to errors of that magnitude, and for that reason may be the least preferred data. Yet it becomes the most important data source during periods of cloudiness, and on many occasions it is the only data available due to the more irregular receipt of higher resolution data.

At this point weather charts should be consulted to determine surface winds and temperatures. Areas of ice movement and formation should be suggested from this data and should agree with indications obtained from other data sets (i.e. cloud patterns, ice formations, sea surface temperatures). Finally, site-specific data should be consulted (ship reports, aircraft observations, GOES altimeter ice edge data, surface observers) and used to adjust results.

1.1.1 Problems In Stratified Sampling. Because stratified sampling utilizes data from several sources, each contributing somewhat different information, it becomes necessary to reconcile these data into a coherent picture of ice conditions. In this process, several problems arise:

1.1.1.1 Time of Data Acquisition. The various data sets used for a particular ice analysis may have been obtained over a time span of up to several days. For instance, the SMMR data is updated on a three-day basis. The data display might be as much as three days old. Even data obtained the same calendar day can differ in age sufficiently that some ice conditions might have changed between observations. Ice floes can easily travel at a rate of 1 kt with the result that they may have moved a quarter of a degree of latitude between, for example, an early satellite image and a late ship observation made the same day. Even more importantly, the location of the freezing front can move even faster than individual ice floes. Therefore, the actual time of observation is very important when comparing and combining ice information from several data sets.

1.1.1.2 Scale and Projection Changes. Sea ice analyses are usually performed using polar-projection maps for display of results.

Satellites obtain data in a way that is not closely related to any standard map projection. Because satellites view the spherical earth from a line of single points, the region directly under the satellite path is least distorted and the distortion increases with distance from this line. Some satellites such as Landsat have a small field of view with the result that distortion at the image edge is small and easily corrected. Because of its wide field of view, the distortion on an uncorrected AVHRR image is immediately obvious. ESMR images are even more distorted than AVHRR images. If computer-rectified images from these sensors are not available, the only alternative is to overlay the imagery with a grid of latitude and longitude coordinates which have been distorted in the same fashion as the image and map back to geographical maps using the distorted coordinates as a guide. This procedure requires a great deal of skill and care and can obviously result in errors. In some cases even after coordinates have been carefully overlaid, proportional dividers should be used to transfer data from the distorted frame to the rectified frame.

In addition to this technique, optical devices such as the Zoom Transfer Scope exist which can optically stretch or shrink an image to match a map.

1.2 HISTORICAL CONTINUITY AND PERSISTENCE

Historical continuity and persistence are very useful tools to the routine sea ice analyst. Historical continuity means that each new sea ice analysis must depend on previous analyses, particularly if one has had some verification of the previous analysis. Clearly, there are limits to the amount of ice formation, removal, or movement which can take place from the time of one analysis to the next. Although these limits depend on location and season, the sea ice analyst should develop an appreciation of these limits and use them to test new ice analyses against previous analyses in terms of the implied changes in ice location, type, concentration and configuration. Changes which do not appear to be reasonable should be checked closely to determine whether they were indeed as great as indicated or that either the new or old analysis was in error. For that reason, data used for previous analyses should be kept available so that previous interpretations can be reevaluated at later dates.

In addition, each ice analysis should be checked against statistical maximum and minimum ice edge observations (Figures III-1 through III-24) to determine whether a new extreme observation is indicated. Although the analysis may be correct, it should be verified simply because new extreme observations are unusual.

Persistence is closely related to historical continuity. Persistence, however, refers more to dynamic situations. For instance, if a series of storms has been advancing the ice edge at the rate of 10 km/day for some time, in the absence of any other data one might expect the advance to continue in the near future. In many cases, persistence has been shown to be the best predictor of future behavior. In many locations the probability of persistence from one day to the next is as high as 80%. That is, there is an 80% chance that whatever was occurring one day will continue the next. In the absence of any other data, persistence would be a good indicator in a case such as this.

However, it should be noted that if there is an 80% chance of persistence from day 1 to day 2, there is also an 80% chance of persistence from day 2 to day 3. Therefore, the chance of persistence from day 1 to day 3 is only .80 x .80 = .64 or 64%. The chance of persistence from day 1 to day 4 = 51%. In other words, persistence falls off with time. In this particular case, the chance of persistence to the 5th day would be only 40%. It is more probable that some other dynamic situation has developed than the original situation seen on day 1 is continuing. Persistence varies from place to place in the arctic and antarctic, but, in general, two to three days persistence is not unreasonable at most locations.

A distinction should be made here between persistence of a dynamic event such as a storm as was discussed above and the persistence of a climatological trend. During a particular year there may be a trend toward enhanced or retarded ice extent in a particular region. Such a trend might be expected to persist beyond a period of a few days' duration. However, if such a trend is to be represented in ice analyses where no direct ice observations are available, other evidence such as climatological data should be used to verify that such a trend is continuing to take place.

What should one do when the time that persistence can reasonably be expected to hold has been exceeded? In the absence of any other data, the most likely situation to occur is the long-term average. For instance, if we have been following the Bering Sea ice edge during October and have not obtained data for several days - long enough for persistence to no longer apply - we can only turn to the long-term average ice edge location during October for guidance. As long as no further information is available, the only reasonable procedure is to return the ice edge to that location in reasonable increments. For instance, if the last projected ice edge location was 50 km south of the average ice edge, it would be absurd to adjust the forecast edge abruptly to the average edge. The reasonable approach would be to make the adjustment over a period of several weeks and then retain that location until new data was acquired.

As discussed above, there may be climatological data available as an indirect indicator of ice edge trend. This is more likely in the northern hemisphere than in the southern hemisphere because of the much greater density of reporting stations there. In that case, the climatological data could be used as an indicator of persistence of a trend in ice edge location. However, the application of such "proxy" data to ice edge location analysis should be performed very carefully.

1.3 ROLE OF STRATIFIED SAMPLING IN PRESERVATION OF CONTINUITY

The stratified sampling approach to data analysis insures that all data sets available will be consulted during each ice analysis. This is important because should one or more data sets suddenly not be available, principal reliance will not be shifted to a data set which was not consulted in recent analyses.

For example, AVHRR imagery is easily interpreted and it is possible that if this data set has been available and sky conditions have been clear, an ice analyst may have come to rely completely on this information source, ignoring harder-to-interpret data sources such as passive microwave data. Difficulties arise when it becomes cloudy and the passive microwave data must be utilized for the first time in several days. Since these data sources were not consulted lately, the analyst would not be familiar with the characteristics and current aspects of interpretation of those data sets. It is very likely that serious errors would be made.

On the other hand, if the passive microwave data had been examined regularly, there would be no great problem when applying those data sets to routine sea ice analysis.

SECTION 2. EXAMPLES OF SEA ICE IMAGERY AND ITS ANALYSIS

This section utilizes realistic examples of sea ice data products used in ice analysis to acquaint the reader with the appearance of sea ice in these various formats and to illustrate the relative utility and limitations of the remote sensing systems used in sea ice analysis. The following pages contain these examples:

Figure	System	Example	Location
IX-1	aerial photo	tabular iceberg	northern Greenland
IX-2	aerial photo	small scale bands	Bering Sea ice edge
IX-3	Landsat	medium scale bands	Bering Sea ice edge
IX-4	Landsat	edge of pack ice	Bering Sea
IX-5	AVHRR	polynyas	New Siberian Islands
IX-6	AVHRR	derived analysis map	McMurdo, Antarctica
IX-7	ESMR	passive microwave, sea ice	Antarctica
IX-8,9,10	Landsat	comparison bands 4,5,7	mid-Atlantic coast
IX-11	GOES	sea ice	Atlantic coast
IX-12	AVHRR	comparison, visual and thermal	southern Greenland
IX-13,14	AVHRR/ESMR	comparison of polynya	Barents Sea
IX-15,16	AVHRR/ESMR	comparison of ice detail	Sea of Okhotsk
IX-17	AVHRR	thermal, linear gray scale	Bering Sea
IX-18	AVHRR	thermal, enhanced gray scale	Bering Sea
IX-19	AVHRR	thermal, "ice table" gray scale	Bering Sea
IX-20	SMMR	passive microwave display,NEDS	Antarctica

FIGURE IX-1. TABULAR ICEBERGS OFF NORTHERN GREENLAND

Although one usually thinks of floating ice shelves in terms of Antarctica, several ice shelves occur off northern Greenland and Ellesmere Island. This oblique aerial photograph shows a group of three tabular icebergs which may have been calved off an ice shelf in northern Greenland. (Note the adjacent annual ice with a much smaller freeboard.) These icebergs were under the influence of the East Greenland Current and were transported directly into the North Atlantic. Similar icebergs are calved from the ice sheets of Ellesmere Island, principally the edge of the Ward Hunt Ice Sheet, and join the Beaufort Gyre. Although strictly speaking, these features are tabular icebergs, they are called ice islands when they are located in the arctic drift ice. Ice islands can be resident in the arctic pack for several decades. The prinicpal mechanisms for their removal are: (1) physical destruction by break-up, largely when they ground (2) transport out of the arctic through the Greenland Sea.

FIGURE IX-2. SMALL SCALE BANDS

This photograph was taken obliquely out the side window of an aircraft at an altitude of approximately 1500 m. The viewing angle here is such that the horizon is in the distance at the top of the photograph. The ocean surface seen at the bottom of the photograph is below the aircraft at an angle of 45°. The photograph looks north, showing a portion of the Bering Sea just south of the drift ice edge. Surface winds are toward the viewer. Bauer (1978) has classifed the streamers of ice seen here as "small-scale bands" and associates them with newly forming ice under windy conditions. Surface observations have found these bands to consist of slush and shuga. In contrast to medium-scale bands, these features are aligned parallel to the wind and are only a few meters wide.

FIGURE IX-3. MEDIUM SCALE BANDS

This Landsat image shows the ice edge in the southern Bering Sea on 19 March 1973. North is at the top of the image. The image scale is 1:1,000,000 or 1 mm = 1 km. In the upper portion of the image, irregularly broken pieces of drift ice can be seen. This is the normal appearance of Bering Sea drift ice and that portion of the image could have been obtained almost anywhere within the Bering Sea ice. However, the ice edge runs across the center of this image and exhibits morphological features found only at the ice edge when a wind is blowing away from the ice edge. Bauer (1978) has described the irregular bands of ice appearing here as an ice edge phenomena appearing under melting conditions. The bands, 3 to 4 km in width, are made up of small pieces of ice and are classified as "medium scale bands." The wind is roughly perpendicular to the medium scale bands.

W169-00 N056:30
22/W167 45 N N57 10/W167-39 MSS

W168-00,
D SUN EL29 AZ154 196-3335-A NASA ERTS E

W169 00

W168-00

N056 30

FIGURE IX-4. BERING SEA ICE EDGE

This Landsat image shows Bering Sea ice conditions near the ice edge in late February. North is at the top of the image. The image scale is 1:1,000,000 or 1 mm = 1 km. An interesting phenomena can be seen. It is immediately apparent that floes of different ages are present. Older, whiter floes are seen frozen into a matrix of younger, grayer ice. This sequence:

(1) ice formation

(2) breaking into floes

(3) freezing floes into younger matrix

(4) ice breaking into floes, etc.

is a characteristic of the Bering Sea ice. It is, in part, a consequence of transport of drift ice southward from the narrow portion of the sea into the much broader portion to the south.

Care must be taken in ascribing thickness directly to degree of whiteness of floes. Although ice generally becomes whiter with thickness, even older thick ice is grayer than snow covered ice. Here, the older, very white floes are most likely snow covered. At the same time, they are probably thicker than the adjacent ice simply because they are older.

It is interesting to note that when the matrix breaks, it seldom breaks along the edges of thicker floes frozen into the matrix.

AD-A145 286 HANDBOOK FOR SEA ICE ANALYSIS AND FORECASTING(U) ALASKA UNIV FAIRBANKS GEOPHYSICAL INST W J STRINGER ET AL. JUN 84 NERPF-CR-84-03 N00228-81-C-H553 3/4

UNCLASSIFIED F/G 8/12 NL

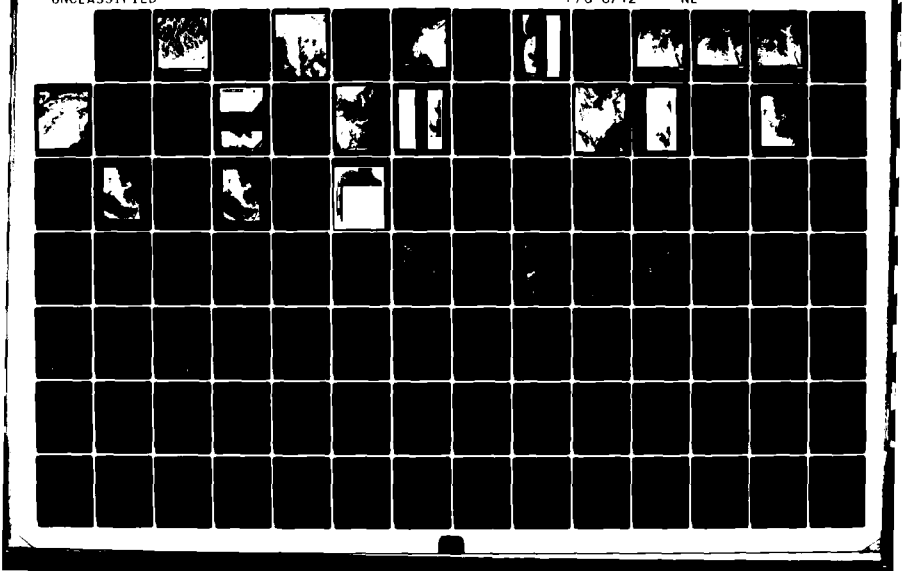

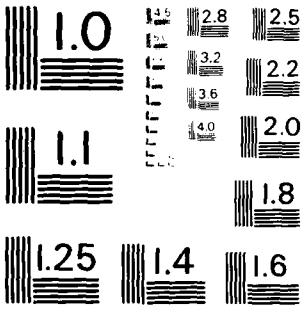

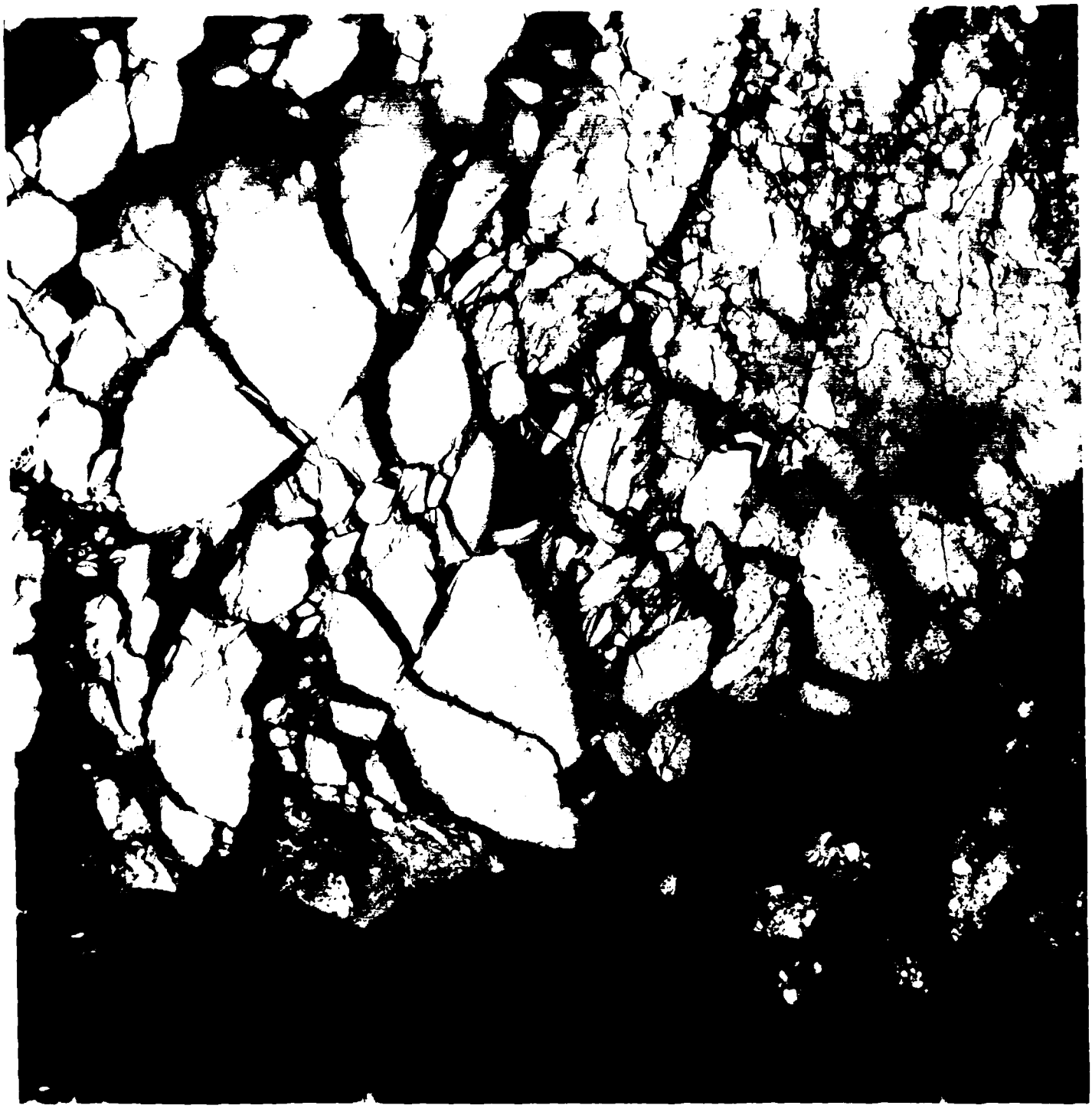

1W169-00 W168-001 N056-301 1W167-00
24FEB74 N57-25/W167-30 N N57-22/W167-26 MSS 7 D SUN EL20 AZ154 196-8104-A-1-N-D-IL NASA ERTS E-1581-21452

FIGURE IX-5. SPRINGTIME SIBERIAN POLYNYAS

This is a portion of an AHVRR image acquired on June 26, 1978. North is at the top of the image. The scale is approximately 1:7,000,000 or 1 mm = 7 km. The New Siberian Islands can be seen as dark areas embedded in fast ice which, even at this date extends to the Siberian mainland. The boundary between fast ice and drift ice can be seen extending to the right (west) beyond the New Siberian Islands. Bands of clouds can be seen above the ice to the north of the islands while larger scattered clouds cover much of the mainland. During spring, polynyas are formed along the Siberian fast ice edge as the drift ice is advected away. Such polynyas can be seen here. Two smaller polynyas can be seen in addition to the large polynya extending over half way across this image. Examination of a good atlas will show that there are small islands located adjacent to these locations. Ice movement can be expected to create polynyas "downstream" of all obstructions such as islands and grounded ice. In this case, "downstream" is to the north.

FIGURE IX-6. ANALYZED PORTION OF TIROS-N
ADVANCED VERY HIGH RESOLUTION RADIOMETER (AVHRR) IMAGE

Shown here is an enlarged portion of a visible band AVHRR image in the vicinity of McMurdo Station in the antarctic. The image was acquired on 13 January 1980 and, thus, represents antarctic summertime conditions.

This highly detailed map of ice conditions could only be drawn by paying careful attention to the location of geographical features by means of a map (and perhaps a shoreline overlay for the satellite image) and also very careful analysis to distinguish clouds from ice. This figure has been constructed so that the map prepared from the image can be raised, exposing the image as it appeared before analysis.

Perhaps the most difficult aspect of this particular analysis was the accurate distinction between ice and clouds. In this regard, the clouds on the right hand side of the figure were no problem. From their patterns, they are clearly clouds. Harder to recognize are the clouds above the water and ice seaward from Terra Nova Bay. Hardest to identify as clouds is the irregularly shaped cloud bank extending between Franklin Island and Mt. Erebus. Perhaps the best indication that these are actually clouds is the fact that they cross over onto and obscure some of the land adjacent to Mt. Erebus.

Once the clouds have been identified, the regions of various ice concentrations can be mapped. See section 2 of Chapter I for definitions of ice concentration categories. At this time of the year, the ice surface can be covered by wet snow and melt ponds. The presence of these conditions on the ice surface can result in a much lower albedo and the possibility that ice will be assigned a lower concentration than is actually present. Note that the lower concentrations indicated on this map are actually higher than the concentration that might first be imagined by the tones and patterns in the region.

Finally, examine the location of McMurdo Station on the image. Its location is marked by a small dark smudge. Human activity creates dust which lowers the albedo of the snow and accelerates its melting. Arctic settlements often become visible this way as the melt season approaches. Even harder to see, but nevertheless visible, is a channel in the ice 10 to 12 nm long, leading from open water to McMurdo. This channel is opened by icebreakers during the spring to facilitate resupply of the station.

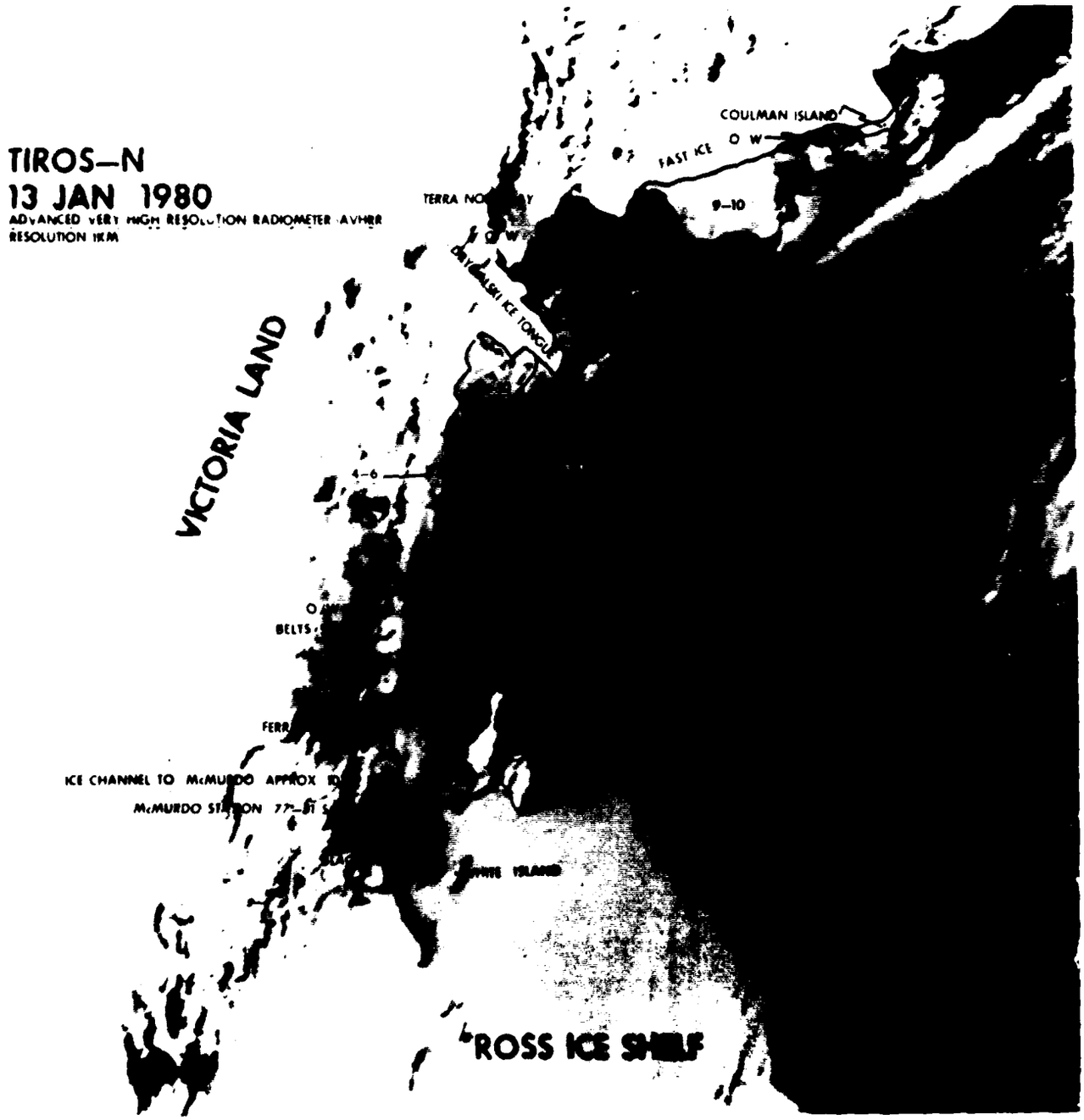
TIROS—N
13 JAN 1980
ADVANCED VERY HIGH RESOLUTION RADIOMETER AVHRR
RESOLUTION 1KM
COULMAN ISLAND
FAST ICE
9—10
VICTORIA LAND
ICE CHANNEL TO McMURDO APPROX
McMURDO STATION
ROSS ICE SHELF

FIGURE IX-7. ESMR IMAGE OF ANTARCTIC ICE CONDITIONS

At first the most readily recognized feature on this image is the southern tip of South America. Just to the right (east) are the Falkland Islands. Our view of Antarctica is aided by the coordinate grid at right. This computer-generated grid corresponds to the ESMR image and shows not only the geographical location of the imaged area, but also the degree of distortion encountered on the wide-angle ESMR data. The grid indicates that the South Pole should be just on the border of the image in the large white field on the ESMR image.

At this point it is useful to discuss several aspects of interpretation of ESMR imagery. As was discussed in Chapter V and VI, ESMR operates in the microwave region where the emissivities of water, land, and sea ice are more important than their temperature in determining their radiative output. Water has an emissivity of 0.50 while the emissivity of first-year ice is 0.92. (Multiyear and glacial ice have emissivities around 0.84.) Therefore, on ESMR we would expect water, emitting lower radiation, to appear white, while first-year ice should appear dark. (ESMR products are usually produced with a negative gray-scale.) Land also has a high emissivity and, therefore, we should not expect to be able to distinguish between land and ice. However, this does not explain the large white areas within the antarctic land mass. This results from two causes. First, this region is glacial ice and, therefore, has a lower emissivity than first-year sea ice. This alone is not sufficient to make glacial ice appear light. Note that the Ross Ice Shelf, the large black indentation into the antarctic continent, is as dark as first-year sea ice located around the rim of the continent. The second and more important reason for the lighter continental areas is that these areas of glacial ice are located at higher elevations and are sufficiently cold that the radiative output is diminished to a point near that of water. The dark line extending upward (east-west) from the inside tip of the Ross Ice Shelf is a series of lower areas separating Lesser Antarctica on the left from Greater Antarctica on the right.

FIGURES IX-8, 9, AND 10. COMPARISON
BETWEEN ICE AS SEEN IN VISIBLE AND NEAR IR BANDS

These images show sea ice as seen on Landsat imagery in band 4 (green light), band 5 (red light), and band 7 (near IR). The region shown contains Washington, D.C. at center and Chesapeake Bay at right. The Mall, a long park extending from the Capitol past the Washington Monument to the Potomac River, can be seen on all three images as a light-colored line extending westward from the center of Washington.

Ice of various thicknesses can be seen in the Potomac River, Chesapeake Bay and many other waterways in this vicinity. Note the particularly heavy concentration of ice in Chesapeake Bay southeast of Baltimore (identified by the radial pattern of major roadways).

Examining these images for ice detail shows that progressively less ice can be seen from band 4 (Fig. IX-8) to band 5 (Fig. IX-9) to band 7 (Fig. IX-10). In general, the shorter wavelengths are not absorbed by water, hence, wet ice can be seen on bands 4 and 5, but not on band 7. Two types of ice are wet: relatively thin forms and flooded forms. In both cases, little near IR is reflected. These examples show why AVHRR band 1 (a combination of Landsat bands 4 & 5) is often used for ice mapping, while band 2 is not. AVHRR band 2 is a near IR band and the imagery does not show all ice forms. AVHRR band 1 maps the full extent of the ice. If one were interested in mapping thin and wet ice types, the ice mapped using band 2 could be subtracted from the area mapped using band 1.

01714-156

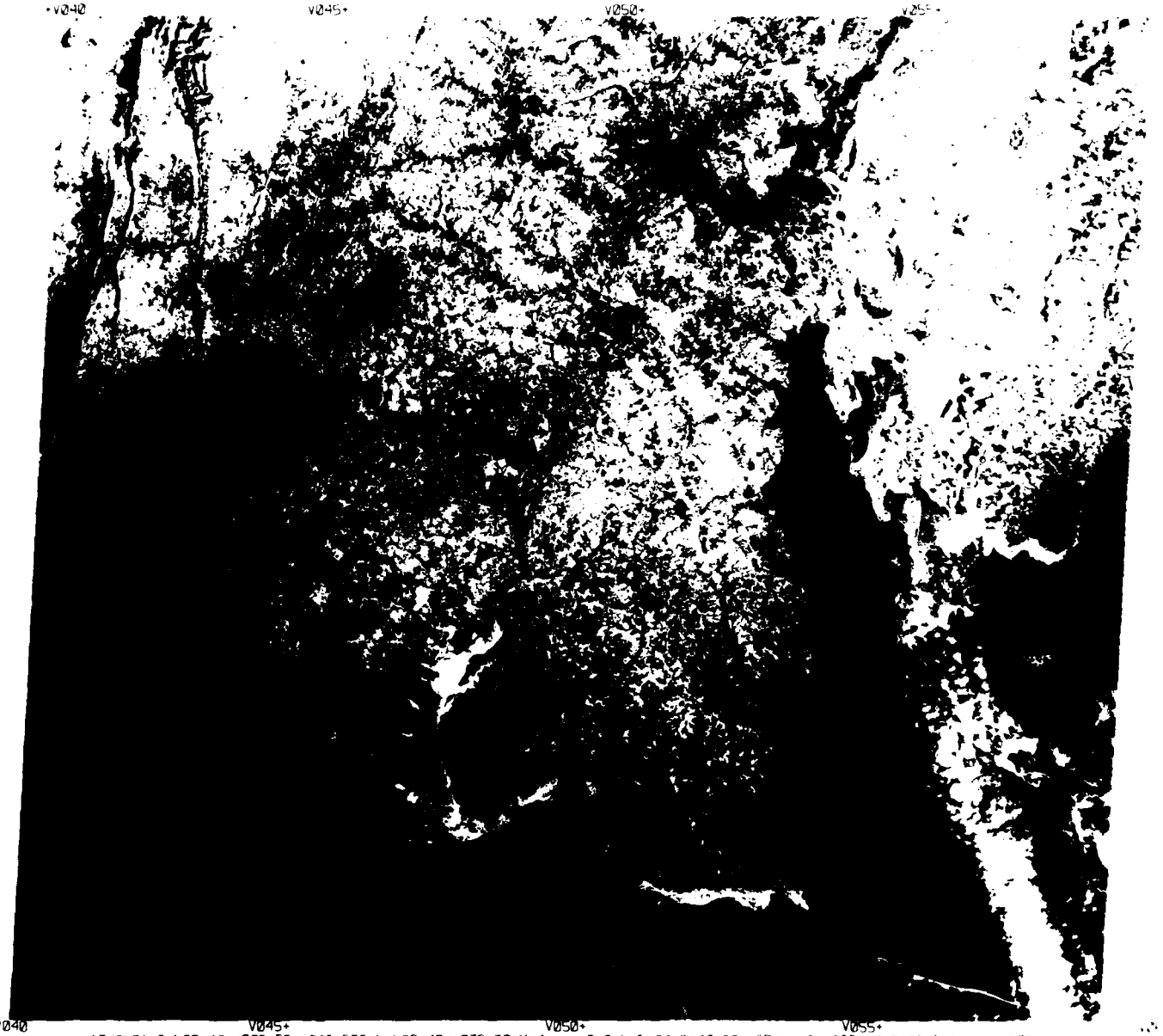

12JAN81 C N38 47/W076 55 USGS EDC N N38 46/W076 50 M 4 D SUN EL22 A147 33H CP N ... NASA ANDSAT E ...506+4

016 033

01714-157

016 033

01714-159

016 D 033

FIGURE IX-11. ICE SEEN ON GOES IMAGERY

One does not normally think of GOES as an ice-detecting satellite. Since it is an equatorial satellite, distortion increases with latitude so that by around 60°N or S, the imagery is essentially useless. However, a considerable amount of sea ice does occur at latitudes lower than 60°, particularly in the northern hemisphere on the east-facing coasts of North America and Asia. The example given here was obtained simultaneously with the Landsat images of Figures IX-8, 9, and 10. This is a very large scale image enlarged from a standard product. The Great Lakes can be seen across the top (north) portion of the image and the eastern U.S. coast is on the lower right-hand side. Chesapeake Bay can be identified by a long line of clouds extending over half its length. The approximate area of the Landsat image has been outlined faintly in black. (Note that the tip of the cloud band appears at the bottom of the Landsat images.)

Close examination of the GOES image reveals the large ice jam seen south of Baltimore on the Landsat image. The ice detected corresponds well with the ice seen on the Landsat band 7 image; note that the thinner ice forms seen on Landsat bands 4 and 5 cannot be seen on the GOES image. More ice can be seen in Delaware Bay, just to the east of Chesapeake Bay.

FIGURE IX-12. COMPARISON OF SUMMERTIME VISUAL AND THERMAL IR ICE IMAGERY

Shown here is a pair of enlargements from AVHRR imagery of the southern tip of Greenland obtained on June 30, 1978 with north at the top of the image. The upper image is from the thermal infrared sensor, while the lower image was obtained from the visual band sensor.

The lower image shows the scene much as we might expect to see it from space. The Greenland ice cap is a solid white. On the fringe of the ice cap, the narrow band of exposed land can be see, and adjacent to this, the ocean. A glance at the thermal image shows that the distinction between warm land and cooler water is more pronounced than on the visual image. On the other hand, the distinction between ice cap and ocean adjacent to land can only be made by use of our knowledge of the geography of the area. Evidently, the ice cap surface and the water around the land are nearly at the same temperature.

Looking at the visual image again, we see cloud patterns across the lower portion of the image. In the left and central portions, the clouds appear in clumps and might be strato-cumulus from their appearance. The clouds in the right-hand corner appear as diagonal streaks. On the thermal imagery, the diagonal clouds appear as the whitest objects in view. (The white circle is a hole in the original image.) The strato-cumulus clouds appear to be near the water temperature as they are nearly invisible against the water. Clearly, the diagonal clouds are considerably colder than the strato-cumulus clouds and anything else on the image. It is, therefore, most likely that they are cirrus since cirrus occur at high altitudes where air is quite cold.

Finally, we are ready to look at the ice on these images. On the visual image, the ice can be seen in swirling streaks along the eastern shore of Greenland and turning to the west along the southern tip of the island and drifting northward along the western side of the island. This ice is following the East Greenland Current, a narrow stream of current down the eastern side of Greenland which curves up around the southern tip of the island. Turning to the thermal image, we cannot see these streams of ice floes. Instead, along the eastern side of Greenland, we see a band of water which must be somewhat cooler than the ocean further east. This must be the cool water of the East Greenland Current.

The reason we do not see the ice is because the water and ice are very nearly at the same temperature, or perhaps are at the same temperature. We must remind ourselves that this image was obtained at the end of June when the sun is high in the arctic sky and there is considerable warming. The ice in the East Greenland Current is melting. It is likely that air temperatures over the ice are above melting temperature and the ice has warmed to its melting temperature somewhere just below 0° C. The East Greenland Current is kept cold by this melting process. As a result, the ice cannot be seen against the water. For this reason, summertime thermal imagery is not a very reliable source of data for ice mapping purposes.

30 JUNE 1978

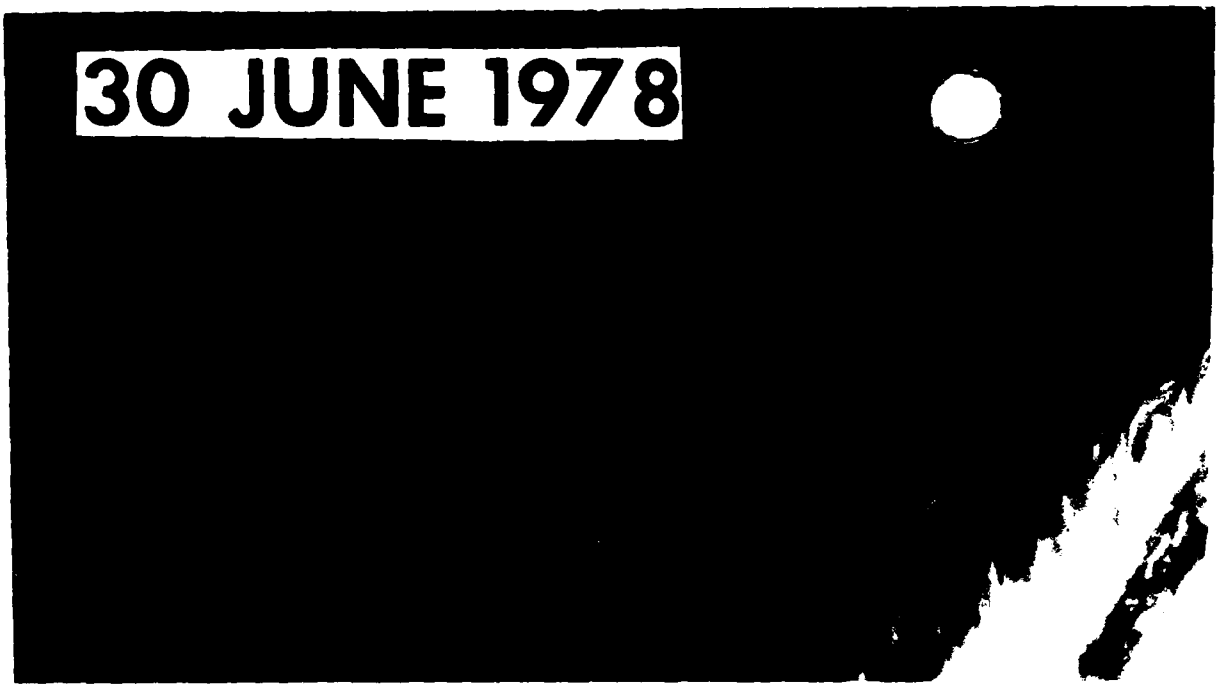

FIGURES IX-13 AND 14. IDENTIFICATION OF POLYNYAS ON ESMR IMAGERY

Figure IX-13 is an AVHRR visual band image showing much of the Barents Sea. The Eurasian mainland is on the right hand side of the image. The islands of Novaya Zemlya are just to the right of lower center, while Severnaya Zemlya is located just above right center. Franz Josef Land is to the left of Novaya Zemlya and Svalbard is in the lower left. Several polynyas which appear as black areas are visible adjacent to these groups of islands.

Figure IX-14 is an ESMR image showing the area of Figure IX-13 at top and extending to Newfoundland at the bottom. Greenland can be seen in the center of the image and Iceland just to its right. The orientation of these images is shown by the dot-matrix coordinate grid provided with the ESMR image. The north pole is located in the upper right-hand region of this grid. Although the wavelengths monitored by ESMR are more sensitive to emissivity rather than temperature, the higher elevations of Greenland are sufficiently cold to emit less radiation than the surrounding warmer ice. Hence, the high interior of Greenland and adjacent higher elevations appear as gray tones. The polynyas of Figure IX-13 are located above Greenland on this image. Close examination will show a remarkable correspondence between the polynyas seen on these two figures.


180:13:58:10 8663 V2B2238 29JUN78 N5 VPEC

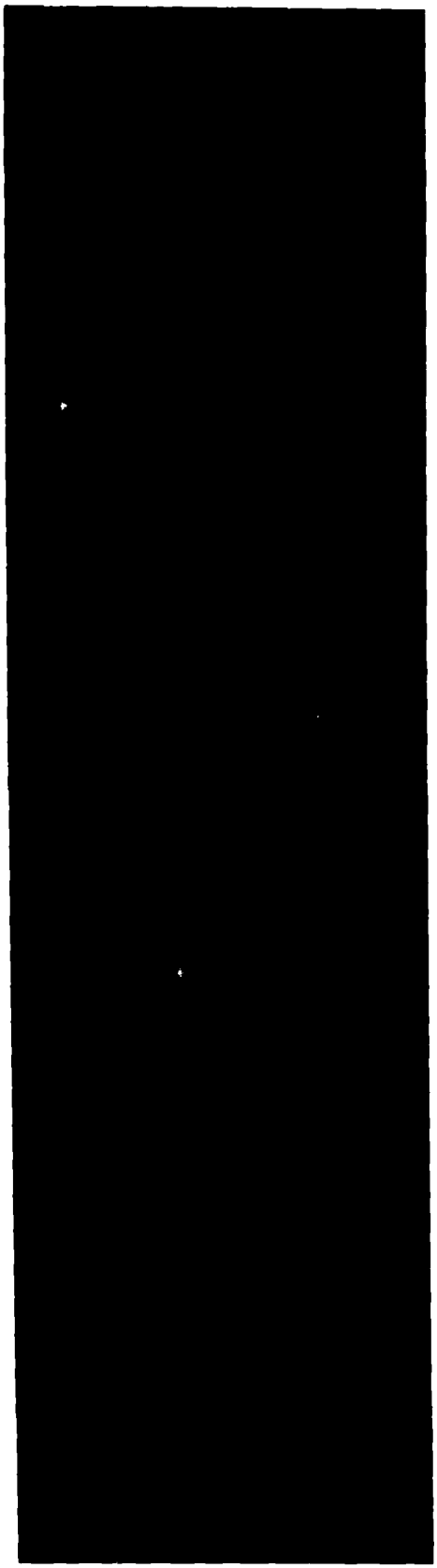

FIGURES IX-15 AND 16. SEA OF OKHOTSK: ICE DETAIL ON MICROWAVE IMAGERY

These two figures have been chosen to show the ice detail which can be detected on passive microwave imagery. The Figure IX-15 is an enlarged portion of a AVHRR visual band image of the coast of Eastern Siberia. The Kamchatka Peninsula, with its characteristic spine of mountains can be seen on the right. The Sea of Okhotsk occupies the central portion, while the Siberian mainland borders the north (top) and western side of the sea. A very bright patch of sea ice can be seen adjacent to the land in the southwest corner of the image. This is a well developed sheet of fast ice. On the right-hand border of this compact coastal ice is the island of Sakhalin.

Several dark areas can be seen within this ice. The group on the left are islands and can be identified by means of an atlas. The large dark area in the center of the ice field is largely open water (a polynya). Above this ice is another area of ice. This patch is not connected to shore and appears to consist of a collection of thin floes.

Turning now to Figure IX-16, we see how this region appears on the low resolution (but all-weather) passive microwave ESMR imagery. The region shown on this enlargement is significantly larger. The most easily identified land feature is the Korean Peninsula in lower Center. The Japanese island of Honshu is directly east (right). The right-hand edge of data cuts through Honshu in a north-south direction and continues up the image, cutting through the northern Japanese island of Hokkaido and then through the Kamchatka Peninsula. The large white area at the top (to the west of the Kamchatka Peninsula) is the Sea of Okhotsk. Within the Sea of Okhotsk is a large dark area with a smaller dark area just below. These are the patches of floes described earlier in the discussion of the Sea of Okhotsk as seen on the AVHRR visual imagery. Note how well these floes contrast with the surrounding water. The larger patch is approximately 200 km in length.

Below these patches, the region of compact coastal ice also discussed in terms of the AVHRR imagery is seen. However, since there is no contrast between this ice and land, it is hard to detect (although a curved band of very thin ice can be seen just above the fast ice). Recall the mention of a group of islands and a polynya. The islands cannot be seen here, but the polynya is visible.

About two inches below this polynya is another faint white patch just north of an indentation in the shoreline. This is Lake Khanka, located just north of the USSR's port of Vladivostok (located at the indentation).

This example shows the utility of the ESMR imagery for mapping ice. It also shows that the best interpretations of this imagery are made with reference to maps, since ESMR does not distinguish well between fast ice and land.

FIGURE IX-17. AHVRR IMAGE WITH LINEAR GRAY SCALE

This is an AHVRR band 3 image of the Bering Sea adjacent to Alaska, obtained December 14, 1979. North is at the top and Bering Strait occupies the top center portion of the image. On this image the strength of radiation is proportional to the degree of darkness, hence, light areas are cold and dark areas relatively warm. Land masses at this time are cold and appear white. Usually, there is an inversion due to radiative cooling of the surface. This inversion is greatest in flat areas and valleys. Hillsides and higher elevations are usually warmer and, therefore, darker. Also, clouds are often warmer than the area they overlie. For instance, most of the Siberian Peninsula is overlain by a thin layer of warm clouds.

The ice edge on this image is reasonably well defined. The ice is colder than the water and appears lighter in tone. Thicker floes radiate less heat than thin floes and appear even lighter in tone than the thinner floes. Examination of the ice edge shows that some fairly large bands of ice perpendicular to the ice edge have formed. This gives rise to the possibility that this is a freezing front and not just a static ice edge. However, although more information may actually be present, this particular data format does not allow precise determination of where freezing is actually taking place.

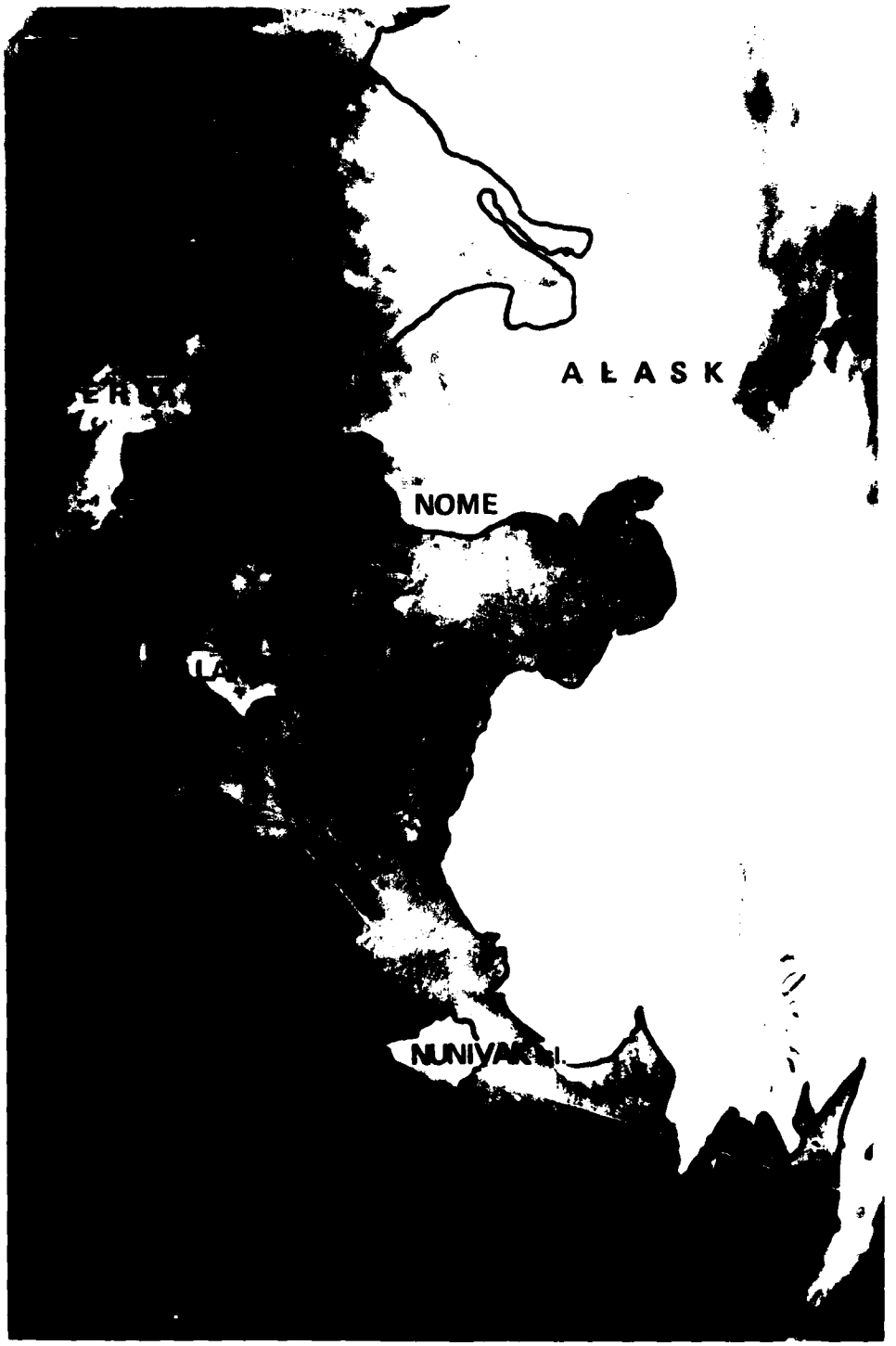
NOME

FIGURE IX-18. AHVRR IMAGE WITH ENHANCED GRAY SCALE

Seen here is the same AHVRR image as shown in Figure IX-17. However, the assignment of gray level to temperature no longer increases linearly from white to dark as temperature increases. Instead, the assignment of gray level is according to the scale presented below.

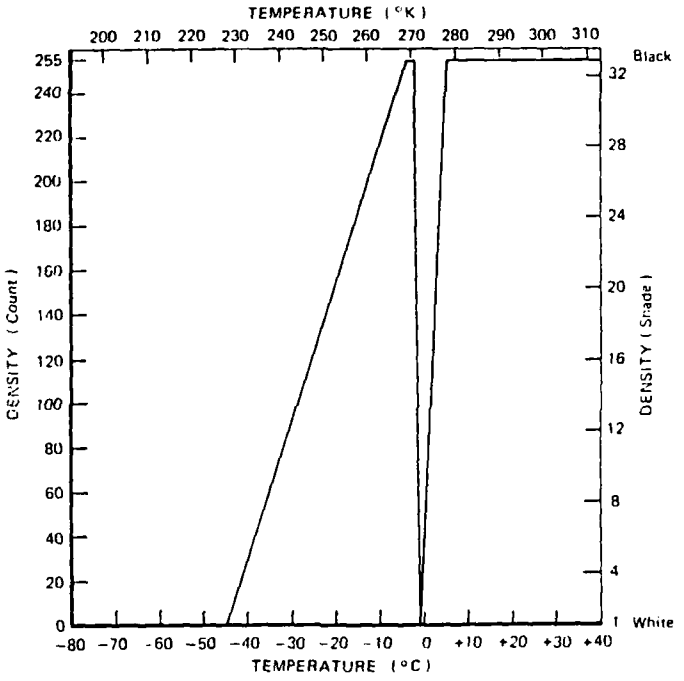

BREAKPOINTS

Segment	From	To
1	<-80°C/000	-45°C/000
2	-45°C/000	- 4°C/255
3	- 4°C/255	2°C/255
4	- 2°C/255	1°C/000
5	- 1°C/000	5°C/255
6	5°C/255	>40°C/255

On this scale, all temperatures above +5° C are black, but so are temperatures between -2° C and -4° C. This is not a problem because these two temperatures are well separated geographically. Note where the ice edge is located. The band of black above the edge is clearly a band of newly formed ice and must be in the temperature range -2° to -4° C.

The other black area is in the ocean at the bottom of the image. This has to be the region above +5° C. The temperatures between +5° C and -1° C have been assigned the entire gray scale. This is the region of cooling ocean water between the black +5° C water and the freezing front. Note that as the water gets cooler, the gray scale assigned is lighter in tone. Between the white representing water at -1° C and the black representing ice at -2° C is a 1° C temperature range represented by the entire gray scale from white to black. Very close examination of this figure shows a scattering of gray pixels along the border between black and white. This is the narrow region where the first freezing is taking place. Going north across the -2° C to -4° C black band, we reach a region with a continuous gray scale. This is the temperature range from -4° C to -45° C. Finally, anything colder than -45° C is absolutely white. Note that -1° C has also been assigned white. However, by now it is possible to distinguish which white areas are relatively warm (most likely water) and which white areas are very cold (most likely interior land surface).

This stepped gray scale makes possible a very accurate determination of the location of the freezing front and the cooling of the ocean surface in its vicinity.

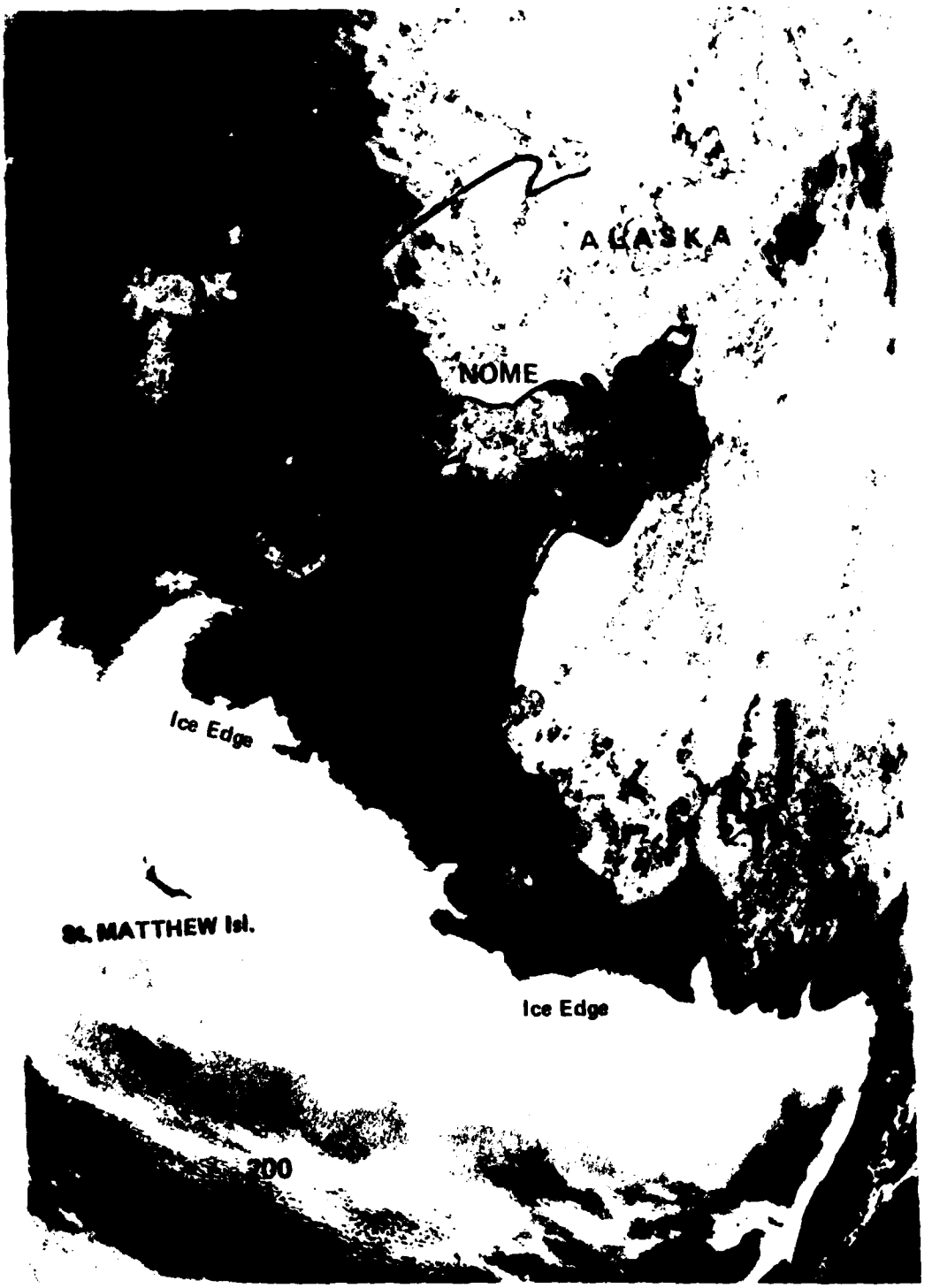
ALASKA
NOME
Ice Edge
St. MATTHEW Isl.
Ice Edge
200

FIGURE IX-19. AHVRR IMAGE WITH 64P/N4P "ICE TABLE" GRAY SCALE

Here again is the same AHVRR image shown in Figure IX-17 and 18. This time the gray scale relationship is even more complicated than that of Figure IX-18. However, it can be easily understood based on an understanding of the gray scale (or enhancement curve) of Figure IX-17. Looking at the gray scale shown here we see that the two are similar except that the region from -2° C to -5° C has been stretched through four dark-to-light gray scale categories. This produces a complicated image, but under the proper conditions, it yields a great deal of information concerning ice formation and growth. For further details see Ahlnas (1979 and 1981).

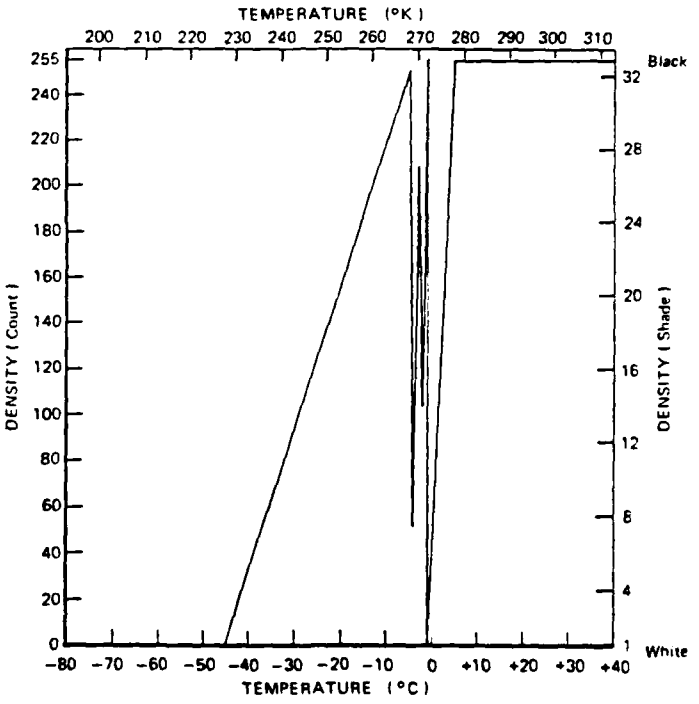

BREAKPOINTS

Segment	From	To
1	<-80°C/000	-45°C/000
2	-45°C/000	- 5°C/250
3	- 5°C/250	- 4°C/052
4	- 4°C/052	-3.5°C/156
5	-3.5°C/156	- 3°C/208
6	- 3°C/208	- 2°C/104
7	- 2°C/104	- 1°C/255
8	- 1°C/255	- 1 C/000
9	- 1°C/000	5°C/255
10	5°C/255	>40°C/255

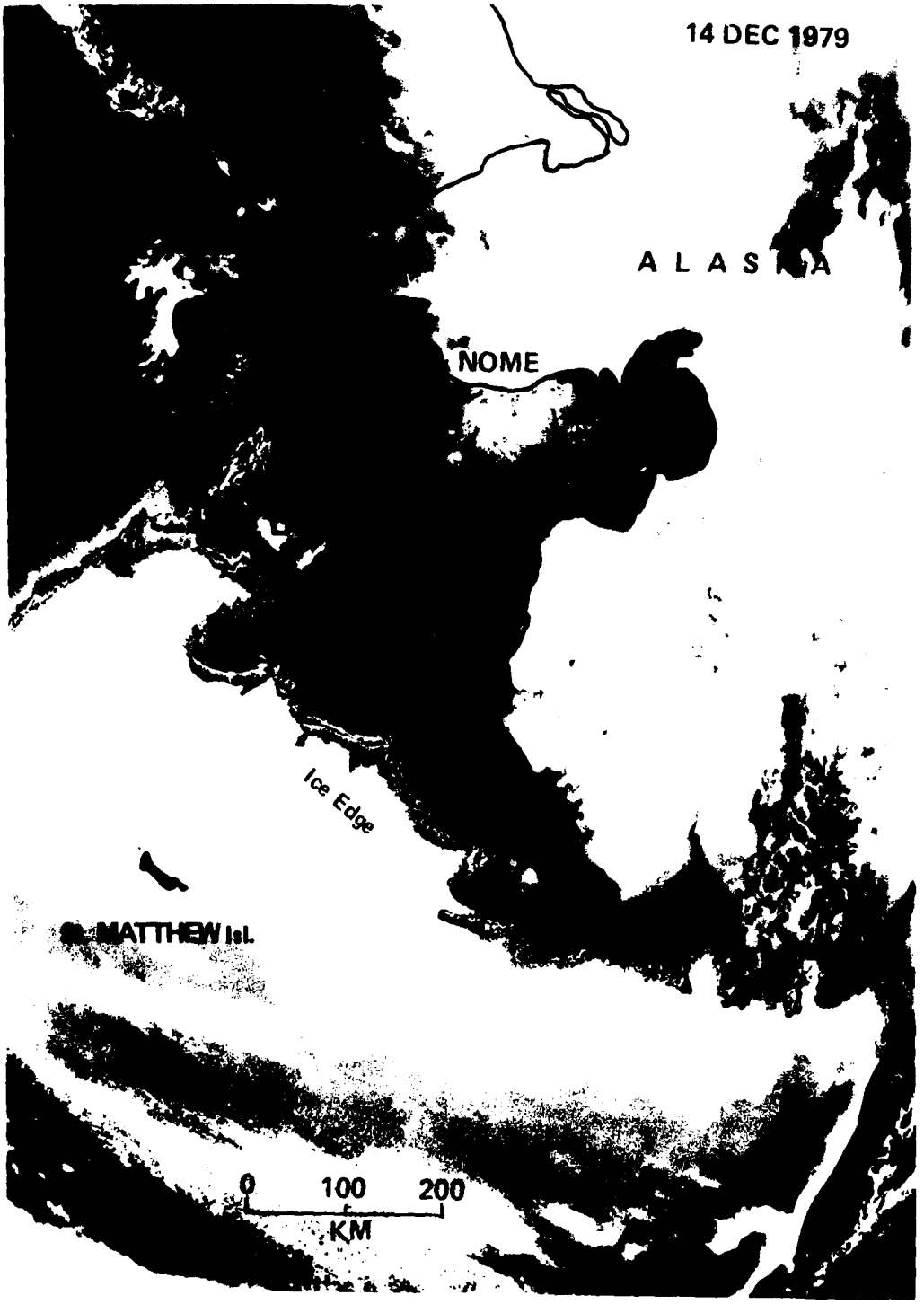
14 DEC 1979
ALASKA
NOME
Ice Edge
ST. MATTHEW Isl.
0
100
200
KM

FIGURE IX-20. ANTARCTIC SMMR DATA AS DISPLAYED ON NEDS

This figure shows the entire continent of Antarctica as seen on the Naval Environmental Display Station (NEDS). The southern tip of South America can be seen at the top of this image. The multiband passive microwave SMMR data has been treated by means of an algorithm utilizing more than one microwave band to produce the multicolor scale of ice concentration seen at the top of the image. As this color bar indicates, high sea ice concentration is shown as red and the scale progresses to light blue representing low sea ice concentration. Very low ice concentration (essentially open sea) is shown as dark blue. The low emissivities of land and glacial ice has been used to mask out continental land and ice masses.

Some aspects of this image should be pointed out. There are blue and black picture elements in the ocean far from sea ice or land, and there is a regular pattern of black picture elements well within the drift ice zone. These obviously misplaced drift ice and land indicators are clearly errors. They result from a number of factors ranging from spacecraft difficulties to lack of algorithm precision. The ice analyst using these data should develop a sensitivity to these sources of error by comparing SMMR data with visual data sets when the visual data is available.

Another feature seen here is what appears to be a patch of intermediate density ice at approximately the 2 o'clock position on the display. This is most likely the effect of a storm creating an area of spray on the ocean surface. Spray has a large emissivity which results in misrepresentation as ice.

LOW SEA
OZ

X. FORECASTING

CHAPTER X. SEA ICE FORECASTING

SECTION 1. INTRODUCTION

The purpose of this chapter is to provide the procedures and background references needed to prepare forecasts of sea ice growth, movement, distribution, and decay. Many of the forecasting procedures employed by the Navy NOAA Joint Ice Center have been adapted from published ice forecasting guides. Space limitations do not allow for the complete reproduction of all the tables and figures used in making the various forecasts. This chapter contains a description of currently utilized techniques from published sources (with references) and detailed descriptions of unpublished procedures with examples.

As with any forecasting procedure, it is desirable that the techniques used to produce the prediction are as objective as possible. However, the measurements of the oceanographic, meteorological, and ice parameters required to increase objectivity in ice forecasting are not always directly available. Consequently, there are no purely objective forecasting techniques. Subjectivity is required in all forecasts. In order to contain that subjectivity within reasonable limits, knowledge relating to median, minimum, and extreme ice extent for specific geographical areas and times of the year are often the most important preliminary information in the preparation of any ice forecast.

1.1 ICE EDGE CLIMATOLOGY

Maximum and minimum ice edge extremes and medians are mapped for the arctic and antarctic and are presented in Chapter III. These figures were produced manually as an interim product.

Computer-determined climatological ice summaries will be produced by the National Climate Center, Asheville N.C. under contract to the Naval Oceanographic Command Detachment, Asheville. The summaries will be constructed from a digital sea ice data base consisting of Joint Ice Center data which is currently under development. The summaries are expected to be completed in 1985.

1.2 ICE FORECASTING OBJECTIVES

At the Joint Ice Center the ice analyst is required to produce ice forecasts representing four time scales. These are:

(1) short-term ice forecasts for the ensuing 24 to 96 hour period which provide close tactical support over a specific locality to an ongoing mission

(2) 7-day ice edge forecasts which are prepared weekly and predict ice edge positions on a hemispheric scale

(3) 30-day ice forecasts which are produced twice monthly and are used primarily for planning purposes in regional areas where fishing, shipping, and military operations are just commencing or may be imminent

(4) seasonal ice forecasts and outlooks which include forecast periods from 60 to 150 days and are used for long-range strategic planning in regional areas.

1.3 PRE-FORECAST EVALUATION AND FORECAST PREPARATION

The first stage in preparing an ice forecast is to subjectively evaluate the recent state of the atmosphere, cryosphere, and hydrosphere to the limit permissible by data availability. The second stage is to review forecast parameters and subjectively determine their likelihood of verification. Listed below are routinely available products used in pre-forecast evaluation and forecast preparation at the Joint Ice Center.

1.3.1 Atmospheric Reports:

1.3.1.1 Synoptic Mean Sea Level Pressure Analyses with Station Plots. These maps are available from the Fleet Numerical Oceanography Center (FNOC) and the National Meteorological Center (NMC) at six hour intervals for the northern hemisphere. FNOC produces maps every twelve hours for the antarctic. Geostrophic winds, surface winds, cloud cover, surface temperature, and surface pressure data can be obtained from these maps.

1.3.1.2 Mean 5-day Mean Sea Level Pressure and Deviation from Normal Analysis. This northern hemisphere map is known as the D-3 MSLP map. Produced at NMC for use in extended range forecasting guidance, the D-3 map is used in evaluating the mean synoptic surface

geostrophic wind patterns for the prior 5-day period. The deviation from normal pressure contours is used to determine areas where anomalous surface pressures are located. Large anomalous surface pressure centers often indicate areas where anomalous ice conditions are observed.

1.3.1.3 Mean 5-day Mean Sea Level Pressure and Deviation from Normal Forecast. This northern hemisphere map is known as the D+3 MSLP forecast map. The D+3 MSLP map and the theoretical ice drift vectors derived from it are the primary ice forecast guidance utilized in 7-day ice forecasts.

1.3.1.4 Mean Monthly Mean Sea Level Pressure and Deviation from Normal Analysis. This northern hemisphere map known as the mean monthly MSLP Analysis is produced twice monthly by the Long Range Prediction Group (LRPG), Climate Analysis Center (CAC) of NMC. The mean monthly analyses are used in a manner similar to mean 5-day analyses.

1.3.1.5 Mean Monthly Mean Sea Level Pressure and Deviation from Normal Forecast. This northern hemisphere map, known as the D+15 MSLP Forecast is produced twice monthly by the LRPG, CAC.

1.3.1.6 30-Day Mean Surface Temperatures Classes. This northern hemisphere map is produced twice monthly by the LRPG and displays classes of analyzed and predicted above normal, normal, and below normal surface air temperatures.

1.3.2 Hydrosphere Reports:

1.3.2.1 Great Lakes Water Surface Temperature Analysis. Produced twice weekly by the NMC, Marine Products Branch, the water surface temperatures provide an indication during freezeup where ice will likely form as the freezing point is approached. The 1°C isotherm is closely monitored for this purpose.

1.3.2.2 National Environmental Satellite Data and Information Service (NESDIS) Sea Surface Temperature Analyses. Available for both the northern and southern hemispheres, the maps indicate areas where ice will likely form as the freezing point is approached. These maps are quite useful when marginal ice zone temperatures are retrieved. The -1°C isotherm is closely monitored for this purpose.

1.3.2.3 Mean Surface Currents. Mean ocean surface currents from a variety of sources are used to evaluate the effects of ocean currents on drift ice. Figures II-1 and II-2 show the major current systems. The Arctic Ocean currents displayed on these and other charts are generally used with considerable caution. In general, polar ocean currents displayed on many charts have been documented with a sparcity of measurements. In areas of continuous ice cover, direct current measurements are scarce and are not seasonally adjusted.

1.3.3 Cryosphere Reports:

1.3.3.1 Joint Ice Center Ice Analyses. A review of a time series of ice charts indicates recent ice formation, expansion, recession, or ablation trends. Comparison of the current analyzed ice edge position with the minimum, median, and maximum ice edge climatology and other oceanographic and atmospheric charts provides insight as to the effects of recent oceanographic trends (e.g. sea surface temperature, waves) and atmospheric trends (e.g. above/below normal air temperatures, wind stress). A continuous series of weekly Arctic Ice Analyses are available from 1972 to present. Antarctic Ice Analyses are available from 1973 to present.

1.3.3.2 Theoretical Ice Thicknesses and Reporting Station Temperature Summaries. Estimations of present ice thicknesses and station temperature summaries for northern hemispheric land stations bordering ice covered seas are routinely available from FNOC. Table X-1 contains a listing of the stations in the routinely monitored network. Figure X-1 identifies the station locations. Gerson (1975) describes and provides a computer listing of the algorithm used to compute the theoretical ice thicknesses from station air temperatures.

1.3.3.3 Theoretical Ice Drift Analyses and Forecasts. Thorndike and Colony (1982) and Skiles (1968) have published relationships relating northern hemispheric mean sea level pressure geostrophic winds and ice drift. The relationships can be utilized with either analyzed or forecast geostrophic wind fields. Figure X-2 identifies the location of grid points at which the theoretical ice drift vectors are computed. Figure X-3 is a partial listing of the FNOC message transmitted through the

Naval Environmental Data Network. It is available upon request at all Navy activities equipped with a Naval Environmental Display Station (NEDS). The FNOC message is computed utilizing the Thorndike and Colony relationship. FNOC produces ice vector analyses at 24-hour intervals extending through 168 hours and forecasts through 72 hours. Extrapolated forecasts are produced from 96 to 168 hours. NMC utilizes the Skiles relationship, producing 168-hour ice vector analyses and ice drift forecasts at 24 hour intervals through 144 hours.

1.3.3.4 Skiles Ice Drift Nomogram. Ice analysts not having access to FNOC and NMC ice drift products or having a mean sea level pressure analysis for which computer-derived ice vectors have not been computed can calculate ice drift from any mean sea level pressure map. Figure X-4 is a scale to convert 4 mb isobaric spacing into a geostrophic wind speed. Figure X-5 is a Skiles ice drift nomogram to convert geostrophic wind speed into ice drift speed and the ice drift deflection from geostrophic direction. The following procedure describes how ice drift vectors can be computed:

(1) From the appropriate mean sea level pressure map (e.g. Mean April Monthly MSLP analysis) locate the vicinity where the drift calculations are to be made. Enter in column a of the Ice Drift Forecasting Table (Table X-2) the distance in degrees latitude between 4 mb isobars. For this example, the isobar spacing between 4 mb isobars in the vicinity of interest is 4 degrees of latitude.

(2) Enter in column b of Table X-2 the latitude where (a) was measured (e.g. 80°N).

(3) Enter in column c of Table X-2 the directions toward which the mean sea level pressure geostrophic winds flow (e.g. 290°).

(4) With the values identified in columns a and b, use the geostrophic wind scale Figure X-4, to determine the geostrophic wind speed in knots. With the value of column a, enter the scale at #1. Proceed vertically until intersecting the 80° latitude diagonal at #2. Proceed horizontally to the left and read the geostrophic wind speed at #3, i.e. 10.2 knots. Enter the geostrophic wind speed in column d of Table X-2.

(5) With the geostrophic wind speed identified in column d of Table X-2, use the Skiles ice drift nomogram (Figure X-5) to determine ice drift deflection and speed. With the geostrophic wind speed of

TABLE X-1

STATIONS IN NETWORK

04202	THULE	21647	MYS SHALAUROVA	72900	HOPEDALE
04210	UPERNAVIK	21824	BUKTA TIKSI	72903	RESOLUTION ISLAND
04220	EGEDESMINDE	21965	OSTROV CHETUREKHSTOLBOVOY	72904	CAPE HOPES ADVANCE
04231	SONDRESTROM	21982	OSTROV VRANGELYA	72906	FORT CHIMO
04250	GODTHAAB	25173	MYS SHMIDTA	72907	PORT HARRISON
04270	NARSSARSSAUQ	25399	MYS UELEN	72909	FROBISHER
04320	DAMATSHAVN	25594	BUKHTA PROVIDENIA	72915	CORAL HARBOR
04330	DANEBORGE	70026	PT BARROW	72917	EUREKA
04340	KAP TOBIN	70086	BARTER IS	72918	ARCTIC BAY
04350	APUTITEQ	70133	KOTZEBUE	72924	RESOLUTE BAY
04360	ANGMAGSSALIK	70200	NOME	72925	CAMBRIDGE BAY
04380	TINGMIARMUIT	70218	NUNIVAK	72938	COPPERMINE
04390	PRINS-CHRISTIANS SUND	70273	ANCHORAGE	72948	CAPE PARRY
20087	MYS GOLOMYANNY	70308	ST PAUL IS	74051	SACHS HARBOR
20292	MYS CHELYUSKIN	70316	COLD BAY	74072	MOULD BAY
20353	MYS ZHELANIYA	70326	KING SALMON	74074	ISACHSSEN
20667	OSTROV BELTY	70350	KODIAK	74081	HALL BEACH
20674	OSTROY DIKSON	72815	STEPHENVILLE	74082	ALERT
20744	MALYE KARMAKULY	72816	GOOSE BAY	74090	CLYDE RIVER
21432	OSTROV KOTELNNY	72818	CARTWRIGHT	74094	CAPE DYER
21504	OSTROV PREDBRAZHEMIA	72819	ST ANTHONY		

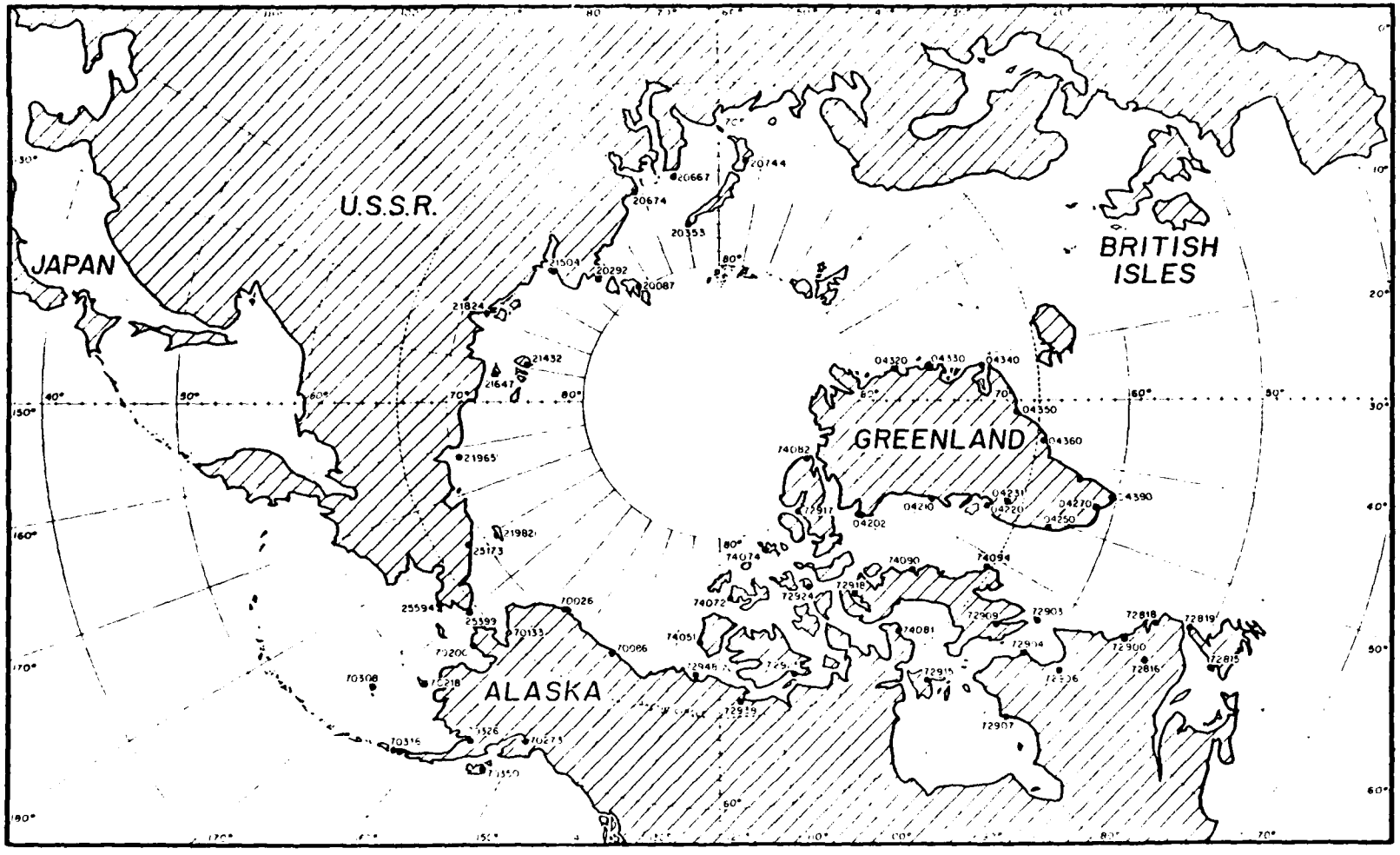

Figure X-1. Map of arctic region showing World Meteorological Organization identification numbers of meteorological stations whose data are routinely available through the Fleet Numerical Oceanography Center (FNOC).

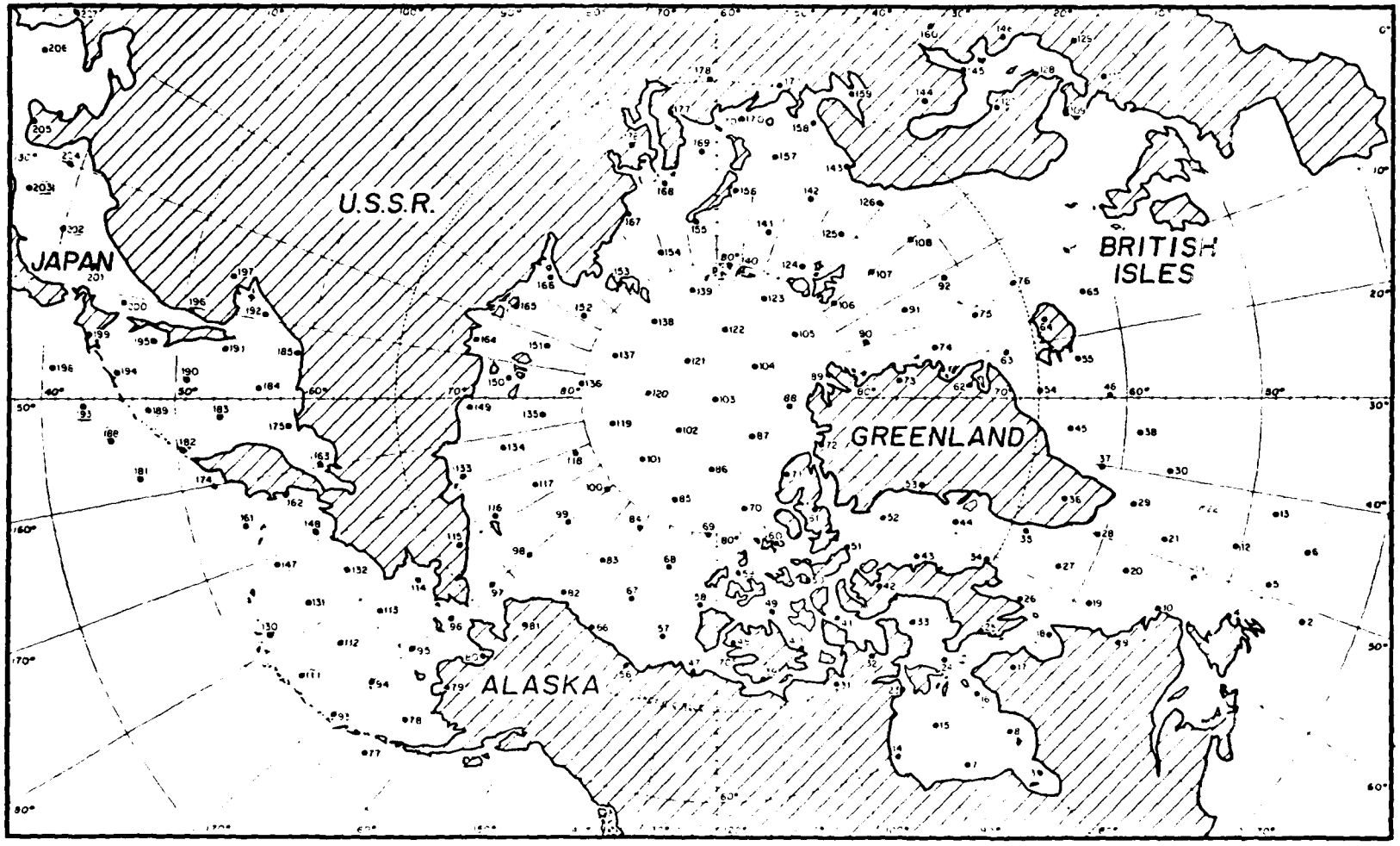

Figure X-2. Map of grid point locations for which theoretical ice drift vectors are computed by Fleet Numerical Oceanography Center ice drift programs.

```
ADVICEDRFT.......(0001),(08/18/83 0912Z) ***..UNCLASSIFIED .***
DRFT
IS IS AN OPS CHECKOUT (PRELIMINARY) PRODUCT.
EASE CONTACT MR. KEN POLLAK, FNOC, AV 878-2169.
TH EVALUATION AND ANY PROBLEMS ENCOUNTERED.
       COMPUTED FREE ICE DRIFT FOR BASE TIME = 83081800
                DD = DIRECTION FROM (DEG/10)
                     NM = TOTAL DISTANCE FOR PERIOD (N.M.)
                      * = FIELDS MISSING (EXTRAPOLATION USED)
                A N A L Y S I S                    F O R E C A S T
DHH: 1100 1200 1300 1400 1500 1600 1700 : 1900 2000 2100 2200 2300 2400 2500
URS: 168  144  120   96   72   48   24  :  24   48   72   96*  120*  144*  168*
  P  DDNM DDNM DDNM DDNM DDNM DDNM DDNM : DDNM DDNM DDNM DDNM DDNM DDNM DDNM
  1  2812 2711 2611 2612 2509 2505 2603 : 2601 2901 2803 2806 2810 2813 2716
  2  2516 2612 2511 2611 2611 2509 2505 : 2604 2506 2607 2609 2610 2612 2613
  3  2517 2616 2613 2710 2705 2502 2001 : 2202 2403 2602 3201 3602 0104 0205
  4  2710 2717 2615 2714 2712 2606 2603 : 2601 1001 2003 2105 2107 2210 2212
  5  2510 2714 2612 2711 2612 2608 2604 : 2603 2604 2705 2707 2708 2709 2711
  6  2618 2814 2812 2812 2811 2709 2705 : 2604 2607 2608 2710 2712 2714 2815
  7  2616 2714 2712 2910 2804 2602 2302 : 1600 0201 3603 3603 3504 3505 3506
  8  2616 2714 2712 2810 2906 2702 2702 : 2002 2601 3303 3405 3408 3410 3413
  9  2816 2817 2815 2813 2909 3004 3002 : 3301 2201 2108 0402 0404 0406 0408
 10  2809 2813 2712 2711 2808 2904 2702 : 0102 0601 1302 1404 1507 1509 1511
 11  2715 2710 2615 2613 2711 2706 2602 : 3602 0303 0503 0602 1002 1402 1603
 12  2621 2819 2716 2713 2712 2707 2603 : 2902 2901 3501 0101 0202 0202 0203
 13  2717 2814 2911 2909 2910 2707 2703 : 2603 2505 2506 2608 2610 2611 2713
 14  3010 3109 3109 3208 3502 3300 1501 : 0701 0301 3601 2901 2602 2503 2405
 15  2608 2705 2705 3006 3303 2901 1901 : 0901 0402 0202 3604 3505 3506 3407
 16  2713 2809 2808 2908 3206 3003 3002 : 1600 0401 0104 3606 3609 3512 3515
 17  2916 2914 2912 2911 3108 3204 3303 : 2702 2401 3501 3604 3606 0108 0111
 18  2715 2714 2712 2811 2908 3104 3402 : 2902 2503 2501 0101 0303 0405 0408
 19  2615 2615 2614 2712 2809 3005 3001 : 3203 3004 2902 3401 0702 0804 0906
 20  2811 2711 2611 2610 2708 2904 2702 : 3204 3105 3003 2502 1903 1706 1609
 21  2709 2811 2711 2610 2608 2705 2603 : 3202 3203 3202 3201 1100 1401 1403
 22  2720 2819 2816 2713 2711 2707 2603 : 2802 2701 1302 1204 1206 1109 1111
 23  0604 0706 0805 0305 3605 3502 0201 : 0501 0401 0102 3503 3404 3405 3306
 24  3106 3406 3405 3506 3408 3204 3202 : 3401 0102 3603 3605 3507 3509 3511
 25  2704 3302 3404 3404 3406 3204 3302 : 3301 0201 0602 0604 0606 0607 0609
 26  2107 2106 2103 2302 3202 3402 0201 : 3302 3202 0102 0403 0504 0506 0607
 27  2510 2510 2410 2409 2706 3103 3501 : 3303 3304 3403 0202 0603 0805 0906
 28  2711 2711 2512 2410 2507 2803 2701 : 3104 3107 3109 3011 3012 3013 3015
 29  2707 2606 2708 2608 2506 2804 2803 : 2802 2905 2906 2907 2907 2808 2808
 30  2815 2814 2913 2911 2808 2806 3004 : 2602 2903 2903 2701 1401 1102 1104
 31  0611 0711 0710 0307 3304 3102 3101 : 3401 3402 3302 3203 3103 3003 2904
 32  0411 0410 0508 0308 3408 3305 3202 : 3301 3402 3303 3204 3205 3207 3208
 33  0306 0208 0207 0207 3507 3305 3302 : 3501 3502 3502 3403 3404 3404 3305
 34  1506 1305 1205 1204 0702 3401 0300 : 3502 3503 3603 0105 0106 0207 0208
 35  2003 2003 2603 2504 2803 3302 3601 : 3603 3507 3611 3614 3617 3621 3624
 36  2306 2208 2307 2307 2306 2701 0101 : 3201 3305 3309 3313 3318 3322 3326
 37  2404 2004 2503 2503 2204 2101 3601 : 2302 2606 2709 2713 2717 2720 2724
 38  2011 2008 3008 3007 2604 2602 3102 : 2303 2605 2708 2710 2712 2713 2715
 39  0612 0612 0411 0207 3504 3403 3402 : 3502 3504 3403 3403 3402 3301 3101
 40  0411 0410 0410 0108 3306 3204 3301 : 3601 3603 3503 3404 3304 3205 3205
 41  0111 0111 0109 3608 3307 3204 3202 : 3501 3401 3302 3303 3204 3205 3206
 42  0606 0407 0305 0305 3604 3403 0101 : 0101 3602 3502 3502 3402 3403 3303
 43  1406 1205 1203 1002 3601 2901 0200 : 3402 3403 3304 3304 3305 3306 3307
 44  0703 0605 0505 0404 0203 3402 3501 : 3603 3606 3609 3613 3616 3620 3624
 45  3603 0502 3601 2701 2204 2003 1301 : 2003 2304 2407 2511 2515 2519 2622
 46  3007 3304 3304 3405 3202 1802 1701 : 2102 2404 2508 2512 2615 2619 2623
 47  0714 0712 0709 0706 0604 0403 0202 : 3301 2501 2002 1904 1806 1808 1810
 48  0413 0412 0310 0108 3606 3605 3603 : 3402 3303 3302 3301 3401 1300 1401
 49  0215 0214 0212 0111 3608 0105 0202 : 0102 3603 3504 3504 3404 3405 3305
 50  0213 0213 0111 0109 0106 0104 0301 : 0201 0102 3503 3404 3304 3305 3206
 51  0708 0608 0507 0405 0304 0303 0501 : 0102 3603 3604 3504 3505 3505 3506
 52  1208 1107 1006 0905 0803 0802 0701 : 0102 3604 3506 3508 3510 3512 3514
 53  1107 1108 1006 0905 0904 0602 0501 : 0301 0204 0108 0112 0116 0121 0125
 54  0306 0405 0404 0103 2903 2404 2001 : 2102 2205 2208 2211 2315 2318 2322
 55  3305 0103 0104 0105 3605 2401 1801 : 2501 2303 2506 2509 2513 2516 2519
 56  0916 1015 1013 1011 0908 0905 0802 : 1801 2002 1904 1805 1807 1709 1710
 57  0810 0810 0808 0805 0703 0302 3601 : 2601 2303 2005 1907 1809 1711 1714
 58  0311 0310 0209 3607 3606 3505 3502 : 2901 2702 2502 2303 2103 2004 1905
 59  0217 0215 0113 0111 0109 0105 0102 : 3101 3102 3104 3105 3106 3107 3108
 60  0420 0317 0315 0312 0309 0305 0202 : 3501 3403 3204 3105 3106 3008 3009
```

Figure X-3. Example of FNOC ice drift message. The right-hand column lists the grid point locations. The left-hand block of figures lists analyzed ice drifts for preceeding times (hours listed at top) and the right-hand block lists forecast ice drifts at future times. The first two numbers in the four-digit ice drift code are the direction from which ice drift occurs (divided by ten) and the second two digits are the magnitude of drift in nautical miles.

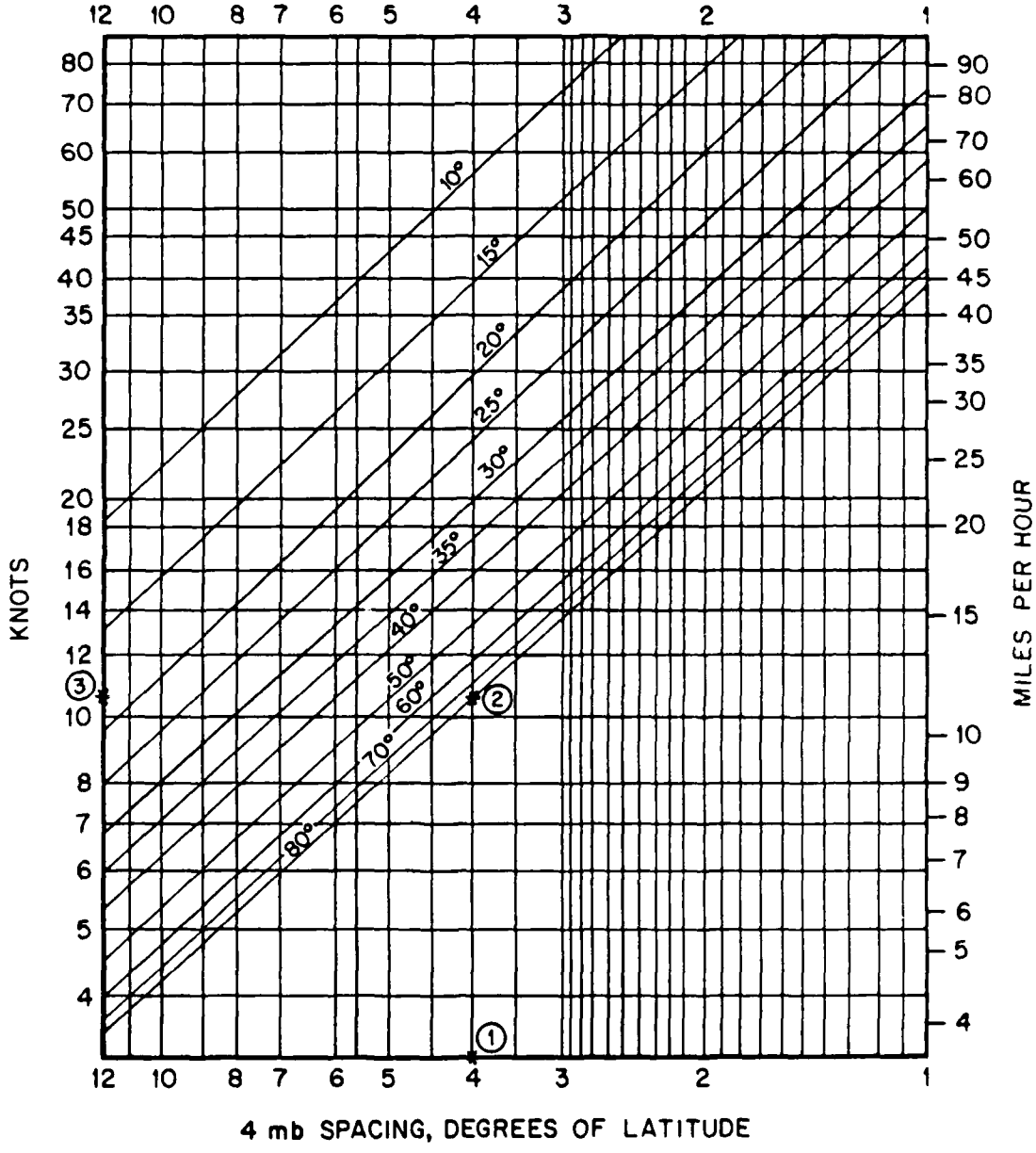

Figure X-4. Nomogram to relate isobaric spacing to geostrophic winds. The spacing, in degrees of latitude between four millibars of atmospheric pressure is found on the horizontal axis. The latiude of the point of observation is provided by the choice of the appropriate diagonal line. Their intersection determines the wind speed, provided by the vertical axes.

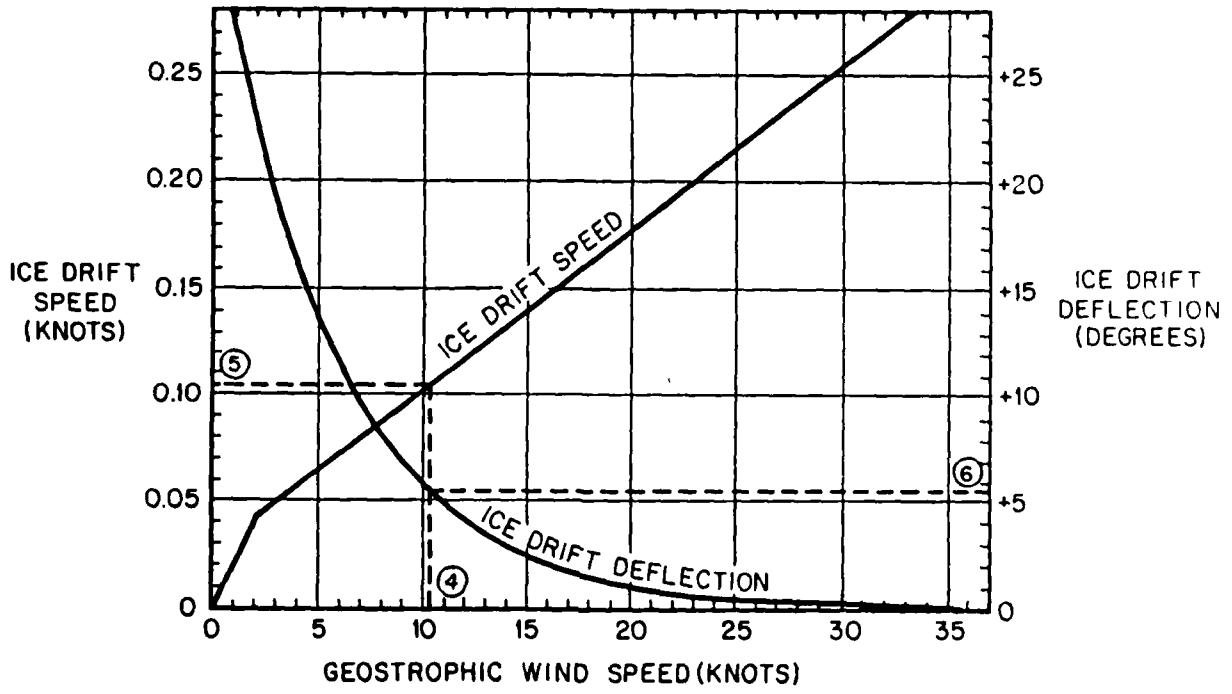

Figure X-5. Skiles Ice Drift Nomogram (Northern Hemisphere). This diagram can be used to relate geostrophic wind speed to ice drift speeds and angles of deflection (from the geostrophic wind vector). The geostrophic wind is read in on the horizontal axis and the resulting ice drift speed is found on the left-hand vertical axis, while the resulting ice deflection is found on the right-hand vertical scale.

ICE DRIFT FORECASTING

TABLE X-2

Month	(a) Enter distance between 4mb isobars from MSLP for vicinity of interest (deg. lat)	(b) Enter latitude where (a) was measured.	(c) Enter direction toward which the geostrophic wind flows (degrees)	(d) With (a),(b) and geostrophic wind nomogram determine geostrophic wind speed (knots)	From Skiles Ice Drift Nomogram and (d) Determine (e) Ice Drift Speed (knots)	(f) Ice Drift Deflection (deg.)	Ice Drift Direction (c)+(f) (degrees)	Distance Ice Drifted (naut.miles)
APRIL	4	80°	290°	10.2	.102	+6	296	73
MAY								
JUNE								

column d, enter at #4 and proceed vertically with a straight line until both the ice drift deflection curve and ice drift speed lines are intersected. From the point of intersection with the ice drift speed line, proceed horizontally to the left and read the ice drift speed at #5. From the point of intersection with the ice drift deflection curve, proceed horizontally to the right and read the drift deflection at #6. Enter the ice drift speed and deflection respectively in columns e and f of Table X-2.

(6) With the direction toward which the geostrophic wind flows in column c, add the ice drift deflection of column f and enter in column g (e.g. 290 + 06 = 296°).

(7) The distance traveled is computed by multiplying the ice drift speed, column e, by the time in hours with which the geostrophic wind blew. In the April example, it would be 30 days x 24 hours/day = 720 hours. The ice drifted .102 nautical miles/hr x 720 hours = 73 nautical miles.

In the example presented, the ice drifted 73 nautical miles toward 296° from the point of origin.

1.4 HYBRID PRODUCTS

A number of hybrid products are routinely produced at the Joint Ice Center to assist in the assimilation of the cause/effect relationship between atmosphere, hydrosphere, and cryosphere. The products are used for diagnostic evaluation (analysis fields only) or for predictions (analysis and forecast fields).

1.4.1 7-Day Ice Forecast Work Charts (Figure X-6). 7-Day Ice Forecast Work Charts are produced each Tuesday and consist of the following fields and parameters:

(1) The Joint Ice Center Eastern or Western Arctic Ice Analysis Chart from the previous week.

(2) The currently analyzed ice edge position.

(3) The most recent 144-hour Ice Drift Vector Forecasts from NMC.

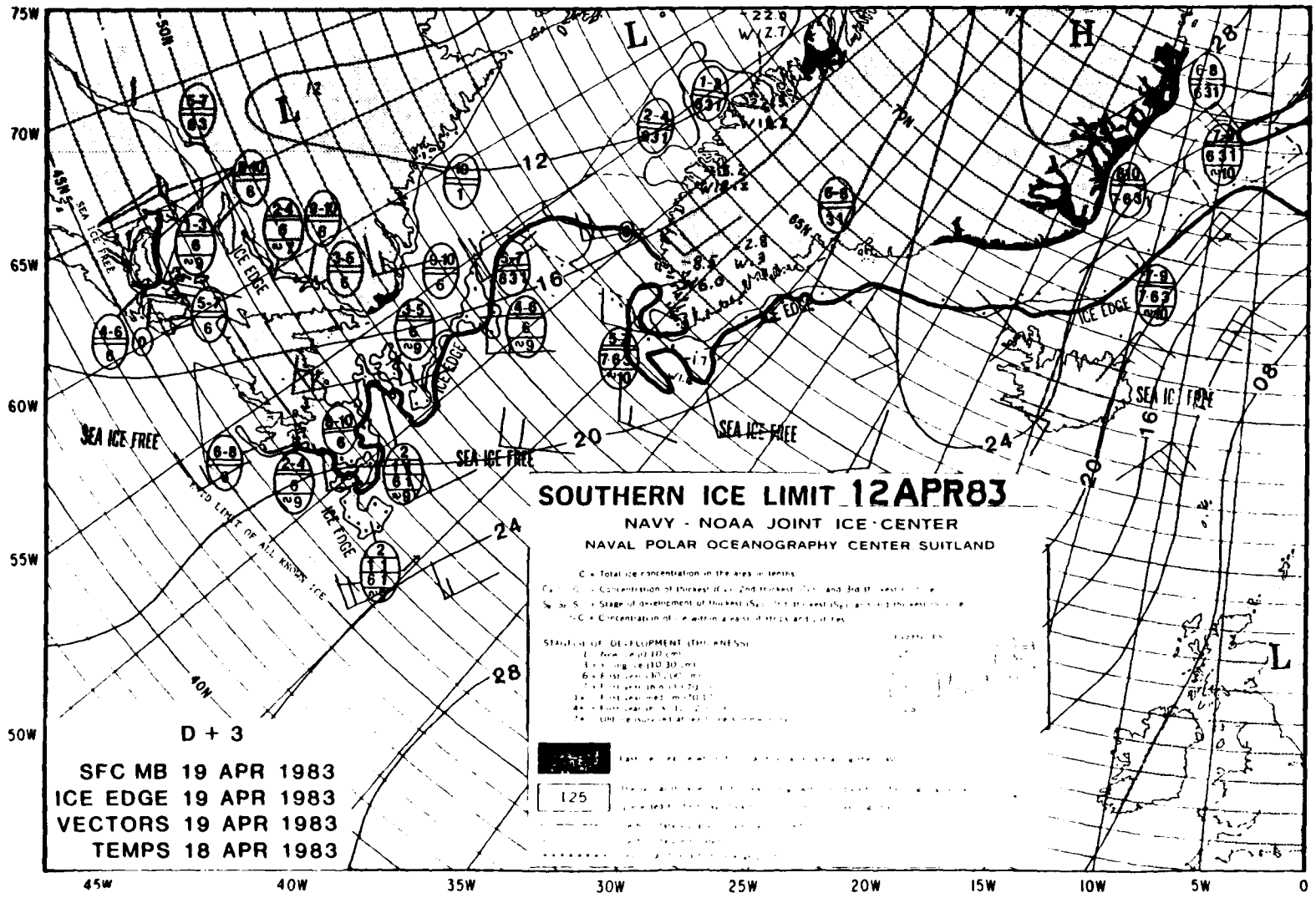

Figure X-6. Example of portion of 7-day Ice Forecast Work Chart. (See X 1.4.1.)

(4) The most recent D+3 MSLP forecast map from NMC.

(5) The most recent average daily station air temperatures and differences from last week at selected arctic station locations.

1.4.2 7-Day Ice Analog Charts (Figure X-7). Each Thursday a 7-Day Ice Analog Chart is produced. These charts have been produced and archived at the Joint Ice Center since 1979. The charts are particularly useful in gaining subjective insight on the cause/effect relationship between hydrosphere, atmosphere, and cryosphere. The charts contain the following fields and parameters:

(1) The Joint Ice Center Eastern or Western Arctic Ice Analysis Chart produced on the previous Tuesday.

(2) The previous week's analyzed ice edge position.

(3) The FNOC 168-hr Ice Drift Vector Analysis spanning the time frame from the most recent Tuesday to the preceeding Tuesday.

(4) The NMC D-3 MSLP analysis spanning the time frame from the most recent Tuesday to the preceeding Tuesday.

(5) The average daily station temperature observed on Tuesday and the difference from the previous Tuesday.

1.4.3 30-Day Forecast Work Chart (Figure X-8). The 30-Day Forecast Work Chart is produced twice monthly upon receipt of 30-day MSLP and temperature forecast guidance products from NMC. The charts contain the following fields:

(1) The most recent Joint Ice Center Eastern or Western Arctic Ice Analysis Chart.

(2) NMC Mean 30-Day MSLP Forecast and Temperature Forecasts.

1.4.4 30-Day Analog Charts (Figure X-9). 30-Day Ice Analog Charts are produced each year after the publication of the annual Eastern/Western Arctic Sea Ice Atlas Publication. The Joint Ice Center currently maintains a running archive extending from 1972. Two charts are produced per month for both the eastern and western arctic. The semi-monthly charts contain the following fields:

(1) The Joint Ice Center Eastern and Western Arctic Ice Analysis Chart dated closest to the first and fifteenth of each month.

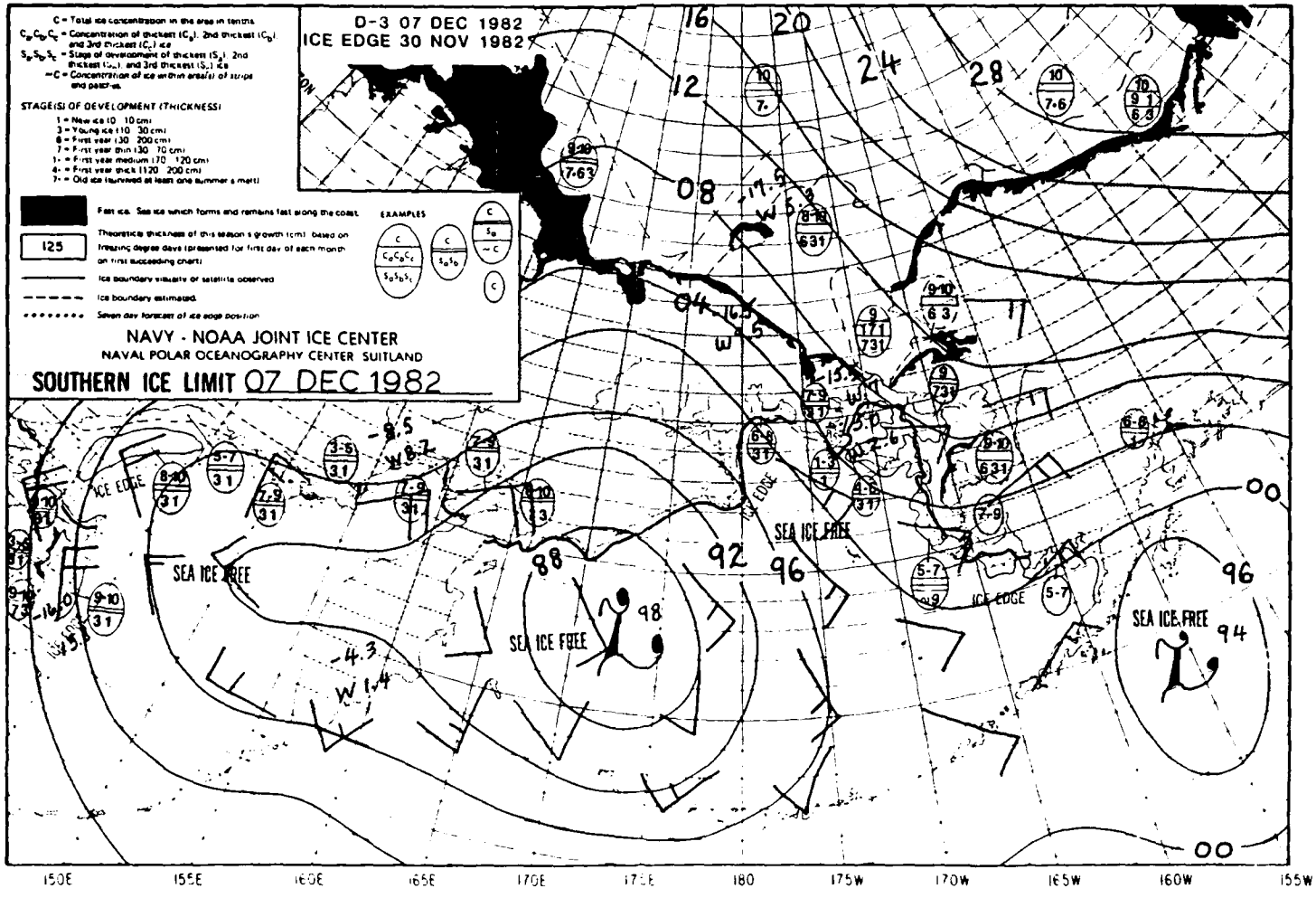

Figure X-7. Example of portion of 7-day Ice Analog Chart. (See X 1.4.2.)

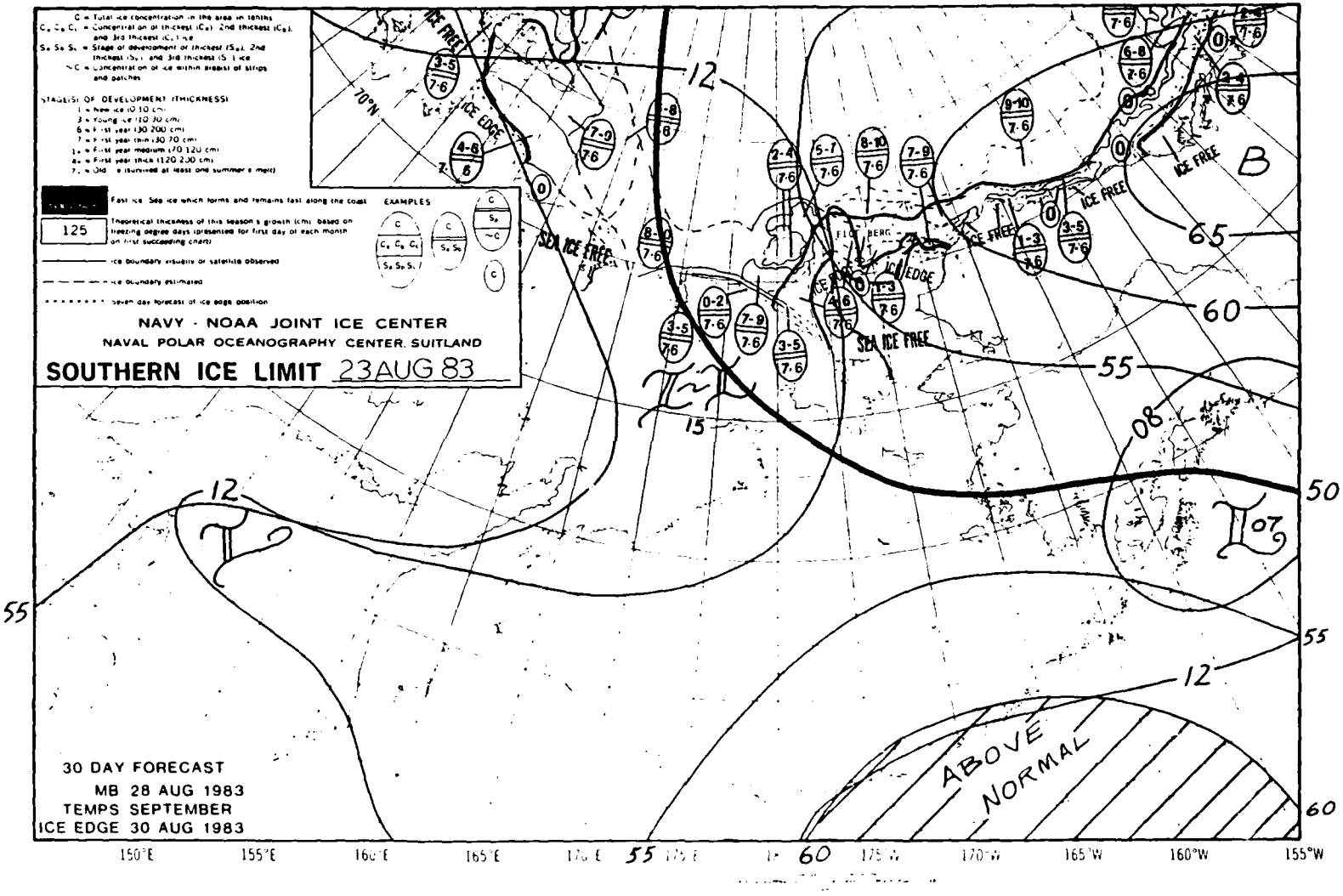

Figure X-8. Example portion of 30-day Forecast Work Chart. (See X 1.4.3.)

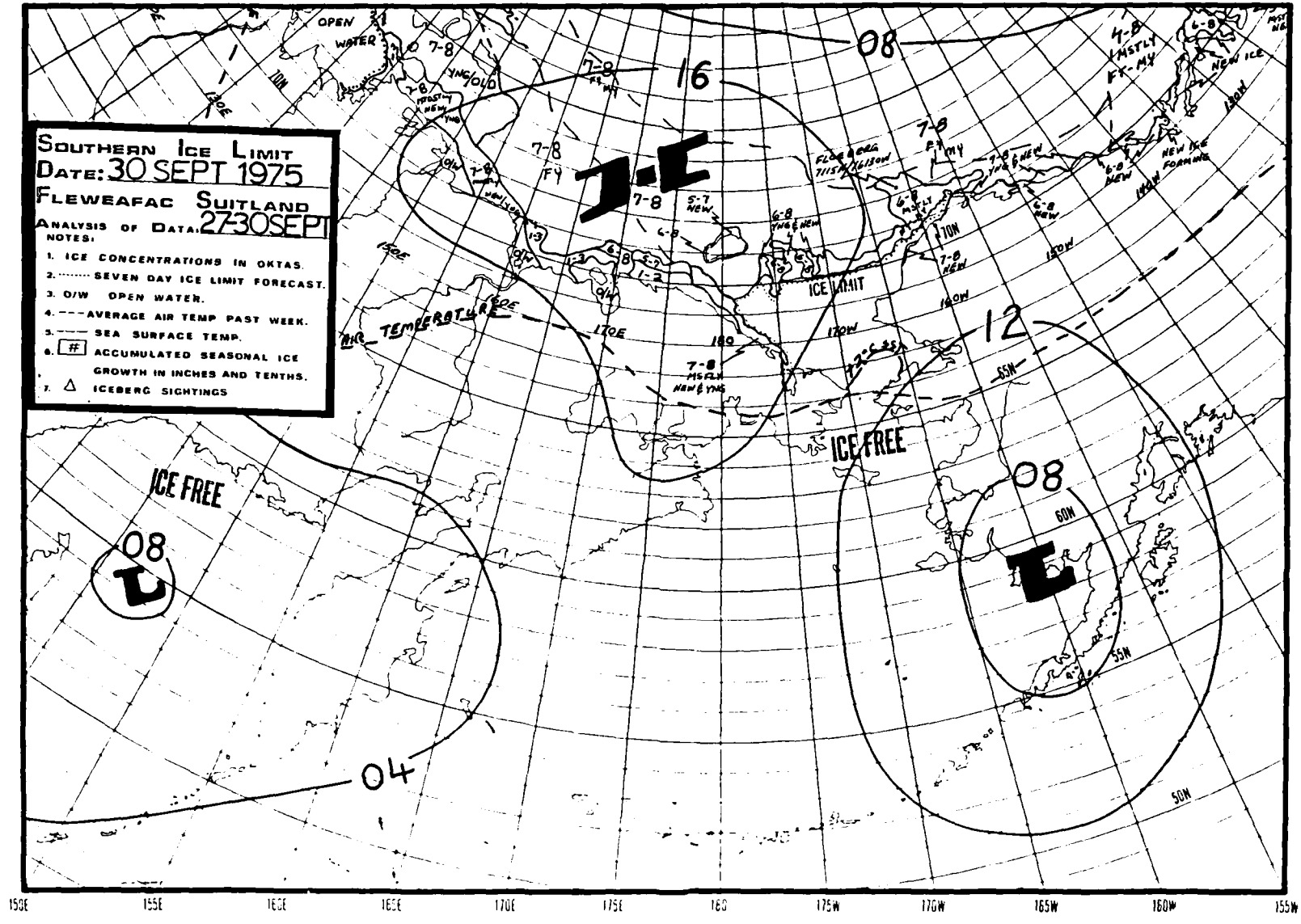

Figure X-9. Example of portion of 30-day Ice Analog Chart. (See X 1.4.4.)

(2) The Mean 30-Day MSLP Analysis for the 30-day period ending closest to the first or mid-month period.

(3) The ice edge location one month prior to the first or midmonth date of the Joint Ice Center Analysis.

1.5 ICE FORECASTING PROCEDURES

1.5.1 Short-Term Ice Forecasts:

1.5.1.1 Detailed Local Scale Forecasts. The first type of short-term ice forecast requires a local scale grid and highly detailed information consisting of the in situ state of ice conditions, including ice concentration and the extent of ridging and hummocking. Because of the lack of local scale automated ice forecast drift models and detailed in situ oceanographic conditions, this type of forecast is rarely made. Wittmann and MacDowell (1964) describe a procedure which is useful for this type of forecast.

1.5.1.2 Trend Forecasts. The second type of short-term ice forecast is a more general trend forecast covering time scales of 24 hours to 96 hours. Trend forecasts are generally appended to ice analysis messages which are transmitted to vessels operating in or near the ice pack. The trend forecast includes, when appropriate, predictions of:

(1) widening, narrowing or closing of navigable leads
(2) changes in expected ice pressure and ridging
(3) changes in concentration
(4) changes in ice edge position
(5) formation of new ice or ablation of in situ ice conditions.

Procedure:

(1) Review local area ice climatology and historical ice analysis charts for similar seasonal time frame.

(2) Review local ocean currents and theoretical ice drift forecasts for effects of wind-driven ice drift. Evaluate the potential ocean and wind-driven effects on leads, ice pressure, ridging, ice concentration, and ice position.

(3) Review theoretical ice thickness and station air temperatures from any local coastal stations. Review NESDIS sea surface temperatures. Evaluate likelihood of ice formation or ice ablation.

Paragraph 2 of Figure X-10 represents a typical short-term ice forecast appended to an ice analysis message.

1.5.2 7-Day Ice Edge Forecast. The 7-Day Ice Edge Forecast is represented as a trend forecast appended to ice analysis messages and as a graphical depiction on the weekly Eastern and Western Arctic Sea Ice Analyses.

Procedure:

(1) Review ice edge climatology and 7-Day Ice Analog charts for the area and seasonal time frame of interest.

(2) Review ocean current charts and NESDIS Sea Surface Temperature Analyses for the area of interest.

(3) With the 7-Day Ice Forecast Work Chart (Figure X-6) subjectively evaluate the combined effects in general order of importance of wind-driven ice drift, ocean currents, and ice formation/ablation. Figure X-11 depicts the graphical 7-Day Ice Edge Forecast represented by a dotted line.

1.5.3 30-Day Forecasts. The 30-Day Eastern and Western Arctic Ice Forecasts are graphic forecasts depicting ice conditions.

Procedure:

(1) Review Alaskan area 15 and 30-Day Ice Forecasting (Potocksky, 1975) and Eastern Arctic 15 and 30-Day Ice Forecasting (Mitchell, 1979) Guides.

(2) Complete the 30-Day Forecast Work Chart (Figure X-8).

(3) By comparing with the ice edge climatology in Chapter III, determine whether the current ice edge position lies nearer the minimum, median, or maximum climatological ice edge position.

(4) Compare the mean 30-day MSLP forecast pattern for the identified verification date with the normal patterns for the same time frames. This may be done by direct comparison with the climatological MSLP normals or with the deviation from normal pressure pattern analysis published with the NMC D+15 guidance product. This comparison will provide a subjective determination of the effect of wind-driven ice advection in great detail (e.g. above normal, normal, or below normal).

UNCLASSIFIED

FEEDBACK COPY

ZCZCCEWF1611IFWF541 LCG LN 042 1162044 JRNL TAPE 289
FTTUNFFA RULKSKD3932 1162044-UUUU--RULGSUU.
ZNR UUUUU
P 261936Z APR 83
FM NAVPOLAROCEANCEN SUITLAND MD
TO USCGC POLAR SEA
INFO CCGDSEVENTEEN JUNEAU AK
MSCO ANCHORAGE AK
BT
UNCLAS //N03150//
SUBJ: SEA ICE CONDITIONS ALASKA
(1.) ICE EDGE FM CST VCNTY 6040N/16505W TO 6055N/16650 6125 16630 61/168 TO CST VCNTY 6015N/16710W RSMG CST VCNTY 6005N/16715W TO 5950/168 5950/169 6020/169 6040/ 16815 6058/16910 6020/170 6010/171 6020/17105 6020/ 17150 5945/173 60/174 5958/17455 6040/17510 6020/177 6110/17710 6030/17750 6030/17850 6010N/17940W ECMG ESTI TO 6005N/17930E 6035/17910 6010/17740 6115/17620 6115/175 6020/17150 5950/17115 TO CST VCNTY 5950N/170[illegible]. 02-04 TENTHS FFITS/STRIPS 06 TENTHS FY/YNG SOUTH AND EAST OF A LN FM CST VCNTY 6415N/161[illegible]2 59 /420/16515 6310/ 16655 6145/16940 6050/16950 6042/17055 TO EDGE 6020N/17105W. 05-10 TENTHS YNG/N NORTH OF A LN FM CST VCNTY 6215N/17205W TO 6245 17855 6220/178 6205/17605 6145/17440 TO CST VCNTY 6145N 17420W. 07-09 TENTHS FY/YNG WEST OF A LN FM CONC BDRY 6205N/17605E TO EDGE 6115N/17620E. 08-10 TENTHS FY YNG/N INRUT RMNDR AREA SOUTH OF A LN FM CONC BDRY 6310N 16655W TO 6305/16810 6325/168 6325/16850 TO CST VCNTY 6370N/1695W RSMG ESTD CST VCNTY 6350N/16815W TO 6430/171 TO CST VCNTY 6425N/17215W. 10 TENTHS FY MED/FY THN/ YNG SOUTH OF A LN FM CST VCNTY 6610N/16950W TO 6620/ 169 TO CST VCNTY 6540N/16805W. LANDFAST ICE 10-20 NM ADJ CST FM CST VCNTY 6855N/166W TO CST VCNTY 7105N/155W. 09-10 TENTHS YNG/N 05-10 NM ADJ FAST ICE FM FAST ICE VCNTY 6858N 166W TO FAST ICE VCNTY 7125N/157W. 10 TENTHS FY WITHIN AN ESTD LN FM CONC BDRY VCNTY 7420N 163W TO 72 170 68 172 6705/169 6720/166 TO CST VCNTY 6745N/16440W. 10 TENTHS CLD FY INRUT RMNDR AREA NORTH OF 6520N/169W.
(2.) 72 HR FCST: FXP COMPACTION OF SEA ICE TO NORTHWEST DUE TO SOUTHEAST WIND. EXP 10-15 NM WIDE LEADS ADJ CST NORTH SLOPE. EXP CONTINUED RECESSION OF ICE EDGE IN BERING SEA.
BT
#7932

CONN
MPOC 511 D
83 APR 27 12 06

Figure X-10. Typical Ice Analysis Message (paragraph 1) with appended short-term ice forecast (paragraph 2).

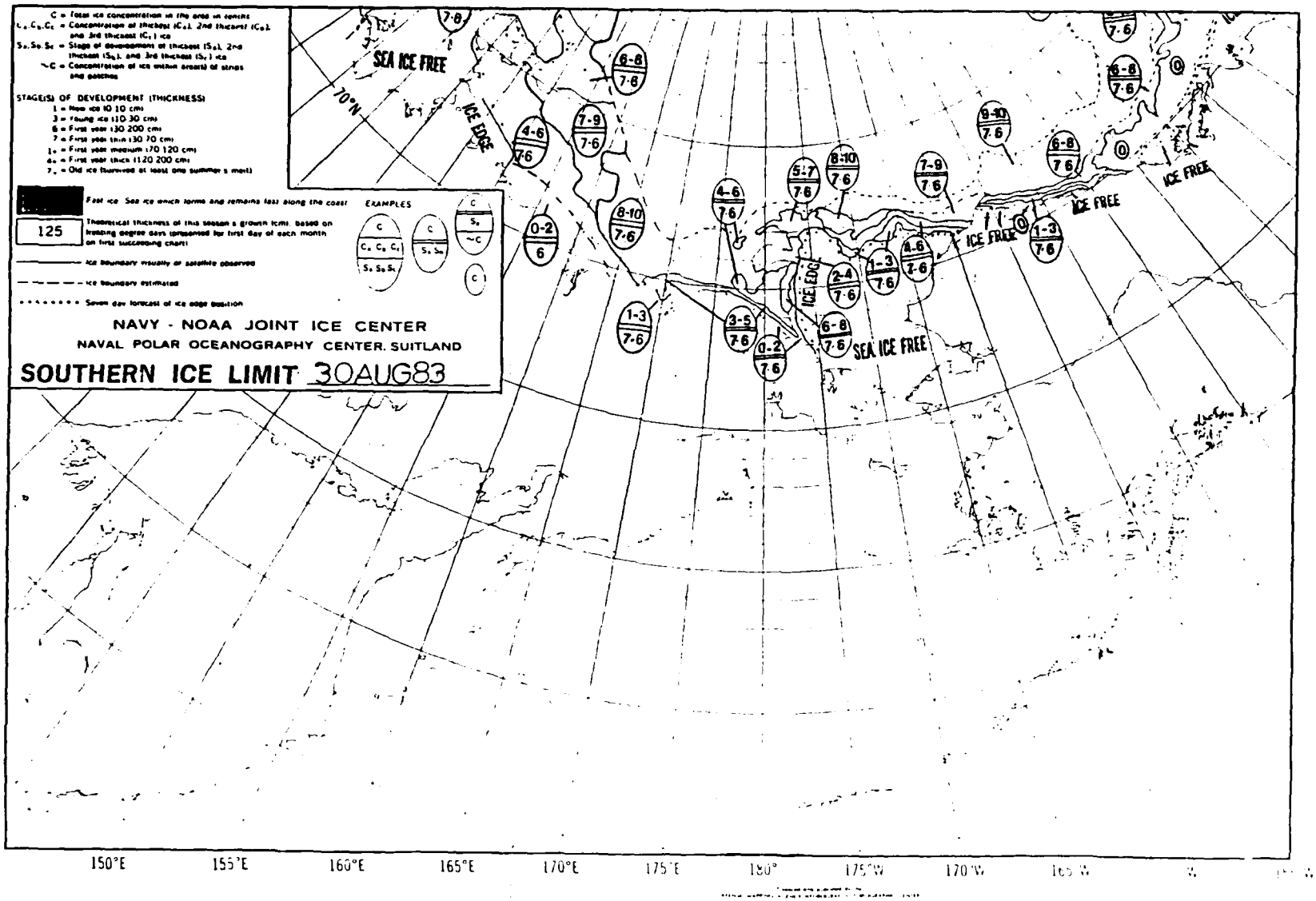

Figure X-11. Example portion of 7-day Ice Edge Forecast. (See X 1.5.2.)

(5) Predict the effects of anticipated above, below, or near normal air temperature patterns.

(6) Having completed (4) and (5) for similar time periods, identify the closest analog from the 30-Day Ice Analog Charts by keying on current/analog ice edge position and predicted/analog mean 30-Day MSLP charts. It may be necessary to combine parts of 2 analogs for a better fit of the predicted pattern.

(7) Complete the forecast by subjectively extrapolating and graphically depicting the forecasted ice edge position and innerpack ice concentration and age.

An example of a completed 30-Day Western Arctic Ice Forecast is presented in Figure X-12.

1.5.4 Seasonal Ice Forecasts. Seasonal ice forecasts are derived by a combination of statistical and analog techniques. The Western Arctic Seasonal Outlook is based primarily on a statistically derived ice severity relationship. The Eastern Arctic Outlook, and the Western Ross Sea/McMurdo Sound Seasonal Outlook are based primarily on analogs and ice climatological statistics. The Eastern and the Western Arctic Outlooks are completed during early May; the Ross Sea and McMurdo Sound Seasonal Outlook is completed during late October. Perchal (1975) provides the necessary statistical summaries necessary for preparing the Ross Sea Outlook. Mitchell (1979) provides useful statistical summaries for the Eastern Arctic Outlook. Appendix X-A is an example of an Eastern Arctic Outlook. Appendix X-B is an example of a Western Ross Sea/McMurdo Sound Outlook.

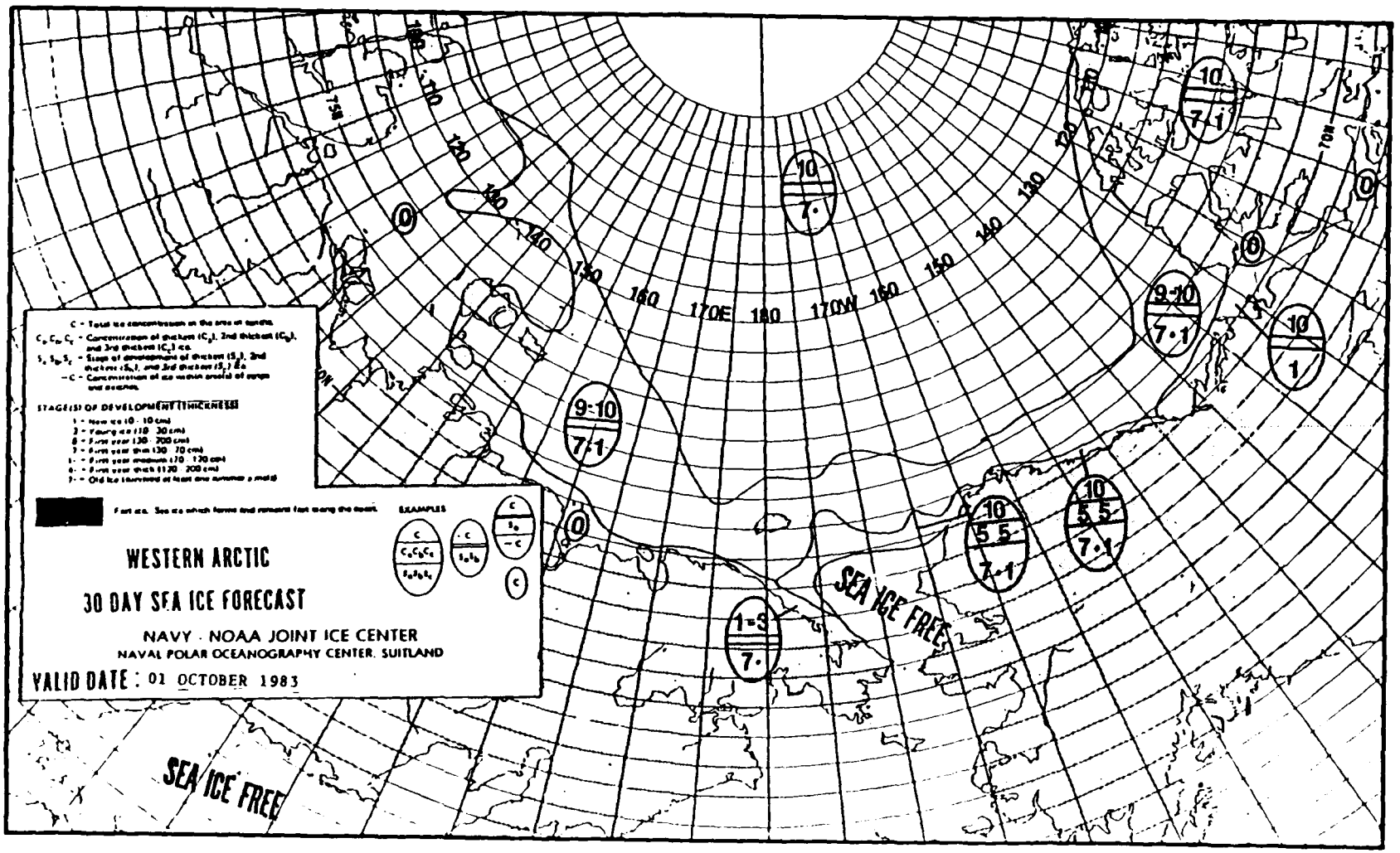

Figure X-12. Example portion of 30-day Western Arctic Ice Forecast. (See X 1.5.3.)

SECTION 2. CURRENT PROCEDURE FOR PRODUCTION OF WESTERN SEASONAL OUTLOOK FOR SEA ICE

This forecast technique was initially developed in late 1975 in response to the requirements of operators involved in resupply of stations along the Alaskan north coast. The need for a method capable of accurately predicting the severity of ice conditions in the navigation season was highlighted by the extreme severity of conditions in 1975. References by Barnett (1976 and 1980) and Rogers (1978) are recommended reading for a better understanding of the initial work. There has been some evolution of this technique since those references were published. These advances are included in this documentation.

The seasonal forecast as described below is prepared in two stages. The first stage in early January of each year is designed to identify indications of an extremely severe season. No formal forecast is prepared at that time unless that extreme is indicated. The second stage is the publication of a formal forecast in early May with the objective of presenting statistically derived, long-range expectations in greater detail.

2.1 STAGE I: PRELIMINARY ANALYSIS OF PRE-SEASON DRIFT PATTERNS

The Western Arctic Seasonal Outlook is prepared in early May with surface pressure data from the January through April time period. There appears to be some evidence, however, that pressure patterns which contribute to such uniquely severe years as 1955 and 1975 can be observed even further in advance of the navigation season. A test has been devised to attempt very early recognition of severe seasons. It should be stressed that while it is strongly suggested that forces which cause a season as extremely severe as 1955 or 1975 may be observed long before the season, the relationships expressed in stage 1 have not been extensively researched. Interpretations are still more subjective than objective.

Test for Extreme Severity:

(1) The initial step is to draw three triangles on the National Meteorological Center's 65 X 65 point or Fleet Numerical Oceanography Center's (FNOC) 63 X 63 point operational grid. These are drawn as dashed lines on Figure X-13. The vertices for these initial triangles

should be as follows: For (Δ1) grid points 67, 68, and 83; for (Δ2) 99, 117, and 118; and for (Δ3) 86, 101, and 102. These triangles represent the July starting point for nine selected hypothetical ice floes.

(2) Next, compute the theoretical drift of these floes for the three month period from 1 July to 1 October. This is done for each triangle vertex by vector addition of the FNOC theoretical 168 hour ice drifts for the 13 weeks of the period. This can be done graphically or by using a program that has been written for performing this addition on a Hewlett Packard calculator (HP-65). The procedure is described in Table X-3.

(3) Plot the new positions of the triangles based on that computation (the solid triangle on Figure X-13).

(4) Compute theoretical ice drift for the three month period from 1 October to 1 January for the same vector points.

(5) Again plot new positions of the triangles (dot-dash triangle on Figure X-13). Note the general drift of these triangles during the period just plotted. Ideally each of the triangles should rotate in a clockwise direction with time and also the group should move in a clockwise direction in relation to each other.

(6) The next step in judging the general drift pattern for the period is to draw three larger triangles using the approximate center point of each of the above triangles as vertices. For the given example draw one triangle using the center point of the three original 1 July triangles (dashed on Figure X-13) as vertices. Plot this triangle as shown in dashed lines on Figure X-14. Then similarly plot two more triangles using the center point of the solid and dot-dash triangles on Figure X-13 as vertices. Figure X-14 shows these triangles. Figures X-15 and X-16 show triangles done in a like fashion from other years. On Figure X-15 note the normal clockwise rotation with a northerly component for the last half of 1973. Conversely, Figures X-14 and X-16 show a marked southerly drift toward the Alaskan coast during the latter half of both 1954 and 1974. In only 3 years of the 29 year period of record (1953-1981) was drift of this nature observed. The fact that two of those occasions were followed by the two most severe ice summers in the period does seem more than coincidental.

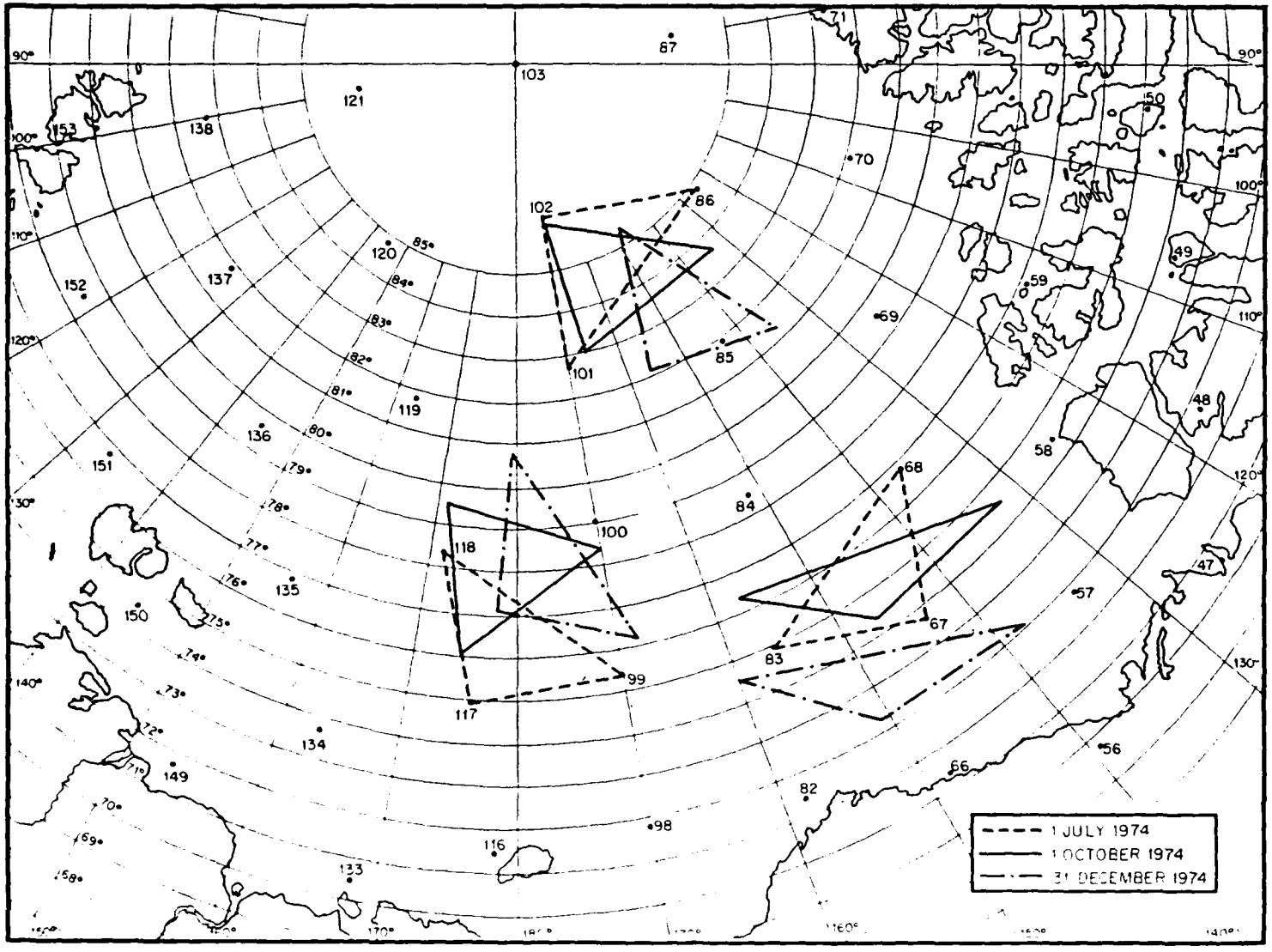

Figure X-13. Pre-season test for extreme ice severity for 1974, step 1. (See X 2.1.)

VECTOR ADDITION PROGRAM - HEWLETT PACKARD 65

TABLE X-3

1. Insert program VA part I.
2. Initialize R/S.
3. Enter angel #1 Key R/S.
4. Enter magnitude #1 Key R/S.
5. This yields x component.
6. Key R/S.
7. This yields y component. Record on tab sheet.
8. Repeat for each vector. Record each.
9. Sum each component (εx and εy).
10. Insert Program VA part II.
11. Initialize R/S.
12. Enter εx Key R/S.
13. Enter εy Key R/S.
14. This yields total magnitude.
15. Key R/S.
16. This yields angle.

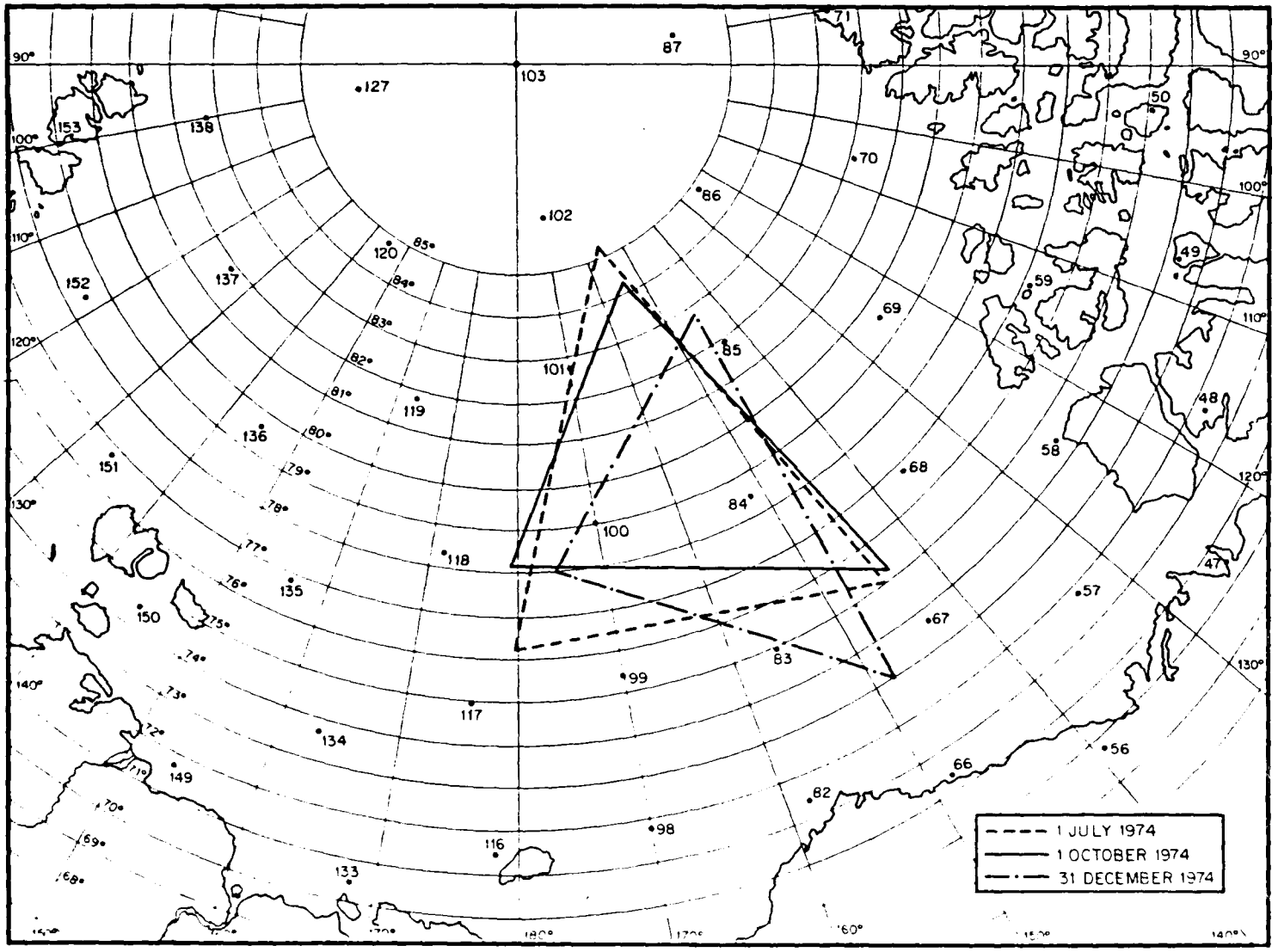

Figure X-14. Pre-season test for extreme ice severity for 1974, step 2.

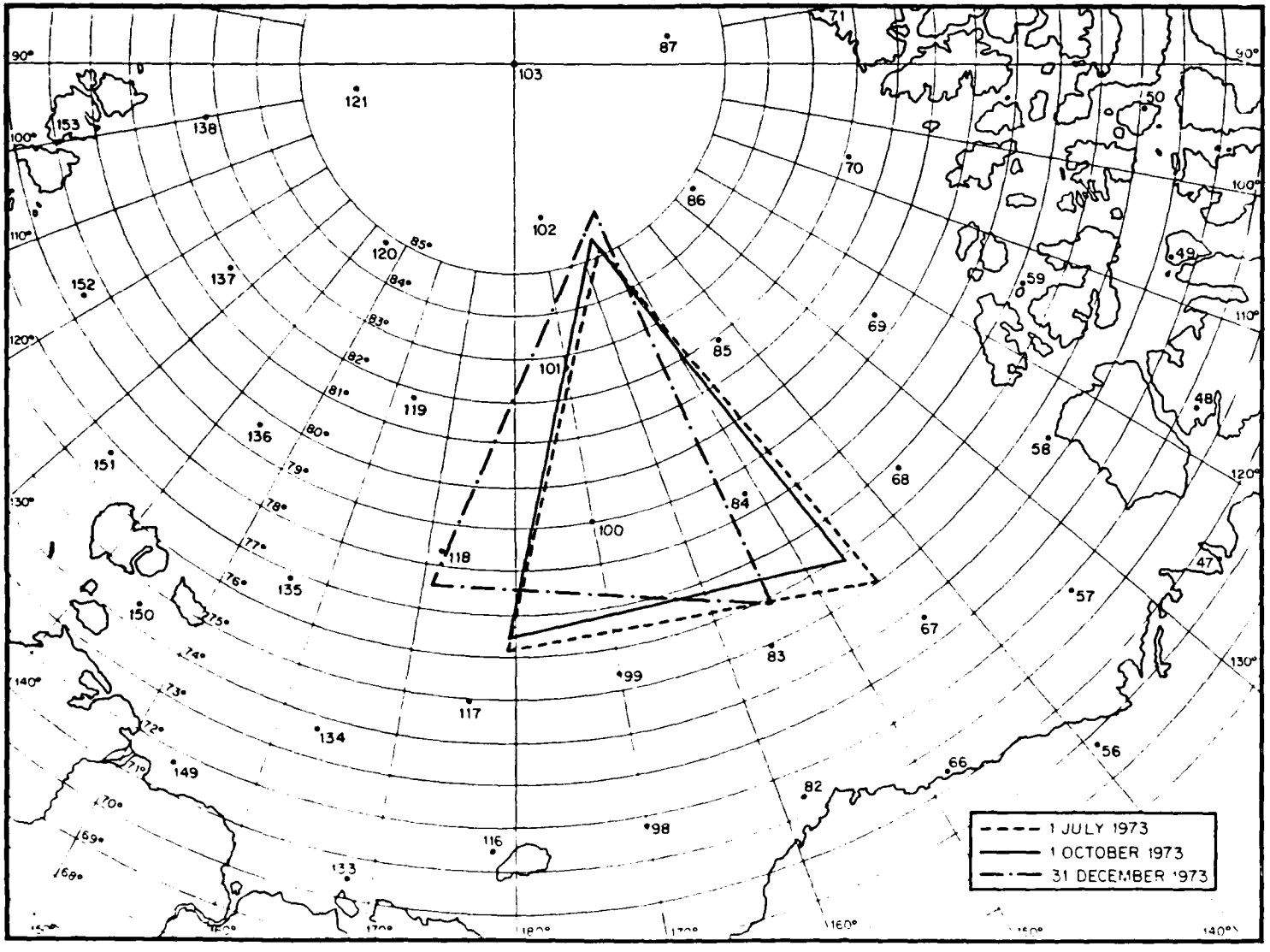

Figure X-15. Pre-season test for extreme ice severity for 1973, step 2.

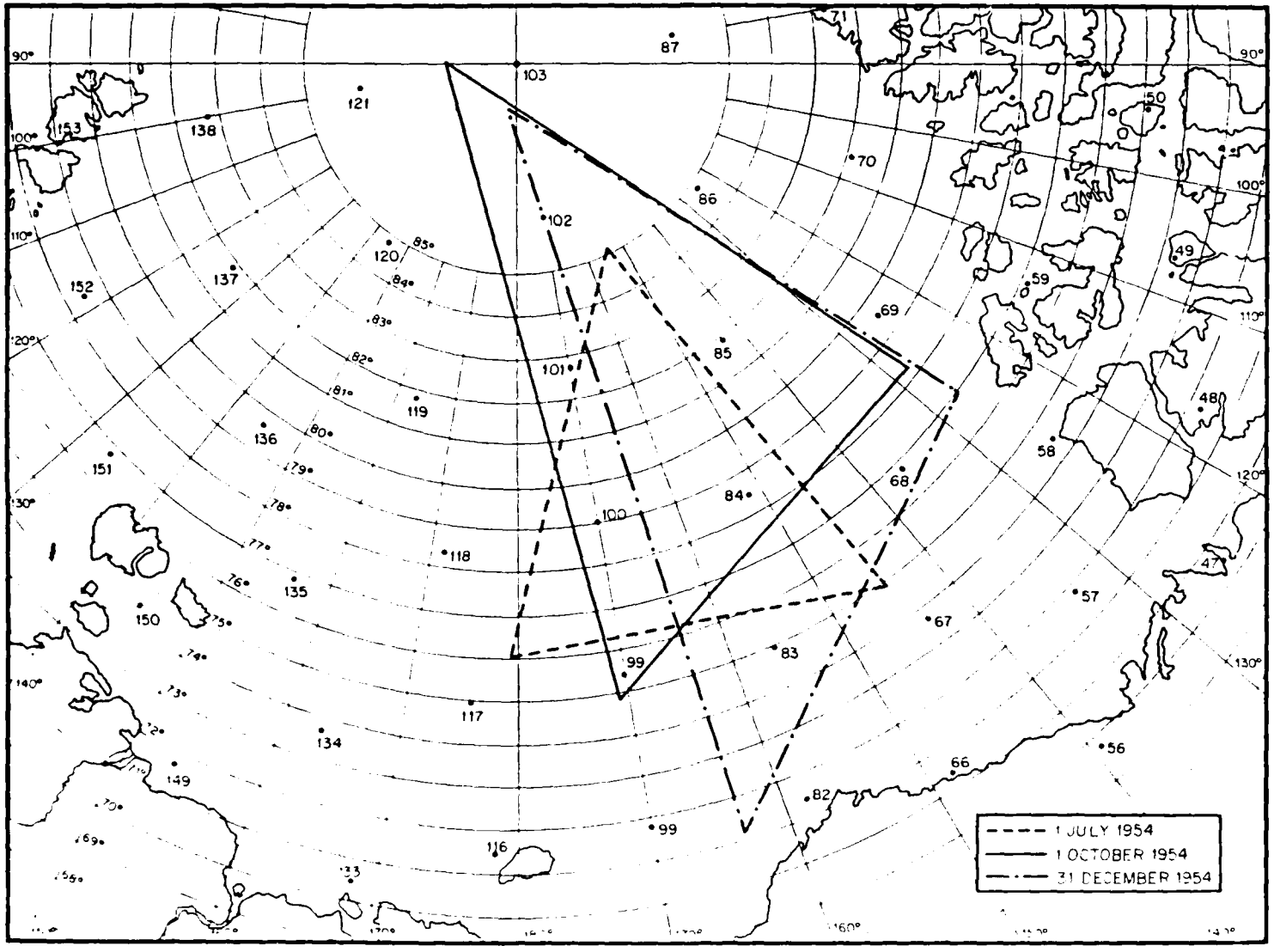

Figure X-16. Pre-season test for extreme ice severity for 1954, step 2.

(7) If an anomalous south or southeast drift toward the Alaskan coast is observed, a season similar to 1955 or 1975 is considered probable. A warning should be passed to consumers in the form of a preliminary forecast. This warning should be issued in January with the statement that an update will be issued in May. There appears to be no further information to be gained from these drift triangles beyond the possibility of signaling an extreme season. No further correlation appears to exist between amount of drift or degree of rotation in this time frame and the succeeding summer ice conditions.

2.2 STAGE II: PREPARATION OF SEASONAL OUTLOOK

There are two methods of forecasting the ice severity parameters listed in Table X-7. Both methods are based on the data gathered in 2.2.1. The method described in 2.2.2 estimates the severity of the coming ice year represented by the forecast severity, S_f, which is then compared to the observed severity, S_o, in previous years. The data for the year with the observed severity closest to the S_f value are used as the predicted values. The method described in 2.2.3 is based on regression equations for individual parameter predictions.

2.2.1 Completing Data Collection Sheet (Table X-4).

(1) Extract surface pressure data for points p_1 through p_{21} from National Meteorological Center (NMC) Prediction Branch printouts (sample, Table X-5).

(2) During April, copy 6-hourly air temperatures for t_1, t_2, and t_3 and compute average temperature for the month. Calculate 1000 millibar height levels (h_1, h_2, and h_3) using surface pressures from NMC and formula (1) from Table X-6.

2.2.2 Forecast Severity Forecast Method.

(1) Find the numerical term representing the forecast severity (S_f) from formula (2) on Table X-6.

(2) Table X-7 lists the observed severity (S_o) calculated for each year from 1953-81. S_o is calculated by adding columns 2,4,5,7 and 8.

(3) Note the relative position that S_f would assume on Table X-7 to make an initial judgement of the forthcoming summer's severity relative to 1953-1981 climatology. To make a more precise identification of a year or years which could be expected to share a similarity with the

TABLE X-4

Data Collection Sheet

GRID POINT	JAN	FEB	MAR	APR
20°N 20°W	p_1 ____	p_2 ____	-	-
25°N 40°W	p_3 ____	p_4 ____	-	-
40°N 160°W	p_5 ____	p_6 ____	p_7 ____	p_8 ____
65°N 180°W	p_9 ____	p_{10} ____	p_{11} ____	p_{12} ____
65°N 160°W	p_{13} ____	p_{14} ____	p_{15} ____	p_{16} ____
75°N 130°W	-	-	-	p_{17} ____
65°N 80°W	-	-	-	p_{18} ____
52°N 100°E	-	-	-	h_1 ____ p_{19} ____ t_1
70°N 140°E	-	-	-	h_2 ____ p_{20} ____ t_2
70°N 130°E	-	-	-	h_3 ____ p_{21} ____ t_3

Table X-5

WESTERN ARCTIC FORECAST EQUATIONS
TABLE X-6

EQUATION 1. Calculating h_1, h_2, h_3:

$$h_i = \left[\ln \frac{p_i}{1000} \right] \left[(287) \frac{t_i}{9.8} \right]$$

$i = 1,2,3$

where p = April surface pressure at appropriate grid point
t = average April air temperature in K°

EQUATION 2. Forecast Severity (S_f):

$S_f = 483.73 + .65x$

where $x = 6.29t + 26.58u - 6.78v - 1.11w$

where $t = p_1 + p_2 + p_3 + p_4 - p_5 - p_6 - 2000$

$u = p_{17} - p_{18}$

$v = p_5 + p_6 + p_7 + p_8 + p_9 + p_{10} + p_{11} + p_{12} - p_{13} - p_{14} - p_{15} - p_{16} - 4000$

$w = 2h_1 + h_2 - h_3$

EQUATION 3. Forecasting distance (nm) from Pt. Barrow north to the ice edge on 10 August (E_A):

$E_A = 18.07 + .03x$ (See x, equation 2)

EQUATION 4. Forecasting distance (nm) from Pt. Barrow north to the ice edge on 15 September (E_S):

$E_S = 114.07 + .19x$

EQUATION 5. Forecasting distance (nm) from Pt. Barrow to the boundary of 5/10 ice concentration on 10 August (C_A):

$C_A = 28.49 + .04x$

EQUATION 6. Forecasting distance from Pt. Barrow north to the boundary of 5/10 ice concentration on 15 September (C_S):

$C_S = 157.06 + .23x$

EQUATION 7. Forecasting opening date for navigation. Initial date entire sea route to Prudhoe Bay from the west is $\leq$ 5/10 ice concentration (D_o) = # of days prior to October 1:

$D_o = 74.19 + .06x$

EQUATION 8. Forecasting closing date for navigation - subjective date based on ice concentration and thickness (D_c) = # of days after October 1:

$D_c = 11.92 + .03x$

EQUATION 9. Forecasting the number of days the entire sea route to Prudhoe Bay is ice free ($\#_f$):

$\#_f = 60.09 + .09x$

EQUATION 10. Forecasting the number of days the entire sea route to Prudhoe Bay is $\leq$ 5/10 ice ice concentration ($\#_c$):

$\#_c = 73.20 + .06x$

OBSERVED SEVERITY INDEX

TABLE X-7

YEAR	1 E_A nm	2 E_S nm	3 C_A nm	4 C_S nm	5 D_o date	6 D_c date	7 $\#_f$ days	8 $\#_c$ days	9 S_o
1958	50	150	50	210	7/19	10/25	92	99	614
1968	25	165	30	200	7/19	10/18	86	91	615
1962	25	150	30	150	7/19	9/30	49+	68+	490
1973	5	80	5	190	7/31	10/20	73	82	486
1954	20	115	20	210	8/1	9/30	38+	61+	484
1963	5	130	5	130	8/13	10/18	67	67	442
1961	15	105	15	135	7/25	9/24	49+	62+	418
1979	0	125	0	125	8/04	10/8	31	56	394
1974	10	100	10	100	8/6	10/5	35	61	351
1978	5	70	30	95	7/25	10/9	35	76	343
1977	5	55	25	85	8/02	10/15	63	74	336
1959	20	65	20	65	7/19	10/6	42	86	331
1982	0	85	0	95	8/3	10/10	21	69	328
1972	0	60	30	90	7/31	10/1	45	63	320
1957	5	45	70	60	8/1	10/6	18	67	250
1981	0	0	35	100	7/26	10/1	0	66	232
1967	15	0	30	50	7/25	10/12	UNK	68	209
1966	5	0	5	45	8/1	10/22	24	65	194
1965	0	10	0	70+	8/25	9/25	25	32	173
1980	15	25	15	25	8/5	9/30	11	42	159
1953	0	0	5	35	7/27	9/16	5	52+	157
1976	0	15	0	15	8/15	10/7	21	53	150
1971	0	0	0	30	8/23	11/1	8	71	147
1960	0	0	20+	20	8/5	9/7	0	34	110
1964	0	0	0	5	8/13	9/20	0	39	92
1956	0	0	0	40	9/7	9/30	0	24	87
1970	0	0	5	0	8/6	9/14	0	32	87
1969	0	0	0	30	9/7	9/18	5	12	70
1955	0	0	5	15	9/13	9/24	0	12	44
1975	5	0	5	0	NEVER	NEVER	0	0	0

1. Distance from Point Barrow northward to ice edge on 10 August (E_A)
2. Distance from Point Barrow northward to ice edge on 15 September (E_S)
3. Distance from Point Barrow northward to boundary of 5/10 ice concentration on 10 August (C_A)
4. Distance from Point Barrow northward to boundary of 5/10 ice concentration on 15 September (C_S)
5. Initial date sea route to Prudhoe Bay $\leq$ 5/10 concentration; route is open to navigation (D_o)
6. Date that combined ice concentration and thickness dictate end of prudent navigation (D_c)
7. Number of days entire sea route to Prudhoe Bay is ice free ($\#_f$)
8. Number of days entire sea route to Prudhoe Bay is $\leq$ 5/10 ice concentration ($\#_c$)
9. Total of Columns 2, 4, 5*, 7 and 8. Observed Severity value.

*Numerical value for Column 5 is the number of days between given date and 1 October.

forthcoming season, follow the procedure outlined on Table X-8. Individual parameters (columns 1-8, Table X-7) can then be forecast by simply lifting the observed data from the year deemed most likely to resemble the forecast year.

2.2.3 Regression Equation Forecast Method. Calculate the forecast for each parameter (columns 1-8, Table X-7) using the regression equations (3) through (10), Table X-6. Columns 2, 4, 5, 7, and 8 can then be totaled to arrive at S_f. If this S_f differs from the one calculated using formula (2), the final forecast can be expressed as a range e.g., "forecast this season to be between the 9th and 12th most favorable of 30 years of record."

2.3 EXAMPLE FORECAST: SAMPLE YEAR 1982

(1) Value of p_1 through p_{21} were extracted from NMC surface pressure tables as follows:

GRID PT	JAN	FEB	MAR	APR				
20N 20W	p_1 1018.0	p_2 1018.0	*	*				
25N 40W	p_3 1020.7	p_4 1025.2	*	*				
40N 160W	p_5 1010.2	p_6 1010.9	p_7 1026.8	p_8 1026.3				
65N 180W	p_9 1014.1	p_{10} 1023.5	p_{11} 1013.2	p_{12} 1014.7				
65N 160W	p_{13} 1016.4	p_{14} 1027.0	p_{15} 1012.3	p_{16} 1013.4				
75N 130W	*	*	*	p_{17} 1017.9				
65N 80W	*	*	*	p_{18} 1013.2				
52N 100E	*	*	*	h_1 164	p_{19} 1020.6	t_1 274.4°K		
70N 140E	*	*	*	h_2 113	p_{20} 1015.2	t_2 256.5°K		
70N 130E	*	*	*	h_3 121	p_{21} 1016.3	t_3 255.7°K		

(2) Calculate S_f from equation (2) on Table X-6:

$$t = p_1 + p_2 + p_3 + p_4 - p_5 - p_6 - 2000$$
$$= 1018.0 + 1018.0 + 1020.7 + 1025.2 - 1010.2 - 1010.9 - 2000 = 60.8$$

$$u = p_{17} - p_{18}$$
$$= 1017.9 - 1013.2 = 4.7$$

$$v = p_5 + p_6 + p_7 + p_8 + p_9 + p_{10} + p_{11} + p_{12} - p_{13} - p_{14} - p_{15} - p_{16} - 4000$$
$$= 1010.2 + 1010.9 + 1026.8 + 1026.3 + 1014.1 + 1023.5 + 1023.2 + 1014.7 - 1016.4 - 1027.0 - 1012.3 - 1013.4 - 4000 = 70.6$$

$w = 2h_1 + h_2 - h_3 = 2(164) + 113 - 121 = 320$
(h calculated with equation 1, Table X-6)

$x = 6.29t + 26.58u - 6.78v - 1.11w = 6.29\ (60.8) + 26.58\ (4.7) - 6.78\ (70.6) - 1.11\ (3.20) =$
$382 + 125 - 479 - 355 = -327$

$S_f = 483.73 + .65x = 483.73 + .65\ (-327) = 483.73 - 213.55 = 271$

(3) Compare $S_f = 271$ with the S_o column of Table X-7. Note that 271 falls between the 320 and 250 values of 1972 and 1957. A preliminary judgement could be made that the 1982 season will be the 14th most favorable of the period of record or just slightly better than average.

(4) Using Table X-8, note that 1972 was only one position from 1982 on the t value index, three positions on the u index, one position on the v index and 3.5 positions on the w index. The 1972 season, with a total position deviation of only 8.5 is clearly the year in which significant surface pressure patterns most resembled 1982. Thus, ice conditions of 1972 and 1957 (which had an S_o value closest to the S_f value of 1982) are presented as examples of conditions expected in 1982. (See Columns B and C in step 5).

(5) Using regression equations (3) through (10) from Table X-6, the following events could be forecast (column A). Columns B and C are values observed in the years 1972 and 1957 respectively. Remember that x was previously calculated to be -327.

Parameter	A Equation Predictions	B 1972	C 1957
Distance to ice edge 10 Aug	8 nm	0 nm	5 nm
Distance to ice edge 15 Sept	52 nm*	60 nm	45 nm
Distance to 5/10 concent. 10 Aug	15 nm	30 nm	70 nm
Distance to 5/10 concent. 15 Sept	82 nm*	90 nm	60 nm
Date open to navigation	7 Aug*[1]	31 Jul	1 Aug
Date closed to navigation	3 Oct [2]	1 Oct	6 Oct
Number of days ice free	31 days*	45 days	18 days
Number of days less than 5/10 concent.	54 days*	63 days	67 days

* parameters used in calculating S_f

(1) 55 days prior to 1 October

(2) 2 days after 1 October

Note that the total of the values upon which S_o is based is 274 which compares closely to the calculated S_f value of 271. Whether to choose one column for the seasonal outlook, either from similar year (B or C) or from the regression equations (A), or some average of the group is a subjective decision.

2.4 FINAL NOTE

The evolution of this forecast technique, since its initial presentation in 1976, has been due in part to further operational research. There are however, still many questions, especially concerning the relationships between summer ice conditions and pre-season strengths of certain remote pressure systems. Seven seasonal outlooks have been produced with this technique. Five were verified with pleasing results. The accuracy of the 1980 and 1981 outlooks was disappointing. There intentionally has been no mention of the five year cycle which has been apparent through the period of record. A longer period of record is needed to judge the utility of including a natural cycle in ice forecasting. Until that time, any utilization of the cycle as a forecast indicator rests on the subjective decision of the forecaster.

These forecast techniques are not considered the final answer (that answer may lie in starting with a clean slate and a different approach), but it is hoped the method will prove its value during the wait.

DEVIATION (=) FROM SAMPLE YEAR - 1982

TABLE X-8

YEAR	t	s	YEAR	u	s	YEAR	v	s	YEAR	w	s	YEAR	TOTAL
1956	31.2	14	1975	-7.6	22	1955	91.7	9	1980	380	10	1953	23.5
55	32.4	13	55	0.0	21	64	87.6	8	63	360	9	54	41
79	39.0	12	64	0.1	20	76	85.0	7	53	355	7	55	50
69	39.9	11	61	0.3	19	56	81.9	6	55	355	7	56	33.5
67	44.0	10	63	0.7	17.5	71	81.4	5	65	355	7	57	21.5
64	44.7	9	71	0.7	17.5	69	77.4	4	70	340	5	58	37
66	45.6	8	65	0.9	15.5	75	77.1	3	64	335	3	59	36.5
59	49.9	7	76	0.9	15.5	73	72.3	2	66	335	3	60	32
65	50.9	5.5	60	1.0	13.5	72	71.8	1	76	335	3	61	59
75	50.9	5.5	78	1.0	13.5	82	70.6	---	79	329	1	62	33.5
60	52.0	4	53	1.5	12	57	67.1	1	77	320	0	63	58.5
57	54.2	3	67	1.7	11	70	66.7	2	82	320	---	64	40
76	54.4	2	59	2.2	10	53	66.2	3	71	315	1	65	37
72	57.9	1	70	2.5	9	77	65.6	4	67	310	2	66	27
82	60.8	---	56	3.0	7.5	74	64.3	5	68	300	3.5	67	33
53	61.4	1.5	79	3.0	7.5	59	64.2	6	72	300	3.5	68	33.5
73	61.4	1.5	69	3.1	6	60	63.7	7	75	295	5	69	28.5
71	62.6	3	81	3.3	5	79	63.6	8	56	290	6	70	22
62	63.4	4.5	57	3.6	4	65	61.2	9	60	280	7.5	71	26.5
74	63.4	4.5	72	3.7	3	67	58.4	10	69	280	7.5	72	8.5
70	64.4	6	62	4.2	2	80	55.3	11	62	275	9	73	18.5
54	65.0	7	77	4.5	1	54	52.5	12	58	270	10	74	22.5
58	67.1	8	82	4.7	---	61	51.8	13	73	250	11	75	35.5
68	68.4	9	74	5.1	1	66	51.0	14	74	245	12	76	27.5
61	76.2	10	66	5.3	2	68	50.1	15	57	239	13.5	77	30
81	76.8	11	58	5.6	3	58	48.7	16	59	239	13.5	78	63.5
80	77.9	12	73	6.3	4	81	48.4	17	54	230	15	79	28.5
63	78.9	13	80	8.2	5	62	48.1	18	78	225	16	80	38
78	80.1	14	68	9.8	6	63	47.2	19	61	220	17	81	51
77	82.8	15	54	11.5	7	78	39.7	20	81	168	18		

The years 1953-82 are listed by numerical order for each of their t, u, v, and w values (as described previously in Table X-6). For each index, years are listed from indicators normally associated with unfavorable conditions at the top of the page to those associated with favorable conditions at the bottom of the page. The sample forecast year 1982 then is assigned a 0 (zero) position deviation value and each other year is assigned a position deviation value equal to the number of postions removed from 1982. These deviations are then accumulated for each year in the right hand column. Those years in which pre-season pressure systems were most similar to 1982 will show the lowest total position deviation; those most dissimilar, the highest total. For instance, all index values for 1972 were quite similar to 1980 and the position for all four index values totaled only 8.5, whereas 1978 was quite dissimilar on all index lists and accumulated total position deviation was 63.5. This is the basis for assuming that other conditions being equal, the 1982 season should approximate the 1972 season

U.S. NAVY-NOAA JOINT ICE CENTER SEASONAL OUTLOOK EASTERN ARCTIC ICE 1983

PREPARED BY
COMMANDING OFFICER
NAVAL POLAR OCEANOGRAPHY CENTER
NAVY DEPARTMENT
4301 SUITLAND RD
WASHINGTON, DC 20390

PREPARED FOR
COMMANDER,
NAVAL OCEANOGRAPHY COMMAND
NSTL STATION, BAY ST. LOUIS, MS 39529

The page numbers in this appendix are those of the original publication.

OUTLOOK - SUMMER 1983

SEA ICE CONDITIONS FOR THE GREENLAND COAST

The eastern Arctic long range outlook is based upon an analogue technique which compares late April ice conditions and freezing day accumulations with those of past seasons.

In figure 1 the ice conditions for April 26, 1983 are analyzed from a synthesis of satellite and conventional data. Satellite data were obtained from NOAA-7 visible and infrared sensors and the NIMBUS-7 scanning multifrequency microwave radiometer. Canadian and Danish ship, shore, and aerial ice reconnaissance reports from the North Atlantic, Labrador Sea, and Baffin Bay were also utilized. Figure 2 depicts the April 26 ice edge relative to the historical April maximum and minimum extremes in both the Labrador Sea and North Atlantic Ocean. The April 26 ice edge position generally exceeds or approximates the historical extremes in both the Labrador Sea and the North Atlantic Ocean. Seasonal frost degree day accumulations for coastal stations bordering the Labrador Sea and Baffin Bay are presented in figures 3 through 7. Each of the stations have observed new or near record maximum theoretical ice thicknesses for 1983. In East Greenland figure 8 shows that the frost degree day accumulation for Angmagssalik is near normal.

Figures 9 through 12 contain ice limit forecasts from May through August. It is predicted that the pack ice conditions in the Labrador Sea and Baffin Bay will be the most severe observed within the last 20 years. Near the East Greenland coast a near normal ice limit is predicted despite the near maximum ice limit currently observed south of 66°N. It is believed that the ice severity in south eastern Greenland in mid-summer is partially dependent upon the amount of ice available for southerly drift by the East Greenland current. The ice source region lies north of 66°N and currently has a near normal ice extent. Opening dates for Thule, Sondrestrom, and Angmagssalik are contained in Table 1.

TABLE 1 PORT OPENING DATES, FORECAST TRENDS

* Escorted

Port	Thule	Sondrestrom	Angmagssalik
Normal Opening Date	12 July	30 May	14 July
Predicted Trend	Later 8-10 Days	Later 4-6 Days	Normal

** Unescorted

Port	Thule	Sondrestrom	Angmagssalik
Normal Opening Date	25 July	08 June	18 August
Predicted	Later 8-10 Days	Later 4-6 Days	Normal

* Concentrations in approaches 7/10 or less and any fast ice will be weakened

** Concentration in approaches and port 1/10 or less.

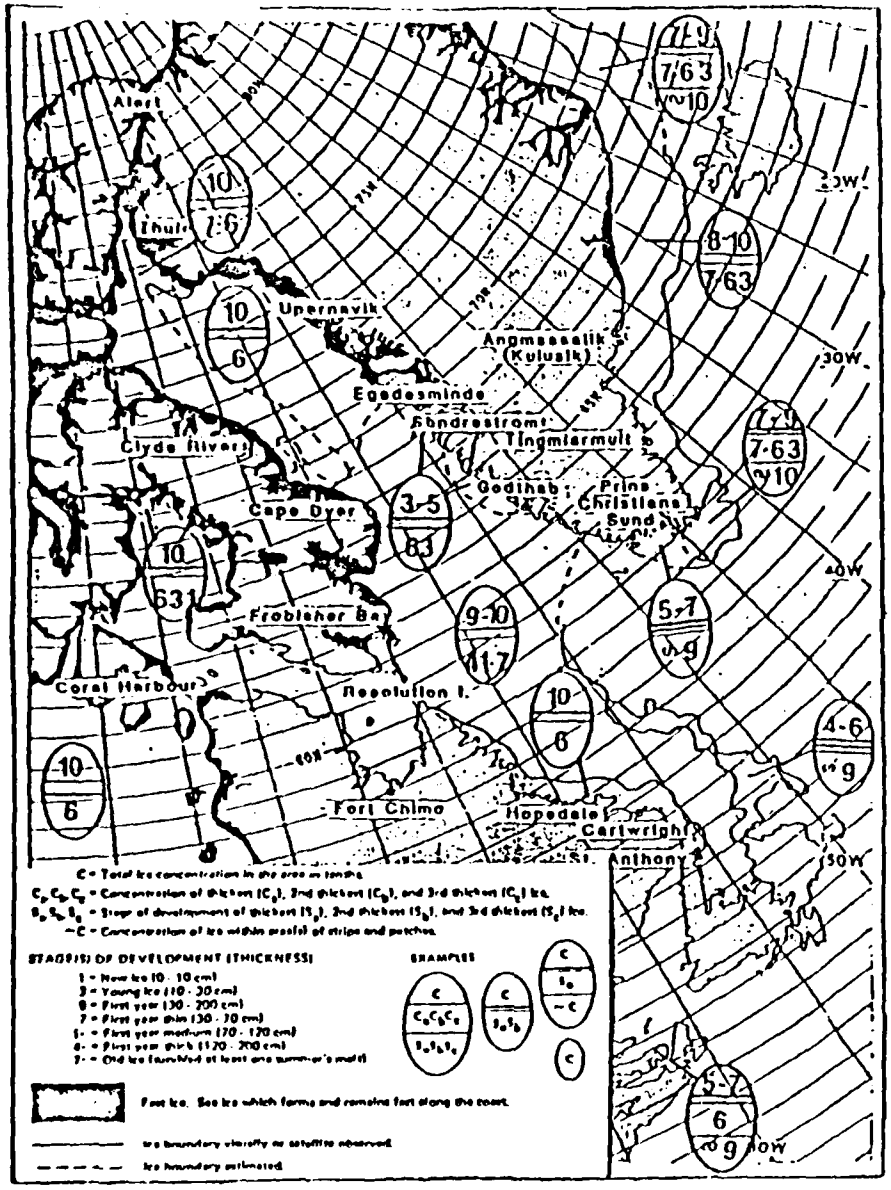

Figure 1. Initial sea ice conditions April 26, 1983

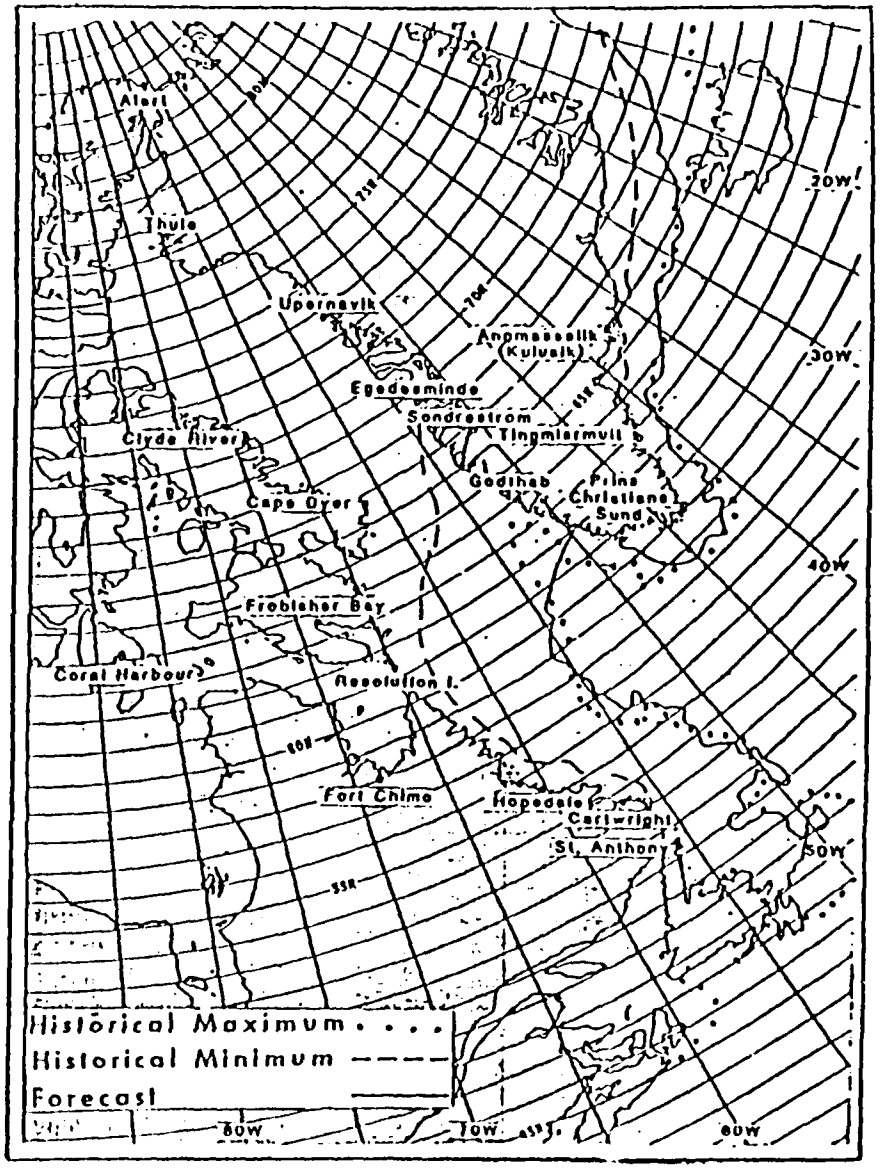

Figure 2. April historical maximum, minimum and observed April 26, 1983 ice edge limit

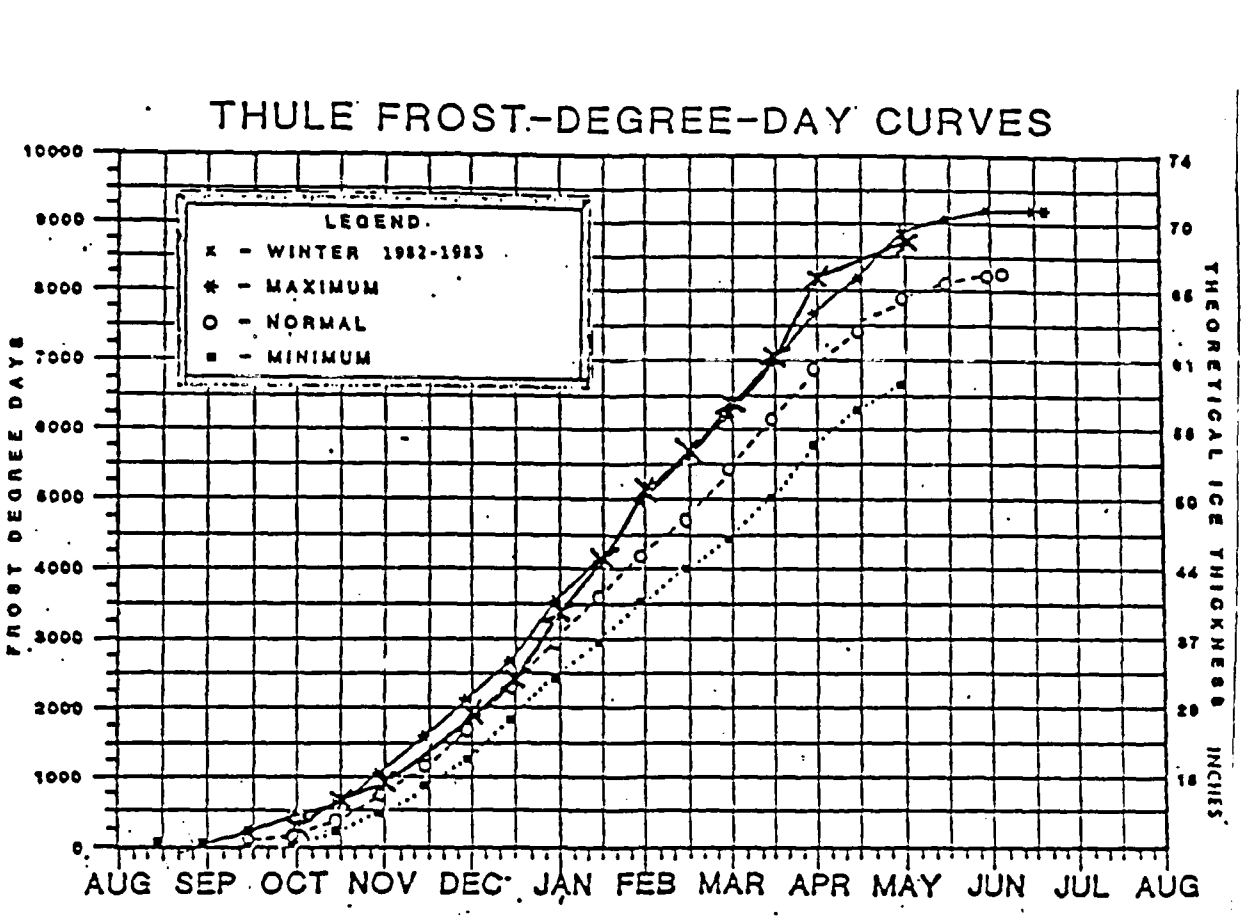

Figure 3. Frost degree day accumulations for Thule, Greenland

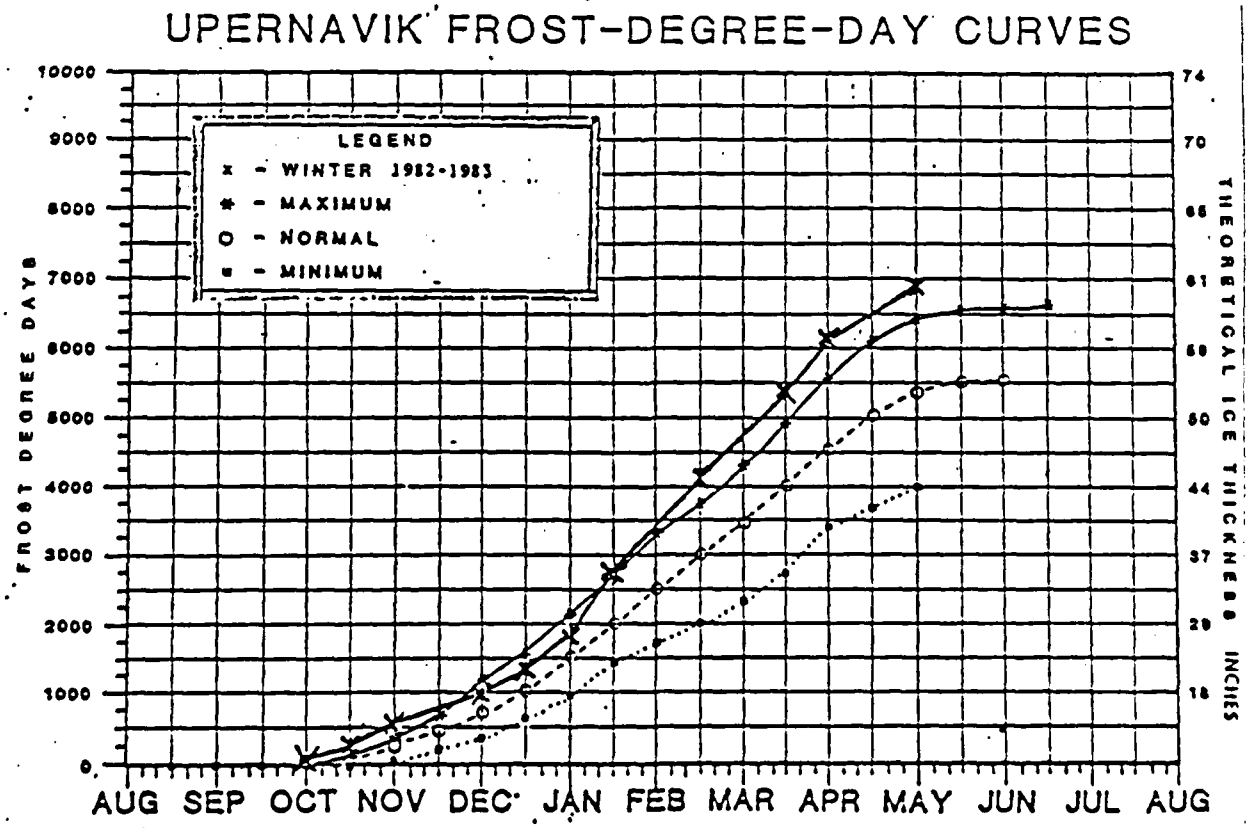

Figure 4. Frost degree day accumulations for Upernavik, Greenland

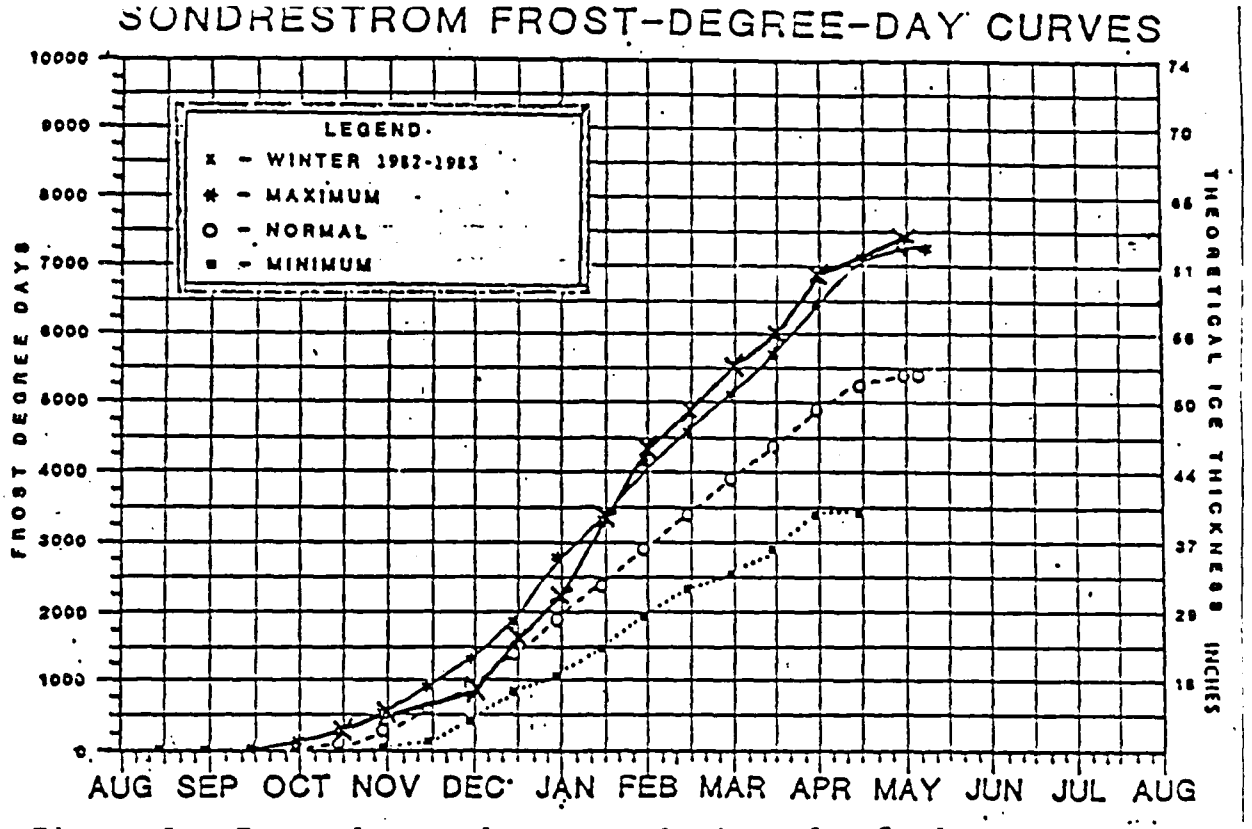

Figure 5. Frost degree day accumulations for Sondrestrom, Greenland

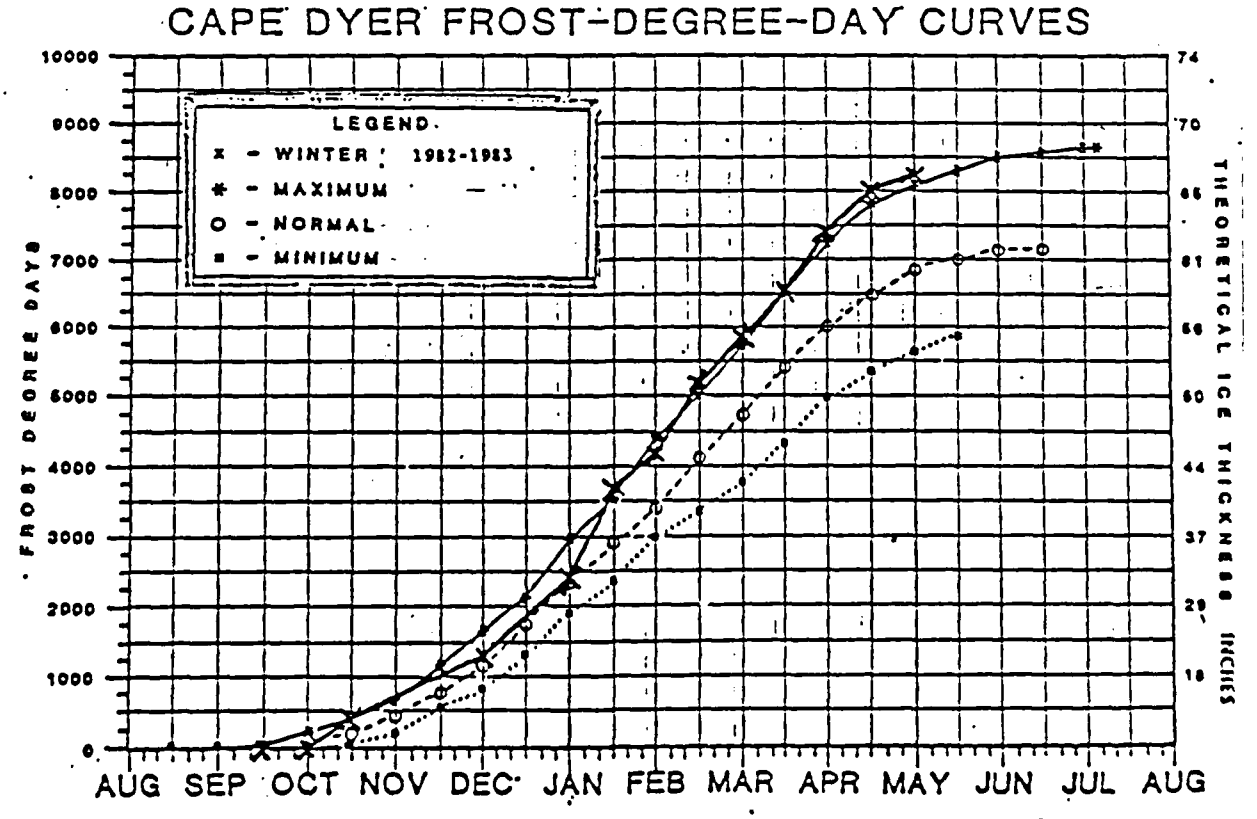

Figure 6. Frost degree day accumulation for Cape Dyer, Canada

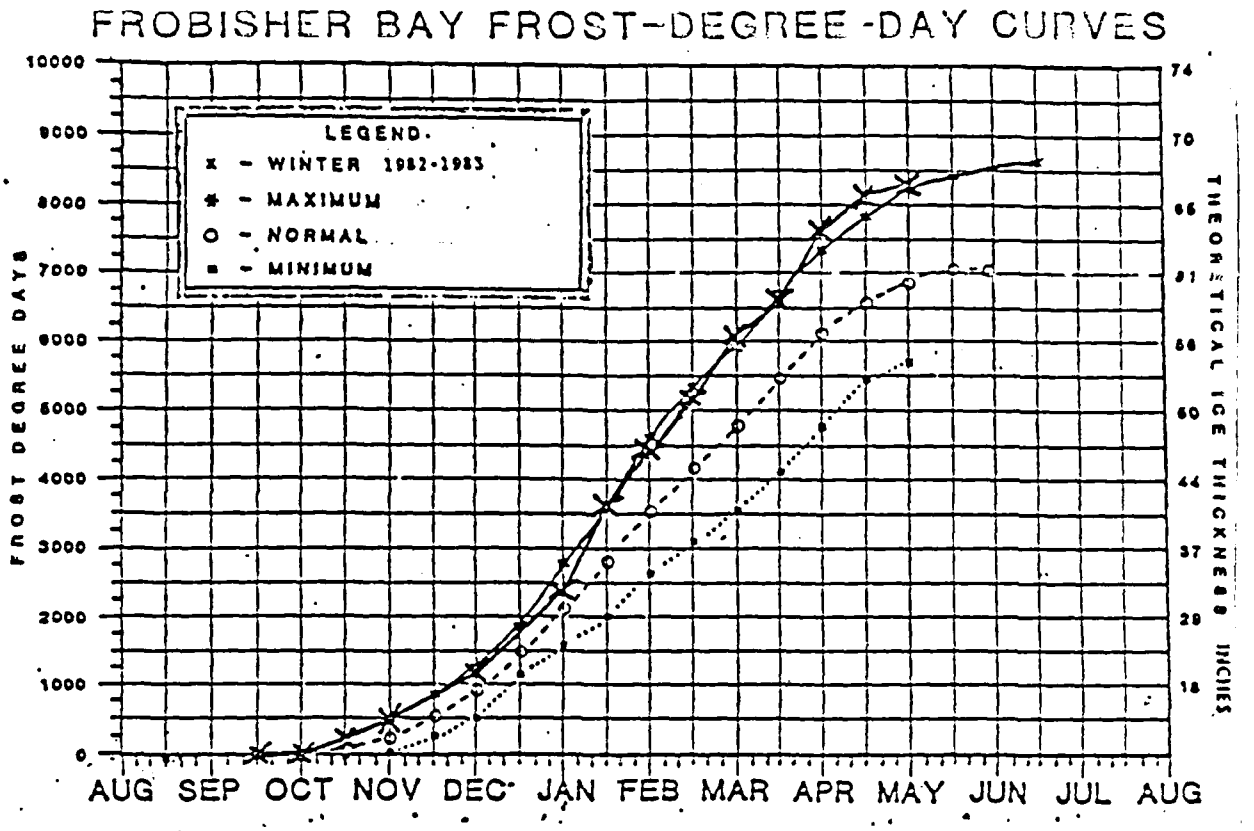

Figure 7. Frost degree day accumulation for Frobisher Bay, Canada

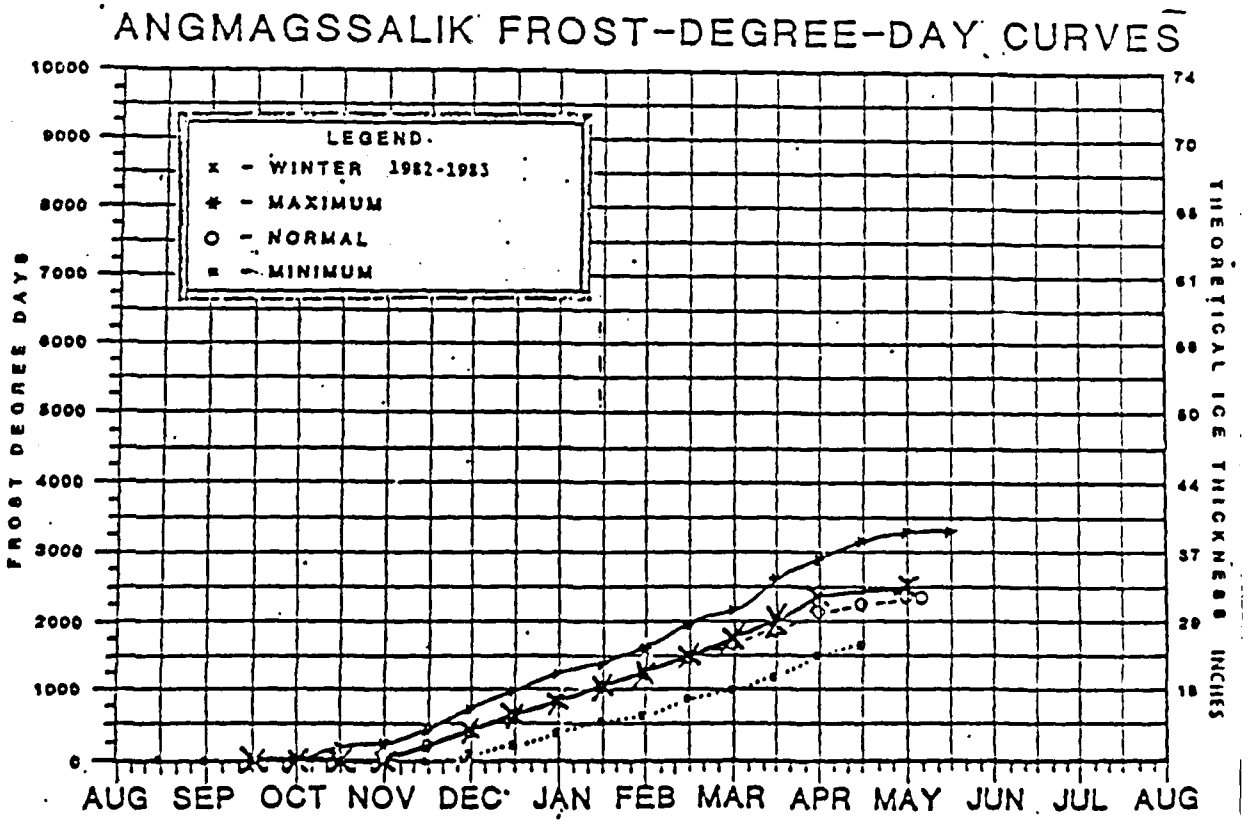

Figure 8. Frost degree day accumulation for Angmagssalik, Greenland

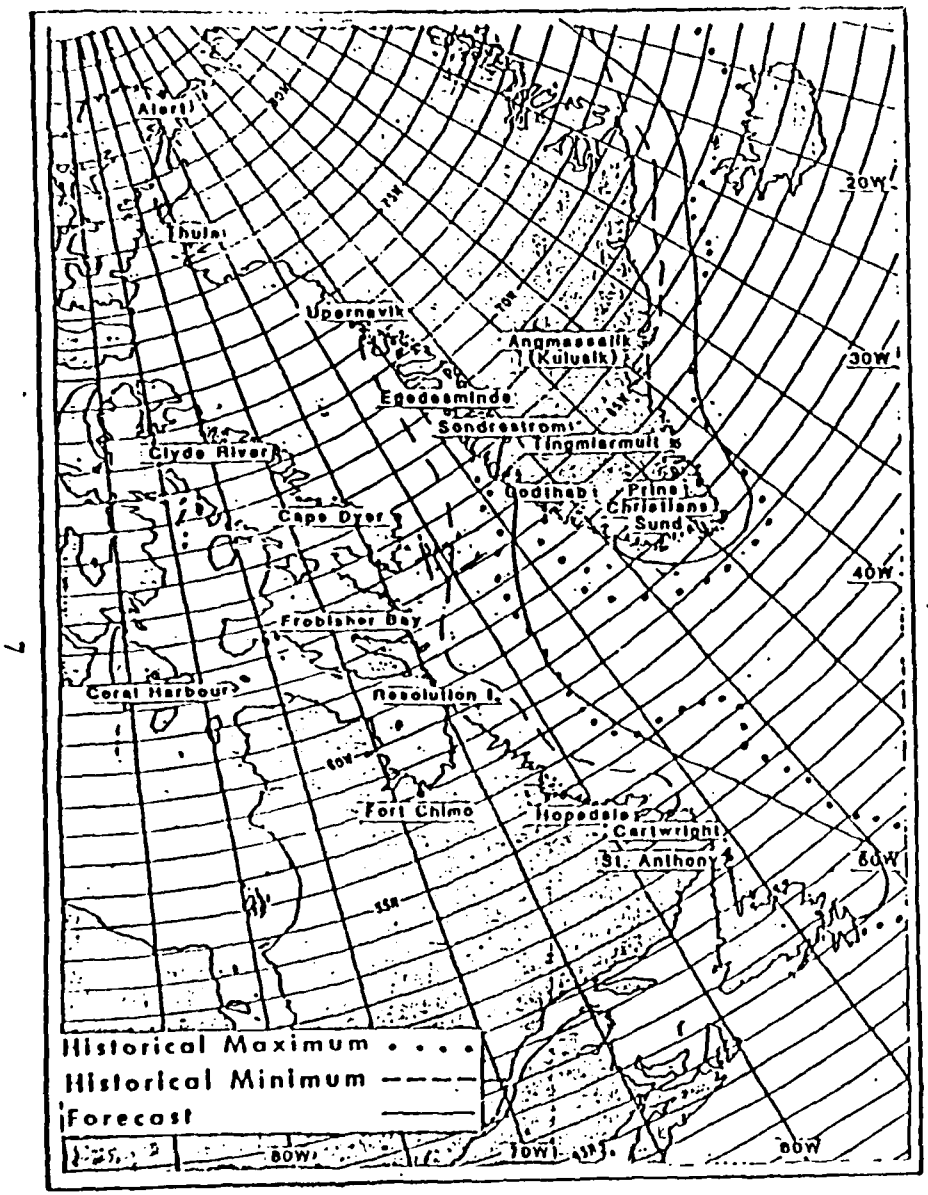

Figure 9. Historical end of May maximum, minimum and May 31, 1983 forecast ice edge position

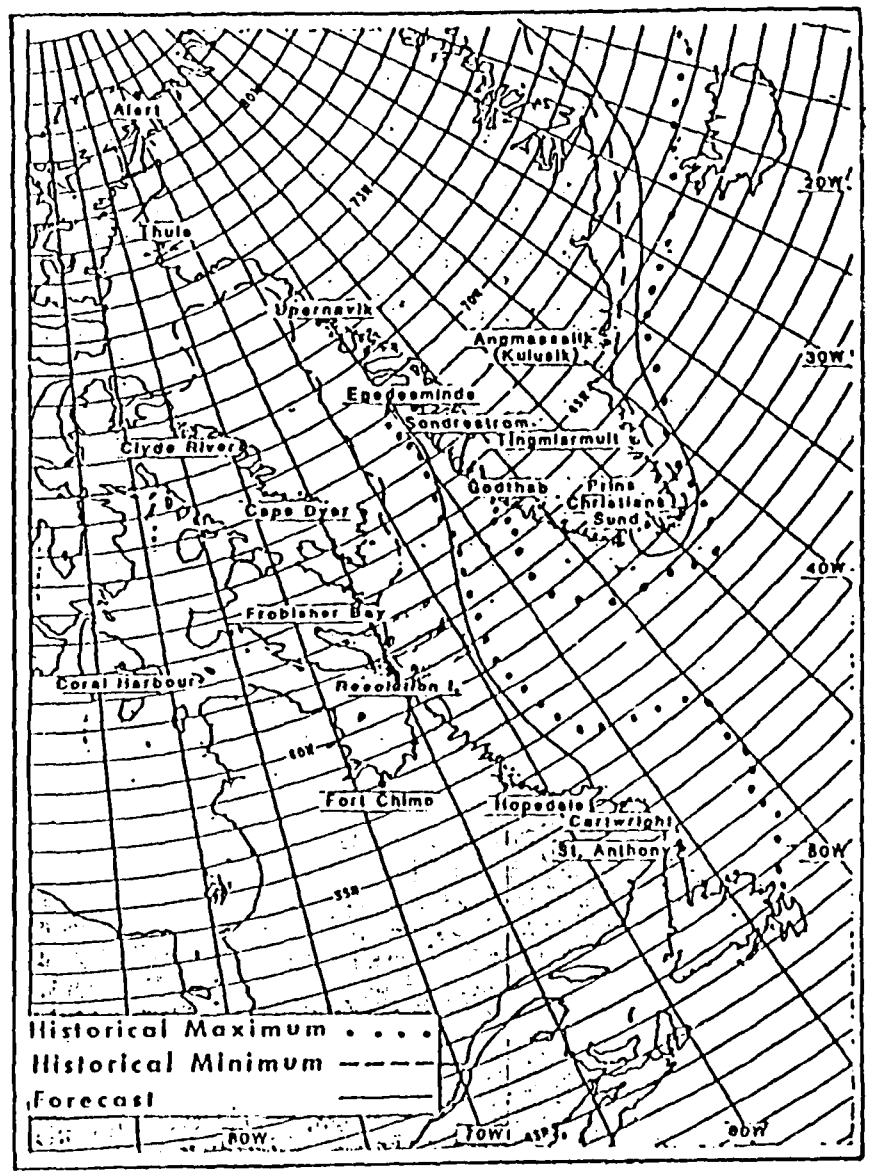

Figure 10. Historical end of June maximum minimum and June 30, 1983 forecast ice edge position

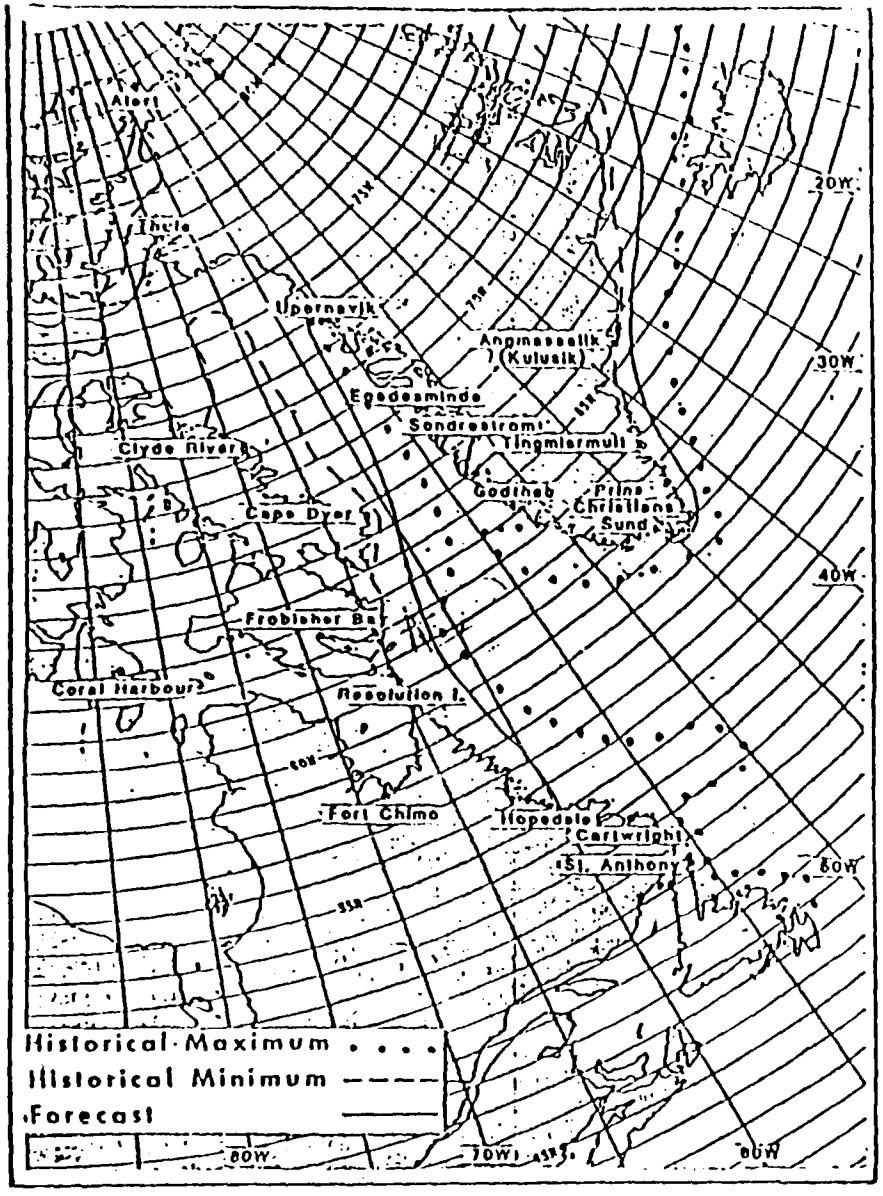

Figure 11. Historical end of July maximum, minimum and July 31, 1983 forecast ice edge position

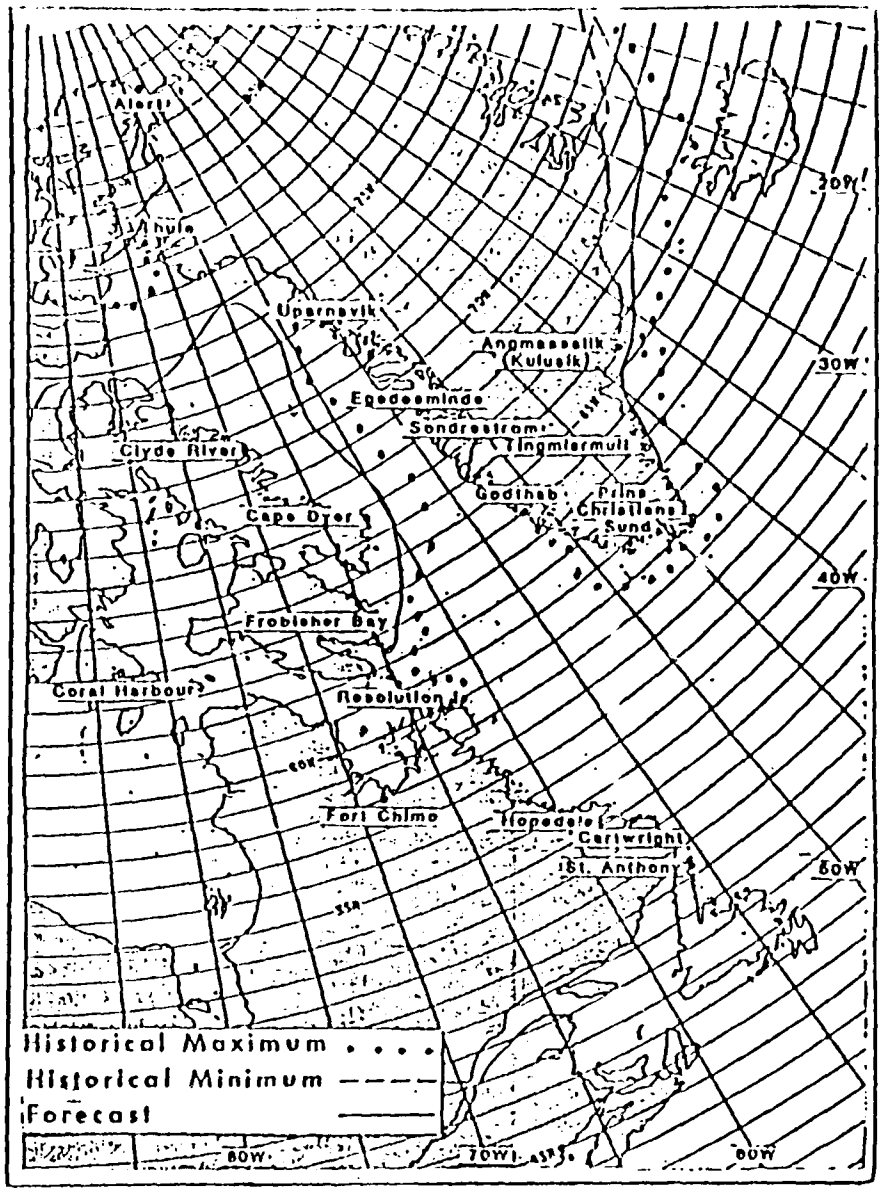

Figure 12. Historical end of August maximum, minimum and August 31, 1983 forecast ice edge position

U.S. NAVY-NOAA JOINT ICE CENTER SEASONAL OUTLOOK WESTERN ROSS SEA AND MCMURDO SOUND 1982-1983

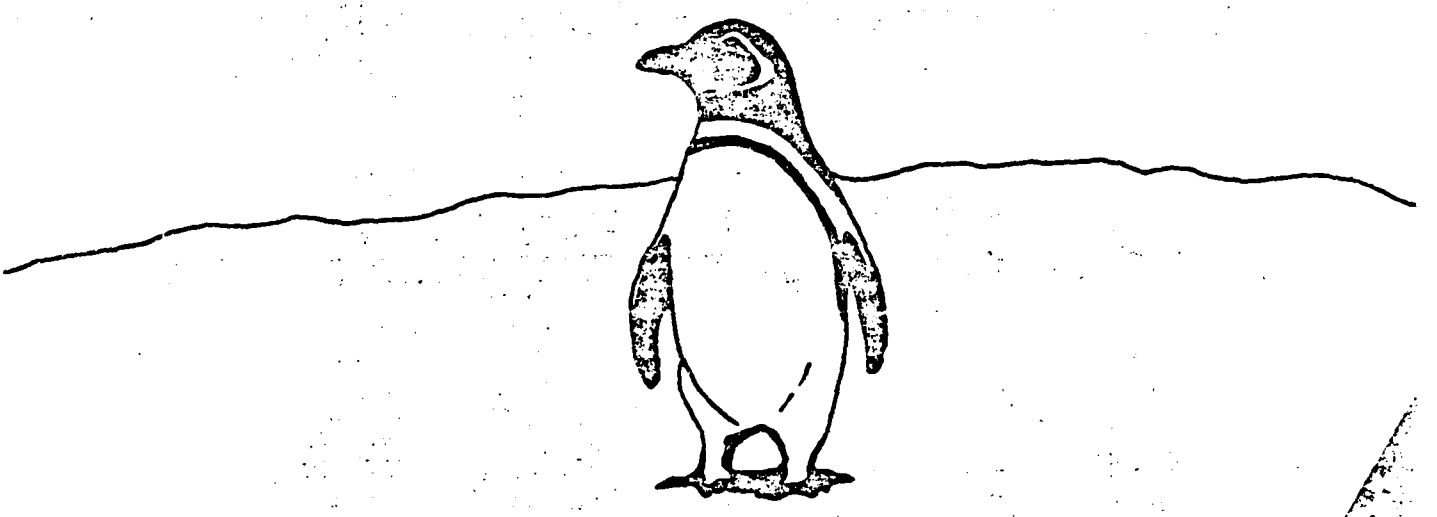

PREPARED BY
COMMANDING OFFICER
NAVAL POLAR OCEANOGRAPHY CENTER
NAVY DEPARTMENT
4301 SUITLAND RD
WASHINGTON, DC 20390

PREPARED FOR
COMMANDER,
NAVAL OCEANOGRAPHY COMMAND
NSTL STATION, BAY ST. LOUIS, MS 39529

The page numbers in this appendix are those of the original publication.

I. Introduction

This outlook forecasts the positions of the northern and southern ice pack edges in the Western Ross Sea and the rate of recession of the fast ice in McMurdo Sound along a typical shipping resupply route to McMurdo Station. The initial analysis of innerpack and fast ice conditions are interpreted from NOAA-7 and NIMBUS-7 satellite imagery. The positions of the ice pack and fast ice edges are predicted from the initial data through an analogue approach using historical data provided in NAVOCEANO Special Publication 265 (Perchal, 1975) and locally archived Ross Sea satellite imagery and satellite derived ice analyses.

II. Initial Ice Conditions

Ross Sea (Figure 1.)

The 28 October 1982 ice edge position extends north of the analyzed 1980 and 1981 location for similar time frames. With the exception of inner pack weaknesses in the vicinity of the Balleny Islands (67S, 163E), Cape Adare (72S, 170E), Drygalski Ice Tounge (76S, 167E) and a narrow shore lead adjacent the Ross Ice Shelf the ice pack is very close (9-10 tenths). The sea ice currently observed consists primarily of first year ice which is thinner and weaker than old ice. The position of the ice edge north of the Ross Sea is 15 nautical miles north of the historical average position (Perchal, 1975).

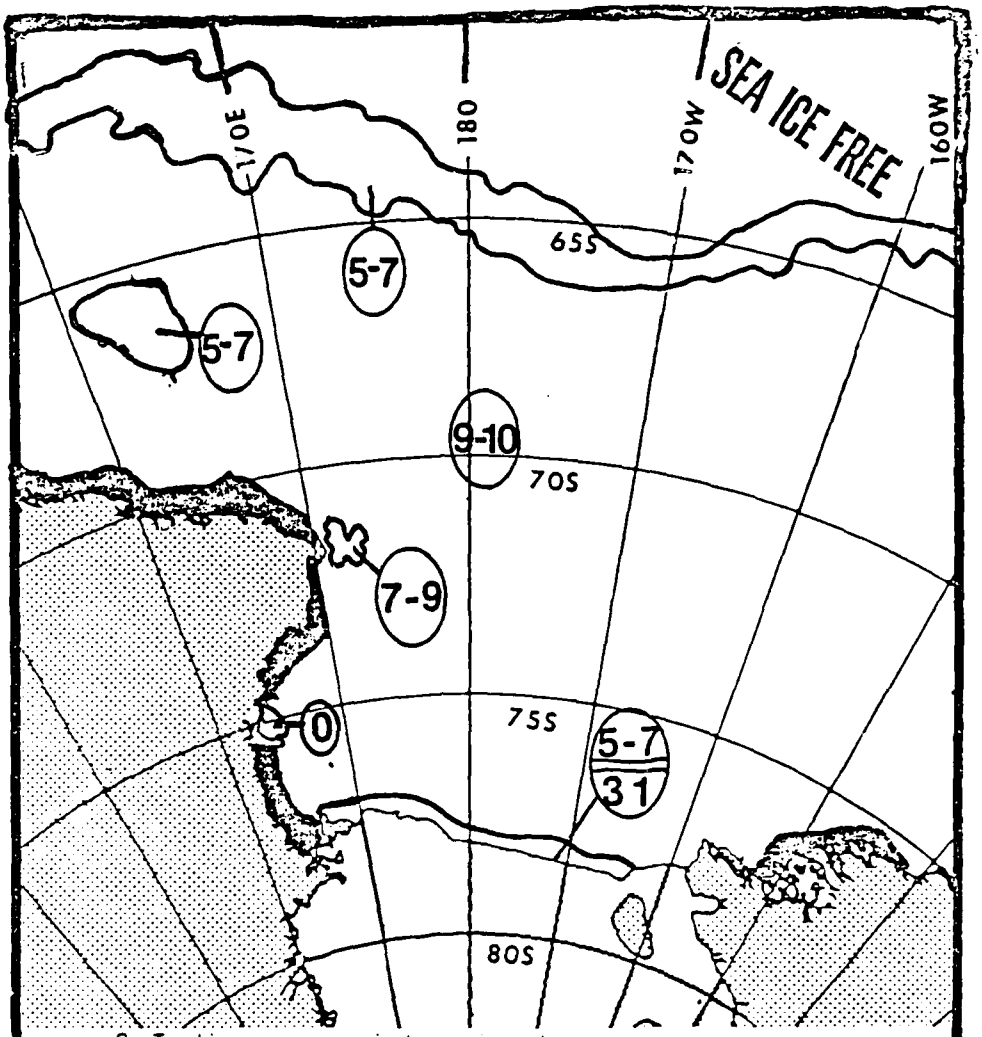

C = Total ice concentration in the area in tenths.

$C_a.C_b.C_c$ = Concentration of thickest (C_a), 2nd thickest (C_b), and 3rd thickest (C_c) ice.

$S_a.S_b.S_c$ = Stage of development of thickest (S_a), 2nd thickest (S_b), and 3rd thickest (S_c) ice.

~C = Concentration of ice within area(s) of strips and patches.

STAGE(S) OF DEVELOPMENT (THICKNESS)

1 = New ice (0 - 10 cm)
3 = Young ice (10 - 30 cm)
6 = First year (30 - 200 cm)
7 = First year thin (30 - 70 cm)
1• = First year medium (70 - 120 cm)
4• = First year thick (120 - 200 cm)
7• = Old ice (survived at least one summer's melt)

EXAMPLES

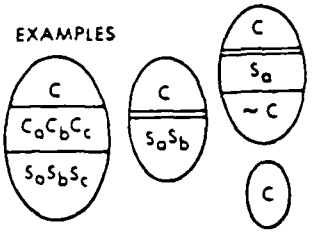

Fast ice. Sea ice which forms and remains fast along the coast.

Ice boundary visually or satellite observed.

Ice boundary estimated.

Figure 1. Initial ice conditions in the Ross Sea, 28 October 1982

McMurdo Sound (Figure 2.)

From NOAA-7 satellite imagery of 28 October 1982, the fast ice has been analyzed as extending 32 nautical miles from Hut Point. As depicted the fast ice extent is normal. In McMurdo Sound north of the fast ice, compact ice conditions consist of 6 tenths of old ice and 4 tenths of first year medium and thick ice.

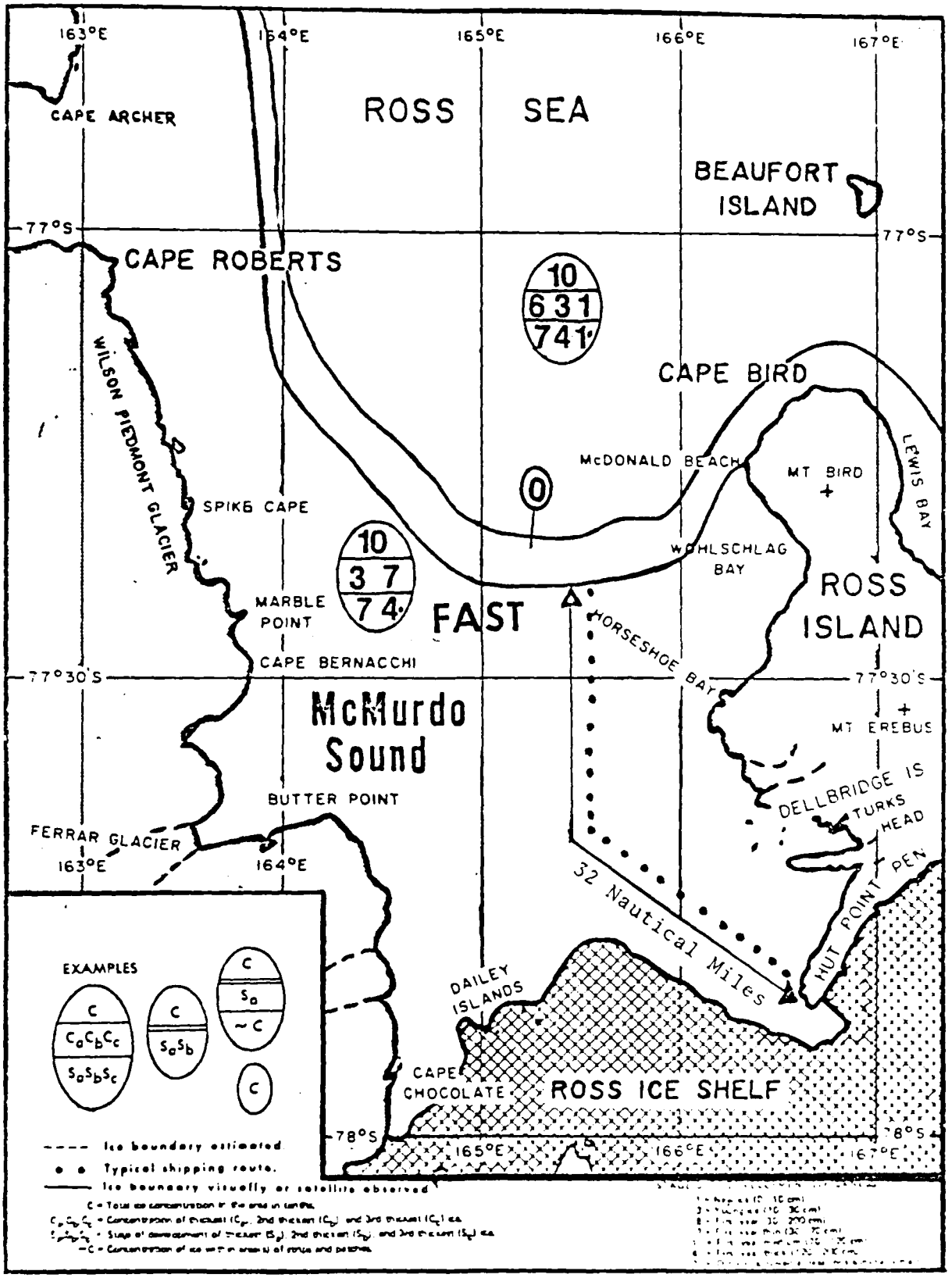

Figure 2. Initial ice conditions in McMurdo Sound, 28 October 1982 and fast ice extent along a typical shipping route

III. Outlook

Ross Sea

The compactness of the overall sea ice conditions in the Ross Sea and the more northerly extent of the northern ice edge indicate less favorable Ross Sea ice conditions for DEEP FREEZE 83. The northern ice edge is expected to recede southward at a rate of approximately 15 nautical miles per week through the first of December and then recede more rapidly. An ice free channel through the ice pack is expected near the twenty-first of January as the southern and northern ice edge positions converge (Figures 3. and 4.).

McMurdo Sound

Due to the normal extent of fast ice in McMurdo Sound (Figure 2.), it is expected that the total breakup to Hut Point will not occur without icebreaker assistance prior to 15 February. The fast ice (Table 1) will recede at normal rates throughout the melt season. By mid-January the fast ice extent is expected to be 12 nautical miles decreasing to 5 nautical miles by early February.

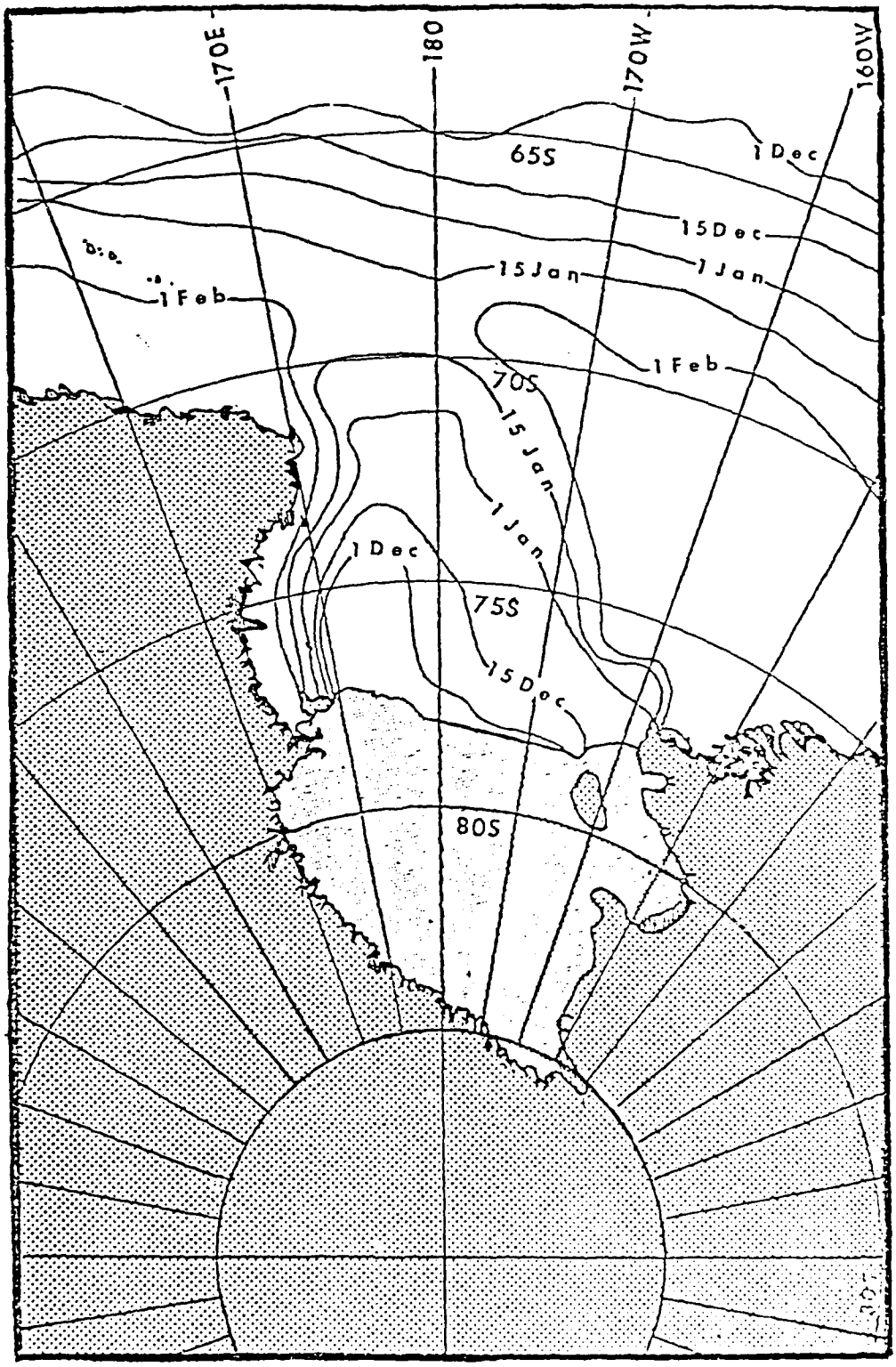

Figure 3. Expected recession pattern in the Ross sea

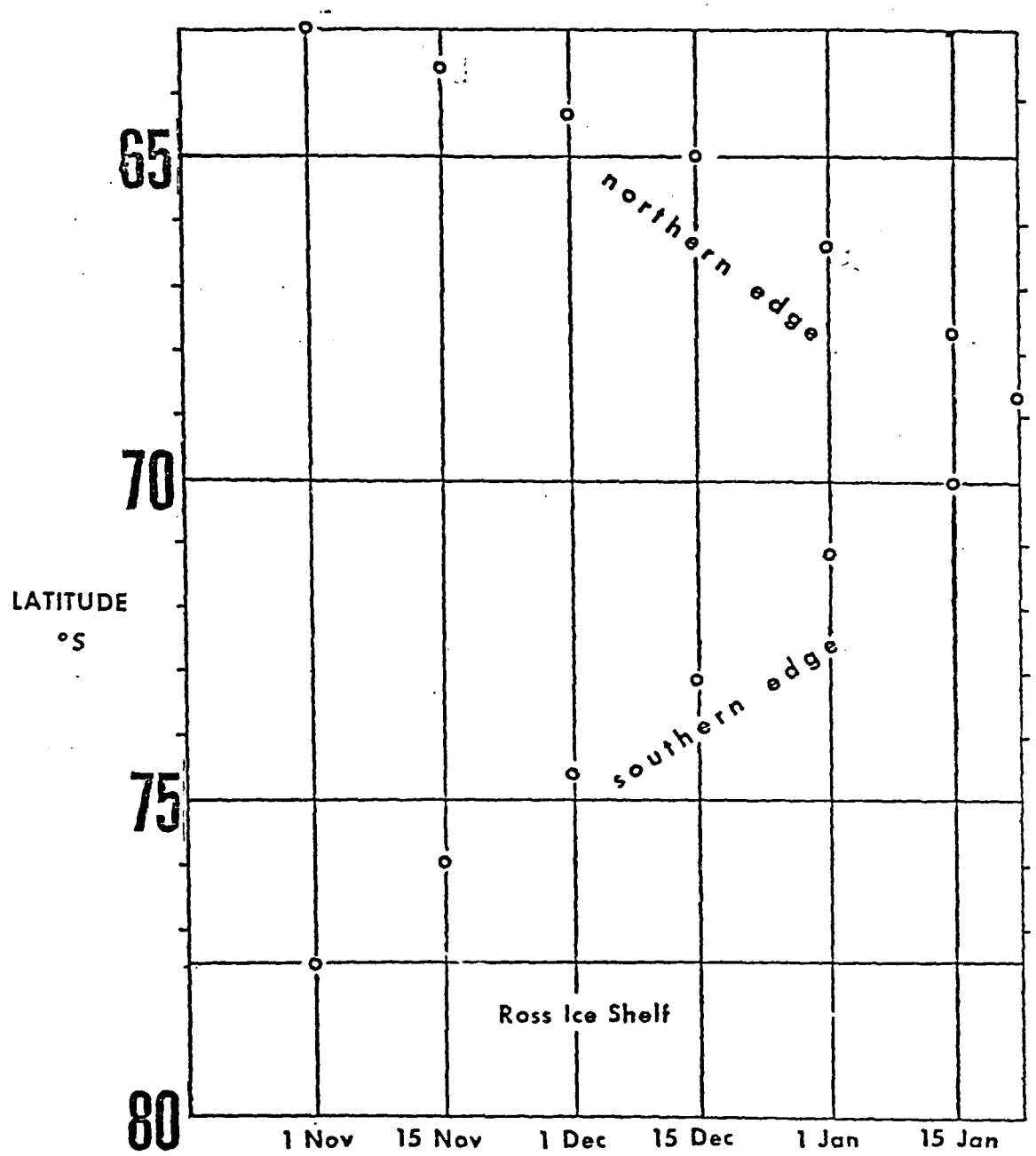

Figure 4. Expected positions of the northern and southern ice pack edges along 175E.

Table 1. Estimated schedule of fast ice recession in McMurdo Sound.

Date	Extent of fast ice from Hut Point** (nautical miles)
01 Nov 82	32
15 Nov 82	27
01 Dec 82	24
15 Dec 82	22
01 Jan 83	17
15 Jan 83	12
01 Feb 83	05
15 Feb 83	0

**The extent of fast ice is determined along a line from the southernmost latitude of the fast ice edge observed between 165° 15'E and 165° 45'E thence due south to a true bearing of 142° extending to Hut Point.

ICE FORECASTING BIBLIOGRAPHY

Ackley, S.F., "A review of sea-ice weather relationships in the southern hemisphere," in Sea Level, Ice and Climatic Change, Proceedings of the Canberra Symposium, December 1979, IAHS Publication No. 131, pp.127-159.

Ahlnas, Kristina, "IR enhancement techniques to delineate surface temperature and sea ice distributions," proceedings of the 13th International Symposium on Remote Sensing of Environment, Ann Arbor, Michigan, April 23-27, 1979.

Ahlnas, Kristina, "Surface temperature enhanced NOAA-satellite infrared imagery for the Bering, Chukchi, and Beaufort Seas and the Gulf of Alaska, May 1974-September 1980," Institute of Marine Science Report R80-2, March 1981.

Allison, Ian, "The role of sea ice in climate variations," prepared for WMO/CAS-JSC-CCCO Joint Meeting of Experts on the Role of Sea Ice in Climate, conference held in Geneva, June 1982.

Allison, Ian, "Antarctic sea ice growth and oceanic heat flux," in Sea Level, Ice and Climatic Change, Proceedings of the Canberra Symposium, December 1979, IAHS Publication No. 131, pp. 161-170.

Barry, R.G., "The data base," presented at NATO Advanced Study on Air-Sea-Ice Interaction, Acquafredda di Maratea, ITALT, September 28-October 10, 1981.

Barnes, James C., David T. Chang, and James H. Willand, "Use of Satellite high resolution infrared imagery to map arctic sea ice," Final report to NASA, Contract No. N62306-68-C-276, August 1969.

Barnett, Don G., "A practical method of long range ice forecasting for the north coast of Alaska. Part I," Fleet Weather Facility Technical Report 1, March 1976.

Barnett, Don G., "A long-range ice forecasting method for the north coast of Alaska," in Sea Ice Processes and Models, Robert S. Pritchard, editor, University of Washington Press, Seattle, pp/ 360-372, 1980.

Bauer, Jane, "Field observations of medium and small scale features of the Bering Sea ice edge in February 1978," in The Interaction of Oil with Sea Ice in the Beaufort Sea, by Seelye Martin, quarterly report to NOAA-OCS Contract 03-5-22-67, Task 6, RU 87, University of Washington, Seattle, Washington, 9/30/78.

Britton, Captain Graham P., "Improvement of marine advisories and optimum track ship routings: the north slope resupply operation in 1975," Sea Use 1-76, Annex G2, Sea Use Environmental Task I.080, March 15 1976.

Campbell, W.J., R.O. Ramsier, H.J. Zwally, and P. Gloersen, "Arctic sea-ice variations from time-lapse passive microwave imagery," Boundary-layer Meteorology, 18, (1), 1980, pp. 99-106.

Carsey, R.D., R.O. Ramseier, W.F. Weeks, "Sea-ice mission requirements for the U.S. FIREX and Canada RADARSAT Programs," report of the bilateral ice study team workshop, Cornwall Ontario, February 11-13, 1981. Prepared by Jet Propulsion Laboratory, California Institute of Technology, Pasadena, CA, January 1982.

Central Intelligence Agency, "Polar Regions: Atlas," GC 78-10040, May 1978.

Crane, R.G., "Seasonal Variations of sea ice extent in the Davis Strait-Labrador Sea area and relationships with synoptic-scale atmosphere circulation," Arctic, 31, (4), December 1978.

Crane, R.G., R.G. Barry, and H.J. Zwally, "Analysis of atmosphere-sea ice interactions in the Arctic Basin using ESMR microwave data," International Journal of Remote Sensing, 3, (3), 1982, pp. 259-276.

Crisci, Richard L., "Objective guidance for forecasting sea ice drift," Alaska Region Technical Procedures Bulletin No. 6, NOAA/National Weather Service, October 1978.

Danard, Maurice, Mark Gray, and Goz Lyv, "The problem of sea ice prediction: a model for computing water temperature, mixed layer depth and initial ice formation," prepared for Forecast Research Div., Meteorological Services, Downsivew, Ontario, May 1982.

Dehn, W.S., "Alaskan Sea Ice," Fleet Weather Facility, Suitland, Maryland, April 1971.

Dwyer, R.E. and R.H. Godin, "Determining sea-ice boundaries and ice roughness using GEOS-3 altimeter data," NASA contractor report 156862, Contract No. NAS6-2947, March 1980.

Dykins, J.E., "Ice engineering - material properties of saline ice for a limited range of conditions," Naval Civil Engineering Laboratory Technical Report R720, April 1971.

Gedney, R.T., R.J. Schertler, R.A. Mueller, R.J. Jirberg, and H. Mark, "An operational all-weather Great Lakes ice information system," NASA Technical Memorandum X-71812, 1976.

Gerson, D.J., "A numerical ice forecasting system," Naval Oceanographic Officer Reference Publication RP-8, 1975.

Gerson, Donald J. and Lloyd S. Simpson, "Wind drift sea ice: a supplement to the Naval Oceanographic office numerical ice forecasting system," Naval Oceanographic Office Reference Publication 8-S, September 1976.

Godin, Raymond H., "Sea ice charts of the Navy/NOAA Joint Ice Center," Glaciological Data, Report GD-11 "Snow Watch 1980," October 1981.

Harr, P.A., "Users manual for a polar ice forecast subsystem-Arctic," NORDA Technical Note 121, Naval Ocean Research & Development Activity, NSTL Station, Miss. 39529, October 1981.

Harr, P.A. and T.C. Pham, "Functional description for modification of the polar ice forecast subsystem-Arctic," NORDA Technical Note 120, Naval Ocean Research & Development Activity, NSTL Station, Miss. 39529, October 1981.

Harr, P.A., T.C. Pham, and J.P. Welsh, "Program maintenance manual, polar ice forecast subsystem-Arctic," NORDA Technical Note 122, Naval Ocean Research & Development Activity, NSTL Station, Miss. 39529, October 1981.

Herman, Gerald, "Atmospheric modelling and air-sea-ice interaction," presented at NATO Advanced Study Institute on Air-Sea-Ice Interaction, Acquafredda di Maratea, ITALY, September 28-October 10 1981.

Hussey, W. John, "The Tiros-N polar orbiting environmental satellite system," presented at Tenth Session of ESCAP/WMO Typhoon Committee, Tokyo JAPAN, October 28 1977.

Jet Propulsion Laboratory, "FIREX Mission requirements document for non-renewable resources," California Institute of Technolgy, Pasadena, California, June 15, 1982.

Kellogg, Thomas B., "Late quaternary changes in the Norwegian and Greenland Seas," Climate of the Arctic, G. Weller and S. Bowling, eds., proceedings of the Twenty-Fourth Alaska Science Conference, Fairbanks, Alaska, August 1973.

Lemke, Peter, "Stochastic description of atmosphere-sea ice-ocean interaction," presented at NATO Advanced Study Institute on Air-Sea-Ice Interaction, Acquafredda di Maratea, ITALY, September 28-October 10, 1981.

McNutt, Lyn, "Comparison of environmental conditions in the Bering Sea and Davis Strait and the effects on microwave signature returns: March and April, 1979," Final Report, NASA Contract NAG 5-161, Ref: A82-13, June 15, 1982.

Malankovitch, M., in Handbuch der Klimatologie, W. Koppen and R. Geiger, editors, Borntraeger, Berlin, Vol. I, Part A, 1930.

Martin, Seelye, "A field study of brine drainage and oil entrainment in first-year sea ice," Journal of Glaciology, 22, (88), 1979, pp. 473-502.

Martin, Seelye, "Frazil ice in rivers and oceans," Ann. Rev. Fluid Mech., 13:379-97, 1981.

Martin, Seelye, Donald J. Avalieri, S. Lyn McNutt, "The Bering Sea ice cover during March 1979: comparison of surface and satellite data with the NIMBUS-7 SMMR," Annual Report NOAA/NESS/SPOC Group Contract #MO-A01-78-00-4335, Ref: A82-4, January 1982.

Mellor, Malcolm, "Mechanical behavior of sea ice," presented at NATO Advanced Study Institute on Air-Sea-Ice Interaction, Acquafredda di Maratea, ITALY, September 1981.

Mitchell, P.A., "Eastern arctic area 15 and 30 day ice forecasting guide," Naval Oceanographic Office Special Publication SP-265, 1979.

NASA, "The Nimbus 7 user's guide," edited by Charles R. Madrid, Management and Technical Services Co., Beltsville, MD, Contract No. NAS 5-23740, August 1978.

AD-A145 286 HANDBOOK FOR SEA ICE ANALYSIS AND FORECASTING(U) ALASKA UNIV FAIRBANKS GEOPHYSICAL INST W J STRINGER ET AL. JUN 84 NERPF-CR-84-03 N00228-81-C-H553 4/4

UNCLASSIFIED F/G 8/12 NL

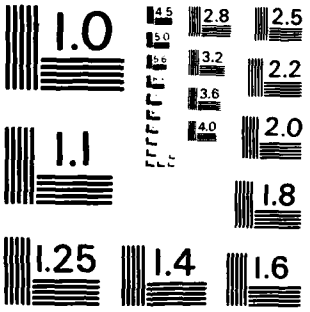

MICROCOPY RESOLUTION TEST CHART
NATIONAL BUREAU OF STANDARDS - 1963 - A

NASA, The Conception, Growth, Accomplishments and Future of Meteorological Satellites, NASA Conference Publication 2257, proceedings of the session on meteorological satellites at the American Meteorological society's 62nd Annual Meeting, San Antonio Texas, January 1982.

NASA, "Antarctic sea ice, 1973-1976: satellite passive microwave observations," SP-459, #NAS 1.21:459, 1983.

NASA (ICEX), "Ice and climate experiment, report of science and applications working group," December 1979.

Naval Environmental Prediction Research Facility, "Navy tactical applications guide, volume 2, environmental phenomena and effects," NEPRF Technical Report 77-04, 1979.

Naval Environmental Prediction Research Facility, "Navy tactical applications guide, volume 1, techniques and applications of image analysis," NEPRF applications report 77-03 Monterey, California, 1977.

Naval Environmental Prediction Research Facility, "Navy tactical applications guide, operational environmental satellites: polar-orbiting satellites, geostationary satellites," NEPRF Technical Report TR 83-02, 1983.

Naval Polar Oceanography Center, "Ice observation handbook," 4301 Suitland Road, Washington, D.C., 1981.

Naval Polar Oceanography Center, "U.S. Navy-NOAA Joint Ice Center seasonal outlook, western Arctic ice 1981," 4301 Suitland Road, Washington, D.C., 1981.

Naval Polar Oceanography Center, "U.S. Navy-NOAA Joint Ice Center seasonal outlook western Arctic ice 1982," 4301 Suitland Road, Washington, D.C., 1982.

Pease, Carol H., and S.A. Salo, "Drift characteristics of northeastern Bering Sea ice during 1980," NOAA Technical Memorandum ERL PMEL-32, July 1981.

Perchal, R.J., "Western Ross Sea and McMurdo Sound ice forecasting guide," Naval Oceanographic Office Special Publication SP-265, 1975.

Potocsky, G.J., "Alaskan area 15 and 30 day ice forecasting guide," Naval Oceanographic Office Special Publication SP-263, 1975.

Reed, John C. and John E. Sater, editors, "The Coast and Shelf of the Beaufort Sea," Arctic Institute of North America, Proceedings of a symposium on Beaufort Sea Coast and Shelf Research, December 1974.

Rogers, Jeffrey C., "Meteorological factors affecting interannual variability of summertime ice extent in the Beaufort Sea," Month Weather Review, 106, (6), June 1978.

NASA, "The Nimbus 7 user's guide," edited by Charles R. Madrid, Management and Technical Services Co., Beltsville, MD, Contract No. NAS 5-23740, August 1978.

NASA, The Conception, Growth, Accomplishments and Future of Meteorological Satellites, NASA Conference Publication 2257, proceedings of the session on meteorological satellites at the American Meteorological society's 62nd Annual Meeting, San Antonio Texas, January 1982.

NASA, "Antarctic sea ice, 1973-1976: satellite passive microwave observations," SP-459, #NAS 1.21:459, 1983.

NASA (ICEX), "Ice and climate experiment, report of science and applications working group," December 1979.

Naval Environmental Prediction Research Facility, "Navy tactical applications guide, volume 2, environmental phenomena and effects," NEPRF Technical Report 77-04, 1979.

Naval Environmental Prediction Research Facility, "Navy tactical applications guide, volume 1, techniques and applications of image analysis," NEPRF applications report 77-03 Monterey, California, 1977.

Naval Polar Oceanography Center, "Ice observation handbook," 4301 Suitland Road, Washington, D.C., 1981.

Naval Polar Oceanography Center, "U.S. Navy-NOAA Joint Ice Center seasonal outlook, western Arctic ice 1981," 4301 Suitland Road, Washington, D.C., 1981.

Naval Polar Oceanography Center, "U.S. Navy-NOAA Joint Ice Center seasonal outlook western Arctic ice 1982," 4301 Suitland Road, Washington, D.C., 1982.

Pease, Carol H., and S.A. Salo, "Drift characteristics of northeastern Bering Sea ice during 1980," NOAA Technical Memorandum ERL PMEL-32, July 1981.

Perchal, R.J., "Western Ross Sea and McMurdo Sound ice forecasting guide," Naval Oceanographic Office Special Publication SP-265, 1975.

Potocsky, G.J., "Alaskan area 15 and 30 day ice forecasting guide," Naval Oceanographic Office Special Publication SP-263, 1975.

Reed, John C. and John E. Sater, editors, "The Coast and Shelf of the Beaufort Sea," Arctic Institute of North America, Proceedings of a symposium on Beaufort Sea Coast and Shelf Research, December 1974.

Rogers, Jeffrey C., "Meteorological factors affecting interannual variability of summertime ice extent in the Beaufort Sea," Month Weather Review, 106, (6), June 1978.

Rogers, Jeffrey C., "A meterological basis for long-range forecasting of summer and early autumn sea ice conditions in the Beaufort Sea," presented at the Fourth International Conference on Port and Ocean Engineering under Arctic Conditions, St. John's, Newfoundland, CANADA September 26-30, 1977, Volume I. pp.952-962.

Schertler, R.J., R.A. Mueller, R.J. Jirberg, D.W. Cooper, J.E. Heighway, A.D. Holmes, R.T. Gedney, and H. Mark, "Great Lakes all-weather ice information system," NASA Technical Memorandum X-71815, presented at the Tenth International Symposium on Remote Sensing of the Environment, Ann Arbor, Michigan, October 6-10, 1975.

Schwalb, Arthur, "The Tiros-N/NOAA A-G satellite series," NOAA Technical Memorandum, NESS 95, August 1979.

Shaw, G., and K. Stamnes, "Arctic haze: perturbation of the polar radiation budget," Annals of the New York Academy of Sciences, Vol. 338, pp. 533-539, May 15, 1980.

Skiles, Frank L., "Empirical wind drift of sea ice," in Arctic Drifting Stations by the Arctic Institute of North America, 1968, pp. 239-252.

Skov, Niels Aage, The Ice Cover of the Greenland Sea: an evaluation of oceanographic and meteorological causes for year-to-year variations, Meddelselser Om Grønland, Udgivne af Kommissionen for Videnskabelige Undersøgelse I Grønland, Bd. 188, Nr2., København, C.A. Reitzels Forlag, 1970.

Thorndike, A.S. and Colony, R., "Sea ice motion in response to geostrophic winds," Journal of Geophysical Research, 87, (C8), 1982.

URSI Commission F. Symposium, Signature Problems in Microwave Remote Sensing of the Surface of the Earth, Lawrence, Kansas, January 5-8, 1981.

Wadhams, Peter, "The seasonal ice zone," Chapter 10, presented at NATO Advanced Study Institute on Air-Sea-Ice Interaction, Acquadfredda di Maratea, ITALY, September 28 - October 10, 1981.

**Walsh, John, "A preliminary digitization of northern hemisphere sea ice data," University of Illinois, DATE and SOURCE UNKNOWN.

Wedler, Edward and James R. Rossiter, "X-band SAR image response from first year ice off Newfoundland," poster paper presented at URSI Commission F Symposium, Lawrence Kansas, January 5-8, 1981.

Welsh, J.P., R. Wessel, P.A. Harr, and T.C. Pham, "Report of FY81 effort for PIFS-N Model," NORDA Technical Note 123, December 1981,

Wittmann, Walter I. and Gordon O. MacDowell, "Manual of short-term sea ice forecasting," Special Publication-82, Oceanographic Prediction Div., U.S. Naval Oceanographic Office, May 1964.

Zubov, N.N., "Arctic ice," translated by Naval Oceanographic Office, American Meteorological Society, printed by Defense Documentation Center for Scientific and Technical Information, Cameron Station, Alexandria, VA, AD426972, 1943.

Zwally, H. Jay, C.L. Parkinson, and J.C. Comiso, "Variability of Antarctic sea ice and changes in carbon dioxide," Science, 220(4601), pp. 1005-1012, 3 June, 1983.